SYNTHESIS AND CHARACTERIZATION OF THE NEUTRAL π-RADICAL MOLECULAR CONDUCTORS

by

Hongzhou Zhang

A thesis

presented to the University of Waterloo

in fulfillment of the

thesis requirement for the degree of

Doctor of Philosophy

in

Chemistry

Waterloo, Ontario, Canada, 2000

The University of Waterloo requires the signatures of all persons using or photocopying this thesis. Please sign below, and give address and date.

ABSTRACT

PREPARATION AND CHARACTERIZATION OF NEUTRAL π-RADICAL MOLECULAR CONDUCTORS

Hongzhou Zhang

University of Waterloo

Advisor:

Dr. Richard T. Oakley

1,3,2- and 1,2,3-dithiazolyl (DTA) radicals have been investigated as building blocks for neutral radical conductors (NRCs). Several new derivatives have been prepared and structurally characterized; their ESR, CV and transport properties have been interpreted in terms of theoretical calculation results.

The electronic properties of 1,3,2-DTA radicals are strongly influenced by the electron-withdrawing power of the fused aromatic residues on 4,5-positions. The shift in reduction potentials from NDTA to TDTA is over 1 V and more importantly, the redox potential which corresponds to the disproportionation energy of the radicals also decreases. This trend follows the theoretical prediction and can be related to a lower Coulombic barrier to charge transport between radical centers in the solid state. However, charge correlation effects still outweigh the electronic stabilization provided by interannular orbital overlap. The large amount of free spins are trapped in the radical molecules and the materials remain Mott insulators with pressed pellet conductivities $<10^{-6}$ S cm^{-1}.

The solid state packing patterns of 1,3,2-DTA radicals are clearly related to their molecular structures. While NDTA favors a herringbone packing, replacement of the

structure-maker CH by N, as in QDTA and TDTA, leads to slipped B stack structures. The dimerization phase transition of 1,3,2-TDTA at low temperature (around 150 K) reveals the weakness of the interaction within the radical stacks. A multiple A tectonic plate π- slippage mechanism was proposed to account for the interconversion of the two phases.

In comparison to their 1,3,2-counterparts, 1,2,3-DTA radicals are inherently better candidates for the design of neutral radical conductors. Guided by the theoretical calculations, many new 1,2,3-DTA derivatives have been explored. In the solid state, 1,2,3-TDTA adopts a slipped B-dimer stack in which the dimers are coupled in a head-to-tail arrangement. The Coulombic barrier is reduced by the improved charge correlation effect and the radical exhibits the highest room temperature conductivity (1×10^{-4} S cm^{-1}) yet obtained for a single-component sulfur based molecular material. Moreover, the decoupled spins at elevated temperatures contribute to an increased conductivity.

A range of 1,2,3-DTA derivatives based on the quinoxaline framework have been synthesized and investigated. Three QDTA radicals were purified and spectroscopically characterized.

ACKNOWLEDGMENTS

This thesis represents the culmination of more than ten years of post-secondary study; the task turned out to be far more difficult than expected. I am delighted that I am close to this last moment. During this long academic journey, I received lots of invaluable help and support from many people and I want to take this opportunity to thank them.

First I want to thank my supervisor, Dr. Richard Oakley. From the first day when I came to Canada I have already felt his warmth and carefulness. It was he who helped me settle down and adapt quickly to my new environment. His theoretical knowledge, experimental skills, enthusiasm, persistence and patience make any problem solvable. Many friends say that few professors like your boss work in the lab and do experiments many times a day. While I was writing this thesis, he revised even commas and periods. I cannot count how much time he put in. He shows me by his behavior what attitude a real scientist should have . I am lucky and grateful to have studied and worked with him.

Dr. Robert Reed was my second advisor for two and a half years although no such real title was on his head. We worked on some projects together and I learned many detailed technical skills from him. He is a fabulous person and I wish him good luck always.

I would like thank my various committee members: Prof. Mark Baker, Prof. Elmer Alyea and Prof. Gary Hanan. As members of my advisory committee, they gave me much help in my comprehensive, seminars and the thesis preparation.

All the crystal structures, magnetic measurements and conductivity properties presented in this thesis came from our collaboration with Prof. Robert Haddon at the University of Kentucky, Prof. Wallace Cordes at the University of Arkansas and Prof. John

Richardson at the University of Louisville. This has beem a fruitful and supportive system.

Many thanks are given to my co-workers in the Oakley lab. Kathryn and I have been in the same labs in Guelph and Waterloo for four years. I also remember the old guys, Greg, Noel, Craig as well as the new friends, Leanne, Dan and James. It has been a nice friendly community.

I also want to thank the Department of Chemistry and Biochemistry at the University of Guelph and the Department of Chemistry at the University of Waterloo, as well as the Graduate Studies Offices of both universities for their outstanding support, personally and financially. I also thank their main office and storeroom staff for their assistance.

And finally, I can never forget my parents, who gave me the chance to pursue this highest academic goal. Their hardwork, consideration and persistence are always remembered.

To Yuezhong and Grace

Table of Contents

LIST OF ABBREVIATIONS

a	Crystallographic lattice repeat along *x* axis
Å	Angstrom
b	Crystallographic lattice repeat along *y* axis
br	Broad (IR peak descriptor)
anal.	Analytical data
BDTA	Benzo-1,2,3-dithiazolyl
BBDTA	Benzo-1,2,4,5-bis(1,3,2-dithiazolyl)
BEDT-TTF or ET	Bis(ethylenedithio)tetramethylfulvalene
bp.	Boiling point
br	broad (IR peak descriptor)
c	Crystallographic lattice repeat along *z* axis
cm	Centimeter
cm^{-1}	Reciprocal centimeter or wavenumber
C	Curie Constant
°C	Degrees Celsius
CDW	Charge Density Wave
CNDO	Complete Neglect of ddifferential Overlap
CT	Charge Transfer
CV	Cyclic Voltammetry
dec.	Decomposing temperature
DC-DTA	4,5-dichloro-1,2,3-dithiazolyl

DFT	Density Functional Theory
DTA	Dithiazolyl
DOS	Density of States
e	Electronic charge
E_F	Fermi level
E_g	Energy gap
e_j	Energy of orbital j
EHMO	Extended Hückel Molecular Orbital
EI	Electron ionization
emu	Electromagnetic unit
Eqn.	Equation
eV	Electron volt
ESR	Electron Spin Resonance
Et	Ethyl group
g	Gram
h	Planc's constant
$\mathbf{H}$	Magnetic field
HOMO	Highest Occupied Molecular Orbital
Hz	Hertz
i	Current
IR	Infrared
$\boldsymbol{k}$	Wave vector
k	Boltzmann's constant

K	Kelvin
LUMO	Lowest Unoccupied Molecular Orbital
m	Metre; medium (IR peak descriptor)
m	Magnetic moment
m_e	Electronic mass
mL	Millitre
mmol	Millimole
M	Magnetization
Me	Methyl group
MHz	MegaHertz
MO	Molecular Orbital
mp.	Melting point
n	Number of charge carriers
N	Number of atoms per unit volume
NDTA	Naphthalene dithiazolyl
NMR	Nuclear Magnetic Resonance
OAH	Odd Alternate Hydrocarbon
ppm	Parts per million
Ply	Phenalenyl
PDTA	Pyrazine dithiazolyl
PTAT	6-amino-7-thiopteridine
PTDTA	Pteridino-[6,7-b]-1,2,3-dithiazolyl
Pm	Pyrimidine

PBDTA	Pyrrole [2,3-b;5,4-b]-bis (1,2,3-dithiazolyl)
PPDTA	1,2,5-thiadiazolo[3,4-b]-pyrazino-1,2,3-dithiazoly-[3,4-b]-pyrazine
Q	Quinoxaline
QAT	2-amino-3-thioquinoxaline
QDTA	Quinoxaline dithiazolyl
q^N	Spin density on N atom
r	Radius
s	Second; strong (IR peak descriptor)
S	Siemens
SOMO	Singly Occupied Molecular Orbital
T	Temperature
T_C	Curie temperature; superconducting transition temperature
T_{MI}	Metal-insulator transition temperature
T_N	Neel temperature
TAF	Tetrathiadiazafulvalene
TCNQ	Tetracyano-*p*-quinodimethane
TTF	Tetrathiafulvalene
TMTSF	Tetramethylselenafulvalene
Torr	Unit of pressure = mm Hg
V	Volt
w	Weak (IR peak descriptor)
x	Crystallographic axis
X	Halogen group

y	Crystallographic axis
z	Crystallographic axis
Z	Atomic number
α	Coulomb integral; crystallographic angle
β	Resonance integral; crystallographic angle
δ	Chemical shift in ppm
γ	Crystallographic angle
μ	Permeability; mobility
μ_o	Permeability in free space
Φ, ϕ	Wavefunction symbols
ρ	Density
σ	Electric Conductivity
χ	Magnetic susceptibility

LIST OF TABLES

LIST OF CAPTIONED FIGURES

LIST OF UNCAPTIONED FIGURES

I-1

I-2

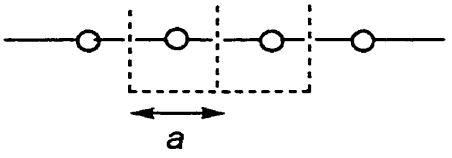

I-3

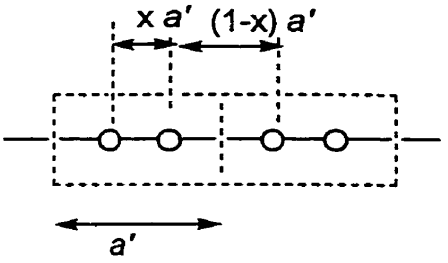

I-4

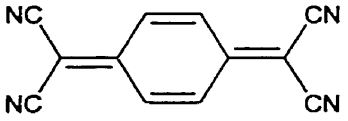

I-5

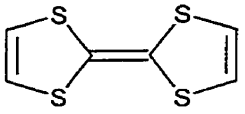

I-6

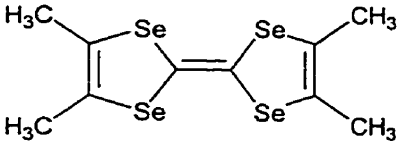

I-7

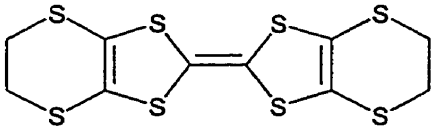

I-8

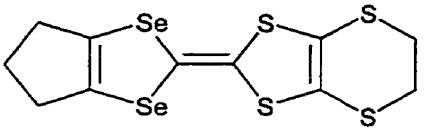

I-9

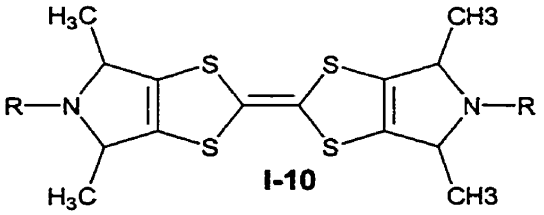

I-10

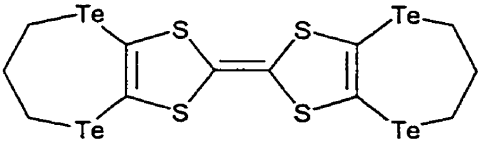

I-11

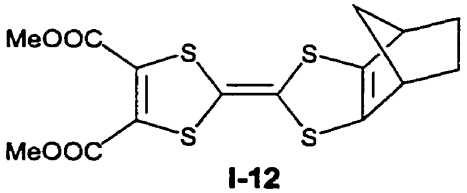

I-12

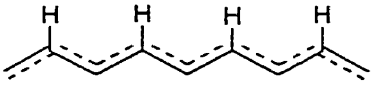

I-13

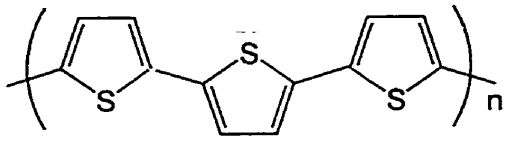

I-14

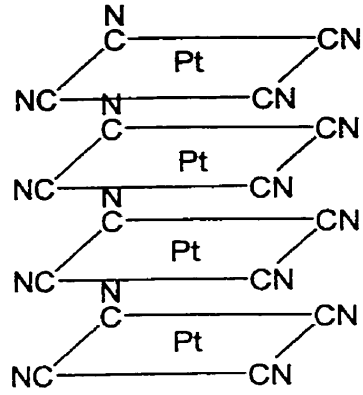

I-15

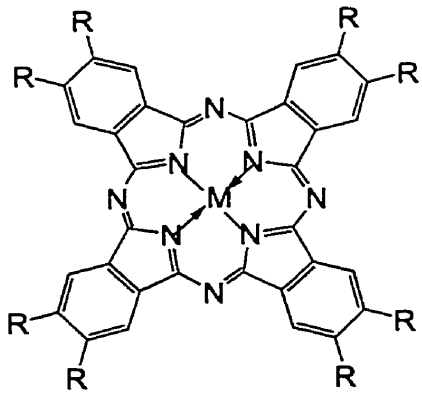

I-16

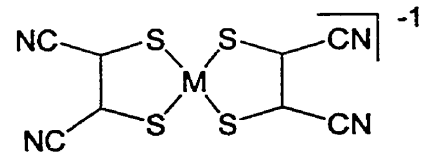

I-17

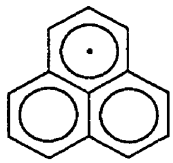

I-18

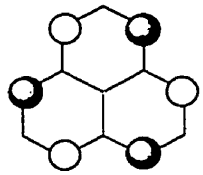

I-19

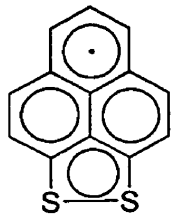

I-20

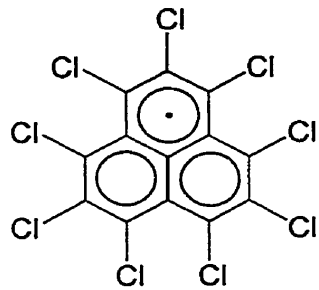

I-21

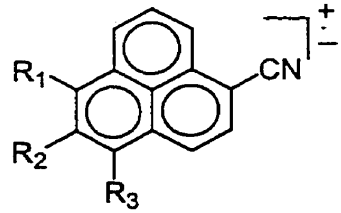

R_1, R_2, R_3 = CH_3O, CH_3S, H

I-22

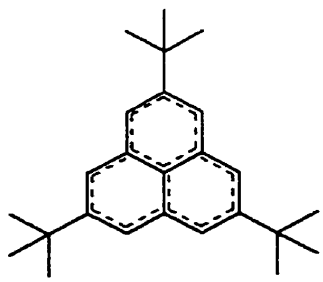

I-23

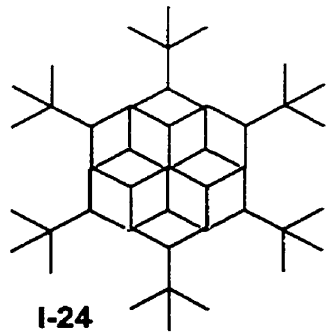

I-24

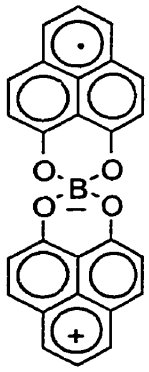

I-25

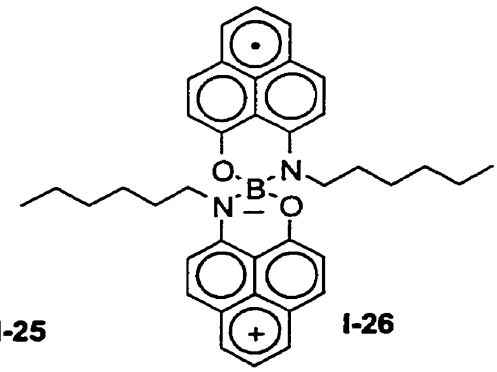

I-26

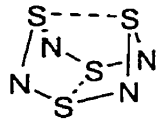

I-27

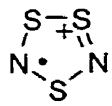

I-28

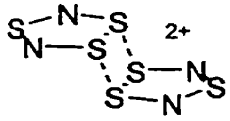

I-29

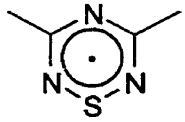

I-30

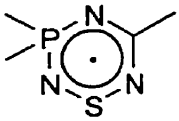

I-31

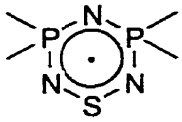

I-32

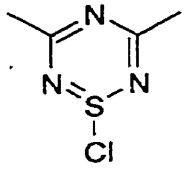

I-33

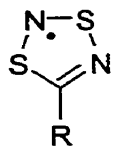

I-34

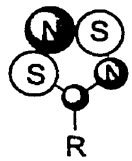

I-35

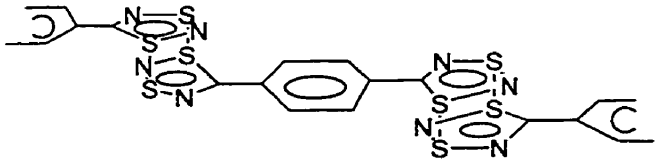

I-36

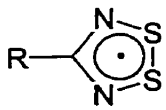

I-37

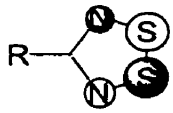

I-38

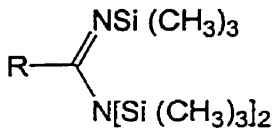

I-39

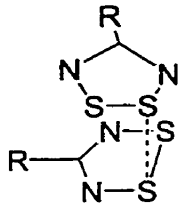

I-40

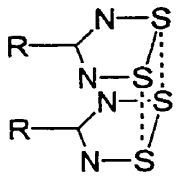

I-41

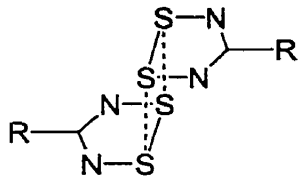

I-42

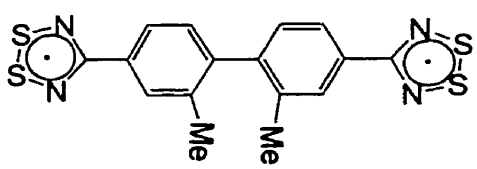

I-43

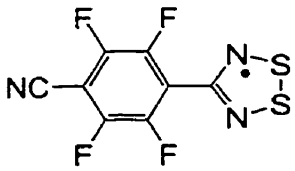

I-44

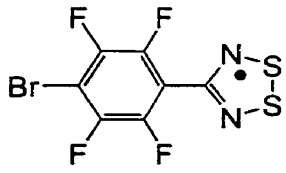

I-45

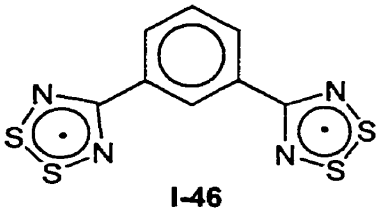

I-46

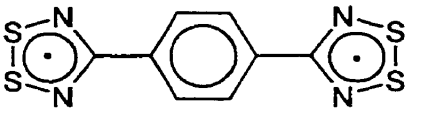

I-47

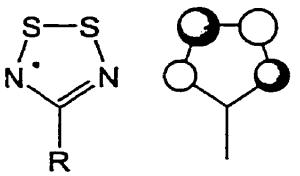

II-1

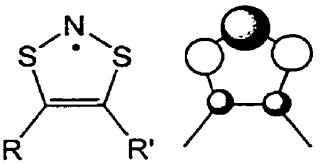

II-2

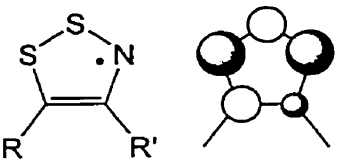

II-3

II-4

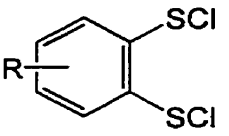

II-5

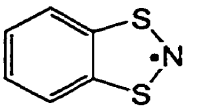

II-6

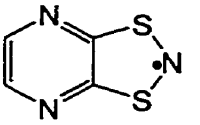

II-7

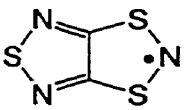

II-8

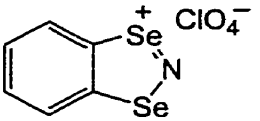

II-9

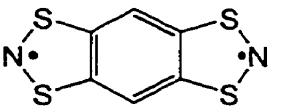

II-10

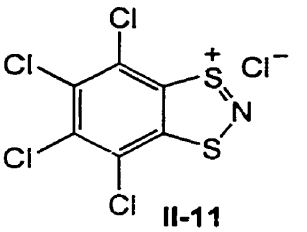

II-11

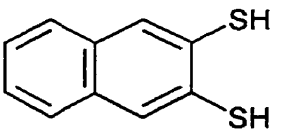

II-12

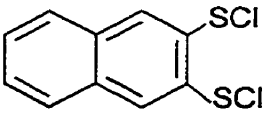

II-13

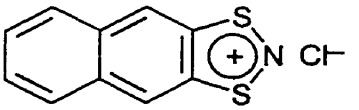

II-14

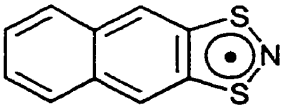

II-15

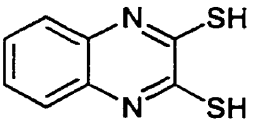

II-16

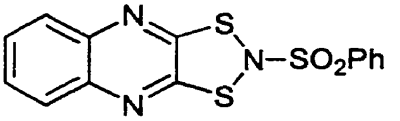

II-17

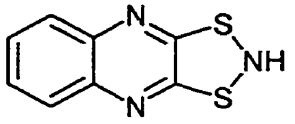

II-18

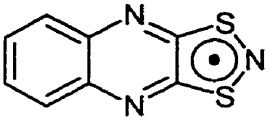

II-19

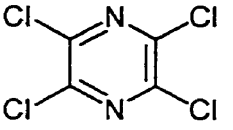

II-20

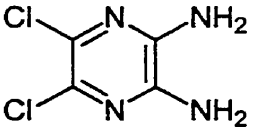

II-21

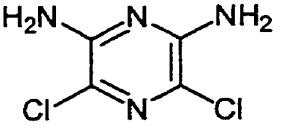

II-22

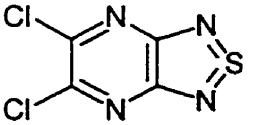

II-23

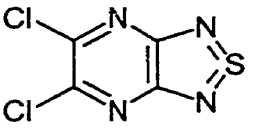

II-23

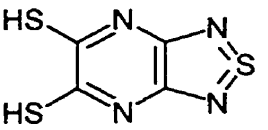

II-24

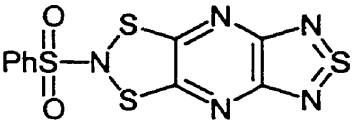

II-25

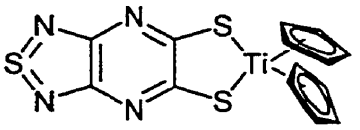

II-26

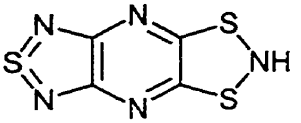

II-27

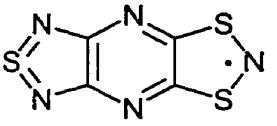

II-28

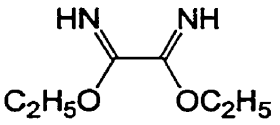

II-29

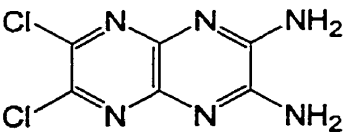

II-30

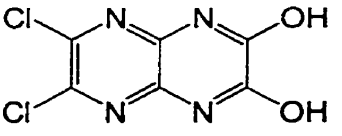

II-31

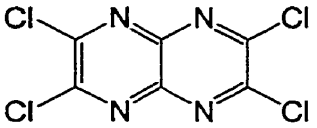

II-32

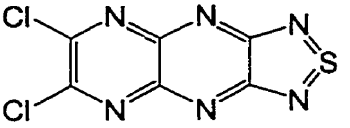

II-33

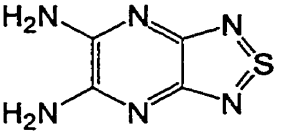

II-34

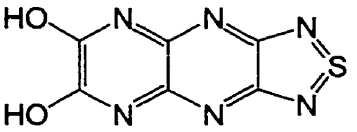

II-35

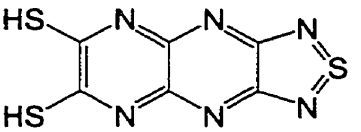

II-36

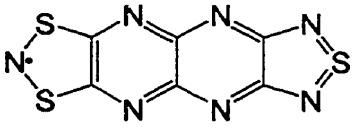

II-37

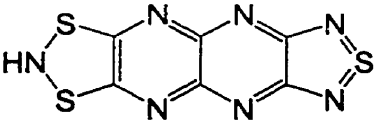

II-38

III-1

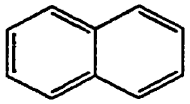

III-2

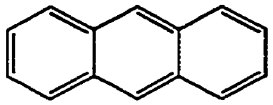

III-3

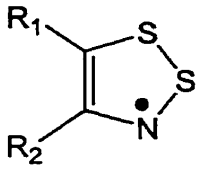

IV-1

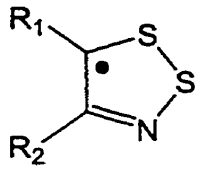

IV-2

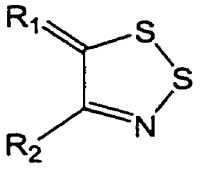

IV-3

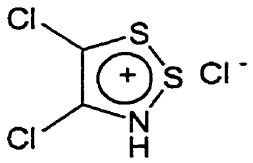

IV-4

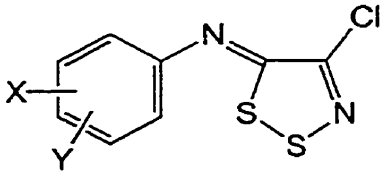

IV-5

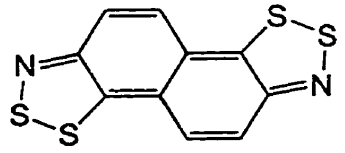

IV-6

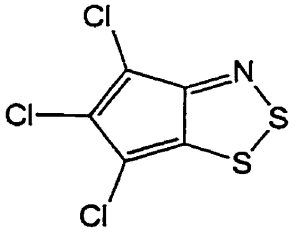

IV-7

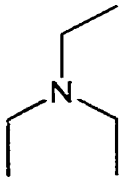

IV-8

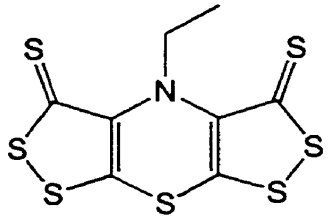

IV-9

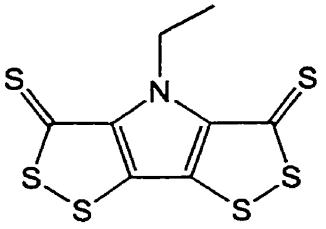

IV-10

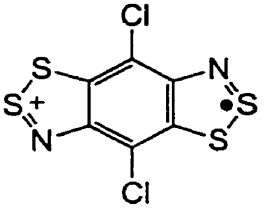

IV-11

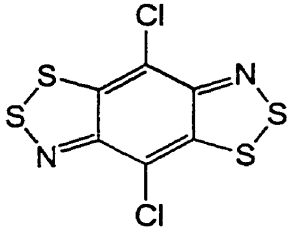

IV-12

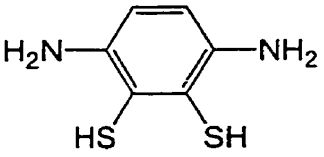

IV-13

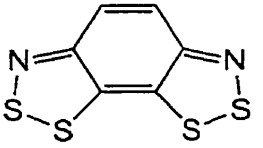

IV-14

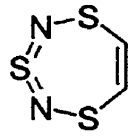

IV-15

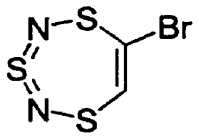

IV-16

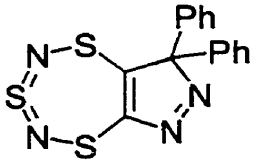

IV-17

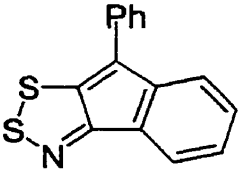

IV-18

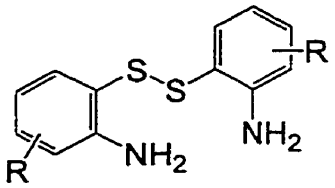

IV-19

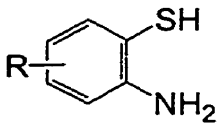

IV-20

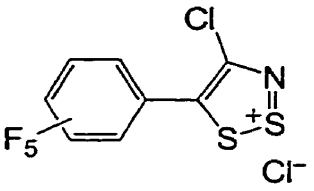

IV-21

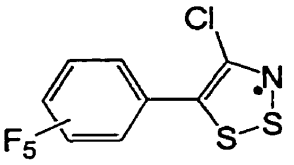

IV-22

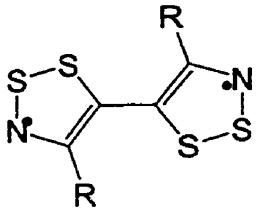

IV-23

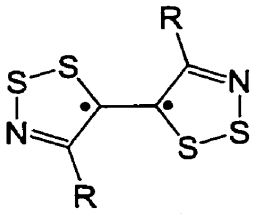

IV-24

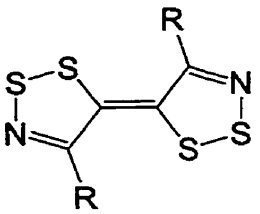

IV-25

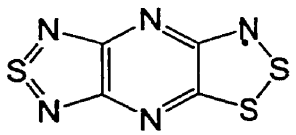

IV-26

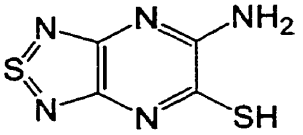

IV-27

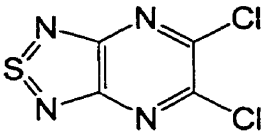

IV-28

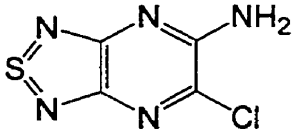

IV-29

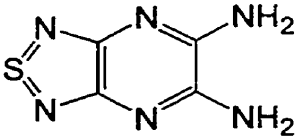

IV-30

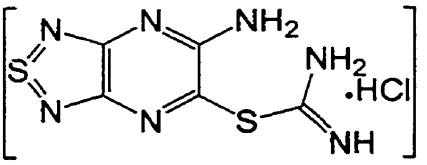

IV-31

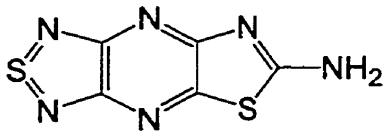

IV-32

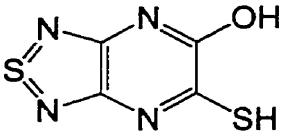

IV-33

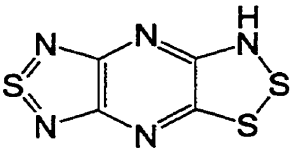

IV-34

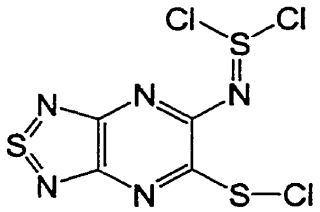

IV-35

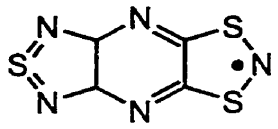

V-1

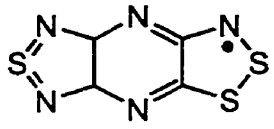

V-2

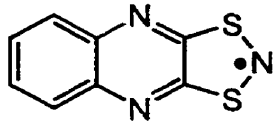

V-3

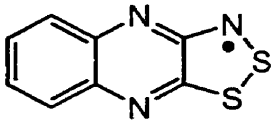

V-4

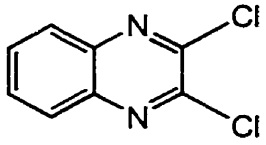

V-5

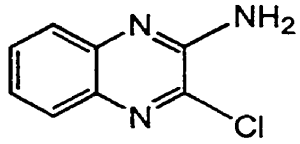

V-6

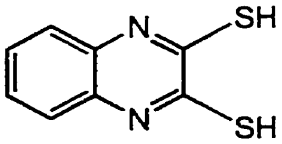

V-7

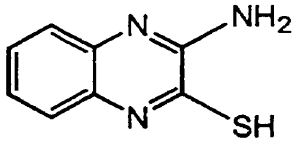

V-8 (QAT)

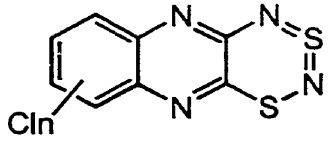

Cl_n-QDTDA (n = 1, 2)

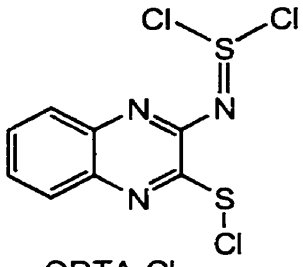

QDTA-Cl_3

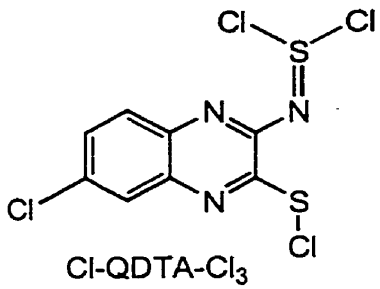

Cl-QDTA-Cl_3

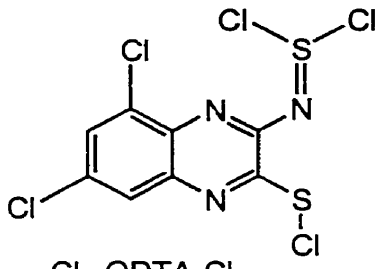

Cl_2-QDTA-Cl_3

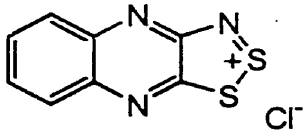

[QDTA][Cl]

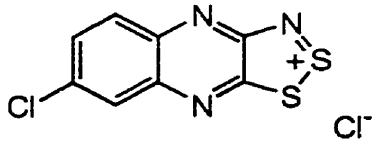

[Cl-QDTA][Cl]

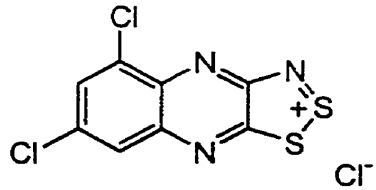

[Cl_2-QDTA][Cl]

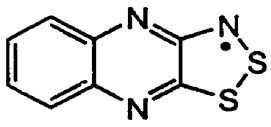

QDTA

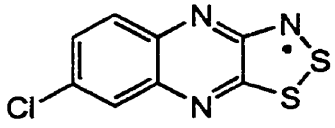

Cl-QDTA

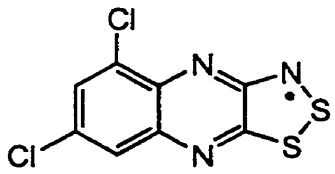

Cl_2-QDTA

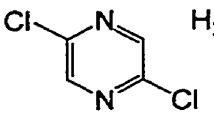

VI-1

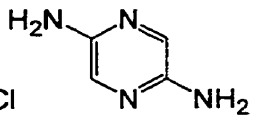

VI-2

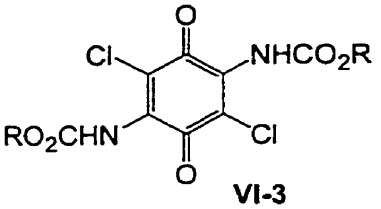

VI-3

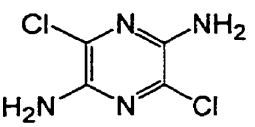

VI-5

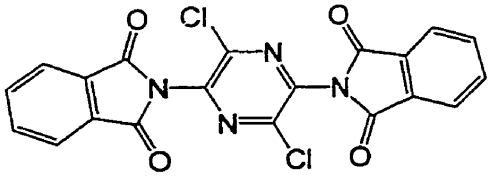

VI-4

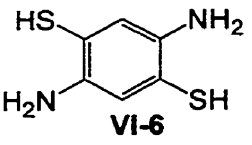

VI-6

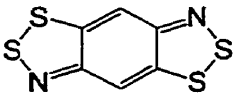

VI-7

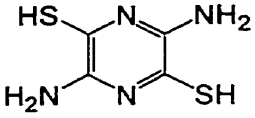

VI-8

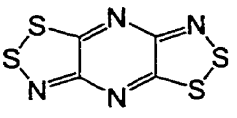

VI-9

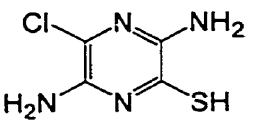

VI-10

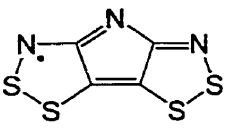

VI-11

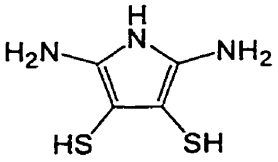

VI-12

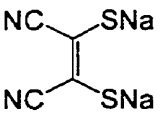

VI-13

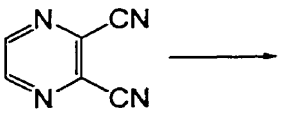

VI-14

VI-15

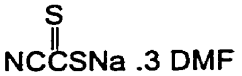

VI-16

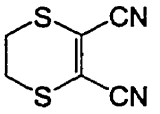

VI-17

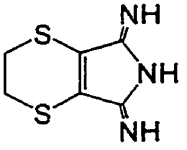

VI-18

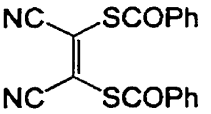

VI-19

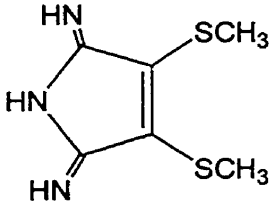

VI-20

VI-21

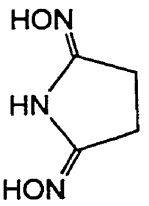

VI-22

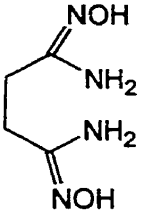

VI-23

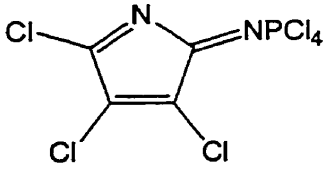

VI-24

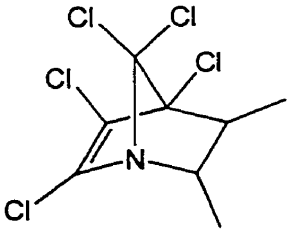

VI-25

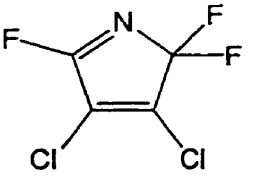

VI-26

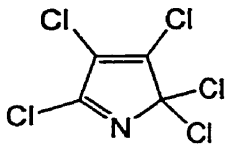

VI-27

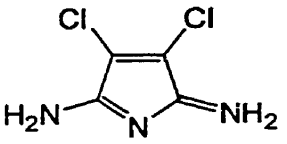

VI-28

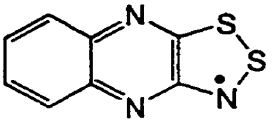

VI-29

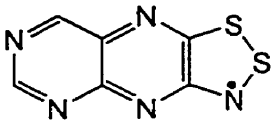

VI-30

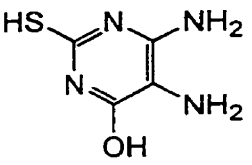

VI-31

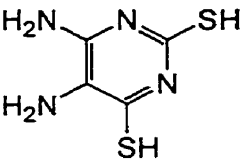

VI-32

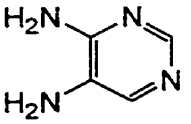

VI-33

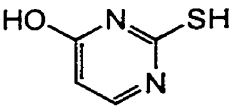

VI-34

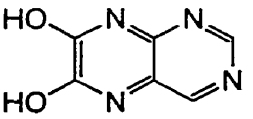

VI-35

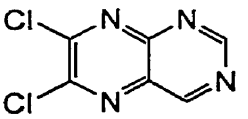

VI-36

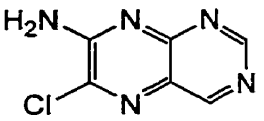

VI-37

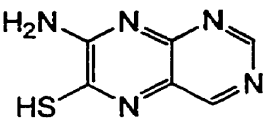

VI-38

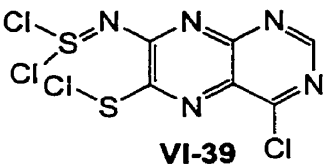

VI-39

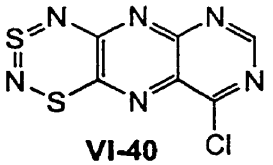

VI-40

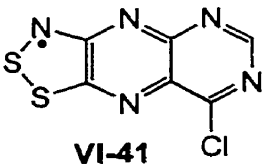

VI-41

Chapter 1 Introduction

Materials science, a hybrid discipline that lies at the interface of physics, chemistry, biology and engineering, has rapidly gained both momentum and recognition in the past three decades. Organic compounds which possess unusual electronic, magnetic and optical properties have been a major focus of research in this area. However, compared to traditional inorganic materials, which have long been used in a variety of applications, organic materials have some inherent disadvantages. Most, for example, have a relatively low melting and/or decomposition point, which restricts their use in high temperature applications. Also, most organic materials are composed of strong localized bonds between carbon and other non-metal elements; these compounds are insulators.

These drawbacks notwithstanding, numerous organic compounds are being synthesized with novel properties. Bearing in mind that the number of organic compounds is immense, there are almost unlimited ways to design and fine tune molecular and bulk properties by changing molecular composition, functionality and structure. Intense effort is now being directed towards the synthesis, characterization and property determination of these materials. A broad knowledge base and a wide range of demanding experimental techniques are required to carry out such research.

This thesis addresses the design and synthesis of a new class of organic solid state conductors based on the use of neutral molecular radicals. Hereafter we will refer to these materials as Neutral Radical Conductors (NRCs). The issues to be covered in the thesis span the evaluation and selection of molecular targets to their preparation and characterization. Inasmuch as the driving force behind this work is related to the electronic structure of

molecular solids, the first section (**1.1**) of this introductory chapter will be used to describe the basics of molecular orbital (MO) theory, as it applies to both molecules and solids. In the course of work for this thesis , many *ab initio* level MO calculations have been carried out (using Gaussian 98), and the general concepts and terms described here will facilitate the understanding of these results. In the following section (**1.2**) a brief history of organic conductors based on charge transfer (CT) salts and polymers will be provided. The high conductivity and even superconductivity of some CT complexes still attracts a great deal of research today. Finally, section **1.3** is used to introduce the concept of a neutral radical conductor (NRC), which is distinct from a CT salt in that it is a single component material. In principle at least the advantage of NRCs is that they obviate the need for charge transfer to generate charge carriers - they are already open shell systems. The initial proposal for an NRC was put forward by Robert Haddon in 1975.[1] The model, as initially described, relied upon the use of odd-alternant hydrocarbons (OAHs), which were believed to enjoy low barriers to charge migration. More recently, and particularly in the Oakley group, attention has focused on the use of heterocyclic thiazyl radicals. As this thesis will show, these materials too can be designed to have good charge migration characteristics. They also enjoy a high degree of thermal stability.

1.1 Band theory and molecular modeling

In the course of designing new molecular materials, it is imperative to develop links between structure and property, both at the molecular and solid state level.[2] Chemists have to be in position to predict how a simple molecular modification will affect not only a molecular property, *e.g.*, ionization potential, but also a bulk property, *e.g.*, conductivity. To

this end molecular orbital theory provides a useful tool for establishing a "cause and effect" relationship. This section will thus provide a working framework, within the language of molecular orbital theory, for describing the electronic structures of both molecules and solids.

1.1.1 Molecular orbitals and energy bands

As a first step, consider the electronic structure of the dihydrogen molecule. Two hydrogen atom's 1s orbitals interact with each other to form two molecular orbitals. It is easy to extend this idea to a one-dimensional chain with large number of the evenly spaced hydrogen atoms. As the number of atoms goes to infinity, and given appropriate boundary conditions, the j^{th} molecular orbital wavefunction ψ_j and energy level E_j can be defined as:

$$\psi_j = \frac{1}{\sqrt{n}} \sum_{m=1}^{n} \exp\left(\frac{2\pi ijm}{n}\right) \Phi_m \qquad (1)$$

$$E_j = \alpha + 2\beta\cos\left(\frac{2\pi j}{n}\right) \qquad (2)$$

where ψ and ϕ represent the molecular and atomic wavefunctions, respectively; α and β are the coulomb and resonance integrals.

The orbital energies are symmetrically located about $E = \alpha$ and for odd-membered chains there is a central nonbonding orbital with the energy of α. The interesting result is that for an infinite one-dimensional chain, the energy level on the bottom is $E_1 = \alpha + 2\beta$, while at the top level $E_n = \alpha - 2\beta$. The energy difference between the highest and lowest levels, the so-called band width, is equal to 4β. In Eqn. 2, j takes all integral values from 0, ±1, ±2, $\pm n/2$. By introducing a new quantum number, the wave vector (k), the energy equation and wavefunctions can be rewritten as:

$$E_k = \alpha + 2\beta \cos(ka) \tag{3}$$

$$\psi_j = \frac{1}{\sqrt{n}} \sum_m \exp(ikma)\ \Phi_{r-m\ a} \tag{4}$$

where a is the unit cell length of the crystal (the H-H separation in a one-dimensional chain of hydrogens atoms) and $k = 2j\pi/na$ with the range of $-\pi/a < k < \pi/a$. At $k = 0$, $E_k = \alpha + 2\beta$, which corresponds to the bottom of the band (the most bonding orbital, **I-1**) while at $k = \pi/a$, $E_k = \alpha - 2\beta$ is the energy of the top of the band (the most anti-bonding orbital, **I-2**). As before the bandwidth equals to 4β. When k is in the range of $-\pi/a$ *and* π/a, the k-value are unique. If k is outside this range, no new wavefunction is obtained, rather the old ones are repeated. The range of unique k-values $(-\pi/a \leq k \leq \pi/a)$ is called the first Brillouin zone.

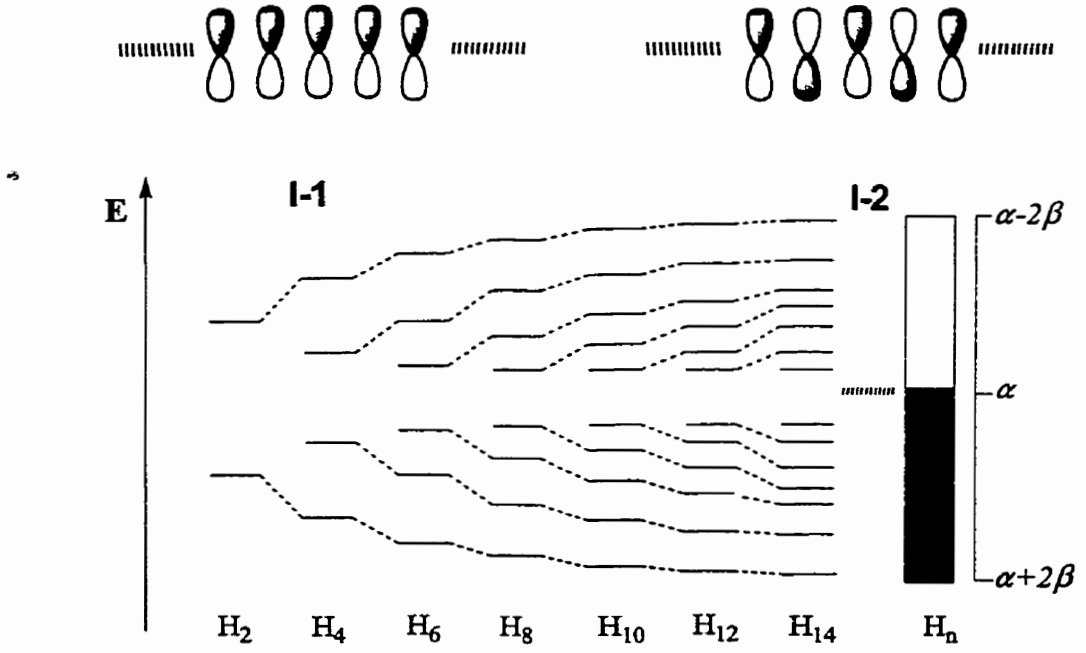

Figure 1.1 The relationship between the orbital energies and the length of a chain of N hydrogen atoms.

Figure 1.1 shows the relation between the energy levels and the length of the atom chain. As is illustrated in the figure, the spread of energy levels increases rapidly at first as the number of the atoms increases, then levels off (to a bandwidth of 4β) as n approaches infinity. The energy differences between adjacent energy levels are so small that they can be viewed as a continuum and treated conveniently as energy bands.

These energy bands can be portrayed in a number of ways. If, for example, one plots E *vs* wave vector k based on Eqn. 3, a symmetrical cosine curve is, of course, obtained. Most of the time, only half of this so-called dispersion curve (from $0 \leq k \leq \pi/a$) is shown (Figure 1.2(a)). Often it is also useful to define the number of states in a narrow range of energy. Values of Density of States, or DOS (Eqn. 5), are plotted as energy against number of levels at particular range of energy (Figure 1.2(b)). The great advantage of the DOS description of energy bands is that it can be experimentally determined by photoelectron spectroscopy.

$$\text{DOS}(E)\, dE = \text{number of levels between } E \text{ and } E + dE \qquad \textbf{(5)}$$

Energy bands, just like molecular orbitals, can be filled, partly filled or completely empty. The lower energy bands, which are made from the core and inner valence shell atomic orbitals, are all filled. Their spread is very narrow since there is no effective resonance interaction between these orbitals, they are basically atomic orbitals which have little impact on chemical or physical properties. Of more interest are the high lying occupied and low lying unoccupied molecular orbitals, as these will form the basis for the corresponding conduction band and valence band of the solid. Accordingly the Fermi level of a solid can be equated with the HOMO of a molecule.

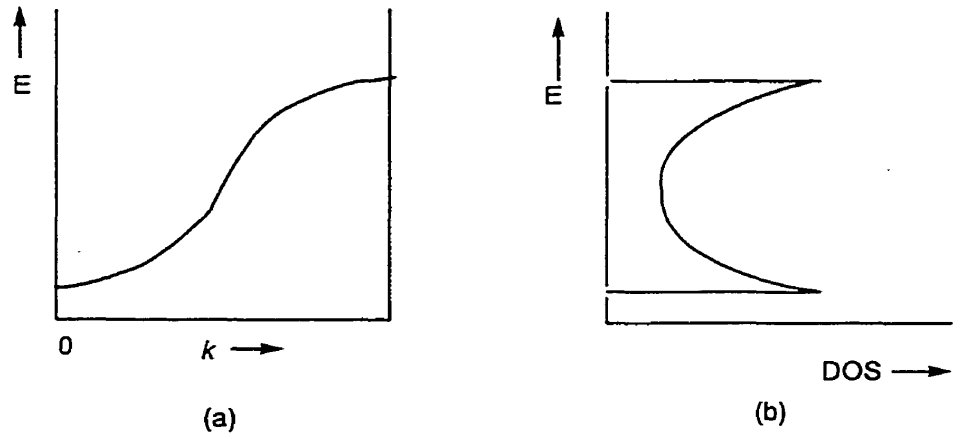

Figure 1.2 *E vs. k* dispersion curve (a). The corresponding DOS picture (b).

Thus far we have used a simple one-dimensional model to introduce a few important basic solid state terms. Since most real materials are two- or three-dimensional, we must extend our language. For the latter systems we must treat k as a vector with components in reciprocal space, and the Brillouin zone is now a two- or three- dimensional area or volume. Under these circumstances it is difficult to show the energy levels $E(k)$ for all k; it is also unnecessary. In the case of a two-dimensional system, for example, special values of k are given names: $\Gamma = (0, 0)$ is the zone center, $X = (\pi/a, 0) = (0, \pi/a)$ and $M = (\pi/a, \pi/a)$. Several such lines (Γ - X, Γ - M, X - Γ) will provide general band dispersion information. The corresponding DOS diagram represents the return to the real space, as an average over the Brillouin zone. The bandwidth in a DOS diagram inherently depends on contributions from all directions in k-space.

1.1.2 Jahn-Teller and Peierls Distortions

Molecular and solid state structures are susceptible to structural distortions. These issues, which collectively are referred to as Jahn-Teller effects in molecules and Peierls

instabilities in solids, are closely related. Both types of distortion originate from partially filled orbitals (or partial-filled energy bands).

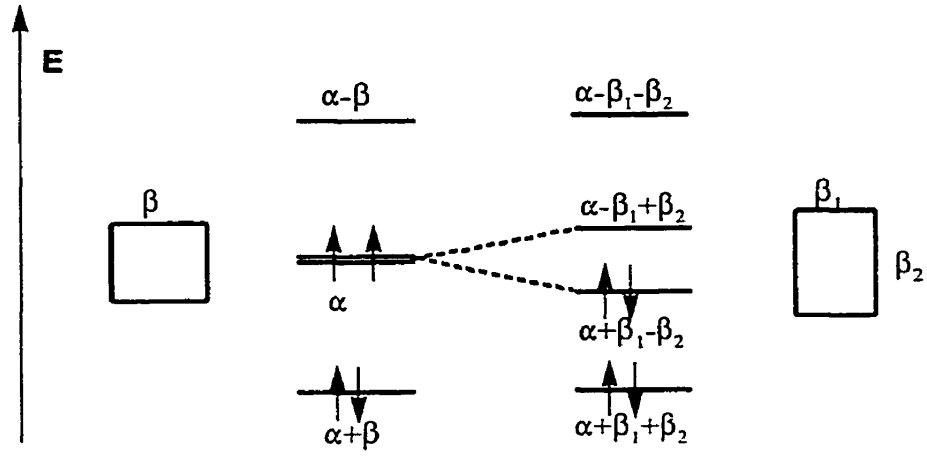

Figure 1.3 Hückel energies for the π molecular orbitals of cyclobutadiene on distortion.

A classic example of a molecular system which suffers from a pseudo first order Jahn Teller distortion is cyclobutadiene. For this molecule, the degeneracy of two highest filled π-levels (Figure 1.3) can be lifted by distortion of the ideal square geometry into a rectangular shape. This leads to a structure with alternating (long/short) bonds around the ring. As illustrated in Figure 1.3 the stabilization energy $\Delta E_T = 2\ (\beta_1 - \beta_2)$.

When we discuss one-dimensional solids, the analog of Jahn-Teller effect, the so-called Peierls distortion,[3] takes over. The structure of polyacetylene provides a convenient example. In the ideal situation (**I-3**), all the C---C bonds are equal and the π-orbitals in each (CH) unit form a half-filled energy band. The energies of the crystal orbitals can be expressed as $E_k = \alpha + 2\beta\cos(ka)$. If we now describe the same system with a new (doubled) unit cell repeat a' (**I-4**), we can still get same form for the energy expression, *i.e.*, $E = \alpha \pm 2\beta\cos(ka'/2)$, where $a' = 2a$.

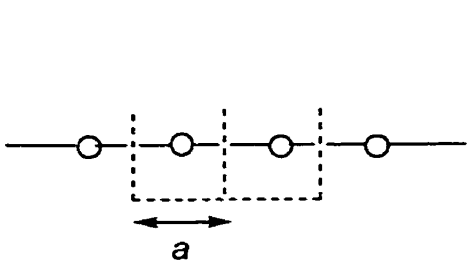

I-3

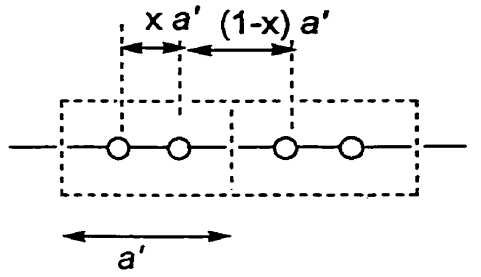

I-4

However if the structure is allowed to distort, such that the bond lengths become alternating (long/short), the interaction integral β is split into different β_1 *and* β_2 (as in the molecular case), and energies of the crystal orbitals are now expressed as:

$$E = \alpha \pm (\beta_1^2 + \beta_2^2 + 2\,\beta_1\,\beta_2 \cos ka')^{1/2} \qquad (6)$$

where at $k = 0$, $E = \alpha \pm (\beta_1 + \beta_2)$ and at $k = \pi/a'$, $E = \alpha \pm (\beta_1 - \beta_2)$. If $|\beta_1| > |\beta_2|$, the energy difference between the symmetric and distorted structure is $\beta_1 - \beta_2$. The DOS diagrams corresponding to the undistorted and distorted structures are shown in Figure 1.4. As can be seen the effect of the distortion is to open a gap at the Fermi level. For polyacetylene the band gap in the distorted structure is about 2 eV, [4] and conductivity is below the low limit of semiconductors.

A Peierls distortion is a characteristic of a one-dimensional electronic system. Some three dimensional solids, in which the electronic structure can be described in terms of three independent - and mutually orthogonal - sub-units, can also display Peierls instabilities. Examples include PbFCl [5] and black phosphorus.[6] Conversely, Peierls instabilities in one-dimensional structures can be suppressed by the incorporation of a degree of two dimensionality. A classic example of this effect is found in the structure of $(SN)_x$ polymer

which, on the basis of its electron count, should suffer from a structural distortion and, as a result, become an insulator. However, as will be shown in section **1.2.4**, interactions between adjacent chains leads to the development of a more two-dimensional structure, as result of which the polymer retains its metallic state.[7] Bechgaard salts (described in section **1.2.2**) also possess appreciable two-dimensional features, so that the structures resist distortions into insulating states.

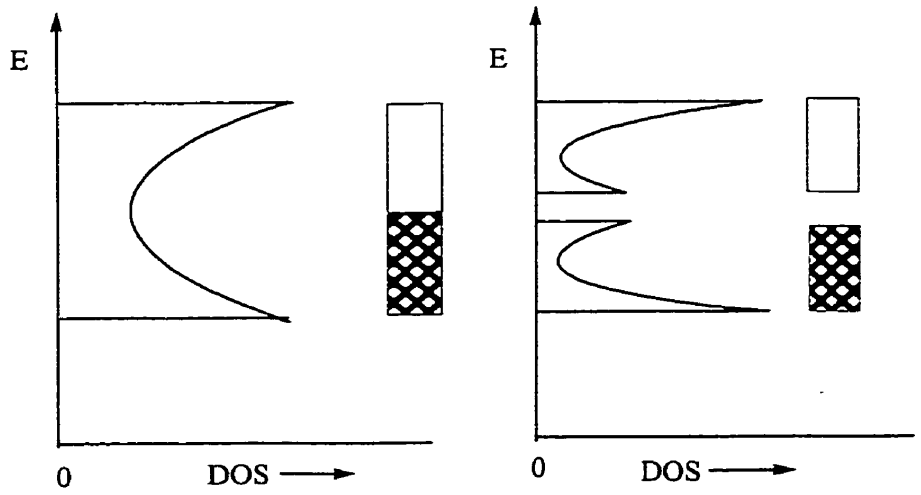

Figure 1.4 Effect of a Peierls distortion in the electronic energy bands of a 1-D system.

1.1.3 Electronic conductivity

One of the most important and interesting solid properties is electronic conductivity. The electronic conductivity, σ, of any material is defined by the expression:

$$\sigma = n\,Ze\,\mu \tag{7}$$

where n is the number of charge carriers per unit volume, Ze is their charge (in the case of

an electron only e is necessary) and μ is velocity of the charge carrier in the presence of an electric field, *i.e.*, its mobility. Band structure is often quoted to explain the magnitude of conductivities of solids. Thus a metal is a material with a partially filled energy band (Figure 1.5(a)), *i.e.*, no thermal activation is required to promote electrons from the valence to the conduction band. As a consequence, and with an applied electric field, electrons can move and generate the net flow of current.

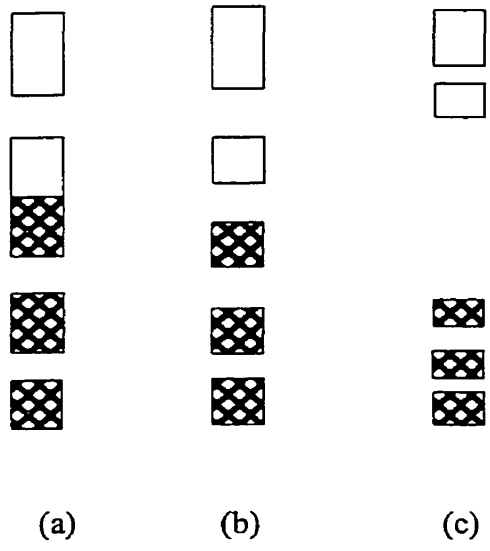

Figure 1.5 Schematic band structure of (a) a metal, (b) a semiconductor and (c) an insulator.

By contrast, the existence of a band gap (E_g) between the valence and conduction band requires that electrons be thermally excited in order to reach the conduction levels where they are free to migrate. With increasing temperature, more electrons are promoted to the conduction band and these activated electrons (along with the holes left in the valence band) can carry the current. The number of activated electrons, as a function of band gap and temperature, is given by the expression:

$$n \propto exp\ (-E_g/2kT) \qquad (8)$$

If the band gap is relatively small, the material is a semiconductor. A large band gap essentially confines the electrons to the valence band, and an insulating state prevails.

These various possibilities are conveniently illustrated with reference to the Group IV elements, all of which have a valence shell configuration ns^2np^2. The strong localized orbital interactions between the carbon atoms in diamond lead to covalent bonds with a large (σ-σ^*) band gap (Figure 1.5). Moving down the Group, larger atoms lead to weaker orbital interactions (a smaller σ-σ^* band gap); the observed band gaps fall accordingly.

	diamond	silicon	germanium	grey tin	lead
E_g(eV)	5.5	1.11	0.67	0.09	0

Thus, while diamond is a perfect insulator, silicon and germanium are important semiconductors, and grey tin and lead are metals at ambient temperatures.

While bulk conductivity in a solid requires that the atomic (or molecular) building block be open shell, so that the resulting solid state material can be described in terms of a partially filled energy band, fulfilment of this condition does not, by itself, guarantee a conductive state. When electrons in a solid move from one atom (or one molecule) to an adjacent one, current flows. However, if the coulombic barrier to charge transfer (U) is large, electrons will be localized. As will be discussed in subsequent chapters, this issue is at the heart of one of the most important problems encountered in the design of neutral radical conductors. As shown in Figure 1.6, if the distance between radical centers is too large, the band width (4β) of the resulting half-filled energy band is too narrow to overcome the charge

transfer barrier U, and the unpaired electrons are trapped on the radical centers, and do not contribute to conductivity. Such a material, in which $4\beta < U$, is referred to as a Mott insulator.[2d]

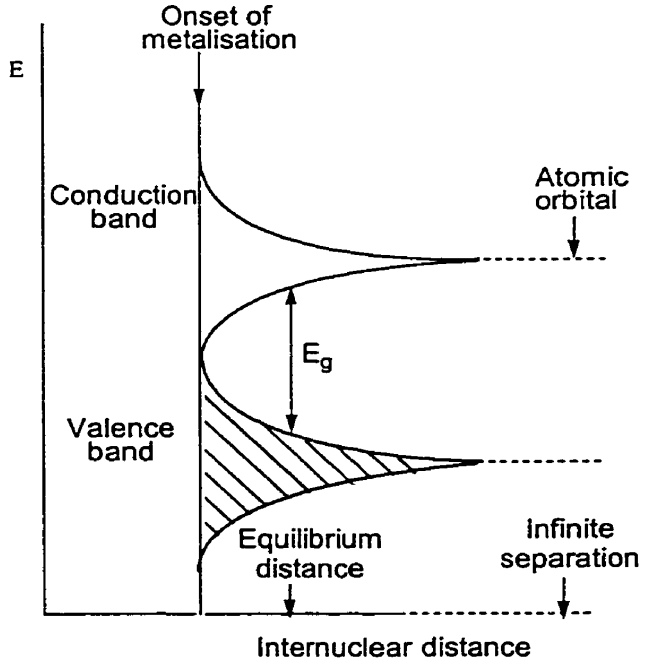

Figure 1.6 Schematic diagram showing band formation with decreasing internuclear distance. Decreasing internuclear distance leads to coalescence of the valence band and conduction band and the onset of metallization.

1.1.4 Magnetic behavior

Magnetism is another important property of both molecules and solids. In this thesis, which explores the synthesis and characterization of neutral radical conductors, solid state magnetic measurements have provided a critical insight into the degree of interaction between unpaired electrons on neighbouring radical centres. This section therefore provides a basic overview of magnetic phenomena. More detailed and advanced coverage may be found in various textbooks.[8]

1.1.4.1 Magnetism in solids

All materials acquire a dipole moment in the presence of the magnetic field $\boldsymbol{H}$; the response of the material is called as the magnetic induction, $\boldsymbol{B}$, or the magnetic flux density. The magnetization, $\boldsymbol{M}$, of the material is defined as the dipole moment per unit volume. The relationship between $\boldsymbol{B}$ and $\boldsymbol{H}$ can be expressed as:

$$\boldsymbol{B} = \mu_0 (\boldsymbol{H} + \boldsymbol{M}) \tag{9}$$

where μ_0 is a universal constant called the permeability of vacuum. In the SI system, μ_0 is defined as $4\pi \times 10^{-7}$ Henries per metre (H m^{-1}). The unit of $\boldsymbol{H}$ is ampères per metre (A/m) but it is often expressed in emu/cm^3, or 1000 A/m. $\boldsymbol{B}$ is represented in units of Vs/m^2 known as Tesla; $\boldsymbol{M}$ has the same units as $\boldsymbol{H}$. The magnetization of a material in general depends on the magnetic field acting on it. For many materials, $\boldsymbol{M}$ is proportional to $\boldsymbol{H}$:

$$\boldsymbol{M} = \chi \boldsymbol{H} \tag{10}$$

where χ, the magnetic susceptibility, is a property of the material and is dimensionless. Eqn. 10 can be rewritten as:

$$\boldsymbol{B} = \mu_0 (1 + \chi) \boldsymbol{H} = \mu_0 \mu \boldsymbol{H} \tag{11}$$

if we define $\mu = 1 + \chi$ and μ is the magnetic permeability. Either χ or μ can be used to characterize a material. In this thesis, χ is used almost exclusively.

1.1.4.2 Classification of materials by magnetic properties

Magnetic susceptibility χ is the most important magnetic property of a material. The value of χ can be either negative or positive; it can be much less or much greater than 1 for different materials. Closed shell molecules with all the electrons paired have no net magnetic moment. In the presence of the magnetic field, however, there is a weak induced

magnetization that opposes the direction of the applied field, with the result of the small negative diamagnetic susceptibility χ.

For all materials with positive magnetic susceptibility, at sufficiently high temperature, the susceptibility decreases with increasing temperature, and follows the so-called Curie-Weiss law (Eqn. 12):

$$\chi = \frac{C}{T \pm \theta} \tag{12}$$

C and θ are positive constants and characteristics of a material. If $\theta = 0$, the material is paramagnetic. Paramagnetism arises from atoms or molecules with unpaired electrons which results in a net magnetic moment in the molecules; χ decreases with increase in temperature since the alignment of the moments of the unpaired electrons becomes randomized at elevated temperatures. Based on statistical thermodynamics, the magnetic susceptibility χ can be expressed in terms of the Curie dependence (Eqn 13). However, in reality many paramagnetic materials follow the modified Curie-Weiss relationship (Eqn. 12).[7]

$$\chi = \frac{N\mu_0 m^2 H}{3kT} = \frac{C}{T} \tag{13}$$

There are several other types of magnetism, such as ferromagnetism, antiferromagnetism and ferrimagnetism, all of which are classes of bulk ordered magnetism. They are characterized by the sign and magnitude of the critical temperature θ (Eqn. 12). A classification of magnetic materials is provided in Table 1.1 and the diagram illustrating the variation of susceptibility for these classes is plotted in Figure 1.7. [7]

Table 1.1 The classification of materials by magnetic properties [7]

Class	Critical temperature	Magnitude χ	χ vs. T
Diamagnetic	None	-10^{-6} to -10^{-5}	Constant
Paramagnetic	None	10^{-5} to 10^{-3}	$\chi = C/T$
Ferromagnetic	Curie temperature θ_C	Large ($<\theta_C$)	Above θ_C, $\chi = C/(T-\theta)$ with $\theta \approx \theta_C$
Antiferromagnetic	Néel temperature, θ_N	Large ($<\theta_C$)	Above θ_N, $\chi \approx C/(T \pm \theta)$ with $\theta \neq \theta_N$; below θ_N, χ decreases, anisotropic
Ferrimagnetic	Curie temperature θ_C	10^{-5} to -10^{-3}	Above θ_C, $\chi \approx C/(T \pm \theta)$ with $\theta \neq \theta_C$

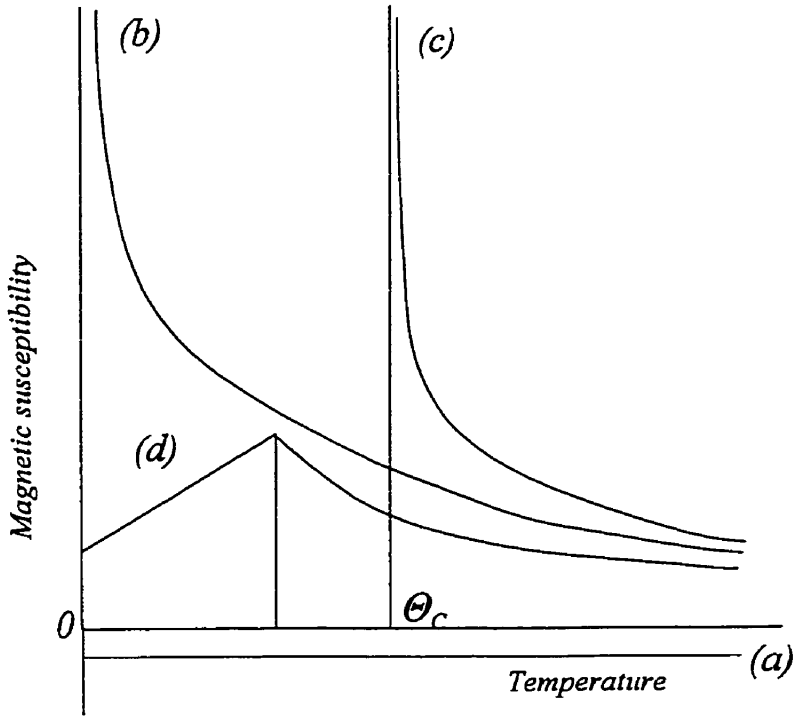

Figure 1.7 The variation of susceptibility with temperature for: (a) diamagnetic; (b) paramagnetic; (c) ferromagnetic (Curie-Weiss); (d) antiferromagnetic materials.

1.2 Organic charge transfer conductors

Most organic materials are inherently poor candidates for electrical conductors, since they are mainly composed of saturated carbon atoms bonded with other electronegative atoms. Electrons are bound tightly around these nuclei and therefore are not free to transport charge. However, it was predicted by McCoy and Moore [9] in 1919 that organic solids could be used as electrical conductors, but it was not until 1954 [10] that the first experimental verification was provided. The experiment involved the doping of perylene (resistivity, $\rho \cong 10^{14}$-10^{16} ohm·cm^{-1}) with bromine to produce a material with $\rho \cong 10$ ohm·cm^{-1}. Two decades later the first molecular crystal (TTF-TCNQ) exhibiting genuine metallic behavior was obtained, [11] and in 1979, the first organic superconductor (a Bechgaard salt) was discovered (with a T_C of 1-2 K under an applied pressure of 5 - 12 kbar).[12] Later on ambient pressure organic superconductors were also prepared.[13] During the past two decades, and inspired by the discovery of the famous $YBaCu_2O_{7-x}$ or "1-2-3" superconductor series,[14] much research has been directed towards new, high Tc organic superconductors. The most notable achievement in this area was the discovery of superconductivity in alkali metal doped fullerides, *e.g.*, K_3C_{60} .[15]

1.2.1 TTF-TCNQ

Most organic materials have closed-shell electronic structures, and in the solid state exhibit wide band (HOMO-LUMO) gaps. They are, in general, insulators or poor semiconductors. In order to induce a conducting state, the band gap should be narrowed or even quenched so that partly free electrons become available to contribute to conductivity. To fulfill this crucial requirement, closed-shell materials can be doped, either by the

injection of extra electrons into the conduction band (reduction) or holes into the valence band (oxidation). Either way the net effect is to produce partially filled electronic bands; electrons (or holes) in these bands will conduct.

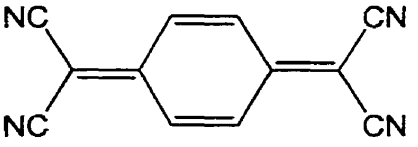

I-5

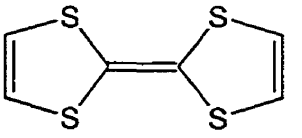

I-6

This concept is the design principle behind TTF-TCNQ type systems. Partial charge transfer between donor and acceptor systems creates two partially filled energy bands. In the 1960s, it was reported that many metal salts of 7,7,8,8-tetracyano-*p*-quinodimethane (TCNQ) **I-5** were semiconductors.[16] Viewed at the molecular level, TCNQ is a powerful electron acceptor (E_{red} = 0.15 V vs. SCE), in which four electron-withdrawing cyano groups are coupled effectively through resonant double bonds. The TCNQ radical anions in these metal salts form plate-like molecular stacks with extended π-electronic systems above and below the molecular plane. The electrons are delocalized and the conductivity is highly anisotropic, indicative of a lack of inter-stack interaction. These materials are thus referred to as one-dimensional conductors. Later on a variety of organic (as opposed to alkali metal) donors were explored to form charge transfer salts with TCNQ. The pivotal experiment involved the organic donor, **I-6**, tetrathiafulvalene (TTF) (E_{ox} = 0.2 V vs. SCE) synthesized by Wudl[17] *etal.* in 1970. Thus, when TTF and TCNQ were put together, the first real organic conductor [TTF][TCNQ] was born;[18] it exhibited a room temperature conductivity of 500 S cm^{-1}, a value which increased to as high as 10^4 S cm^{-1} at a temperature of 59 K.

The crystal structure of TTF-TCNQ consists of segregated stacks of TTF and TCNQ

molecules that interleave each other in a herringbone packing pattern (Figure 1.8). The conductivity is highly anisotropic along the stacks because of strong overlap of π-orbitals between adjacent molecules in stacks and weak interaction between the stacks.

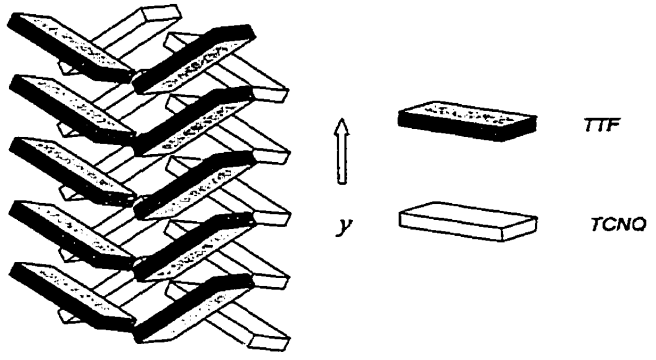

Figure 1.8 Solid state packing in TTF-TCNQ.

Researchers around the world rapidly embraced this new area of research, and generated a very large number of modifications in both the donor and acceptor components. This led to the discovery of systems with even higher conductivities. This period could be referred as the first golden age of CT conductors. For example, it was a natural progression to replace the sulfur atoms in TTF by larger selenium atoms,[19] to make a more powerful electron donating system (TSeF) and to improve intermolecular overlap in the solid state. [TSeF][TCNQ] shows the high room temperature conductivity (800 S cm^{-1}) and greater stability than the sulfur counterpart. The tellurium analogue of TTF-TCNQ provides even higher conductivity (2200 S cm^{-1}).[20]

Torrance[21] arranged donors and acceptors into four classes in terms of their conductivities and stoichiometries. Several important intermolecular effects and interactions were classified. He concluded that the materials with incomplete charge transfer (*i.e.*, $\rho < 1$,

where ρ denotes the degree of charge transfer.) may display high conductivities. By contrast for those systems where charge transfer is complete (*e.g.*, alkali metal salts of TCNQ) the conductivity is lower. In the case of TTF-TCNQ, the extent of charge transfer has been estimated (determined from X-ray and neutral diffraction experiments) [22] at $\rho = 0.59$, producing two partially filled energy bands, as illustrated in Figure 1.9. At the same time, Coulombic repulsion is diminished by strong π-interaction in the stacks. All these factors favor a metallic conductivity.

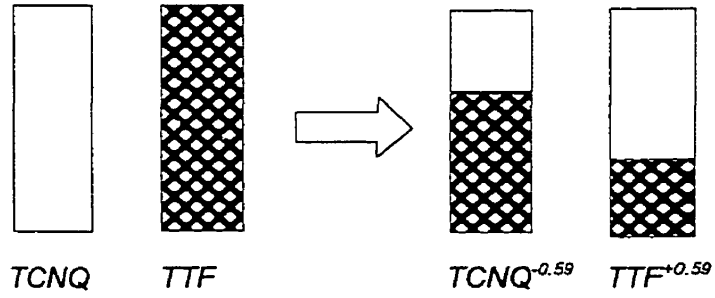

Figure 1.9 The schematic view of the incomplete charge transfer in TTF-TCNQ.

Torrance [23] also established the importance of balancing the ionization potential (IP) of the donor and electron affinity (EA) of the acceptor in order to obtain partial charge transfer. These concepts can be illustrated by reference to the charge transfer process shown in Eqn 1.14.

$$D^0 + TCNQ^0 \underset{IP - EA}{\overset{E_M}{\rightleftharpoons}} D^+ + TCNQ^- \qquad (14)$$

There are two factors that determine the equilibrium for this reaction. One is the lattice or Madelung energy E_M gained if the crystal is ionic. The second effect, which

counterbalances the first, is the molecular energy of charge transfer, equal to the difference (IP - EA). By measuring solution electrochemical potentials E_{ox} (donor) and E_{red} (acceptor), one can obtain an estimate of both IP and EA. Torrance demonstrated that many of the differences in the behavior of the charge-transfer solids can be comprehended in terms of electrochemical cell potential ΔE, where $\Delta E = E_{ox} - E_{red}$. For a given acceptor (TCNQ) he noted that donors with high (Na) or low (perylene) reduction potentials did not form good conductors with TCNQ; However, intermediate systems (such TTF) were very effective. Thus the working adage "a little charge transfer goes a long way" was born.

1.2.2 Bechgaard salts

After the discovery of the unusually high conductivity of TTF-TCNQ, numerous modifications were made to the basic TTF framework, one of which produced tetramethylselenafulvalene (TMTSF), **I-7**,[24] in which all of the sulfur atoms of TTF are replaced with selenium. The intent of this change was to increase the electronic interactions both within and between the molecular π-stacks; four methyl groups were added in order to produce some slippage in the stacks. In addition, the use of two organic components was simplified by the use of a simple inorganic counterion. This was initiated to remove the properties of the molecular acceptor species from the solid in order to focus on TMTSF itself.

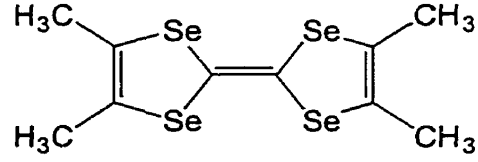

I-7

Bechgaard started the systematic studies on the salts of TMTSF and monovalent inorganic counter ions, such as PF_6^-, AsF_6^-, ReO_4^- and TaF_6^-. These salts were found to be superconductors under applied pressures (5 - 12 kbar). In 1981, $(TMTSF)_2ClO_4$ was discovered to be the first ambient pressure organic superconductor with a $T_c = 1.4$ K.[12] The early suggestions by Kraus [25] became reality after 60 years.

In comparison to TTF-TCNQ, which is basically a one-dimensional synthetic conductor with $\sigma_{\parallel}/\sigma_{\perp} > 10^4$, $(TMTSF)_2X$ showed appreciable two-dimensional behavior. All $(TMTSF)_2X$ compounds possess the same triclinic crystal structure at room temperature. As a representative of the whole series, the crystal structure of a Bechgaard salt ($X^- = PF_6^-$) is shown in Fig 1.10. The basic pattern is such that the nearly flat TMTSF molecules form zigzag stacking, parallel to the high conductivity x axis.[26] The stacks also contact each other through inter-stack Se - Se interactions which provide 2-dimensionality to this system. These extensive Se --- Se interactions form the infinite sheet network which stabilizes the metallic state with respect to the structural instabilities associated with 1-D structures.

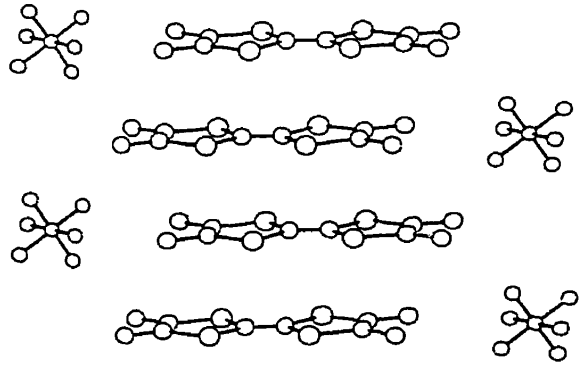

Figure 1.10 Stacking of TMTSF molecules in $(TMTSF)_2(PF_6)$ (hydrogen atoms omitted).

Bechgaard salts led to the second wave of searching for new synthetic conductors. A wide variety of inorganic counter ions could be used to form the salts with TMTSF molecules, and the relationship between different counter ions and the resulting structural and transport properties of salts was studied extensively.[12]

1.2.3 ET salts

Another important modification of TTF was the bis(ethylenedithio)-tetrathiafulvalene (BEDT-TTF) or "ET" system, **I-8**. This molecule was first reported by Mizuno[27] and because of the presence of eight sulfur atoms in the molecule, it is a remarkably effective electron donor. Electro-oxidation in the presence of the linear symmetric inorganic anions, such as I_3^-, IBr_2^-, AuI_2^-, provides the 2:1 stoichiometric (ET_2X) salts. These salts were discovered to be the first ambient pressure superconductors based on ET.[28] Many other monovalent anions have since been explored.[29]

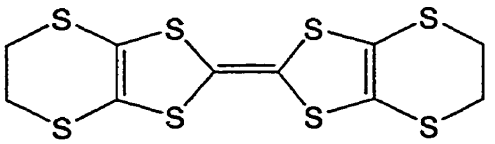

I-8

The crystals of ET salts are mainly prepared by electrochemical methods and, in contrast to Bechgaard salts, which have a common crystal structure, ET salts display a variety of packing patterns. In all of these the ET molecule is nearly planar over the central fulvalene portion, but exhibits large deviations from planarity ("ruffling") for the terminal ethylene dithio groups. In the structures of ET salts, lateral interactions become important and comparable in magnitude to the face-to-face interactions. As a result, corrugated sheet

networks of S---S interactions are formed.[30] In $(ET)_2 (ClO_4) (TCE)_{0.5}$, for example, the electrical resistivity shows only a small anisotropy ($\rho_\perp/\rho_{//} \simeq$ 1-2) within the conducting plane. This suggests a true two-dimensional electronic structure. Theoretical studies reveal that both intra- and inter-stack contacts contribute to the electrical properties and band structure.

Just as the modification of the TTF framework resulted in the discovery of Bechgaard salts, numerous variations of ET have been explored. For example, the complete or partial replacement of S atoms with other chalcogens, *i.e.*, selenium and tellurium, such as **I-9**, **I-10**, **I-11** has been achieved.[31, 32]

In summary, the discovery of TTF-TCNQ has led to extensive research on several generations of TTF analogues, and these materials continue to hold the spotlight in the organic synthetic metal arena. Variations in strategy are numerous.[33] For example, compounds such as **I-11, I-12,** which are electron donors or the combination of donor and acceptor, have been investigated.[34] The radical cation of **I-9** was claimed showing ambient pressure superconductivity.[35] A new series of pyrrole based TTF derivatives **I-10** has recently been pursued.[36] TTF has also been inserted to polymers and later connected with C_{60}, C_{70}.[37]

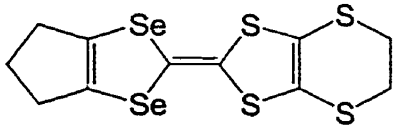

I-9

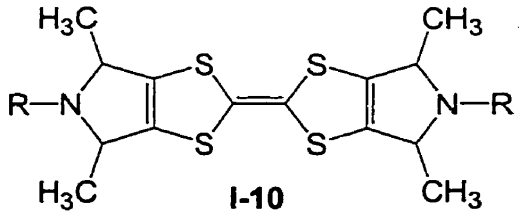

I-10

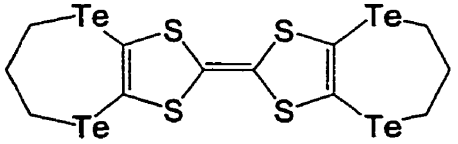

I-11

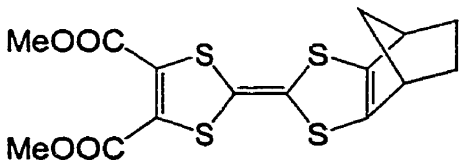

I-12

1.2.4 Organic conducting polymers

Work on organic conducting polymers goes back to the benchmark work of Shirakawa and Ito in the early 1970's.[38] They found that polyacetylene $(CH)_x$ **I-13** could be prepared as films with metallic lustre and that the conductivity of these films could be increased by 13 orders of magnitude by suitable doping.[39] In 1990, Tsukamoto[40] achieved a conductivity of 10^5 S cm^{-1} for doped **I-13**. These conductivities are comparable to the best elemental metal conductors.

I-13

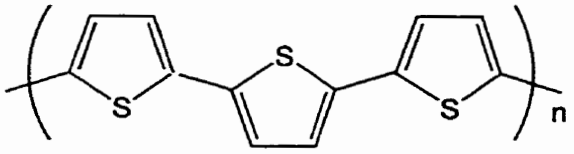

I-14

Charges doped into the polymer are stored in states such as solitons, polarons, and bipolarons, which include a charge and a lattice distortion that surrounds it. Theoretical calculations and experimental work have stressed the importance of interchain interactions and the need for three-dimensionality of the electron states in order to avoid one-dimensional localization. Indeed, there is evidence that the metallic states are three-dimensional, though the transport properties are highly anisotropic.[41]

Various dopants have been used with polyacetylene in order to increase the conductivities and many doping methods have been developed. In addition to a range of derivatives of $(CH)_x$, many aromatic polymers, such as polypyrrole, poly-(phenylacetylene), poly(p-phenylene sulfide) have been evaluated. Among them, the doped poly(thiophene), **I-14** attracts much interest as a result of its good stability toward oxygen, moisture and heat (stable to 250°C). The unique electroluminescent, field effect transistor (FET) and non-linear

optical properties of this latter material and its oligomeric counterparts make it a potential candidate in microelectronic and photonic devices.[42]

In addition to the organic conductor polymers discussed thus far, there are some inorganic polymeric conductors which deserve discussion. Foremost amongst these, especially from the perspective of this thesis, is $(SN)_x$ (Figure 1.11) prepared by the solid state polymerization of S_2N_2.[43, 44] This material is a metallic conductor at room temperature and becomes a superconductor at 0.26 K.[45] Similar to the charge transfer conductors discussed above, various donors and acceptors can be inserted to $(SN)_x$ chains. For example, bromine was found to increase the conductivity ten times at room temperature at the ratio of $(SNBr_{0.4})_x$.[46]

In $(SN)_x$ polymer each unit SN has three π-electrons, two of which occupy a π-bonding orbital while the third enters a π^* anti-bonding orbital. When a linear one-dimensional polymer is formed, a half-filled energy band results from the singly occupied π^* orbital. As pointed out by the X-ray determination,[6] the polymer chains are parallel with good close interchain contacts. The conductivity ratio ($\sigma_{\parallel}/\sigma_{\perp} \sim 15$ at 298 K) confirms significant orbital overlap between chains. As a result of these lateral interactions between the $(SN)_x$ chains the structure is resistant to a Peierls instability.

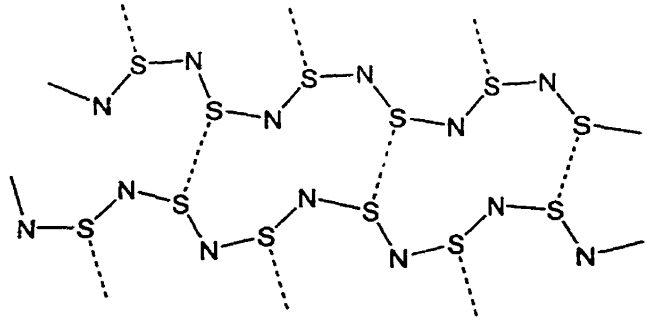

Figure 1.11 Schematic structure of $(SN)_x$, with interchain S---S contacts as dashed lines.

In addition to $(SN)_x$ there are a variety of concatenated metal polymers which can be doped into conductive states. For example, the so-called Krogmann salts[47] consist of partially oxidized tetracyanoplatinate (POTCP) salts **I-15**. The metal dithiolate complex, for example, **I-17**, $[M(S_2C_2R_2)2]^{n-}$ (M = Ni. Pd, Pt,Cu, Co, or Fe and R = CN, Me, H, CF_3 or C_4H_4.) also forms one-dimensional stacks. In both cases, the optimized conductivity along the *z* axis goes as high as 200 S cm^{-1}. This idea of using π-stacked metal containing rings has been extended to include metallomacrocyclic molecules[48] like **I-16**. Graphite intercalated compounds [49] have also received much attention.

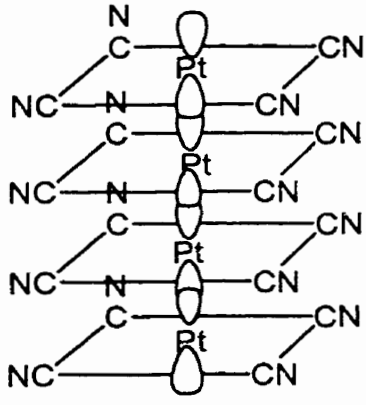

I-15

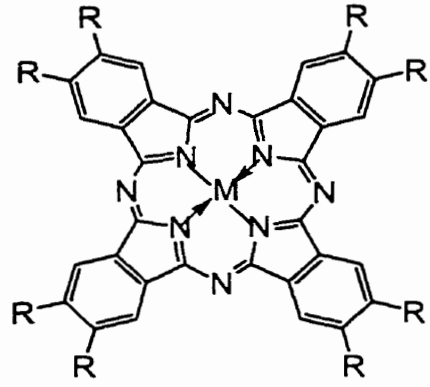

I-16

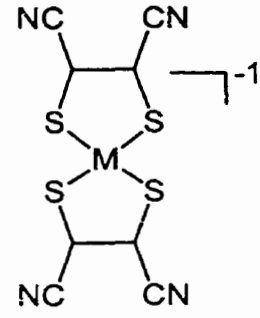

I-17

1.3 Neutral radicals, a new class of synthetic conductor

1.3.1 Introduction

In the materials discussed above, the building blocks whether molecular or polymeric, are closed shell species. The frontier electrons are paired to form the filled valence and empty conduction bands. Typically there are wide band gaps which serve as a barrier to charge transport, and the native (undoped) materials are insulators (a few fall in the semiconductor

region). In order to form highly conducting materials, both types need some doping process to generate partially filled bands, either by oxidation or reduction (p- or n-type doping). As an alternative to the charge transfer methodology the Oakley group has pursued the use of neutral radicals as building blocks for synthetic or "organic" conductors.

Neutral radical molecules are not closed shell; they have one unpaired electron at the frontier orbital level. In the solid state this gives rise to a half-filled energy band, which should provide a channel for electron transport. In a sense elemental metals can be considered to be neutral radical conductors. In the case of sodium, for example, the single valence shell 3s electrons form, in the solid state, a half-filled three-dimensional energy band; electrons move almost freely in any directions. At this level, neutral molecular radicals, just like metals, should be perfect candidates for an organic conductor. The built-in unpaired electrons makes any doping process unnecessary.

There is, however, a problem with the model, as outlined above. The body centered lattice of sodium gives rise to a stable, three-dimensional electronic structure. By contrast the solid state electronic structure of many organic π-radicals is highly anisotropic, almost one-dimensional in most cases, and this features gives rise to instabilities (Peierls distortions) which lead to the creation of a band gap at the Fermi level, and the formation of an insulating or semiconducting ground state.

These solid state issues aside, stable neutral radicals are not common. Indeed the word "radical" itself implies "extreme" and radical species (like $CH_3 \cdot$) are usually highly reactive, transient species. In the mid 1970's Griller and Ingold[50] suggested the use of the words "stable" and "persistent" to categorize various groups of radicals. Within this scheme there are several classes of radicals, which are *extremely* stable under ambient condition.

These include nitric oxide, nitroxides, nitronyl nitroxides, verdazyls, and some thiazyl heterocycles (see **1.4** section). In this thesis, we use the term "stable" radical to mean a material that can be separated and characterized in the solid state at or even above room temperature. The materials can also be stored indefinitely, in an inert atmosphere if necessary, without decomposition.

1.3.2 The phenalenyl radical; a perfect model with disadvantages

The idea of a synthetic conductor based on the use of a neutral radical was first proposed by Haddon in 1975.[1] Understanding the energetics of charge transfer in the solid state through such a system can be viewed, at the simplest level, in terms of the relative energies of the triad of oxidation states - cation, neutral radical, and anion - available to the molecular (radical) building blocks. Then, and now, Haddon has focused on a special class of neutral radicals known as Odd Alternate Hydrocarbons (OAHs), which possess a non-bonding SOMO (singly occupied molecular orbital). Because the SOMO is non-bonding, addition of an electron to such the orbital, to form an anion, or removal of an electron from it, to form a cation, should require a minimum structural reorganization, a feature which should facilitate charge transfer in the solid sate. Moreover, because they are neutral species, in the solid state, neutral radical stacks should prefer closer packing, thereby increasing interactions (and the resonance integral β) within and between stacks. All these factors favor large band widths and higher conductivity.

The Haddon model used the phenalenyl (PLY) radical, **I-18,** as a primary example of an OAH. As noted above, its SOMO **I-19** is non-bonding orbital, and the calculated disproportionation energy ΔH_{disp} for the reaction $2\ PLY^{\bullet} = PLY^{+} + PLY^{-}$ is 5.23 eV, a

value comparable to that found for 2 $TTF^{+\bullet} = TTF^{0} + TTF^{+2}$ (5.03 eV).[51] However, although the PLY radical can be observed by ESR spectroscopy in solution, and characterized electrochemically, it associates with C---C bond formation below -30°C in solution, to yield a diamagnetic dimer. Various modifications of the PLY framework have been explored, including, for example, 1,9-dithiophenalenyl **I-20** and perchlorophenalenyl, **I-21**. These radicals were characterized early on by ESR spectroscopy, but no structural results were obtained at the time.[52]

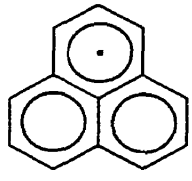

I-18

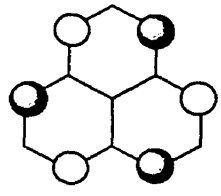

I-19

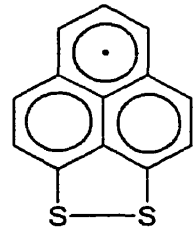

I-20

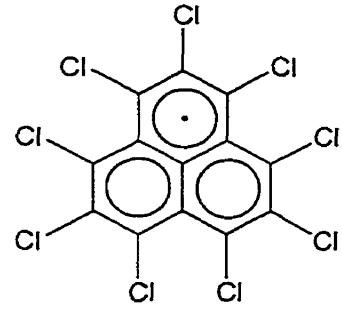

I-21

A few years later Nakasuji and coworkers[53] reported acceptor-PLY-donor systems, **I-22**. The use of methoxy or methylthio groups as the donors at the electronically active α position and cyano group as acceptors at the β position of PLY improved its redox properties. CV experiments showed a lower potential difference which suggested both cation and anion states interact with substituents. Although no solid state structure was available, the materials were characterized by ESR spectroscopy. In the solid state the material displayed a (pressed pellet) conductivity of 10^{-5} S/cm (at room temperature).

More recently the solid state structure and magnetism of the pentakis(isopropyl) cyclopentadienyl radical were reported. This was the first example of the neutral hydrocarbon radical to be characterized by X-ray crystallography. However, the steric protection afforded

by the five isopropyl groups, prevents interaction between the molecules. The molecules are essentially isolated, and too far apart to form an effective conduction band.

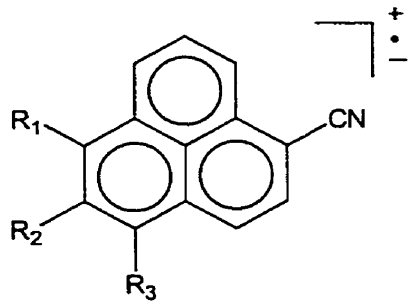

R_1, R_2, R_3 = CH_3O, CH_3S, H

I-22

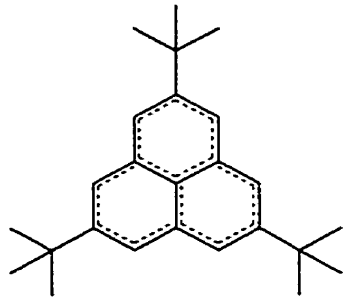

I-23

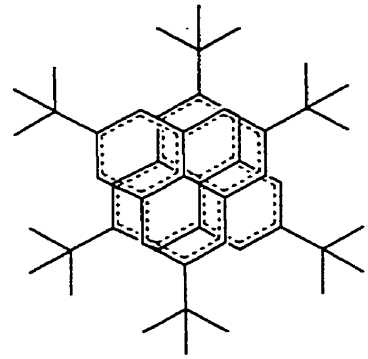

I-24

In an attempt to follow this steric protection route to prevent C-C bond formation in phenalenyl, the 2,5,8-tri-*tert*-butyl-phenalenyl radical, **I-23**, was recently prepared and its crystal structure was fully analyzed.[54] While single C--C bond formation is suppressed the radicals still associate - as centrosymmetric π-dimers (**I-24**) in which steric interactions between the *tert*-butyl groups is minimized. The bulk magnetic measurement discloses the strong bonding interaction in the radical dimers.

In order to avoid the dimerization problem, which is inherent with an exactly half-filled band, and also to help reduce the high coulombic barrier to charge transfer associated with this degree of band filling, the Haddon group has created[55] a modified PLY radical in which a boron atom is used to bridge two 9-oxidophenalenone units via a spiro-linkage, *i.e,* **I-25**.[56] ESR and cyclic voltammetry experiments on both **I-25** and the N-hexyl variant **I-26** show that PLY rings do not act independently but are quite strongly coupled. The unpaired electron is delocalized over the whole molecule.[57]

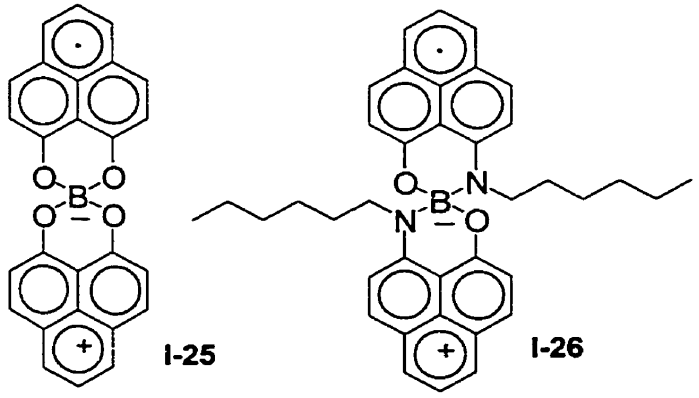

The oxidized N-hexyl salt $[\mathbf{I\text{-}26}]^{+}\ BPh_4^{-}$ salt can be reduced by cobaltocene in an H-cell. Diffusion of the solutions through the intervening glass frit gives rise to crystal nucleation, and long needle-like crystals, suitable for X-ray work can be obtained within a week. The most significant feature of the crystal structure of **I-26** (Figure 1.12) is the lack of intermolecular carbon-carbon dimerization, which is usually suppressed by employing the bulky substituents at the active positions of the phenalenyl nucleus. Apparently the radical molecules do not interact strongly, since the shortest distance between them is longer than van der Waals contacts. However, this material exhibits a room-temperature conductivity of $\sigma = 0.05$ S/cm which is the *highest yet observed* for any neutral radical conductor. The activation energy, E_a was calculated as 0.13 eV, which is very low value comparing to other radical systems.

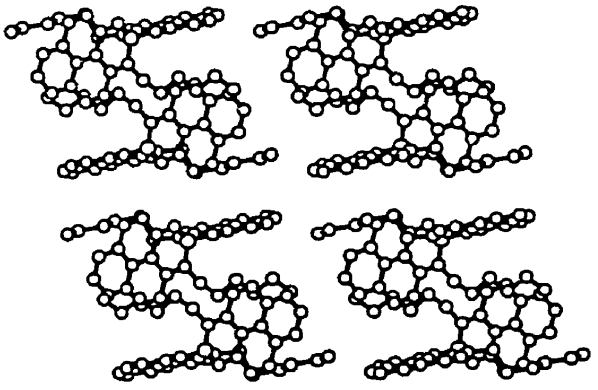

Figure 1.12 Crystal packing of **I-26** in the *xz* plane.

1.4 Heterocyclic thiazyl radicals

A wide range of binary cyclic and open chain thiazyl compounds is known; some examples are shown in Figure 1.13. Their basic chemistry was established in the first half of the 20th century, but it was not until the 1980's that the relationships between the chemistry and molecular and electronic structure of these systems were really established. The chemistry of binary thiazyl rings has been reviewed by Chivers and Oakley.[58] Thiazyl chain compounds and their properties have been reviewed by Rawson and Longridge[59] and Rees.[60]

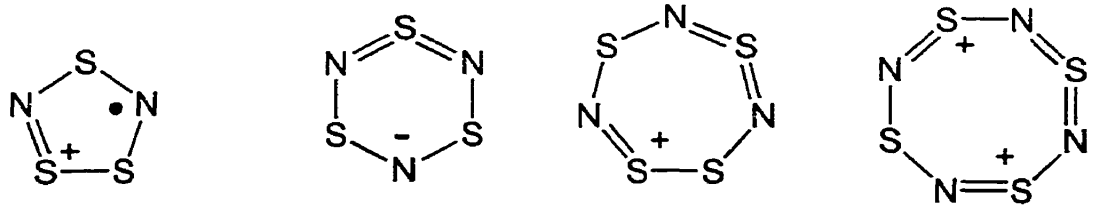

Figure 1.14 Some common cyclic thiazyl compounds.

In any cyclic S_xN_y system, each sulfur provides two electrons to a cyclically delocalized π-system, while nitrogen donates one, so thiazyl rings are electron-rich in comparison to unsaturated organic compounds. Ring systems with both $4n+2$ (aromatic) and $4n$ (anti-aromatic) electron counts have been characterized; the latter are prone to structural distortions. Thus the S_4N_4 molecule, **I-27**, perhaps the most well-known sulfur nitride, exists not as a 12π-electron ring but rather as a folded cage-like structure with two weak transannular S---S linkages of 2.576 and 2.586 Å at room temperature [61] and 2.595 and 2.590 Å at 120 K,[62] which are considerably longer than a single S---S bond (2.047Å in cyclo-S_8). The existence of a *stable* binary 7π-electron radical cation $S_3N_2^{+\cdot}$ **I-28** and its dimer $[S_3N_2]^{2+}$

I-29 was also established.[63]

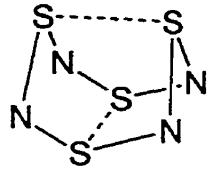

I-27

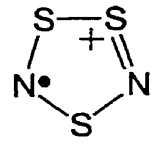

I-28

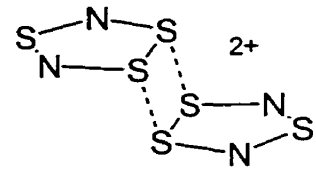

I-29

Starting in the late 1970's, researchers in Europe, U.S.A. and Canada started to explore the design of organic variants of binary SN rings, in the belief that ternary CSN rings would be more stable than their purely binary counterparts (most binary SN molecules are contact explosives). In particular neutral isoelectronic variations on the $S_3N_2^{+\cdot}$ radical cation were sought. Scheme 1.2 (below) shows some of the possibilities which were pursued.

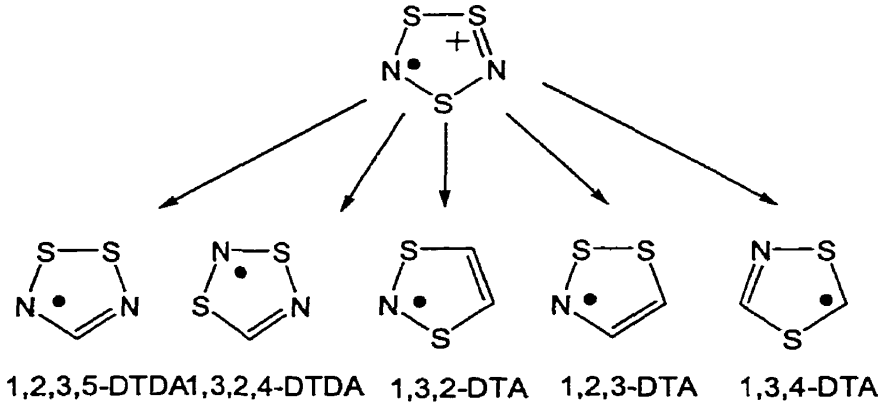

Scheme 1.2

In addition to these five-membered ring dithiazolyls (DTA's) and dithiadiazolyls (DTDA's), a variety of six-membered 7 π-electron thiatriazinyls (Scheme 1.3), containing both carbon and/or phosphorus, were investigated. Collectively these systems constitute the molecular building blocks on which all of the molecular materials used in this thesis are based. In the following subsections, and starting with the thiatriazinyls shown below, brief overviews of these radical systems are provided.

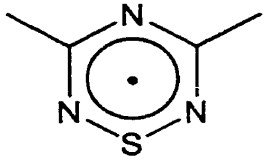

I-30

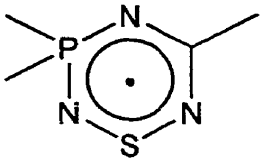

I-31

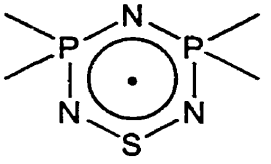

I-32

Scheme 1.3

1.4.1 1,2,4,6-thiatriazinyl radicals

Thiatriazinyls **I-30** are prepared through condensation of an imidoylamidine with sulfur dichloride, followed by reduction of the consequent thiatriazinium cation **I-33** with triphenylantimony.[64] Thiatriazinyl radicals are indefinitely stable in the absence of oxygen, and the crystal structure of the 3,5-diphenyl derivative (and its selenium variant) have been reported. In both cases the radicals dimerize through the chalcogen , with d(E---E) = 2.7Å (E = S) and 2.9Å (E = Se).[65]

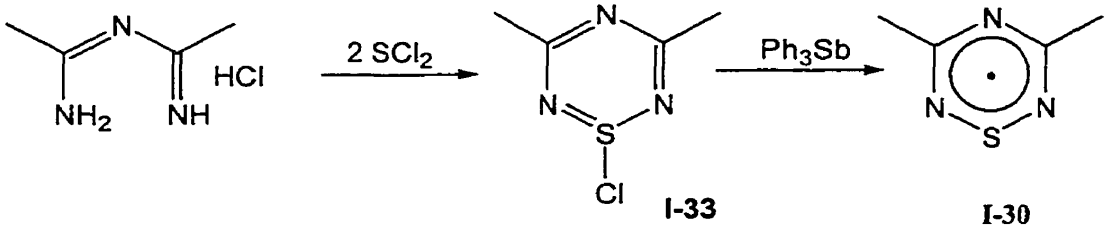

I-33 I-30

Scheme 1.4

The ESR spectra for both E = S and Se have been recorded.[66] The unpaired electron is delocalized over the whole ring with nearly equal hyperfine coupling to the three nitrogens. When the carbon atoms of the ring are partly (**I-31**) or completely (**I-32**) replaced by phosphorus atoms, the route for electron delocalization is blocked and the unpaired electron is confined on the NSN part of the ring.[67]

1.4.2 1,3,2,4-Dithiadiazolyl radicals (DTDA)

The favored synthetic route to 1,3,2,4-dithiadiazolyl radicals **I-34** involves the 4+2 cycloadditon of a nitrile and the S_2N^+ cation, to form the cyclic dithiadiazolylium cation. Subsequent reduction generates the corresponding radicals (Scheme 1.5).[68]

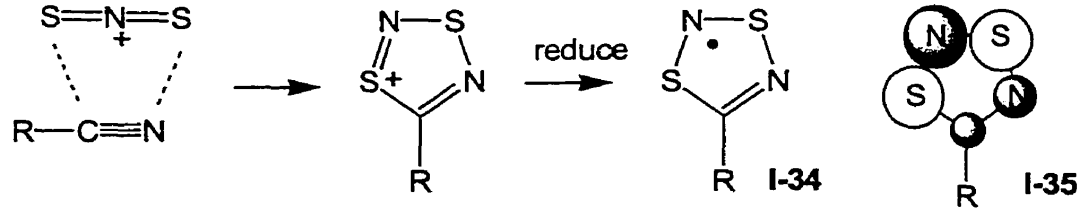

Scheme 1.5

Of the two possible dithiadiazolyl isomers (1,2,3,5- and 1,3,2,4), the latter is the less thermodynamically stable.[69] In solution 1,3,2,4-DTDAs easily convert to their 1,2,3,5-counterparts. The isomerization reaction has been interpreted in terms of the bimolecular mechanism illustrated in Figure 1.14. CNDO calculations[70] have suggested a photochemically allowed (thermally forbidden) process, and the reaction can certainly be activated photochemically.

Several 1,3,2,4-DTDA radicals, with different 5-substituents, have been synthesized. Their ESR spectra display similar features; the unpaired electron is confined to the SNS portion of the ring. The hyperfine coupling constants and the first ionization potentials change little with changes in the 5-substituents, an observation which can be understood in terms of the properties of its SOMO **I-35**.

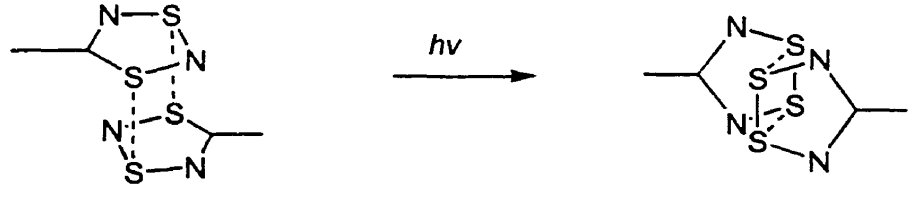

Figure 1.14 The proposed mechanism of the isomerization of 1,3,2,4-dithiadiazolyl radicals.

Due to the instability of these systems with respect to isomerization, only one example of this family, the 1,4-phenylene bridged diradical, has been successfully crystallized and analyzed by X-ray methods. The crystal structure reveals a staircase-like array of molecules linked by centrosymmetric DTDA dimers, *i.e.*, **I-36**.[71]

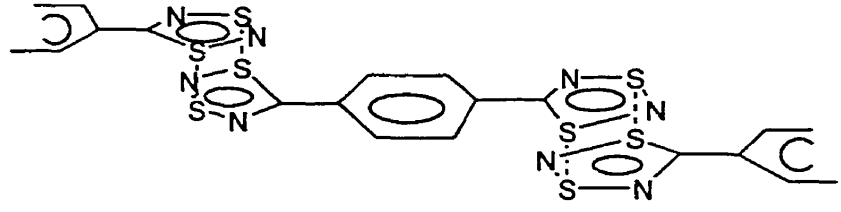

I-36

1.4.3 1,2,3,5-dithiadiazoyls

Since they are the more stable isomers, 1,2,4,5-dithiadiazoyl radicals **I-37** have attracted far greater synthetic attention. Generally, the preparation of 1,2,3,5-DTDA radicals involves the reduction of dithiadiazolylium cations. Such cations are usually generated through the reaction of protonated[72] or silylated amidine (**I-39**)[73,74] with sulfur dichloride (SCl_2). The corresponding diselenadiazolyl radicals can be made in a similar fashion when selenium dichloride is selected.[75] The formation of the dithiadiazolylium cations by the one-step reaction of $S_3N_3Cl_3$ with a nitrile has also been explored;[76] however, the reaction is complex and often affords lower yields (Scheme 1.6).

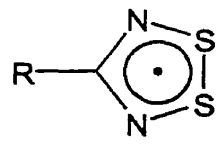

I-37

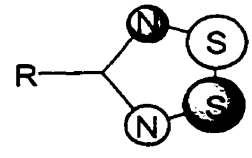

I-38

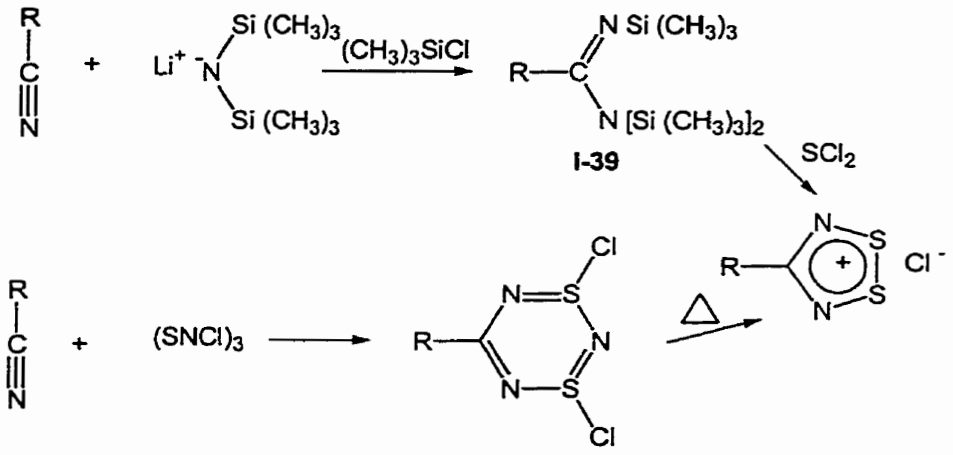

Scheme 1.6

The 1,2,3,5-DTDA radical ring **I-37** has a π-SOMO **I-38** in which the carbon atom resides on the nodal plane. Therefore any conjugate or resonant interactions of substituents on carbon contribute a negligible effect to the radical's electronic properties. All 1,2,3,5-DTDA derivatives possess similar ESR pattern with the intensity ratio of 1:2:3:2:1, which corresponds to coupling to two equivalent ^{14}N nuclei. The hyperfine coupling constants shows almost no effect of substituents.[77]

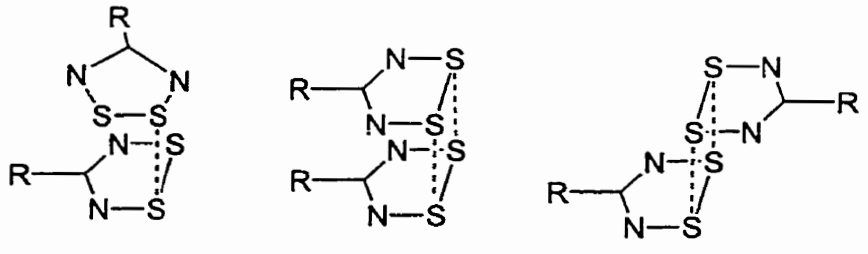

I-40 **I-41** **I-42**

Many 1,2,3,5-DTDA derivatives have been synthesized and crystallographically characterized. Most radicals dimerize in the solid state. The dimerization modes include twisted dimers (**I-40**) (R= CH_3, $N(CH_3)_2$) with one S---S connection,[78, 79] *cis* (**I-41**) and *trans* (**I-42**) co-facial dimers with all S atoms involved.[80] In the case of polyfunctional

systems, stacks with alternate long and short dimers may be formed.[81] When the bridging group become more sterically demanding, such as **I-43**, the big torsion angle of *ca.* 75° prevent any π stacking of the diradicals. One end of the molecule is dimerized in a head-to-tail fashion, while the other end remains completely unassociated.[82] By calculation (R = H)[83] the dimerization energy has been estimated in the order of 30 kJ /mol while the energy difference between different dimerization modes is quite small (around 5 kJ/mol).

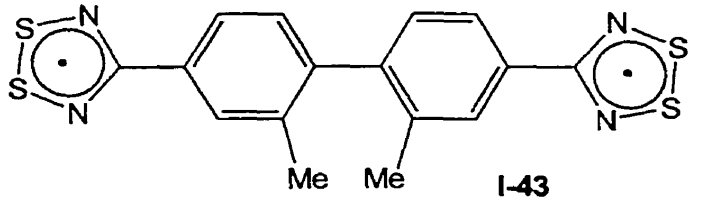

I-43

While the dominant tendency of 1,2,3,5-DTDA radicals is to associate, the solid state structure of the fluorinated 1,2,3,5-DTDA radical **I-44** consists of discrete radical molecules; a fortuitous combination of the fluorinated aromatic ring and the strong CN-S interaction effectively competes with the natural tendency to form spin-paired dimers. Two phases have been characterized. The β-phase has an effective moment of 1.55 μ_B (1.60 μ_B for α-phase) at room temperature and shows weak canted ferromagnetism at 36 K.[84]

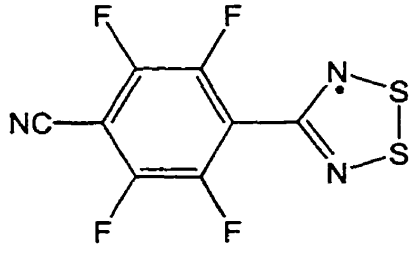

I-44

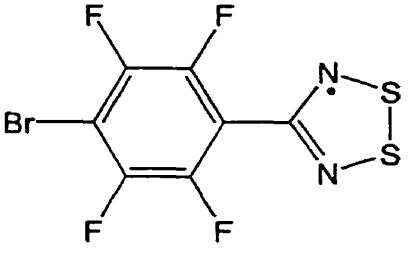

I-45

Dimerization is also suppressed when the cyano group in **I-44** is replaced by a bromine atom, as in **I-45** [85] Since the difference of electronegativity between Br and S is

much less than that of S and N (in CN), it was suggested that the interaction between Br and N of heterocyclic ring might determine the crystal packing, and the close in-plane contact leads to the retention of paramagnetism. The effective moment is measured to be 1.45 μ_B at room temperature. An undoped dithiadiazolyl radical having uniform stack in the solid state has also been reported,[86] but recent work in our laboratory has determined that this conclusion was the result of a crystallographic error.[87]

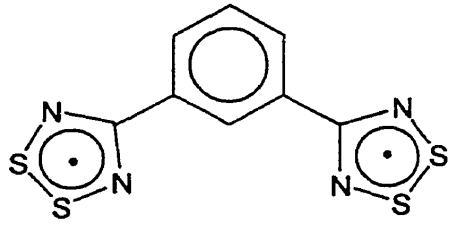

I-46

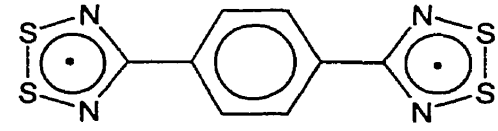

I-47

Dithiadiazolyl based diradicals and even triradicals have been explored. Actually, many different bridging elements have been considered and several targets successfully synthesized and crystallographically characterized. As examples, [1,3-S], **I-46** and [1,4-S] **I-47** adopt stacked dimer and herringbone dimer patterns in the solid state, respectively. The 1,3,5-benzene bridged triradical system crystallizes as girder-like stacks with a bond alternation pattern.[80 c] By contrast the 1,3,5-triazine bridged triradical does not form the desired columnar stacking.[88]

Compound **I-46** has tetragonal crystal structure that belongs to the space group $I4_1/a$. This consists of stacks of diradical molecules linked vertically in a zig-zag fashion through alternate ends by long S-S contacts (Figure 1.15, left). On the other hand, **I-47** belongs to the space group $P2_1/n$ and consists of herring-bone dimers (Figure 1.15, right). Transport measurements have shown that [1,4-S] **I-47** is essentially diamagnetic and an insulator

through all available pressures (0 - 26 k bar). Compound **I-46**, like its 1,4-counterpart, is a room temperature insulator at all available pressures (0 - 26 k bar), but single-crystal measurements give a conductivity of 1 x 10^{-7} S cm^{-1} in all directions at 470 K.[72]

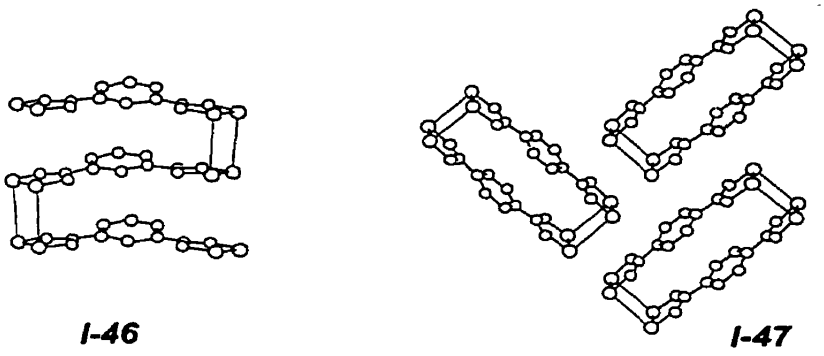

I-46 *I-47*

Figure 1.15 The packing structure of [1,3-S](left) and [1,4-S] (right). Stacked dimers and herring-bone dimers, respectively.

These large polyfunctional dithiadiazolyl radicals form air and thermally stable high density materials, with "tight" interdimer contacts. However, they are poor conductors. If selenium atoms are incorporated in this system, magnetic and conductivity data are consistent with thermally activated conduction, with band gaps of 0.5 - 1.5 eV.[80]

1.4.4 Doping of DTDA radicals

The conductivity of DTDA stacks can be improved by p-doping with halogens (typically iodine). The benefit is two-fold. First, partial oxidation of the radical stack moves the level of band-filling away from half-filled, so that the structure is no longer susceptible to dimerization (although other charge density wave distortions are possible). Secondly, and perhaps of greater importance, the coulombic barrier to charge transfer is reduced by shifting the level of filling away from the half-filled position. The effects of doping were first observed for the prototypal radical HCN_2S_2. Two crystal phases, triclinic and monoclinic,

were obtained based on different sublimation conditions. In both phases, dimer stacks are formed. The triclinic phase exhibits a unusual structural feature, with a near hexagonal cavity contained within a "cylinder" formed from six π-dimer stacks.[89] Doping of this structure by resublimation in the presence of iodine affords a rigorously hexagonal structure with uniform stacking (stack repeat distance = 3.35 Å). Iodine fills the columnar cavity, affording an overall stoichiometry of $[HCN_2S_2]_6[I]_{1.1}$. The dramatic change in structure leads to high conductivity. At room temperature, a pressed pellet measurement gives $\sigma = 10$ S/cm, which is eight orders of magnitude higher than that of the parent radical.[88]

Following on from this work doping experiments were performed on bifunctional DTDA radicals, including those shown above (**I-46, I-47**).[90, 91] By cosublimation of the sulfur radicals, charge transfer salts of general formula [diradical][I] could be obtained. These crystallize in orthorhombic or tetragonal space groups, and consist of columnar arrays of evenly spaced π-stacks interspersed by columns of disordered iodines. These doped materials display high, weakly metallic conductivity ($\sim 10^2$ S/cm) at room temperature, but all fall into insulating ground states around 200 K.

1.5 Objectives of the thesis

Electronic conduction is associated with a partially occupied energy band. All metals, be they elemental metals, metal oxides or organic charge transfer complexes, conform to this tenant. Within this context the premise of a neutral radical conductor (NRC) holds appeal. Unfortunately, a partially occupied one-dimensional energy band is inherently susceptible to Peierls distortion. As a consequence, a band gap is opened at the Fermi level and material will fall into an insulating or semiconducting state.

Figure 1.16 illustrates this issue graphically. Accordingly, a stacked column of π-radicals, should give rise to a half-filled energy band and a metallic ground state (case A). If the structure is one-dimensional, dimerization, *i.e.*, a Peierls instability, occurs, generating herringbone stacking (case C) or π-dimer stacks (case B). In both cases, a band gap is created at the Fermi level. Bifunctional DTDA radicals, **I-46** and **I-47** are perfect examples of types B and C.[72] Dimerization can be suppressed, and in later chapters examples will be provided, but if this suppression is accompanied by a loss in bandwidth, *i.e.*, a lack of interaction between neighbouring molecules, then the structure is frozen into a Mott insulator state - the unpaired electrons are isolated in the molecular plates. This state is illustrated by case D.

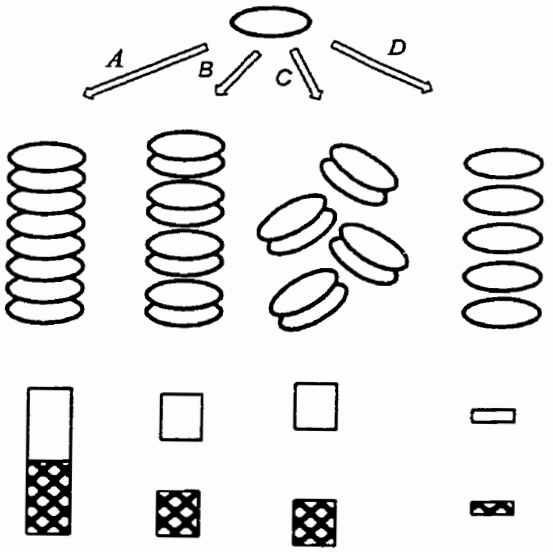

Figure 1.16 Packing patterns of neutral radicals and the corresponding band electronic structures.

To achieve the perfect structure with the perfect property (case A), several conditions must be met. Firstly the radicals must be thermally stable. 1,2,3,5-dithiadiazolyls (DTDAs) and their selenium counterparts certainly fulfil this condition. The nodal plane at carbon in

the radical SOMO makes the electronic structure of the radical relatively inert to substituent effects, so that trends in solid state arrangements can be, and have been, assessed without variations in the energetics of charge migration. However the inability to fine tune the energetics of charge transfer by chemical modification is also a serious design flaw, since without doping these materials are Mott insulators, *i.e.*, the barrier to charge transfer U is larger than the bandwidth 4β. In addition, the relatively localized nature of the SOMO DTDAs (the unpaired electron is confined to the 5-atom rings) leads to a dominance of dimerized structures.

In the mid to late 1990's, and after working on DTDA for several years, the Oakley group shifted the focus of its research towards the 7π dithiazolyl (1,3,2- and 1,2,3-DTA) systems (Scheme 1.2) as these possess relatively open - and more readily tunable - electron distributions. This thesis represents part of this general thrust. Work on the 1,3,2-variants, with different substituents in the 4,5-positions, is described in Chapter 2. Chapter 3 serves as an intellectual watershed. With the series of 1,3,2-dithiazolyl (DTA) radicals safely in hand, we carried out a series of computations on more ambitious model systems, based on both 1,3,2-DTA and 1,2,3-DTA frameworks, in order to identify target molecules with good charge transfer characteristics (a low U).

$$R + R = R^{+} + R^{-} \qquad U \approx \Delta H_{disp} = IP - EA \qquad (15)$$

The value of U can be equated, loosely, with the gas phase disproportionation energy of two radicals (Eqn 1.15), which is equal to the difference between the ionization potential (IP) and electronic affinity (EA). Molecular systems were therefore sought in which the difference (IP-EA) was a minimum. From this computational "interlude" we concluded that 1,2,3-DTAs were potentially more promising targets than 1,3,2-DTAs. They are, however,

the more difficult of the two DTA system to synthesize. We have nonetheless made progress, and Chapter 4 provides a benchmark study on one particular 1,2,3- system, one which has provided the best results - in terms of transport properties - ever found for a thiazyl based radical. Chapter 5 reports the synthesis and characterization of a whole family of derivatives based on 1,2,3-QDTA and finally, Chapter 6 provides results of ongoing work on variations on the 1,2,3-DTA theme.

1.5 References

1. (a) Haddon, R. C. *Nature*, **1975**, 256, 394. (b) Haddon, R. C. *Aust. J. Chem.*, **1975**, *28*, 2343.
2. The simple band theory section was mainly based on the following reference books. (a) Hoffmann, R. "*Solid and Surfaces, A Chemist's View of Bonding in Extended Structures*" VCH, **1988**. (b) Duffy, J. A., "*Bonding, Energy Levels & Bands in Inorganic Solids*" Longman Scientific & Technical, **1990**. (c) Smart, L.; Moore, E. "*Solid State Chemistry, An Introduction*" Second Ed. Chapman &Hall, **1996**. (d) Burdett, J. K. "*Chemical Bonding in Solids*" Oxford, **1995**.
3. R. F. Peierls, "Quantum Theory of Solids", Oxford Press: London, **1953**.
4. Kertész, M. *Adv. Quantum Chem.* **1982**, *15*, 161
5. Tremel, W.; Hoffmann, R. *J. Am. Chem. Soc.* **1987**, *109*, 124.
6. Burdett, J. K. *Progr. Sol. St. Chem.* **1984**, *15*, 173.
7. Cohen, M. J.; Garito, S. F.; Heeger, A. J.; MacDiarmid, A. G.; Mikulski, C. M.; Saran, M. S.; Kleppinger, J. *J. Am. Chem. Soc.* **1976**, *98*, 3844.
8. (a) Jakubovics, J. P. "*Magnetism and Magnetic Materials*", The Institute of Metals, **1987**. (b) Jiles, D. " *Introduction to Magnetism and Magnetic Materials*", Chapman and Hall, Suffolk, Great Britain, **1991**.

9. McCoy, H. H.; Moore, W. C. *J. Am. Chem. Soc.* **1911**, *33*, 1273.

10. Ahamatu, H.; Inokuchi, H.; Matsunaga, Y. *Nature*, **1954**, *173*, 168.

11. Ferraris, J.; Cowan, D. O.; Bloch, A. N. *J. Am. Chem. Soc.* **1973**, *95*, 948.

12. Bechgaard, K.; Carneiro, K.; Rasmussen, F. G.; Olsen, H.; Rindorf, G.; Jacobsen, C. S.; Pederson, H. J.; Scott, J. E. *J. Am. Chem. Soc.* **1981**, *103*, 2440.

13. Bechgaard, K.; Carneiro, K.; Eg, O.; Olsen, H.; Rasmussen, F. G.; Jacobsen, C. S; Rindorf, G. *Mol. Cryst. Liq. Cryst.* **1982**, *79*, 271.

14. Hor, P. H.; Meng, R. L.; Wang, Y. Q.; Gao, L; Huanh, Z. J.; Bechtold, J.; Forster, K.; Chu, C. W. *Phys. Rev. Lett.* **1987**, *58*, 1891.

15. Hebard, A. F.; Rosseinsky, M. J.; Haddon, R. C.; Murphy, D. W.; Glarum, S. H.; Palstra, T. T. M.; Ramirez, A. P.; Kortan, A. R. *Nature*, **1991**, *350*, 600.

16. (a) Acker, D. S.; Harder, R. J.; Hertler, W. R.; Mahler, W.; Melby, L. R.; Benson, R. E.; Mochel, W. E. *J. Am. Chem. Soc.* **1960**, *82*, 6408. (b) Siemons, L. J.; Bierstedt, P. E.; Kepler, R. G. *J. Chem. Phys.* **1963**, *39*, 3523.

17. Wudl, F.; Smith, G. M.; Hufnagel, E. J. *J. Chem. Soc., Chem. Commun.* **1970**, 1453.

18. Ferraris, J.; Cowan, D. O.; Walatka, V. J.; Perlstein, J. H. *J. Am. Chem. Soc.* **1973**, *95*, 948.

19. Engler, W.; Patel, V. V. *J. Am. Chem. Soc.* **1974**, *96*, 7376.

20. McCullough, R. D.; Kok, G. B.; Lerstrup, K. A.; Cowan, D. O. *J. Am. Chem. Soc.* **1987**, *109*, 4115.

21. Ferraro, J. R.; Williams, J. M., in "*Introduction to Synthetic Electrical Conductors*" Academic Press, **1987**, pp. 13-23.

22. Weyl, C.; Engler, E. M.; Bechgaard, K.; Jehannom, G.; Etemand, S. *Sol. St. Commun.* **1976**, *19*, 925.

23. Torrance, J. B. *Mol. Cryst. Liq. Cryst.* **1985**, *126*, 55

24. (a) Bechgaard, K.; Cowan, D. O.; Bloch, A. N. *J. Chem. Soc., Chem. Commun.*, **1974**, 937. (b) Shu, P.; Bloch, A. N.; Carruthers, T. F.; Cowan, D. O. *J. Chem. Soc.,*

Chem. Commun. **1977**, 505. (c) Braam, J. M.; Carlson, K. D.; Stephens, D. A.; Rehan, A. E.; Compton, S. J.; Williams, J. M. *Inorg. Synth.* **1986**, *24*, 132. (d) Moradpour, A.; Peyrussan, V.; Johansen, I. Bechgaard, K. *J. Org. Chem.* **1982**, *48*, 388. (e) Bechgaard, K.; Jacobsen, C. S.; Mortensen, K.; Pedersen, H. J.; Thorup, N. *Solid state commun.* **1980**, *33*, 1119.

25. Kraus, H. J. *J. Am. Chem. Soc.* **1913**, *34*, 173.

26. Thorup, N. G.; Rindorf. G. H.; Soling, H.; Bechgaard, K. *Acta Cryst.* **1981** *B37*, 1236

27. Mizuno, M.; Garito, A. F. Cava, M. P. *J. Chem. Soc., Chem. Commun.* **1978**, 18.

28. Williams, J. M.; Ferraro, J. F.; Thorn, R. J.; Carlson, D.; Geiser, U.; W.; Wang, H. H.; Kini, A. M.; Whangbo, M. "*Organic Superconductors*", Prentice Hall Inorganic and Organometallic Chemistry Series, **1992**.

29. Ferraro, J. R.; Williams, J. M. "*Introduction to synthetic electrical conductors*", Academic Press, **1987**, pp. 44-59.

30. Friend, R. H.; Jérome, D.; Fabre, J. M.; Giral, L.; Bechgaard, K. *J. Phys. C*, **1978**, *11*, 263.

31. Suzuki, T.; Yamocho, H.; Srdanov, G.; Hinkelmann, K.; Wudl, F. *J. Am. Chem. Soc.* **1989**, *111*, 3108.

32. Tsutsui, K.; Takimiya, K.; Aso, Y.; Otsubo, T. *Tetrahedron Lett.* **1997**, *38*, 7569.

33. Gribble, G. W.; Gilchrist, T. L. "*Progress in Heterocyclic Chemistry*", **1997**, 195.

34. (a) Karikomi, M.; Kitamura, C.; Tanaka, S.; Yamashita, Y. *J. Am. Chem. Soc.* **1995**, *117*, 6791. (b) Naito, T.; Kobayashi, H.; Kobayashi, A. *Bull. Chem. Soc. Jpn.* **1997**, *70*, 107. (c) Aitkenmr. A.; Hill, L. *Phosphorus Sulfur Silicon Relat. Elem.* **1997**, *120/121*, 423. (d) Shimada, S; Masaki, A.; Hayamizu, K.; Matsuda, H.; Okada, S.; Nakanishi, H. *Chem. Commun.* **1997**, 1421.

35. Kata, R. K.; Yamamoto, K. Y.; Tajima, H.; Sawa, H. *J. Chem. Soc., Chem. Commun.* **1997**, 947.

36. Zong, H.; Chen, W.; Cava, M. P.; Rogers, R. D. *J. Org. Chem.* **1996**, *61*, 8117.

37. (a) Liacay, J.; Mas, M.; Molins, E.; Veciana, J.; Powell, D.; Rovira, C. *J. Chem. Soc.*, Chem. Commun. **1997**, 659. (b) Alam, M. M.; Watanabe, A.; Ito, O. *Bull. Chem. Soc. Jpn.* **1997**, *70*, 1833.

38. (a) Shirakawa, H.; Ito, T.; Ikeda, S. *Polym. J.* (Tokyo), **1973**, *4*, 460. (b) Ito, T.; Shirakawa, H.; Ikeda, S. *J. Polym. Sci. Polym. Chem. Ed.* **1974**, *12*, 11.

39. (a) Chiang, C. K.; Fincher, C. R.; Park, Y. W.; Heeger, A. J.; Shirakawa, H.; Louis, E. L.; Gau, S. C.; MacDiarmid, A. G. *Phys. Rev. Lett.* **1977**, *39*, 1098. (b) Park, Y. W.; Denenstein, A.; Chiang, C. K.; Heeger, A. J.; MacDiarmid, A. G. *Solid State Commun.* **1979**, *29*, 747.

40. Tsukamoto, J. *Adv. Phys.* **1992**, *41*, 509.

41. (a) McCall, R. P.; Scherr, E. M.; MacDiarmid, A. G.; Epstein A. J. *Phys. Rev. B* **1994**, *50*, 5094. (b) Tanaka, J.; Tanaka, C.; Miyamae, T.; Shimizu, M.; Hasegawa, S.; Kamiya, K; Seki, K. *Synth. Met.* **1994**, *65*, 173.

42. Kahlman, R. S., Epstein, A. J. "*Handbook of Conducting Polymers*" Second Ed. Marcel Dekker, Inc., **1998**, pp. 727-742 and 847-880.

43. Walatka, V. V.; Labes, M. M.; Perlstein, J. H. *Phys. Rev. Lett.* **1973**, 1139.

44. (a) Burt, F. P. *J. Chem. Soc.* **1910**, 1171. (b) Cohen. M. J.; Garito, A. F.; Heeger, A. J.; MacDiarmid, A. G.; Mikulshi, C. M.; Saran, M. S.; Kleppinger, J. *J. Am. Chem. Soc.* **1976**, *98*, 3844.

45. Greene, R. L.; Street, G. B.; Suter, L. J. *Phys. Rev. Lett.* **1975**, *34*, 577.

46. Yoffe, A. D. *Chem. Soc. Rev.* **1976**, *5*, 51.

47. Krogmann, K.; Hausen, H. D. *Z. Anorg. Chem.* **1968**, *358*, 167. through Ferraro, J. F.; Williams, J. M. "*Introduction to synthetic electrical conductors*", Academic Press, **1987** pp. 139-154, and 195-198.

48. Halina, D. W.; Lyding, J. W.; Ratajack, M. T.; Kannewurf, C. R.; Marks, T. J. *J. Am. Chem. Soc.* **1980**, *102*, 7854.

49. Dresselhaus, M. S.; Dresselhaus, G. *Adv. Phys.* **1981**, *30*, 139.

50. Griller, D.; Ingold, K. U. *Acc. Chem. Res.* **1975**, *9*, 13.

51. The IP, EA and ΔH_{disp} values of PLY and $TTF^{+\cdot}$ were calculated at B3LYP/ 6-31G** level to compare with those of the DTA radicals.

52. (a) Haddon, R. C.; Wudl, F.; Kaplan, M. L.; Marshall, J. H.; Cais, R. E.; Bramwell, F. B. *J. Am. Chem. Soc.* **1978**, *100*, 7629. (b) Haddon, R. C.; Chichester, S. V.; Steele, S. M.; Marshall, J. H.; Mujsco, A. M. *J. Org. Chem.* **1987**, *52*, 711.

53. Nakasuji, K.; Yamaguchi, M.; Murata, I.; Yamaguchi, K.; Fueno, T.; Ohya-Nishiguchi, H.; Sugano, T.; Kinoshita, M. *J. Am. Chem. Soc.* **1989**, *111*, 9265.

54. Goto, K.; Kubo, T.; Yamamoto, K.; Nakasuji, K.; Sato, K.; Shiomi, D.; Takui, T.; Kubota, M.; Kobayashi, T.; Yakusi, K.; Ouyang, J. *J. Am. Chem. Soc.* **1999**, *121*, 1619.

55. Chi, X.; Itkis, M. E.; Patrick, B. O.; Barclay, T. M.; Reed, R. W.; Oakley, R. T.; Cordes, A. W.; Haddon, R. C. *J. Am. Chem. Soc.* **1999**, *121*, 10395.

56. Haddon, R. C.; Chichester, S. V.; Marshall, J. H. *Tetrahedron,* **1986**, *42*, 6293.

57. R. C. Haddon, private communication.

58. (a) Chivers, T. *Chem. Rev.* **1985**, *85*, 341. (b) Oakley, R. T. *Can, J. Chem.* **1993**, *71*, 1775.

59. Rawson, J. M.; Longridge, J. J. *Chem. Soc. Rev.* **1997**, 53.

60. Rees, C. W. *J. Heterocyl. Comp.* **1992**, 639.

61. Sharma, B. D.; Donohue, J. *Acta. Crystallogr.* **1963**, *16*, 891.

62. Delucia, M. L.; Coppens, P. *Inorg. Chem.* **1978**, *17*, 2336.

63. Gillespie, R. J.; Kent, J. P.; Sawyer, J. F. *Inorg. Chem.* **1981**, *20*, 3784 and 4053.

64. Oakley, R. T., Reed, R. W., Cordes, A. W.; Craig, S. L., Graham, J. B. *J. Am. Chem. Soc.* **1987**, *109*, 7745.

65. (a) Boeré, R. T.; Cordes, A. W.; Hayes, P. J.; Oakley, R. T.; Reed, R. W.; Pennington, W. T. *Inorg. Chem.* **1986**, *25*, 2445. (b) Hayes, P. J.; Oakley, R. T.; Cordes, A. W.; Pennington, W. T. *J. Am. Chem. Soc.*, **1985**, *107*, 1346.

66. Cordes, A. W.; Hayes, P. J.; Josephy, P. D.; Koenig, H.; Oakley, R. T.; Pennington, W. T. *J. Chem Soc., Chem. Commun.* **1984**, 1021.

67. Bestari, K.; Cordes, A. W.; Oakley, R. T.; Young, K. M. *J. Am. Chem. Soc.* **1990**, *112*, 2249.

68. (a) Parsons, S.; Passnore, J.; Schriver, M. J.; Sun, X. *Inorg. Chem.* **1991**, *30*, 3342. (b) Wudl, F. *J. Am. Chem. Soc.* **1983**, *103*, 7064.

69. (a) Burford, N.; Passmore, J.; Schriver, M. J. *J. Chem. Soc., Chem. Commun.* **1986**, 140. (b) Chung, Y. L., Pairhurst, S. A.; Gillies, D. G.; Preston, K. F.; Sutcliffe, L. H. *Magn. Reson. Chem.* **1992**, *30*, 666.

70. Alange, G. G.; Banister, A. J.; Luke, A. W., Rawson, J. M.; Whitehead, R. J. *J. Chem. Soc., Dalton Trans.* **1992**, 1277.

71. Banister, A. J.; Rawson, J. M.; Clegg, W.; Birkby, S. L. *J. Chem. Soc., Dalton Trans.* **1991**, 1099.

72. (a) Alange, G. G.; Banister, A. J.; Bell, B.; Millin, P. W., *J. Chem. Soc., Perkin, Trans. I,* **1979**, 1192. (b) Cordes, A. W.; Goddard, J. D.; Oakley, R. T.; Westwood, N. P. C. *J. Am. Chem. Soc.* **1989**, *111*, 6147.

73. Cordes, A. W.; Haddon, R. C.; Oakley, R. T.; Schneemeyer, L. F.; Waszczak, J. V.; Young, K. M.; Zimmerman, N. M. *J. Am. Chem. Soc.* **1991**, *113*, 582.

74. Cordes, A. W.; Chamchoumis, C. M.; Hicks, R. G.; Oakley, R. T.; Young, K. M.; Haddon, R. C. *Can. J. Chem.* **1992**, 919.

75. Belluz, P. D. B.; Cordes, A. W.; Kristof, E. M.; Kristof, P. V.; Liblong, S. W.; Oakley, R. T. *J. Am. Chem. Soc.* **1989**, *111*, 2495.

76. Apblett, A., Chivers, T. *J. Chem. Soc., Chem. Commun.* **1989**, 96.

77. (a) Lee, F. L.; Preston, K. F., Williams, A. J.; Sutcliffe, L. H.; Banister, A. J.; Wait, S. T. *Magn. Reson. Chem.* **1989**, *27*, 1161. (b) Markovski, L. N.; Polumbrik, O. M.; Talanov, V. S.; Shermolovich, Y. G. *Tetrahedron, Lett.* **1982**, *23*, 761. (c) Fairhurst, S. A.; Sutcliffe, L. H.; Preston, K. F., Banister, A. J.; Partington, A. S.; Rawson, J. M.; Passmore, J.; Schriver, M. J. *Magn. Reson, Chem.* **1993**, *31*, 1027.

78. (a) Banister, A. J.; Hansford, M. I.; Hauptmann, Z. V.; Wait, S. T.; Clegg, W. *J. Chem. Soc., Dalton trans.* **1989**, 1705. (b) Höfs, H. U.; Bats, J. W.; Gleiter, R.; Hartmann, G.; Mews, R.; Eckert-Maksic, M.; Oberhammer, H.; Sheldrick, G. W. *Chem. Ber.* **1985**, *118*, 3781.

79. Torroba, T. *J. Prakt. Chem.* **1999**, *341*, 99.

80. (a) Cordes, A. W.; Haddon, R. C.; Hicks, R. C.; Kennepohl, D. K.; Oakley, R. T.; Palstra, T. T. M.; Schmeeneyer, L. F.; Scott, S. R.; Waszczak, J. V. *Chem. Mater.* **1993**, *5*, 820. (b) Davis, W. M.; Hicks, R. G.; Oakley, R. T.; Zhao, B.; Tayor, N. J. *Can. J. Chem.* **1993**, *71*, 180.

81. (a) Andrews, M. P.; Cordes, A. W.; Douglas, D. C.; Fleming, R. M.; Glarum, S. H.; Haddon, R. C.; Marsh, P.; Oakley. R. T.; Palstra, T. T. M.; Schmeeneyer, L. F.; Trucks, G. W.; Tycko, R.; Waszczak, J. V.; Young, K. M.; Zimmerman, N. M. *J. Am. Chem. Soc.* **1991**, *113*, 3559. (b) Cordes, A. W.; Haddon, R. C.; Hicks, R. G.; Oakley. R. T.; Palstra, T. T. M.; Schmeeneyer, L. F.; Waszczak, J. V. *J. Am. Chem. Soc.* **1992**, *114*, 5000.

82. George, N. A. *Ph. D. thesis*, University of Guelph, **1997**, 145.

83. Cordes, A. W.; Bryan, C. D.; Davis, W. M.; de Laat, R. H.; Glarum, S. H.; Goddard, J. D.; Haddon, R. C.; Hicks, R. C.; Kennepohl, D. K.; Oakley, R. T.; Scott, S. R.; Westwood, N. P. C. *J. Am. Chem. Soc.* **1993**, *115*, 7232.

84. (a) Banister, A. J.; Brickebank, N.; Clegg, W.; Elsegood, M. R. J.; Gregory, C. I.; Laverder, I.; Rawson, J. M.; Tanner, B. K. *J. Chem. Soc., Chem. Commun.* **1995**, 679. (b) Banister, A. J.; Brickebank, N.; Laverder, I.; Rawson, J. M.; Gregory, C. I.; Tanner, B. K. Clegg, W.; Elsegood, M. R. J.; Palacio, F. *Angrew. Chem. Int. Ed. Engl.* **1996**, *35*, 2533.

85. Guillermo, A.; Davies, J. E.; Hartley, M.; Palacio, F.; Rawson, J. M.; Smith, J. N. B.; Steiner, A. *J. Chem. Soc., Chem. Commun.* **1999**, 1393.

86. Banister, A. J.; Batsanov, A. S.; Dawe, O. G.; Herbertson, P. L.; Howard, J. A. K.; Lynn, S.; May, I.; Smith, J. N. B.; Rawson, J. M.; Rogers, T. E.; Tanner, B. K.; Antorrena, G.; Palacio, F. J. *J. Chem. Soc., Dalton trans.* **1997**, 2539.

87. Beer, L.; Cordes, A. W.; Myles, D. J. T.; Oakley, R. T.; Taylor, N. J. *Cryst. Eng. Comm.* **2000**, 20.

88. Cordes, A. W.; Glarum, S. H.; Haddon, R. C.; Hallford, R.; Hicks, R. C.; Kennepohl, D. K.; Oakley, R. T.; Palstra, T. T. M.; Scott, R. S. *J. Chem. Soc., Chem. Commun.* **1992,** 1265.

89. Bryan, C. D.; Cordes, A. W.; Haddon, R. C.; Hicks, R. C.; Kennepohl, D. K.; MacKinnon, C. D.; Oakley, R. T.; Palstra, T. T. M.; Perel, A. S.; Scott, R. S; Schmeeneyer, L. F.; Waszczak, J. V. *J. Am. Chem. Soc.* **1994,** *116*, 1205.

90. (a) Bryan, C. D.; Cordes, A. W.; Haddon, R. C.; Hicks, R. C.; Oakley, R. T.; Palstra, T. T. M.; Perel, A. J. *J. Chem. Soc., Chem. Commun.* **1994**, 1447. (b) Bryan, C. D.; Cordes, A. W.; Goddard, J. D.; Haddon, R. C.; Hicks, R. C.; MacKinnon, C. D.; Mawhinney, R. C.; Oakley, R. T.; Palstra, T. T. M.; Perel, A. S. *J. Am. Chem. Soc.* **1996**, *118*, 330.

91. (a) Bryan, C. D.; Cordes, A. W.; Fleming, R. M.; George, N. A.; Glarum, S. H.; Haddon, R. C.; Oakley, R. T.;Palstra, T. T. M.; Perel, A. S.; Schmeeneyer, L. F.; Waszczak, J. V. *Nature*, **1993**, *365*, 821. (b) Bryan, C. D.; Cordes, A. W.; Fleming, R. M.; George, N. A.; Glarum, S. H.; Haddon, R. C.; MacKinnon, C. D.; Oakley, R. T.; Palstra, T. T. M.; Perel, A. S. *J. Am. Chem. Soc.* **1995**, *117*, 6880.

Chapter 2 1,3,2-Dithiazolyl (DTA) Radicals

As indicated in Chapter 1, 1,2,3,5-dithiadiazolyl (**II-1**) radicals are very stable species, with flexibility for modification in the nature of the 4-substituent. However, the nodal properties of the SOMO of these radicals leads to very little electronic interaction between the substituent and ring.[1] Delocalization of charge, so as to improve the redox properties of the radical, and to help suppress dimerization, is not possible. By contrast, the SOMO distributions of 1,3,2- and 1,2,3-dithiazolyl (**II-2** and **II-3**) radicals are such that there is significant spin density at carbon, particularly in the 1,2,3-variants (**II-3**).[2] This feature opens the way for modification of molecular properties since, by attachment of single substituents at the 4,5-positions, or by creating fused ring structures, the unpaired electron can be delocalized away from the five membered ring.

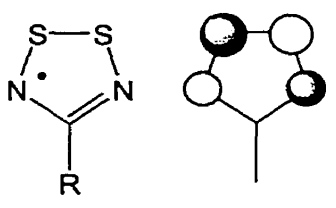

II-1

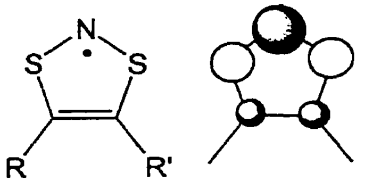

II-2

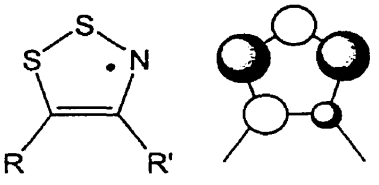

II-3

This chapter describes the first stages of exploration designed to take advantage of this feature. Our initial intent was to design, synthesize and study catacondensed ring systems based on 1,3,2-radicals. The subsequent chapters will describe the results of work on the 1,2,3-systems.

2.1 Introduction to 1,3,2-DTA radicals

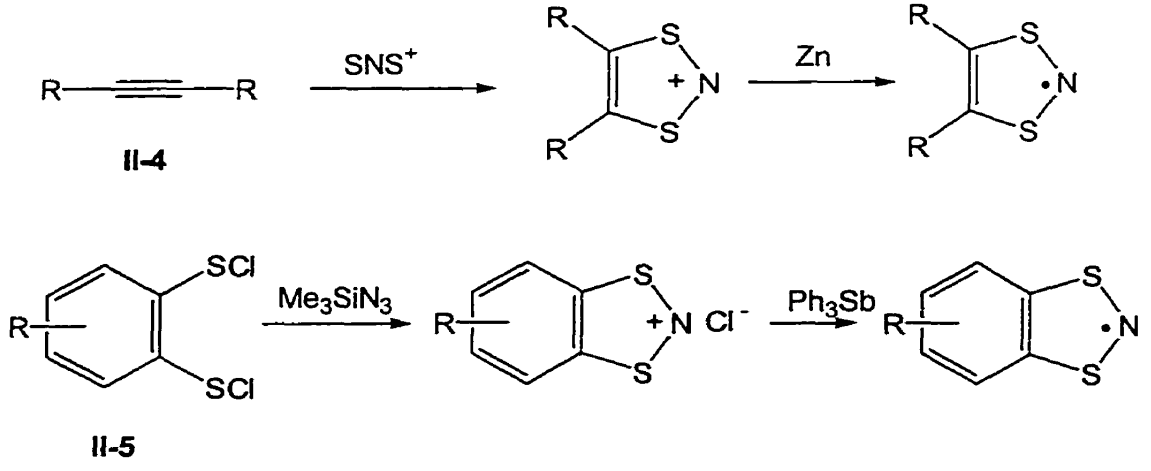

Scheme 2.1

In attempting to build polycyclic 1,3,2-DTA radicals we were able to take advantage, at least initially, of known synthetic technology. As the work progressed, a number of new synthetic strategies were developed. The 1,3,2-DTA ring has been known for several decades and high yield methods have been developed for the generation of monocyclic and bicyclic derivatives. For example, the Passmore group has utilized the reaction of the SNS^+ cation with acetylenes, **II-4**, to produce a wide range of 4,5-substituted dithiazolylium cations.[3] Reduction of these cations, typically with zinc, then affords the radicals (Scheme 2.1). Another useful cyclization involves the condensation of a bis(sulfenyl chloride), **II-5** with trimethylsilyl azide; the 1,3,2-DTA rings **II-6**, **II-7** and **II-10** were obtained *via* this route.[4,5,14] Indeed the parent 1,3,2-dithiazolylium chloride cation ([**II-2**]$^+$ with R, R' = Cl) was obtained by this approach, too.[6] Similarly, benzo-1,3,2-diselenazolylium chloride (**II-9**) was generated from the corresponding bis(chloroseleno) derivative.[7] Other reagents and routes have also been explored. For example, N,N-dichlorobenzenesulfonamide was discovered to form the 1,3,2-dithiazolyl ring with 2,3-dithioquinoxaline.[8] A more unusual

route to generate the 1,3,2-DTA ring, is *via* ring contraction of a dithiazepine derivative with the concomitant chlorination. However, only the cation associated with the tetrachlorobenzo group (**II-11**) was reported.[9]

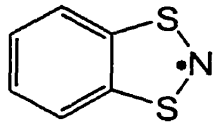

II-6

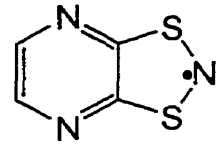

II-7

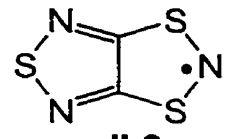

II-8

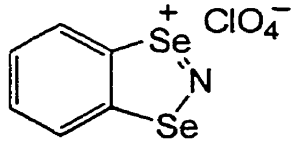

II-9

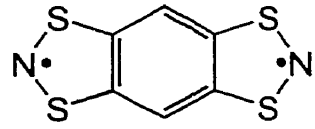

II-10

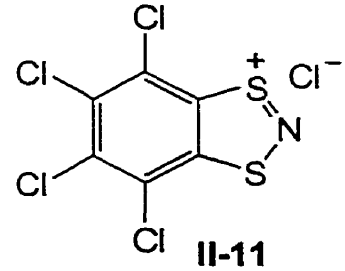

II-11

ESR studies have been carried out on a variety of 1,3,2-systems with a wide range of substituents in the 4- and 5- position. Unlike 1,2,3,5-DTDA radical systems in which the hyperfine patterns are very similar (generally five-line patterns with g-values in the order of 2.01 regardless of R substituents), the coupling constant to nitrogen in 1,3,2-DTA system varies with the R and R' groups over a relatively broad range. For example, the monocyclic 4,5-bis(trifluomethyl)-1,3,2-dithiazolol-2-yl **II-2** (where R =R' = CF_3), and other radicals in this type have a_N values of about 1.1 mT.[10] When cyano groups replace trifluoromethyl groups in **II-2**, a_N = 1.087 and no hyperfine coupling interaction from the nitrogens of the cyano groups could be discerned.[11] For polycyclic 1,3,2-DTA systems, such as PDTA and QDTA, the anisotropic hyperfine coupling constants on pyrazine ring nitrogens (0.0654 mT and 0.1272 mT) clearly shows that the unpaired electron spin density is delocalized to the pyrazine rings.[12] That is to say , when the larger aromatic systems are fused to 4,5- position

of 1,2,3-DTA, the unpaired electron becomes more delocalized and therefore the radical state is stabilized.

Prior to this work relatively little was known about the solid state properties of 1,3,2-DTAs. As shown in Figure 2.1, the 4,5-dicyano (**II-2** R=R'=CN) derivative forms a simple cofacial dimer.[8] The pyrazine-based radical (PDTA, **II-7**) dimerizes similarly, but with the formation of one-dimensional dimer stacks.[12] By contrast, the benzo-derivative (BDTA, **II-6**) [13] has a similar molecular structure to PDTA, but dimerizes in a centrosymmetric fashion (Figure 2.1(right)). Thus the dimerization and the solid state arrangements of 1,3,2,-DTAs are similar to these of 1,2,3,5-DTDA radicals.

d (S---S) = 3.145Å d (S---S) = 3.175Å

Figure 2.1 The crystal structures of 4,5-dicyano-1,3,2-DTA (left) and benzo-1,3,2-DTA.

The trithiatriazapentalenyl radical (TTTA, **II-8**) represents a sharp contrast to the previous examples. In the solid state, at room temperature, *no* dimerization is observed. Instead the crystal structure consists of evenly-spaced slipped π -stacks.[14] The low temperature solid structure was reported recently[15] and it consists of the paired radical molecules, which is similar to our discovery on 1,3,2-TDTA (**II-28**) discussed later in this chapter. A more recent example of a slipped π -stack structure is benzo-1,2:4,5-bis (1,3,2-dithiazolyl) diradical (BBDTA, **II-10**).[16]

The latter two examples, both of which are fused ring radicals, provide credence to the idea that the association of 1,3,2-DTA radicals can be suppressed. It was partly on the basis of these observations that we began the exploration of 1,3,2-DTA radicals fused with different aromatic rings. More extensive delocalization of the unpaired electron, as would be afforded by polycyclic aromatics, should further militate against dimerization. The following sections describe the synthesis and characterization of such systems, called NDTA, QDTA, TDTA and PPDTA.

2.2 2,3-naphthalene-1,3,2-dithiazolyl, (NDTA)

2.2.1 Synthesis

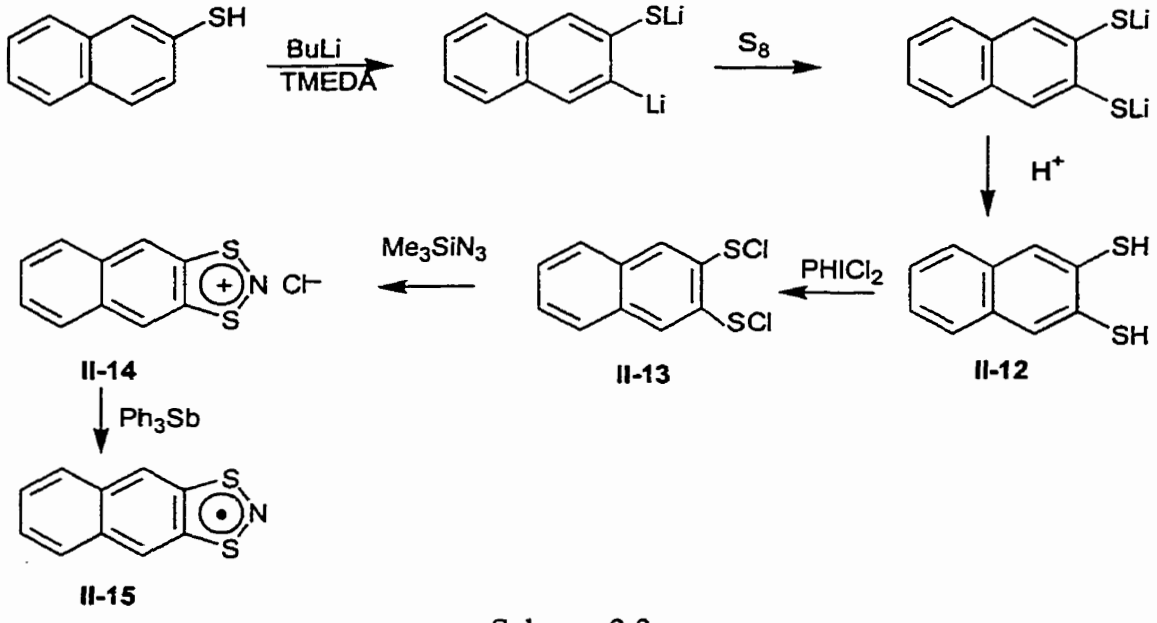

Scheme 2.2

The NDTA framework was developed (Scheme 2.2) using a known synthetic sequence.[17] Thus, 2,3-naphthalene-dithiol (**II-12**) prepared by orthometallation of commercially available 2-naphthalenethiol, followed by treatment of the lithiated material

with sulfur. The dithiol, **II-12** was then oxidized with iodobenzene dichloride to give 2,3-naphthalene-bis(sulphenyl chloride) (**II-13**). It should be noted that this oxidation required very stringent control of the oxidizing conditions. An excess of $PhICl_2$, or the use of more vigorous oxidants, *e.g.*, chlorine, leads to chlorination of the aromatic ring. The product **II-13** was condensed with trimethylsilyl azide in CH_2Cl_2 solution to afford 2,3-naphthalene-1,3,2-dithiazolylium chloride cation(**II-14**). Reduction of the cation with triphenylantimony in acetonitrile gave the crude purple NDTA radical (**II-15**). The total synthetic process is described in Scheme 2.2.

The reduction of [NDTA]Cl (**II-14**) with triphenylantimony, to afford the neutral radical (**II-15**), was the most technically demanding, as the NDTA radical is extremely sensitive to atmospheric oxygen. Purification of the radical, and the growth of crystals suitable for X-ray and transport property measurements, was best achieved using the three-zone tube furnace illustrated in Figure 2.2. The furnace contains of three temperature zones (T_1, T_2 and T_3) which were set to allow sublimation and fractionation of the radical over a period of several days. For the initial sublimations we usually used a dynamic vacuum (ca. 10^{-2} Torr) , while subsequent sublimations were performed using sealed evacuated tubes. Given prepurified materials, this latter procedure afforded larger, more defect free, crystals.

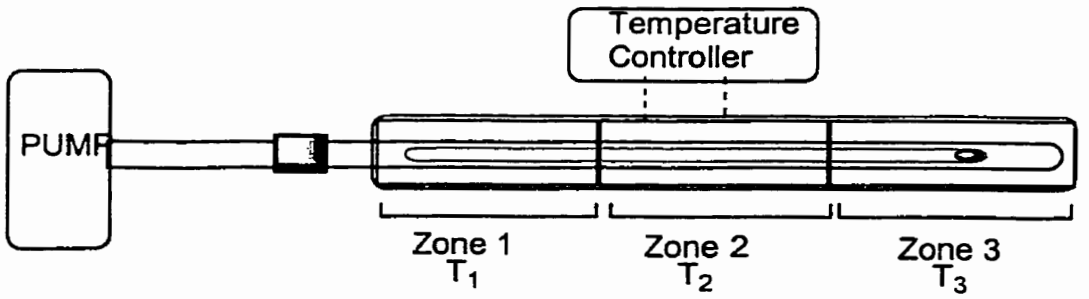

Figure 2.2 A schematic diagram of sublimation apparatus.

2.2.2 Crystal structure

Earlier in this chapter we met several different crystal structures based on the 1,3,2-DTA framework. In accord with our hopes, the NDTA radical does not dimerize (at room temperature) in the solid state. Instead, the crystal structure consists of discrete molecules of NDTA, with two molecules per asymmetric unit; the planes of molecules in the same unit are approximately perpendicular each other. The internal bond lengths of the two rings (mean d(S---N) = 1.645Å, mean d(C---S) = 1.748Å) are very similar to those in dimeric derivatives [14] and disclose the fact that dimerization effects minimal electronic reorganization. The crystal structure consists of anti-parallel ribbons of radicals along *z* direction (Figure 2.3 left). If viewed down the *z* direction (Figure 2.3 right) the packing pattern of the ribbons resembles the close-packed herringbone arrangement found in many polycyclic aromatics,[18] *e.g.*, naphthalene[19] and anthracene.[20] As noted already there is no dimerization of NDTA radicals, and the closest intermolecular S---S contacts are well outside the van der Waals separation of 3.6Å.[30]

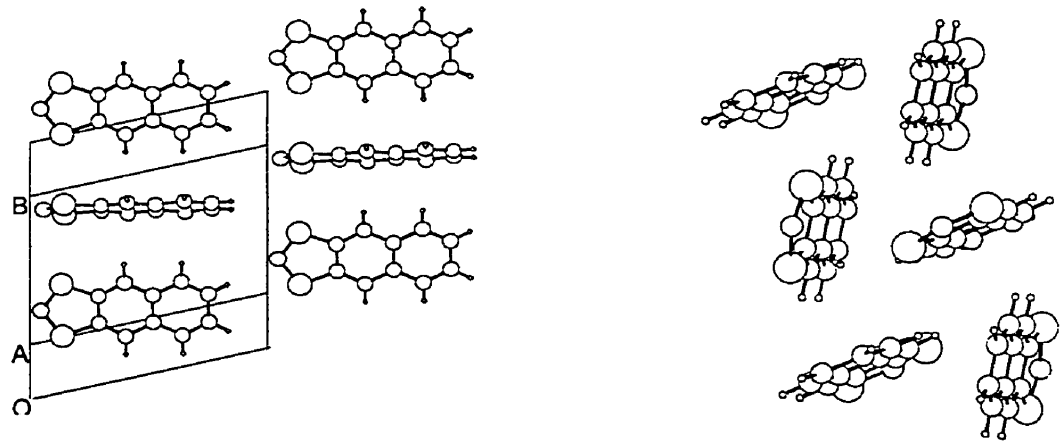

Figure 2.3 Herringbone packing of NDTA radicals viewed along and down *z* direction.

2.2.3 Magnetic properties

The bulk magnetic susceptibility of NDTA has been measured over the temperature range 5 - 400 K on a SQUID magnetometer.[21] The plot of χ_M *vs.* T is shown in Figure 2.4. Analysis of the susceptibility data for NDTA indicates that it is essentially paramagnetic above 200 K, with θ = 1.3 K. In an ideal case, the radical state which holds the unpaired electrons, should display paramagnetism and obey the Curie law in an actual magnetic measurement. However, not all the unpaired electrons contribute to paramagnetism, for example, the dimerization occurs. In order to estimate the availability of free spin, the ratio of the effective magnetic moment and to that expected for a S = ½ system, *i.e.*, the fraction of free Curie spin, f, is determined from the formula $f = 8\chi T/3$. For NDTA, $f = 0.80$ mol $^{-1}$. Below 200 K there is a phase transition to a more strongly antiferromagnetically coupled state with θ = 10.7 K and f = 0.53 mol^{-1}. The nature of this phase transition, and the accompanying structural changes was not pursued.

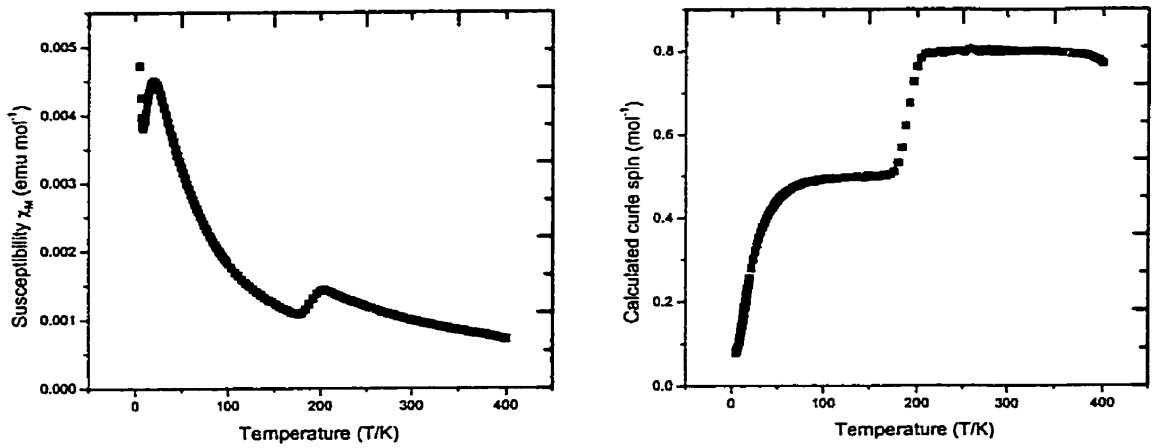

Figure 2.4 Magnetic susceptibility χ_M of NDTA as a function of temperature (left) and the calculated fraction of Curie spins *vs.* temperature (right).

The pressed pellet conductivity at room temperature for NDTA was estimated at less than 10^{-6} S cm^{-1}. This is not surprising given the herringbone crystal structure. The radical molecules can not form an effective energy band to overcome the Coulombic energy barrier. The large free spin is trapped inside the molecules and NDTA is a Mott insulator.

2.3 2,3-Quinoxaline-1,3,2-dithiazolyl, (QDTA)

Our initial work on NDTA provided us with the confidence that dimerization can be overcome by fusing large aromatic groups onto a 1,3,2-DTA ring. In order to continue the exploration of the substitutent effect on structural pattern, we turned to the quinoxaline-based 1,3,2-DTA radical, QDTA (**II-19**). When two nitrogen atoms replace carbon on the aromatic substituent, what will happen to the radical's solid state and electronic properties?

2.3.1 Synthesis

The preparation of QDTA (**II-19**), by treating the corresponding benzenesulfonamide derivative (**II-17**) with ammonia, has been reported in the literature.[8] From commercially available 2,3-dichloroquinoxaline, quinoxaline-2,3-dithiol (**II-16**) was easily prepared by treatment with thiourea followed by hydrolysis of the corresponding bis(thiouronium) salt.[22] The dithiol was then combined with N,N-dichlorobenzenesulfonamide[23] in ether to yield the sulfonamide (**II-17**) as an air stable crystalline solid. When this compound was first reported it was suggested that the radical could be obtained directly from **II-17** by thermolysis. However, in our hands this was not the case. Indeed, attempted thermolysis (150°C/10^{-3} Torr) to generate QDTA radical (**II-19**) resulted in the sublimation of **II-17** in the form of

translucent yellow crystals. **II-17** was very sensitive to base. Bubbling ammonia gas in dichloromethane solution immediately generates a green slurry of the corresponding imide. After washing with toluene and hexane, the yellow green imide **II-18** was separated. Our initial experiments with **II-18** did not support the report[8] that it could be thermally decomposed to form QDTA radical. The material was sublimed unchanged during the course of an attempted thermal decomposition. We were then forced to reassess the literature procedure for the generation of QDTA from the imide **II-18**. To this end we explored a variety of oxidants. The first approach involved cosublimation of the imide with an excess of PbO_2 through a temperature gradient of 100-30°C/10^{-3} Torr. While this was successful in generating crystals of QDTA, a more efficient and simpler route was found later. Treatment of the imide in CH_2Cl_2 solution with aqueous $K_3Fe(CN)_6$ would generate the radical. Extraction from aqueous solution by CH_2Cl_2 and evaporation of the organic layer yielded crude QDTA radical which was subsequently purified by fractional vacuum sublimation through a temperature gradient of 40-70°C /10^{-2} Torr as black rod-like crystals. The synthetic route was presented in Scheme 2.4.

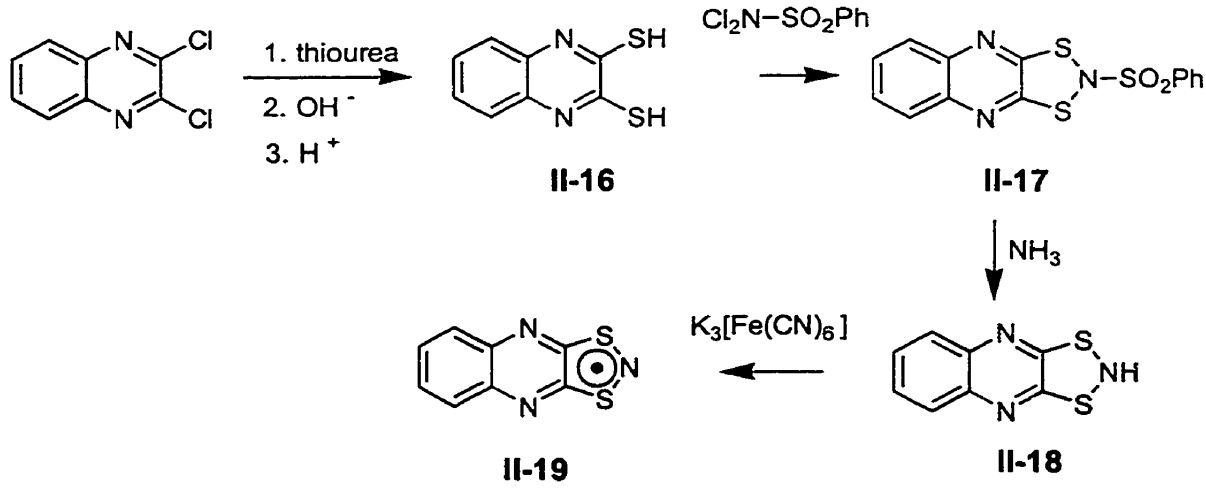

Scheme 2.4

The redox chemistry of QDTA is thus in stark contrast to that of NDTA. While NDTA is extremely sensitive to air, QDTA is stable in the aqueous, indeed molecular oxygen can be used to oxidize imide to the radical. The conversion of the imide to QDTA was a reversible process, *i.e.*, combination of a CH_2Cl_2 solution of QDTA with an aqueous solution of sodium dithionite regenerated the imide, which could be isolated from the organic layer.

2.3.2 Crystal structure

The crystal structure of QDTA is very different from that of NDTA, even though they have similar molecular structures. The crystals belong to the $P2_1$ space group. The internal bond lengths of the heterocyclic ring of QDTA (mean d(S---N) = 1.649Å, mean d(C---S) = 1.736Å) are typical of those seen in simple dimers [comparing to BDTA (mean d(S---N) = 1.646Å, mean d(C---S) = 1.744Å) in Table 2.1].[14] However, in the solid state, QDTA consists only of undimerized radicals.

Table 2.1 Comparison of bond lengths (Å) observed in related 1,3,2-dithiazolyls.

Bond	QDTA	TTTA	BDTA	BBDTA	NDTA
S---N	1.649 (10)	1.651 (5)	1.646 (4)	1.648 (2)	1.645 (7)
C---S	1.736 (10)	1.728 (5)	1.744 (5)	1.733 (6)	1.748 (6)

As shown in Figure 2.5, the molecules lie in ribbon-like chains, but the ribbons adopt a slipped π-stack pattern similar to that observed for TTTA[15]. Apart from intermolecular contacts associated with the cell repeat distance(3.7105 Å), there is only one S---S contact inside 4.0Å (d_1) linking radicals in adjacent stacks.

Studies on the related polycyclic aromatics,[19] such as naphthalene [20] and anthracene[21] have showed that the solid state packing arrangements for these materials can be divided into two motifs: structures composed of herringbone (or T-shaped) molecular pairs, and those made up of slipped stack pairs. These studies also indicate that the mutual orientation of the molecular planes in the crystal are affected by the relative importance of intermolecular C---C *versus* C---H contacts, with the C---H interactions favoring the herringbone type packing arrangement. If we compare the structure difference in stacking between NDTA (**II-15**) an QDTA (**II-19**). It seems that the similarity of the NDTA structure to those of simple polycyclic aromatics favors the herringbone arrangement,[19] but when N atoms replace CH groups in the side ring, this preference is reduced while in QDTA, the slipped stack structure prevails.

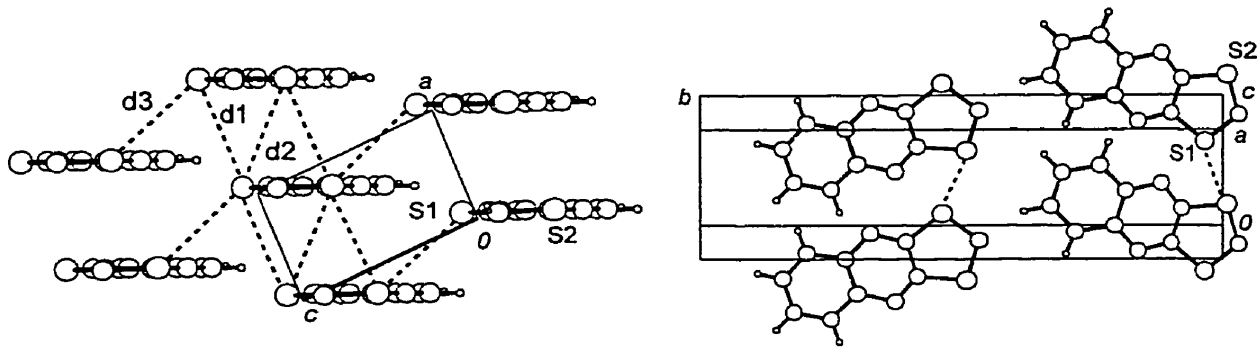

Figure 2.5 Crystal structure of QDTA. Slipped π-stack structure of QDTA. Intermolecular S---S contacts are shown with dashed lines; $d_1 = 3.840$ Å (left). Top view of QDTA. dashed line shows S---S contacts in the same layer (right).

When the substituents on the DTA ring become more aromatic and electron withdrawing, the interaction (intermolecular S---S) between two DTA ring is reduced and

the dimerization enthalpy is slightly weakened. Possibly this is why in QDTA, dimerization does not occur. A similar situation may apply for TTTA (**II-8**).

2.3.3 Magnetic properties

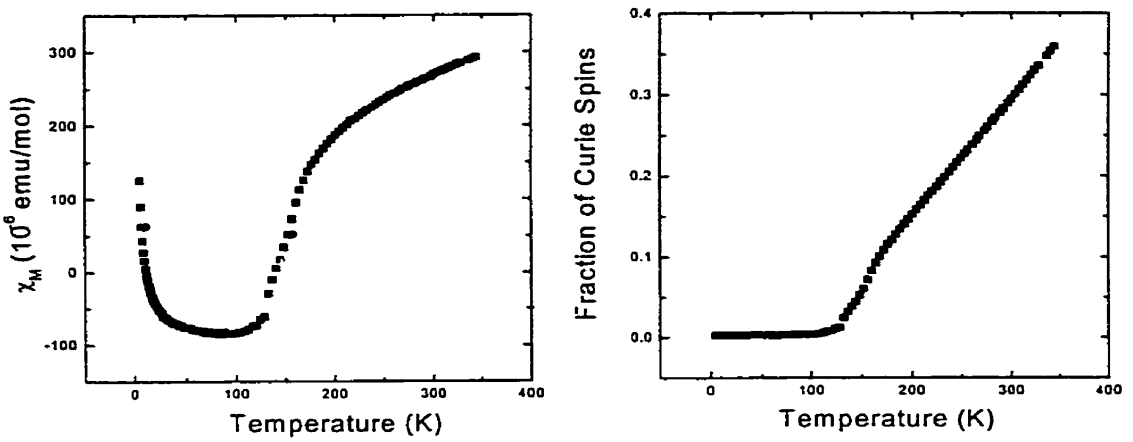

Figure 2.6 Magnetic susceptibility χ (left) and fraction of Curie spin (right) of QDTA as the function of temperature.

The bulk magnetic susceptibility of QDTA, plotted as a function of temperature is shown in Figure 2.6. The low temperature susceptibility is consistent with a diamagnetic ground state, with $\chi_0 = -99\times 10^{-6}$ emu mol^{-1}, $\theta = -0.1$ K and the calculated Curie spin $f =$ 0.003 mol^{-1}. Above 120 K the susceptibility slowly rises and, at room temperature, f is about 0.3 mol^{-1}. QDTA, in the solid state, takes on a slipped π-stack structure, in which the electron are nominally unpaired. However, at room temperature the free spin count is only 30% of that calculated for non-interacting centers. Presumably this partial quenching reflects some kind of intermolecular exchange interactions between the plates up and down the π-stack. Upon cooling to 120 K, all the spins are quenched, indicative of some sort of phase

transition in this temperature region. Pressed pellet measurements indicate room temperature conductivity is less than 10^{-6} S cm^{-1}. As in the case of NDTA, the large fraction of spin density can not contribute to actual conductivity. These spins were trapped inside the molecules and therefore the radicals become Mott insulators.

2.4 1,2,5-thiadiazolo[3,4-b]- 1,3,2- dithiazolo[3,4-b]-pyrazin-2-yl (1,3,2-TDTA)

The crystal structure results on NDTA and QDTA confirmed that dimerization can be suppressed if the large aromatic groups are attached onto the 1,3,2-DTA ring. In the case of NDTA which holds six CH "structure makers", the herringbone structure is produced. In QDTA, the number of CH groups is reduced to four, and the molecules take on a slipped π stacked structure in the solid state. In the trithiatriazapentalenyl radical (TTTA, **II-8**), there are no CH groups at all and a slipped π stack arrangment again prevails. The replacement of the CH group by nitrogen seems to play an important role in promoting this type of packing.

With these issues in mind, we decided to pursue the ternary, tricyclic radical 1,2,5-thiadiazolo[3,4-b]-1,3,2-dithiazolo[3,4-b]-pyrazin-2-yl (**II-28**), since it combines in one system all the attributes of QDTA and TTTA. In this so-called TDTA molecule, all CH groups have been replaced with N atoms, so the CH-ring effect is avoided.

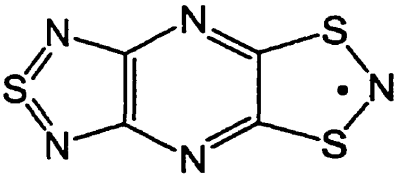

II-28

2.4.1 Synthesis

As in the preparation of QDTA, the ideal starting point for 1,3,2-TDTA required the generation of a dithiol, namely is 5,6-dithio-1,2,5-thiadiazolo[3,4-b]pyrazine (**II-24**). However, neither this compound nor any of its immediate precursors are commercially available. The starting point for this chemistry was 2-chloropyrazine, a simple monocyclic molecule onto which we built two extra rings.

As a first step in the synthetic sequence, tetrachloropyrazine (**II-20**) [24] was made from 2-chloropyrazine and excess of PCl_5 at 280°C in a pressure reactor. Initially we used thick-wall glass (Carius) tubes to carry out this reaction. These experiments were confined to small scale (typically 1-2 g chloropyrazine). Later a Parr bomb reactor (300 mL) with a controlled heating system was acquired. This allowed us to scale up the reaction so that we could generate 30 g of tetrachloropyrazine in one batch. At the end of each bomb reaction, the pale yellow solid was extracted with ether and extracts combined, washed with H_2O, dried over anhydrous Na_2SO_4 and rotary evaporated to give a white, pale yellow solid. White plates were obtained by recrystallization from methanol (Scheme 2.5).

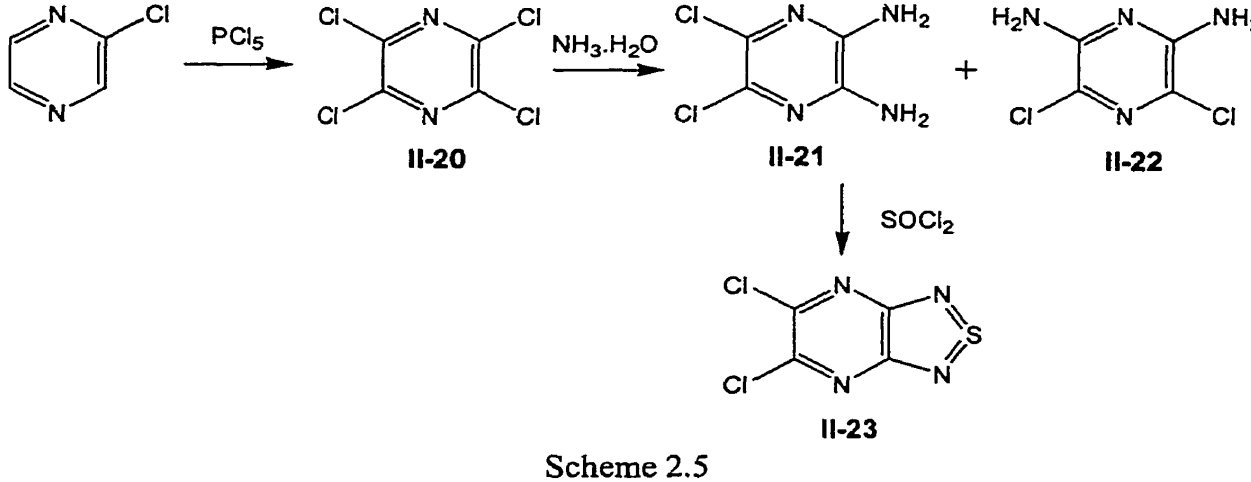

Scheme 2.5

We encountered less trouble when we made diaminodichloropyrazine (**II-21**).[25]

Initially tetrachloropyrazine reacts with ammonium hydroxide in a sealed tube reactor at 140°C for 16 hours; later the steel bomb was used to increase the productivity. Eventually we realized that the product of this reaction was actually a mixture of 2,3-diamino-5,6-dichloropyrazine (**II-21**) and 2,6-diamino-3,5-dichloropyrazine (**II-22**) in an approximately 1:1 ratio. The two isomers could be separated by recrystallization from methyl ethyl ketone, in which the 2,3-isomer is far less soluble that the 2,6-compound.[26] In the next step, 5,6-dichloro-1,2,5- thiadiazolo[3,4-b]pyrazine (**II-23**) was made by modification of literature procedure.[27] This was a difficult reaction, which required optimization of time, temperature and solvent. Initially we used mixtures of **II-21** and **II-22**, excess of $SOCl_2$, the mixed **II-22** and the excess of S_2Cl_2 (sulfur) gave a dark brown slurry. After several tries, the whole process was optimized. The best results came from reacting 2,3-diamino-5,6-dichloropyrazine with $SOCl_2$ for 7 hours, using pyridine as catalyst and refluxing xylene as a solvent. The large pale yellow plate of **II-23** was obtained by recrystallization from ethyl acetate.

The dithiol **II-24** was made easily by mixing **II-23** and thiourea in anhydrous ethanol under reflux. The red thiouronium salt was hydrolyzed with base to give a clear red solution. Acidification with HCl or acetic acid gave the product which was used without further purification in the following step.

Because the synthesis of QDTA from the dithiol derivative was so successful, we expected that this synthetic approach would be applicable to our new system without much revision. Surprisingly however, attempts to synthesize TDTA *via* this route failed completely. The necessary sulfonamide intermediate **II-25** could not even be prepared by the reaction of **II-24** with benzene-N,N-dichlorosulfonamide (shown in Scheme 2.6).

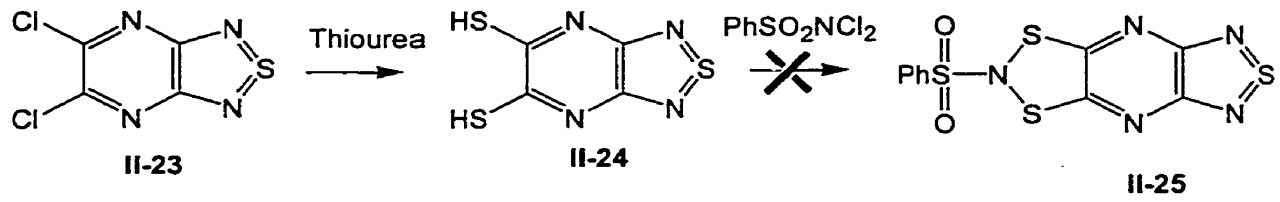

Scheme 2.6

We therefore questioned whether dichlorobenzenesulfonamide itself was active enough towards the reaction with **II-24**. In order to increase the reactivity of **II-24**, the dithiol was reacted with sodium ethoxide to make the disodium salt (scheme 2.7), which was then reacted with titanocene dichloride to convert it to the dark green titanocene derivative **II-26**. This latter material was purified by Soxhlet extraction with CH_2Cl_2 for several days.

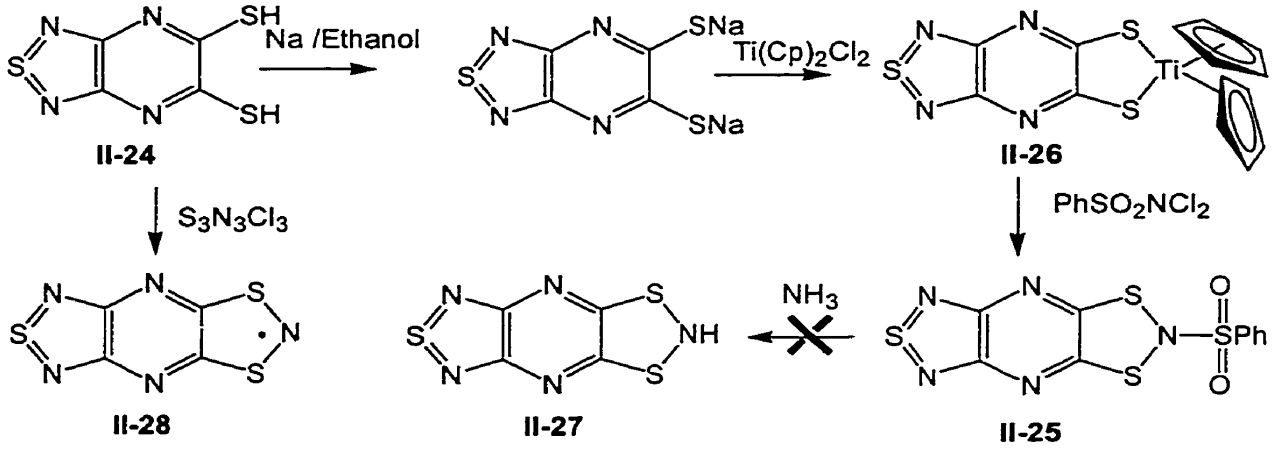

Scheme 2.7

We then turned back to make the desired sulfonamide derivative. When **II-26** and N,N-dichlorobenzenesulfonamide (Scheme 2.7) were mixed together in acetonitrile, $(Cp)_2TiCl_2$ was immediately regenerated and the slurry turned red brown. However the similar solubilities of product and byproduct made the later separation process difficult. The mixture was extracted with hot toluene to remove most of the red $(Cp)_2TiCl_2$. The solid

residue obtained by evaporation of the solvent was then recrystallized from hot acetonitrile. Yellow needles of **II-25** were collected after cooling the solution in the freezer to -20°C. It was with some disappointment that we discovered that treatment of this sulfonamide with ammonia did not lead to the expected imide (**II-27**), but rather to the recovery of benzene-sulfonamide and starting dithiol **II-24**.

However, we were eventually able to find a very fast, and relatively easy method for the generation of 1,3,2-TDTA (**II-28**), *in a single step*, from dithiol, **II-24**. The reaction involved treating the dithiol with trithiazyl trichloride $S_3N_3Cl_3$. In the course of this reaction the chloride salt of the binary cation $S_4N_3^+$ was produced as a side product, along with the neutral (unoxidized) form of TDTA, **II-28**. Under forcing conditions (excess chlorine gas) TDTA can be oxidized to what we presume is a chloride salt of the corresponding dithiazolylium cation, but this material readily reverts to the neutral material (with loss of chlorine) on heating of 60°C. The crystal for structural determination was grown by fractional sublimation at 110-60° C/ 10^{-2} Torr.

2.4.2 ESR spectra

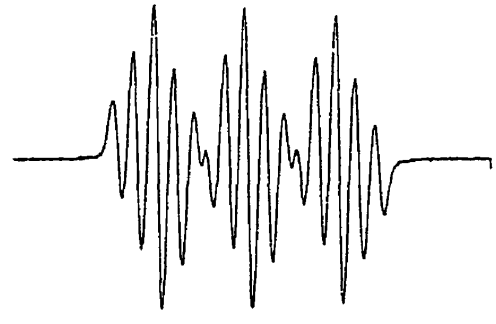

Figure 2.7 X-band ESR spectrum of TDTA (in CH_2Cl_2, sweep width 0.50 mT).

Values of the g-factors and isotropic hyperfine coupling constants a_N for NDTA, QDTA, TDTA, and several related 1,3,2-dithiazolyl radicals [28] are provided in Table 2.2, along with computed (B3LYP/6-31G**) estimates of the spin density q_N on nitrogen. For TDTA the ESR spectrum is illustrated in Figure 2.7.

Table 2.2 ESR measurements: *g*-values, hyperfine coupling constants a_N (mT) and calculated (B3LYP/6-31G**) spin densities q_N for 1,3,2-dithiazolyls

compds	g	a_N [a]	q_N [a]
DTA (R = H)[11]	2.0071	1.066	0.459
BDTA	2.0069	1.101	0.464
TTTA [15]	2.0061	1.112 (0.084)	0.465 (0.039)
NDTA	2.0067	1.106	0.458
QDTA [8]	2.0065	1.089 (0.129)	0.456 (0.037)
TDTA	2.0071	0.950 (0.207)	0.435 (0.060)

[a] Values in parentheses refer to the nitrogen atoms in the pyrazine ring (QDTA, TDTA) and thiadiazolo ring (TTTA).

All the radicals show the expected features for a 1,3,2-dithiazolyl radical, *i.e.*, a large coupling to the nitrogen within the DTA ring. Taken together, however, the spectra reveal a progressive and significant decrease in this internal a_N value along the series NDTA, QDTA, and TDTA. Coupled to this trend is a larger a_N value in the pyrazine ring of TDTA (relative to QDTA). These experimental results follow closely the trends in computed spin

densities. The singly occupied molecular orbital (SOMO) of TDTA extends well out onto the pyrazine ring. In essence the thiadiazolopyrazine ring is an extremely effective sink for spin density, much more so than simple benzenoid aromatic residues, such as in BDTA or NDTA, or even simple thiadiazole units such as TTTA.

2.4.3 Magnetic susceptibility

In the solid state NDTA is essentially paramagnetic at room temperature, as expected from its herringbone packing pattern, which affords little opportunity for intermolecular exchange coupling. Upon cooling it undergoes two phase transitions, with eventual loss of paramagnetism. The slipped π-stack structure of QDTA leads to a room temperature magnetic susceptibility with only 30% of that expected for a free spin system. Presumably this partial quenching reflects some intermolecular exchange interactions between the plates up and down the stack. Upon cooling the fraction of free spins slowly decreases, so that by 120 K all paramagnetism is quenched.

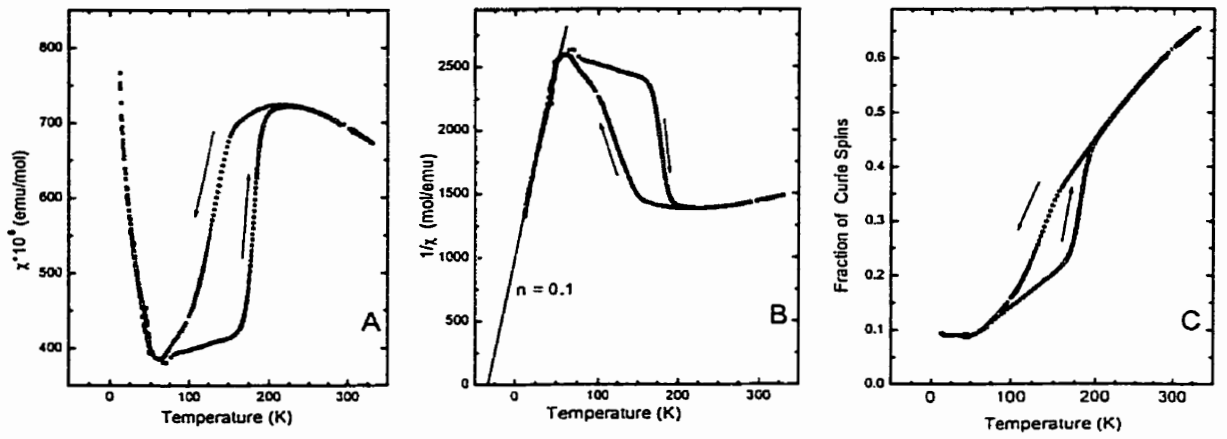

Figure 2.8 Magnetic susceptibility χ of TDTA as a function of temperature (A). Plot of $1/\chi$ vs T for TDTA (B). Fraction of free Curie spins of TDTA as function of temperature (C).

The result of magnetic susceptibility measurements on TDTA, taken over the temperature range 4-330 K, is shown in Figure 2.8A. It is clear that there is a hysteretic phase transition in the vicinity of 150 K. In fitting the data we have used a calculated diamagnetic susceptibility correction of -92 ppm emu/mol. From the fit to the low-temperature data (Figure 2.8B) we obtain a Weiss constant for the ordering transition of about -34 K. This is the same order of magnitude as the hysteresis, and on this basis we assign an antiferromagnetic interaction as the origin of the phase transition. These two parameters have been used in Figure 2.8C to obtain the fraction of Curie spins as a function of temperature. It can be seen that the Curie spins count is temperature dependent throughout the whole temperature range (down to near 50 K).

For the NDTA and QDTA systems the structural origins of the observed magnetic changes as a function of temperature in terms of variations in crystal structure were not investigated. While dimerization of some form provides a facile explanation for the loss of paramagnetism, the exact nature of how this process might occur is not known. In contrast to these materials, the ground state of TDTA is antiferromagnetic, and this unusual observation, coupled with the hysteretic phase transition observed in the region of 150 K, prompted us to explore the crystal structure of TDTA above and below the phase transition observed in the magnetic measurements. As discussed above, the hysteretic phase transition in the vicinity of 150 K originated from dimerization of radical molecules.

2.4.4 Crystal structure

The compounds NDTA, QDTA are similar at a molecular level, however, their room-temperature solid-state structures are quite different. NDTA crystallizes as herringbone

arrays, while QDTA adopts a slipped π-stack structure similar to that found for TTTA[15]. The different packing patterns exhibited by NDTA and QDTA provide a striking example of the effect of the presence, or absence, of CH---ring van der Waals interactions.[29] When such structure-making "tilted-T" contacts are possible, as in NDTA, then the well-known close-packed or herringbone arrangement is observed. When the opportunity for such interactions is reduced by CH/N replacement, as in QDTA, then a slipped π-stack structure is favored. In TDTA (**II-28**) there are no CH units at all, and extension of the previous argument would suggest a slipped π-stack structure, as in QDTA and TTTA, [5,15]or perhaps a stacked dimer structure, as in PDTA[13]. In fact, both possibilities are correct.

We have investigated three crystal structures in the course of this thesis work and the selected bond lengths are listed in Table 2.3. The structure of compound **II-25**, the benzenesulfonamide derivative of TDTA, was determined to establish the effect of substitution on ring planarity and to create bench mark bond lengths and angles for comparison with those of the radical (vide infra). The crystal structure consists of discrete molecules of **II-25**, with two molecules per asymmetric unit, differing primarily in the degree of torsion about the N-SO_2Ph bond. Both, save for the substituted nitrogen atoms, are planar within 0.085Å, and the three-atom SNS envelope "flaps" make dihedral angles of 137.89(15) and 143.17(15) with the adjacent SCCS planes. These features are similar to that found in the toluenesulfonamide of 4,5-dicyano-DTA.[8]

The crystal structure of TDTA, based on material grown by fractional sublimation at 110-60°C/10^{-2} Torr, was determined at both 293 and 150 K. These two temperatures are respectively above and below the phase transition observed in the magnetic measurements. While crystal selection and data collection at 293 K was a relatively simple task,

characterization of the low temperature phase was extremely difficult. In most cases the crystals fractured, often violently, upon cooling, and on those occasions when the crystal displayed a sufficient lifetime at low temperature to allow data collection, the intensity of the data was low in comparison to the room-temperature response. The best refinement, the one reported here, is from a partial data set ($\theta_{max} = 21.5$) obtained from a crystal which fractured after 36 hours at 150 K.

As shown in Figure 2.9, at room temperature crystals of TDTA belong to the triclinic space group $P\bar{1}$, with two radicals per unit cell. The space group remains unchanged at 150 K, but the unit cell is dramatically different, containing two dimeric units. At 150 K there are three interannular S---S contacts, all of which are greater than 3.4Å. As such these contacts are significantly longer than the interannular S---S "bonds" in other DTA dimers, e.g., dicyano-DTA (see Figure 2.1), and fall perilously close to the van der Waals separation for two sulfurs (3.6Å).[30] Interestingly, of the three distances the shortest is between the two "tail" sulfurs (S_C---S_C). Dimerization has virtually no effect on the bonds within individual molecules; the bond lengths in the low- and high-temperature structures are almost identical. Dimerization does not lead to any significant puckering of either of the molecular halves, both of which remain planar to within 0.05Å.

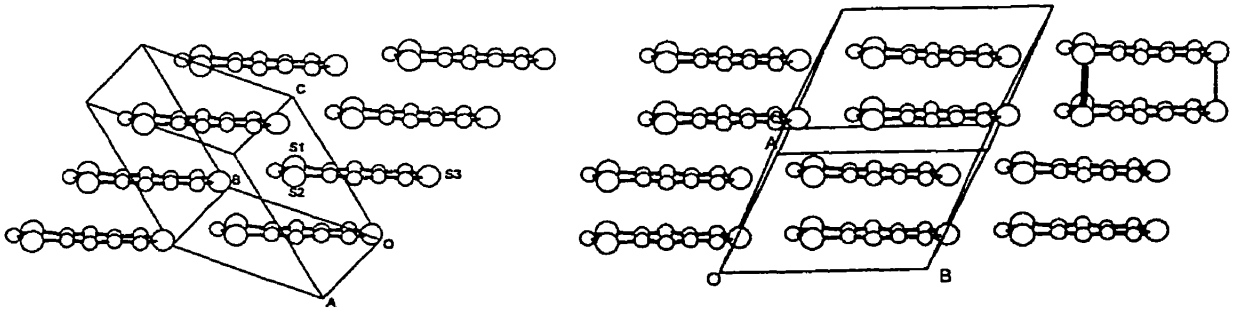

Figure 2.9 Crystal structure of TDTA at 293 K (left) and 150 K (right), respectively.

Table 2.3 . Mean structural parameters (Å) in **II-25** and TDTA (**II-28**) [b]

	II-25	TDTA (**II-28**)	TDTA (**I-28**)
T, K	293	293	150
N_A---S_A	1.73 (3)	1.636 (3)	1.627 (14)
S_A---C_A	1.755 (16)	1.728 (2)	1.73 (3)
C_A---C_A	1.467 (6)	1.448 (2)	1.45 (2)
C_A---N_B	1.297 (3)	1.320 (2)	1.319 (14)
N_B---C_C	1.368 (4)	1.356 (3)	1.357 (15)
C_C---C_C	1.424 (4)	1.447 (2)	1.44 (3)
C_C---N_C	1.333 (10)	1.334 (4)	1.33 (4)
$S_A \cdots S_A$	---	---	3.48 (5)[a]
$S_C \cdots S_C$	---	---	3.401 (5)[a]
N_C---S_C	1.620 (2)	1.620 (8)	1.614 (17)

[a] Intradimer contacts, [b] Atoms grouped by labeled ring as shown below.

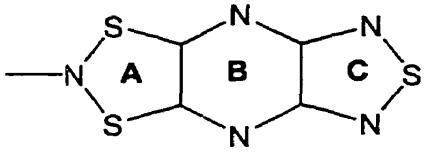

The structural differences observed between TDTA and its sulfonamide derivative **II-25** are largely restricted to the dithiazolyl ring and follow the pattern expected upon reduction of any 1,3,2-dithiazolyl, notably a lengthening of the S---N and S---C bonds.[16, 17] That bond length (shown in Table 2.3) changes extend into the pyrazine ring provides

additional evidence for the extent of delocalization of the SOMO in TDTA. The structures consist of ribbons of radicals (or dimers) layered into slipped π-stacks just like those found in QDTA; only the degree of slippage is more marked in the present case.

At 293 K the lateral slippage between adjacent layers is such that equivalent atoms are separated by 4.454(1) Å, *i.e.*, the unit cell repeat. In the 150 K structure slippage of the dimeric units is similar. For example, the tail sulfur (S_C) of one dimer is 4.556(5) Å from the tail sulfur (S_C) in the dimer above it. Outside of the intradimer S-S contacts already noted there are several short intermolecular (head-to-tail) S---S interactions (3.350(5)Å and 3.357(5)Å).

The association of TDTA radicals at low temperature is not, in itself, a novel finding. Spin pairing by dimerization, *i.e.*, covalent bond formation, is the fate of most sterically unencumbered radicals like most DTDAs. What is interesting in the present system is the fact that the association does not lead to a complete quenching of paramagnetism. Also of interest is the mechanism of the phase transition; how do the two structures interconvert?

In many DTDA systems which we have studied, the stacking of plates has been almost invariably superimposable. Dimerization requires little more than the coupling of the lattice to a charge density wave parallel to the stacking direction, so as to produce the characteristic oscillation in interplanar spacing along the stack.[31] In slipped stacks such as TDTA dimerization requires displacive motion of layers of molecules across the stacking direction rather than along it. The abrupt, almost explosive fracturing of single crystals of TDTA upon rapid cooling is reminiscent of the so-called "jumping crystal" phenomenon described by others.[32] Literature precedent for plate slippage interconversions in molecular crystals are, however, few. The closest analogy that we have found is the so-called

martensitic[33] phase transition observed in ttatt-perhydropyrene.[34]

Our suggested mechanism for the structural interchange in TDTA is built on the premise that lateral displacement or slippage of molecules within the crystals is reversible,[35] as implied by the magnetic behavior, and that the crystal symmetry is maintained throughout the phase transition. Accordingly, the interconversion of the two structures can be envisaged as taking place within the confines of a common P supercell. Analysis of the separate lattices for the two phases of TDTA reveals two similar supercells comprised of eight layers of the 293 K structure and four layers of the 150 K structure (Figure 2.9). The dimensions of these cells are listed in Table 2.4 and three views of the 1,3,2-TDTA packing at 293 K (left) and 150 K (right) are shown in Figure 2.10. Individual layers, or plates, within the *x y* plane of these supercells experience very little internal reorganization, indeed, the a and b vectors and the associated angle are virtually identical. To a first approximation, conversion of the room-temperature lattice into the low-temperature structure can be envisaged as taking place by a series of lateral displacements of these layers along the x direction, in a tectonic platelike fashion. The relative motion of the plates can be understood with reference to the simplified representation shown in Figure 2.11. Accordingly layers 2, 3, and 4 all shift in the same direction but to different extents. The largest shift (over 4Å) is for layer 4. The motion of layers 5, 6, and 7 mirror these movements but in the opposite sense (Figure 2.11), *i.e.*, a large shift for layer 5, with smaller shifts for layers 6 and 7. Insofar as these shifts are in opposite directions, the strain on the structure from the associated sheer forces between layers 4 and 5 must be considerable; the process amounts to a microscopic earthquake! It is not surprising, therefore, that crystals of TDTA tend to shatter easily on cooling, as internal strain builds up in the high temperature structure and then is suddenly released.

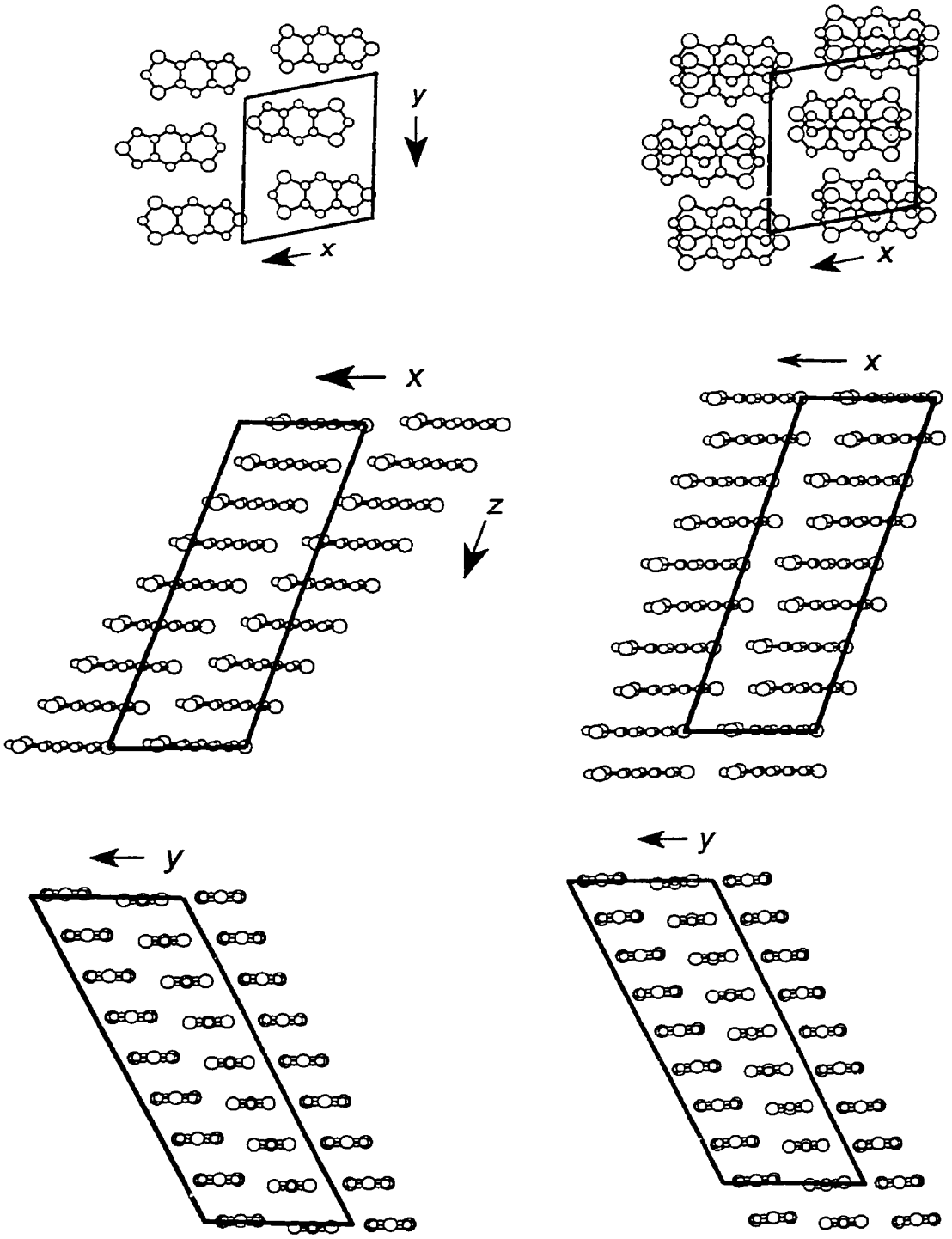

Figure 2.10 Three views of the TDTA packing at 293 K (left) and 150 K (right). Above: sheets of radicals/dimers. Center: ribbons of radicals/dimers. Bottom: end-on view of ribbons. Supercells (see Table 2.4) are shown with heavy lines.

Table 2.4 Supercell vectors [a] and dimensions [b] for TDTA **II-28**.

	293 K		150 K	
a	9.660 (2)	[110]	9.593 (4)	[010]
b	11.408 (4)	[111]	11.300(4)	[101]
c	31.926 (6)	[710]	29.96 (3)	[400]
α	118.78 (2)		113.70(5)	
β	75.68 (2)		74.64 (5)	
γ	77.23 (2)		77.57 (3)	

[a] Supercell vectors expressed relative to standard cell.

[b] The values of a, b, c are in Å; α, β and γ are in deg.

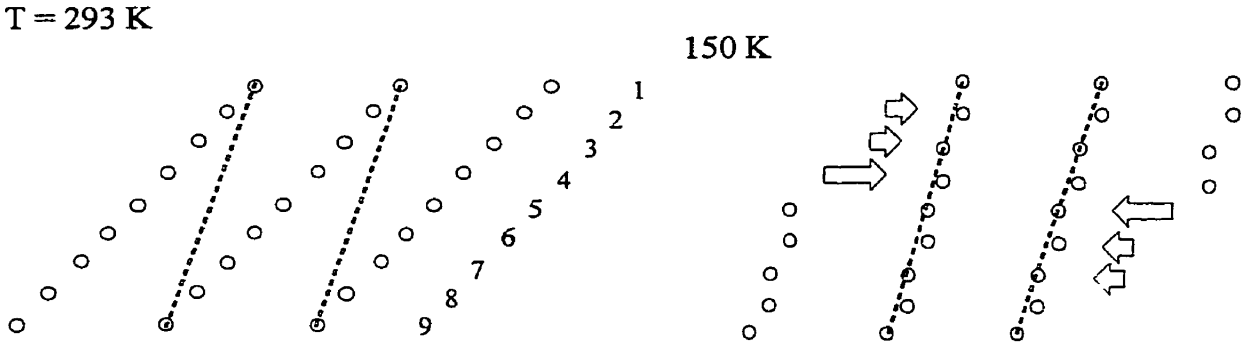

Figure 2.11 Qualitative views of the two phases of TDTA, illustrating the direction and magnitude of "tectonic plate" slippage during the phase transition. The common supercell is shown with dashed lines.

The hysteresis in the magnetic measurements (Figure 2.8) can likewise be attributed to this kinetic effect (see below). That the phase transition failed to occur (at 150 K) on one occasion underscores the importance of structural defects in acting as nucleation sites.

While the one-dimensional model for the motion of layers is conceptually appealing, it is incomplete. The discrepancy in the magnitude of the supercell *c* vectors, and the angles, signals "tectonic plate" motion in the *y* direction as well as along *x*. The extent of motion along *y* is, however, much smaller than along *x*. A refinement of the supercell model, made by doubling the supercell from 8 to 16 layers, produces discrepancies in *c* and α of similar magnitude, but opposite sign. Clearly, an even larger supercell is required for a perfect match, but the conclusions of such a treatment would not differ qualitatively from those resulting from the simple eight-layer model presented here.

About 18 months later after our results were published, the structure of TTTA, **II-8**, was re-examined. It was found that, similar to TDTA **II-28**, it experiences an analogous phase transition (dimerization process) below 200 K. The magnetic susceptibility measurements indicated a first order phase transition with a wide hysteresis loop and sharp changes at the boundary (230 K - 305 K).[16]

2.5 1,2,5-thiadiazolo[3,4-b]-1,3,2-dithiazolo[3,4-b]pyrazino[3,4-b]pyrazin-2-yl, PPDTA, II-37

From NDTA, QDTA, to 1,3,2-TDTA, the experimental results reveal that the fused aromatic residues on 4,5-positions of 1,3,2-DTA can effectively reduce the Coulombic barrier to charge transport. The theoretical prediction on the trend of (IP-EA) values have been confirmed by experiments (cyclic voltametry measurements and theoretical calculations will be discussed in Chapter 3). The more spin density that is stripped away from the DTA ring, the more resistant are the radicals to dimerization. We therefore sought an even larger, more delocalized, target. Given 1,3,2-TDTA as a starting point, we decided to

pursue the four ring system: 1,2,5-thiadiazolo[3,4-b]-1,3,2- dithiazolo[3,4-b]pyrazino[3,4-b]pyrazin-2-yl, simply called PPDTA.

2.5.1 Building the skeleton of PPDTA

In order to build this radical, we decided to expand 1,3,2-TDTA by inserting another pyrazine ring. The diamino derivative **II-30** became the key to succeed. It was well known that fused nitrogen-rich heterocycles can be made by the coupling reaction of diamino and dichloro compounds.[36] The Oakley group has the experience with this system using the diethyloximidate **II-29**.[37] This approach was therefore adopted to fabricate the necessary pyrazino[3,4-b]pyrazine skeleton. The first step was to make the 2,3-diamino functionality (**II-30**) shown in Scheme 2.8.

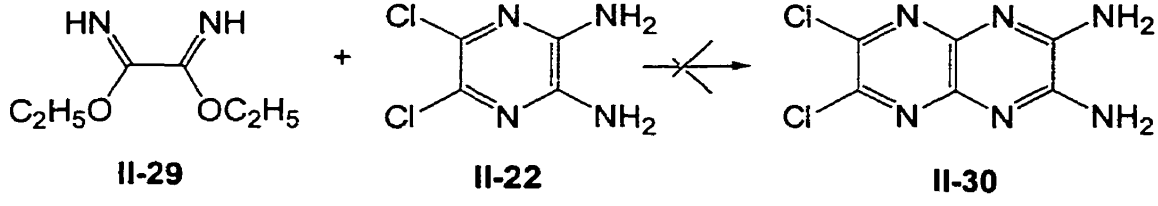

II-29 **II-22** **II-30**

Scheme 2.8

The preparation of diethyl oximidate was not easy. Eventually good quality **II-29** was obtained by careful control of the chlorine bubbling rate, but the expected coupling reaction with 2,3-diamino-5,6-dichloropyrazine (**II-22**) was not successful. After a variety of solvents, catalysts and reaction conditions were tested, no sign of 2,3-diamino-6,7-dichloropyrazino-[2,3-b]-pyrazine (**II-30**) was evident.

On the other hand, the parent pyrazino[3,4-b]pyrazine and its derivatives, such as **II-31** are known. **II-31** has been made from **II-22** with diethyl oxalate and NaOEt in absolute

ethanol[38] or by other methods. [39, 40] We presumed that if 2,3,6,7-tetrachloropyrazino[3,4-b]pyrazine (**II-32**) can be obtained by chlorination of **II-31**, its properties should be similar to those of tetrachloropyrazine (**II-20**). We believed that the key immediate **II-33** should be accessible through the route shown in Scheme 2.9. Compound **II-32** was obtained from **II-31** using PCl_5 in $POCl_3$.[41] However, while tetrachloropyrazine reacts with ammonium hydroxide generating 2,3 and 2,6-diamino isomers, the anologous reaction of **II-32** with ammonium hydroxide was unsuccessful. **II-32** is more reactive than tetrachloropyrazine to nucleophile reagents such as ammonium hydroxide. Multiple substitution seems to be unavoidable. Later we explored potassium phthalimide. However, even under carefully controlled conditions, a mixture of mono, di, tri and even tetramino derivatives was generated. Faced with this problem we decided to pursue another approach, using the intermediate **II-23** (from the 1,3,2-TDTA project) as an entry point.

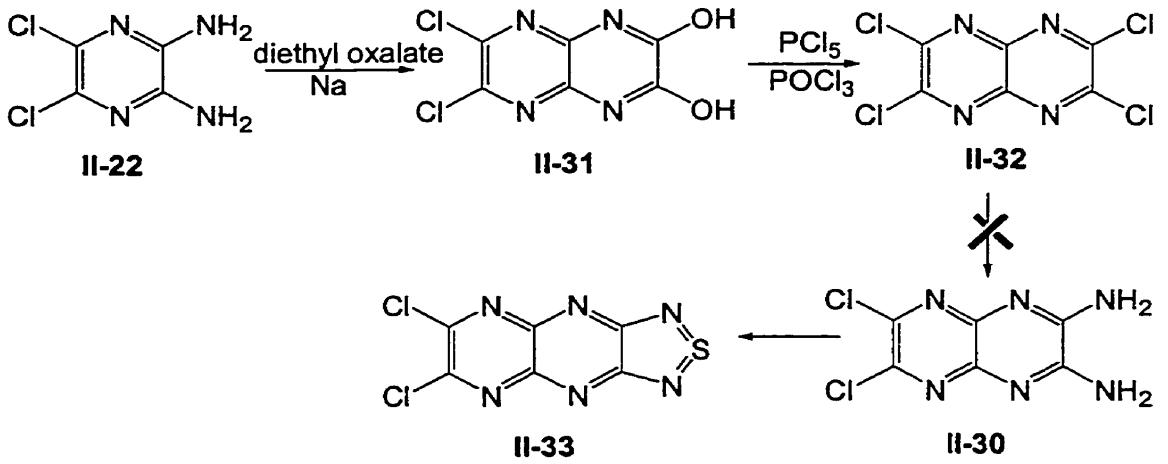

II-22 **II-31** **II-32** **II-30** **II-33**

Scheme 2.9

As shown in Scheme 2.10, 5,6-diamino-1,2,5-thiadiazolo[3,4-b]pyrazine (**II-34**) was prepared by the standard method,[42] and the fusion and derivation of the second pyrazine ring[38] (**II-35**) and dichloroPP derivative (**II-33**) also worked well. The preparation of the

dithio derivative (**II-36**) was similar to that in the synthesis of TDTA.

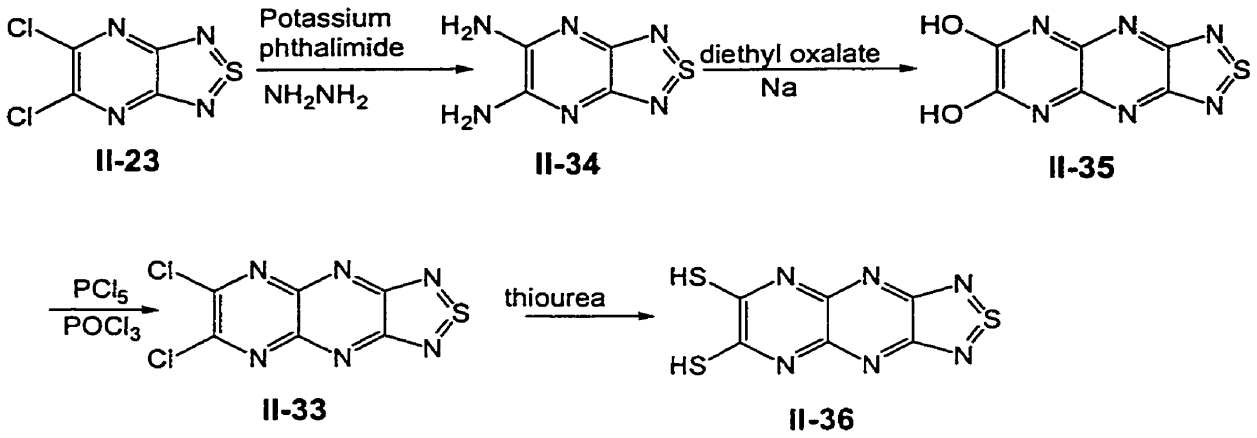

II-23 **II-34** **II-35**

II-33 **II-36**

Scheme 2.10

2.5.2 Formation of 1,3,2-DTA ring

Attempts to generate the desired PPDTA using the reaction of **II-36** and $S_3N_3Cl_3$ as we had done for TDTA,[43] met with mixed success. Numerous experiments were done and the sublimed products were analyzed by DEI mass spectrometry, but always the $[M+1]^+$ peak dominated. We therefore believed that we had formed the imide **II-38** rather than the desired radical.

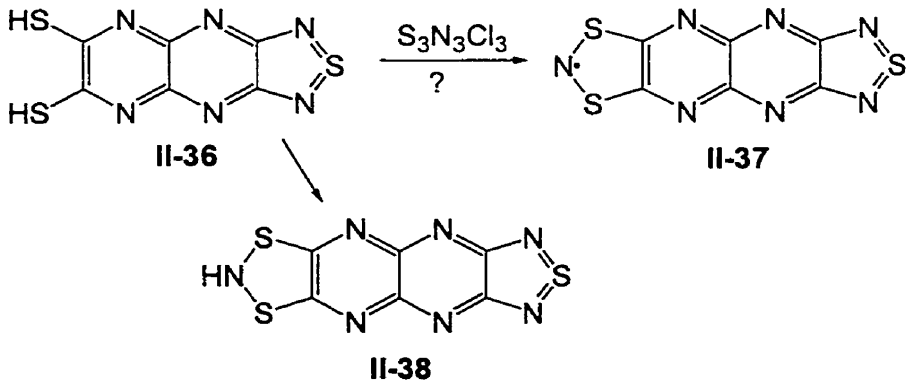

II-36 **II-37**

II-38

1,3,2-DTAs are relatively open systems. The fused aromatic structures greatly reduce the spin density on DTA ring. Especially in 1,3,2-TDTA, for example, 1,2,5-dithiazolo[3,4-

b]pyrazino group is very powerful electron-withdrawing group, resulting in a very high IP value. By way of comparison, while NDTA is extremely sensitive to air, the cation state of TDTA is not favored. In fact, the TDTA radical is stable under the strong oxidizing reagent $S_3N_3Cl_3$. Theoretical calculations predict that PPDTA (**II-37**) has an even higher IP value and therefore the cation and even radical states are, we presume, hard to access.

This project cost us much time. From the commercially available starting material 2-chloropyrazine, more than ten steps were required. We therefore moved away from 1,3,2-DTAs altogether, and began to focus on their 1,2,3-isomers which, for reasons to be discussed in Chapter 3, we believed were inherently better targets.

2.6 Summary and conclusions

A range of synthetic methods now exists for the attachment of the 1,3,2-DTA radicals to organic and heterocyclic frameworks. In contrast to the behavior of 1,2,3,5-DTDA radicals, the redox chemistry of the DTA residue is markedly dependent on the donor/acceptor properties of the rest of the molecule. The shift in reduction potentials between NDTA and TDTA is over 1 V. More importantly the attachment of extremely electron withdrawing substituents, as in TDTA, leads to a decrease in the cell potential corresponding to the disproportionation energy of the radical. This decrease can be related to a lower barrier to charge transport between radical centers in the solid state and augurs well for the use of DTA derivatives in the design of single component neutral radical conductors. The crystal structure of TDTA at 298 K consists of slipped π-stacks. However, while this configuration formally fulfills the structural criteria for a neutral π-radical conductor, *i.e.*, evenly spaced plates, charge correlation effects still outweigh the electronic

stabilization afforded by interannular orbital overlap, and the material remains a Mott insulator, with a pressed pellet conductivity $<10^{-6}$ S cm^{-1}. It is not difficult, however, to imagine more extended heterocyclic frameworks in which the ΔH_{disp} is further diminished by increasing the value of EA, and we are certainly pursuing the design and synthesis of such materials. An electronegative molecular metal, akin to the polymer $(SN)_x$,[44] may be possible. The major solid-state reorganization that accompanies the dimerization of TDTA represents, to our knowledge, the first full characterization of such a process for a slipped π-stack structure. While the magnetic susceptibility changes that accompany the phase change, *i.e.*, the reduction in free spins, are clearly understandable in terms of the observed solid-state rearrangement, it is noteworthy that some paramagnetism persists after dimerization and that the structure is a ground state antiferromagnet. This observation suggests that the intermolecular resonance interaction between the radical halves of the dimer is extremely weak, comparable to the magnitude of the exchange interaction between the two unpaired electrons.

2.7 Experimental section

Preparation of 2,3-dithionaphthalene, II-12 [18]

100 mL of cyclohexane and TMEDA (44 mL, 292 mmol) were added to a 1L round-bottomed flask and cooled to 0°C in an ice bath. Under an atmosphere of N_2, butyllithium (177 mL, 283 mmol) was introduced via a syringe to a dropping funnel and then added to the flask. A solution of 2-naphthalenethiol (14.97 g, 93.6 mmol), dissolved in 90 mL of cyclohexane was then added dropwise to this solution. When the addition was finished, the ice bath was removed and the slurry was allowed to stir overnight at room temperature.

Sulfur (8.99g, 280 mmol) was added to the orange slurry at room temperature; and the slurry turned pale yellow and the flask became quite warm. The mixture was stirred overnight. The cyclohexane was removed *in vacuo* and replaced with 150 mL of distilled THF. To this red solution, $LiAlH_4$ (3.53 g, 93.4 mmol) was slowly added. The red solution turned dark yellow and was gently refluxed overnight. The next day the heating mantle was removed and the solution was cooled with an ice bath. 400 mL of aqueous HCl (2.5 M) was poured onto the above solution and the pH value adjusted to *ca.* 1. This acidic solution was extracted with 2 × 500 mL of ether and the organic layers were combined, washed with 2 × 200 mL of HCl (5%) and 300 mL of brine solution. The organic phase was dried over $MgSO_4$ for 30 minutes and then rotary evaporated to a yellow solid. It was recrystallized from toluene twice and sublimed as a white crystalline solid . Yield. 6.0 g, 31 mmol, 33%. ^1H NMR ($CDCl_3$) 7.88 (s, 2H), 7.65 and 7.40 (AA'BB', 4H), 3.86 (s, 2H). IR (4000-400 cm^{-1}): 3051 (w), 2557 (w), 1570 (w), 1500 (w), 1315 (m), 1256 (w), 871 (m), 802 (m), 766 (w), 527 (w), 479 (w) cm^{-1}.

Preparation of Naphthalene-2,3-bis(sulfenyl chloride), II-13.

Freshly prepared iodobenzene dichloride (4.88 g, 17.8 mmol) was slowly added portionwise to a stirred solution of naphthalene-2,3-dithiol, **II-12**(1.55 g, 8.1 mmol) in 50 mL of CH_2Cl_2 at 0°C, and the resulting mixture allowed to warm slowly (2 h) to room temperature. The solvent was then removed in *vacuo* from the filtrate to leave a yellow crystalline solid that was recrystallized from 15 mL CH_3CN to give naphthalene-2,3-bis(sulfenyl chloride), **II-13** (1.62 g, 6.2 mmol, 77%). mp, 90-93°C. IR (1600-400 cm^{-1}) 1618 (w), 1569 (m), 1311 (w), 971 (w), 899 (w), 880 (s), 770 (w), 755 (vs), 722 (w), 470 (s) cm^{-1}. ^1H NMR ($CDCl_3$) 8.1 (s, 2H), 7.85 and 7.55 (AA'BB', 4H). Anal.

calcd for $C_{10}H_6NS_2Cl_2$: C, 45.99, H, 2.32; Cl, 27.15. Found: C: 46.17; H, 2.40; Cl, 27.40.

Preparation of Naphthalene-2,3-(1,3,2-dithiazolyl), NDTA, II-15.

A solution of trimethylsilyl azide (0.55 g, 4.8 mmol) in 10 mL of CH_2Cl_2 was added dropwise to a stirred solution of naphthalene-2,3-bis(sulfenyl chloride), **II-13** (1.2 g, 4.6 mmol) in 40 mL CH_2Cl_2. Slow bubbling of N_2 was observed, and the solution changed to a dark red color. A cherry red precipitate of naphthalene-2,3-(1,3,2-dithiazolylium chloride) **II-14** was also produced. After 2 h the solid was filtered off, washed with 2 × 20 mL CH_2Cl_2, and dried in *vacuo*. IR (1600-400 cm^{-1}) 1557 (w), 1350 (w), 1323 (w), 1264 (m), 1154 w), 1073 (m), 965 (w), 883 (s), 801 (w), 783 (m), 750 (s), 601 (w), 551 (w), 429 (w), 477 (m), 429 (m) cm^{-1}. This crude salt was slurried in 60 mL of CH_3CN and reduced by the addition of a solution of triphenylantimony (0.81 g, 2.3 mmol) in 10 mL CH_3CN at 0°C. After 1 h the crude product was filtered off and dried in *vacuo*. Purification was effected by fractional sublimation at 80-50°C/10^{-2} Torr, to afford purple plates of NDTA, **II-15** (0.28 g, 1.4 mmol, 30% based on bis(sulfenyl chloride)), mp 149-50°C. IR (1600-400 cm^{-1}) 1315 (w), 1269 (w), 1195 (w), 874 (vs), 767 (s), 700 (s), 693 (m), 480 (m), 470 (w) cm^{-1}. MS (m/z): 204 (M^+, 100%), 158 ([M-NS]$^+$, 15%), 140 (6%), 114 (11%), 102 12%), 69 (4%). Anal. calcd for $C_{10}H_6NS_2$: C, 58.80, H, 2.96; N, 6.86. Found: C, 59.03; H, 3.12; N, 6.83.

Preparation of 2,3-dithioquinoxaline, II-16 [22]

In the 500 mL side-armed RBF, the 2,3-dichloroquinoxaline (16.8 g, 84 mmol) and thiourea (33.4 g, 440 mmol) in 250 mL of anhydrous ethanol were heated to reflux under

N_2. The orange clear solution turned to a yellow slurry after reflux about half an hour. 2 hours later, the slurry was left to room temperature and poured to 500 mL of aqueous KOH (40 g) solution. The resulting orange solution was heated to gentle boiling for a while, then acetic acid was added to neutralize the base and generate the brown precipitate of 2,3-dithioquinoxaline. The precipitate was filtered off, washed with large amount of water and air dried for next step. Yield: (15.65 g, 80 mmol, 95%). Different batches gave yields ranging from 75%- 95%. mp. >250°C. IR (4000-400 cm^{-1}): 3083 (br, w), 1629 (w), 1607 (m), 1559 (w), 1502 (m), 1482 (s), 1360 (s), 1325 (s), 1252 (m), 1147 (s), 1059 (m), 829 (s), 739 (s), 621 (s), 594 (s), 524 (s) cm^{-1}.

Preparation of N-benzenesulfonamide-1,3,2-dithiazolo[4,5-b]quinoxaline, II-17. [8]

N,N-dichlorobenzenesulfonamide (5.8 g, 31 mmol) was added in one portion to a 250 mL side-armed RBF containing, 2,3-dithioquinoxaline **II-16** (5.0 g, 26 mmol) in 75 mL of ether. The slurry so formed was allowed to stir overnight. The solid was filtered, washed with 50 mL of acetonitrile and dried in vacuum. The followed recrystallization from chlorobenzene gave yellow crystals (6.08 g, 18 mmol, 68%). mp. 191°C (lit. 195°C). IR (4000-400 cm^{-1}): 1580(w), 1556(w), 1305(w), 1300(w), 1178(m), 1159 (s), 1129(s), 1084(m), 821(m), 780(w), 779(s), 747(s), 683(s), 597(s), 568(s), 497(w), 467(w), 415(s) cm^{-1}.

Preparation of 1,3,2-dithiazolo[4,5-b]quinoxaline, QDTAH, II-18.

Anhydrous ammonia gas was gently bubbled through a slurry of sulfonamide **II-17**

(2.00 g, 5.76 mmol) in 100 mL of CH_2Cl_2 held at 0°C, to produce an off-white thick precipitate in a green solution. After 15 min the gas flow was halted, and the precipitate of benzenesulfonamide filtered off. The solvent was removed in *vacuo* from the filtrate, and the residual solid extracted with 100 mL of warm toluene (under nitrogen). The mixture was again filtered (to remove residual benzenesulfonamide), and the solvent was again removed in *vacuo*. The yellow green product (0.91 g, 4.4 mmol, 76%) was recrystallized from hot ethanol as pale yellow needles of QDTAH **II-18**, dec 122-24°C. IR: (NH) 3168 cm^{-1} and (1600-400 cm^{-1}): 1559 (w), 1247 (w), 1161 (m), 1130 (w), 1092 (m), 1016 (w), 1008 (w), 932 (m), 770 (m), 757 (s), 669 (w), 643 (m), 595 (m), 466 (w), 412 (m) cm^{-1}. ^1H NMR ($CDCl_3$): 4.89 (s, NH), 7.62 and 7.86 (AA'BB', 4H). MS (m/z): 206 (M^+, 100%,), 160 ([M - NS]$^+$, 61%), 102 (33%), 77 (21%), 51(18%). Anal. calcd for $C_8H_5N_3S_2$: C, 46.36, H, 2.43; N, 20.27. Found: C, 46.53; H, 2.27, N, 20.06.

Preparation of 1,3,2-dithiazolo[4,5-b]quinoxalin-2-yl, (QDTA), II-19 [8]

Crude QDTAH **II-18**, prepared as described above from the sulfonamide **II-17** (2.18 g, 6.3 mmol), was dissolved in 100 mL of CH_2Cl_2, the solution was treated with a solution of potassium ferricyanide (2.0 g, 6.1 mmol) in 100 mL of H_2O, and the two-phase mixture was vigorously stirred for 8 h. The dark blue organic layer was then separated, dried over sodium sulfate, and evaporated to dryness to leave QDTA **II-19** as a blue/black crystalline solid (1.0 g, 4.8 mmol, 77% from sulfonamide). The product was purified by fractional sublimation over the range 90-45°C/10^{-2} Torr to yield black needles, mp. 137-140°C (lit. 132°C). IR (4000-400 cm^{-1}): 1546 (w), 1168 (m), 1137 (w), 1108 (w), 1016 (w), 955 (w), 752 (s), 693 (w), 598 (w), 595 (w) cm^{-1}.

Preparation of Tetrachloropyrazine, II-20 [24]

Commercially obtained 2-chloropyrazine (15 g, 131 mmol) and phosphorus pentachloride (110 g, 528 mmol) were put in a PARR bomb reactor and heated at 280°C for 16 hours. The reactor was then cooled to room temperature, and the HCl gas generated during the reaction slowly released. The residual PCl_5 was destroyed by adding H_2O to the bomb carefully. The pale yellow solid was extracted by 3 × 250 mL ether and the combined extracts dried over anhydrous $MgSO_4$ for 30 min. Rotary evaporation gave a white crystalline crude product; white plate-like crystals were grown by recrystallization from methanol. Yield (25 g, 114 mmol, 87%). mp, 100°C (lit. 99°C). IR (1600-400 cm^{-1}): 1412 (w), 1316 (s), 1304 (s), 1218 (w), 1197 (w), 1159 (s), 1075 (s), 1045 (m), 658 (s), 475 (m) cm^{-1} .

Preparation of 2,3-diamino-5,6-dichloropyrazine II-21 [25]

150 mL of commercial ammonium hydroxide (28-30% w/w) was added to tetrachloropyrazine, **II-20** (20 g, 92 mmol) in the bomb reactor and heated to 140°C for 16 hours. The reactor was cooled to room temperature; the pale yellow crystals were filtered off and washed with H_2O. The crude product was a mixture of 2,3-diamino-5,6-dichloropyrazine **II-21** and 2,6-diamino-3,5-dichloropyrazine **II-22** (total: 13 g, 72 mmol, 78%) in an approximately 1:1 ratio. Separation of the isomers was achieved by using methyl ethyl ketone (MEK) as recrystallization solvent.[26] Thus the mixture (10 g, 46 mmol) was dissolved in boiling MEK (100 mL). After hot filtration to remove any insoluble material, the solution was allowed to sit in the freezer for an hour. The recrystallized yellow solid was filtered and dried in the oven with the total recovery of 33% of 2,3-diamino-5,6-

dichloropyrazine **II-21** from tetrachloropyrazine. Characterization: **II-21**, mp. >250°C. IR (4000-400 cm-1): 3439 (s), 3291 (m), 3202 (m), 1629 (s), 1537 (w), 1499 (s), 1332 (s), 1224 (w), 995 (s), 670 (m), 434 (s). **II-22**, dec. 212°C (lit. 218-220°C), IR (4000-400 cm-1): 3489 (m), 3464 (m), 3390 (m), 3308 (w), 3166 (w), 1641 (s), 1610 (s), 1554 (m), 1534 (m), 1351 (w), 1324 (w), 1248 (s), 1115 (m), 1069 (m), 745 (m), 479 (w) cm^{-1}. These two isomers can not be separated by TLC with CH_2Cl_2, However TLC works well with ether as eluent. (R_f for **II-21**: 0.39 and R_f for **II-22**: 0.63).

Preparation of 5,6-dichloro-1,2,5-thiadiazolo[3,4-b]pyrazine, II-23 [27]

Isomeric mixtures of 2,3-diamino-5,6-dichloropyrazine **II-21** and 2,6-diamino-3,5-dichloropyrazine **II-22** (15.4 g, 86 mmol) were used for a large scale reaction with $SOCl_2$ (22.6 g, 190 mmol) in 300 mL of xylene. This slurry was refluxed with the catalyst of 1 mL of pyridine for 7 hours under the N_2. The dark red slurry was allowed to evaporate in the fumehood and the residue extracted with 500 mL of methylene chloride. These extracts were passed through a short silica column, and the solvent removed (rotary evaporator) to afford a yellow solid which was recrystallized from ethyl acetate to give pale yellow plate-like crystal of **II-23**, (6.84 g, 33 mmol, 38.4%). If the pure 2,3-diamino isomer **II-21** was used instead, up to 80% yield was achieved. mp, 180°C (lit. 180-2°C). IR (1600-400 cm^{-1}): 1524 (m),1309 (w), 1255 (s), 1179 (s) (s), 1039 (m), 1008 (s), 892 (s), 940 (s), 711 (m), 663 (m), 550 (s), 458 (s) cm^{-1}. MS (EI, m/e): 206 (M^+, 100%), 171 ($[M-Cl]^+$, 84%), 119 (10%), 93 (23%), 58 (25%).

Preparation of 5,6-dithio-1,2,5-thiadiazolo[3,4-b]pyrazine, II-24

A mixture of 5,6-dichloro-1,2,5-thiadiazolo[3,4-b]pyrazine **II-23** (6.3 g, 30 mmol) and thiourea (13.9 g, 183 mmol) in 120 mL of anhydrous ethanol were refluxed for 2 hours. The brown red slurry so formed was filtered, and the product dissolved in 300 mL of aqueous 1M NaOH solution to give a clear red solution. The dithiol derivative was reprecipitated by the addition of aqueous acetic or hydrochloric acid solution, washed by a large amount of water, and dried in the oven, yield: 5.05 g, 24 mmol, 81%. MS (EI, m/e): 202 (M^+, 100%), 169 ($[M-SH]^+$, 13%), 143 (25%), 116 (29%), 85 (70%), 58 (45%), 45 (54%). IR (4000-400 cm^{-1}): 3500-3050 (mw), 1542 (m), 1321 (m), 1264 (m), 1219 (m), 1131 (m), 834 (m), 808 (m), 751 (m), 667 (m), 618 (m), 544 (m), 505 (m) cm^{-1}. Dimethyl derivative was prepared for characterization. IR (4000-400 cm^{-1}): 1508 (m), 1316 (m), 1250 (w), 1151 (s), 1048 (s), 976 (w), 873 (s), 811 (s), 654 (m), 545 (s), 440 (m) cm^{-1}. MS (EI, m/e): 230 (M^+, 48%), 215 ($[M-CH_3]^+$, 100%), 200 ($[M-2\ CH_3]^+$, 22%), 116 (17%). Anal. calcd for $C_6H_6N_4S_3$:C, 31.32%, H, 2.79%, N, 24.36%. found: C, 31.29%, H, 2.63%, N, 24.33%.

Preparation of $TDPS_2TiCp_2$, II-26.

Dithiol derivative **II-24** (1.50 g, 7.4 mmol) was added to a solution of sodium ethoxide prepared from sodium (0.34 g, 14.8 mmol) and anhydrous ethanol (30 mL). The resulting slurry was stirred under N_2 for 90 minute, and then the solid filtered off and dried in *vacuo* to yield the crude red-brown disodium salt (1.70 g, 6.9 mmol). This solid was added to 100 mL of CH_3CN, and finely powdered Cp_2TiCl_2 (1.72 g, 6.9 mmol) was slowly added to the stirred mixture. The red-brown solid was slowly converted into a dark green solid. After 15 hours the crude product was filtered off, and Soxhlet extracted exhaustively (72 h)

with CH_2Cl_2. Addition of toluene to the extracts and slow rotary evaporation of the dark green solution afforded green black microcrystals of $TDPS_2TiCp_2$ **II-26** (1.06 g, 2.8 mmol, 42%), mp > 300°C. IR (1600-400 cm^{-1}), 1379 (m), 1351 (m) 1309 (w), 1248 (w) 1114 (s), 1083 (br, w), 937 (br, w), 882 (m), 829 (br, s), 816 (m), 731 (br, w), 652 (m), 626 (w), 558 (w), 444 (w), 411 (m) cm^{-1}. Anal. calcd for $C_{14}H_{10}N_4S_3Ti$: C, 44.45; H, 2.66; N, 14.81. Found: C, 44.61; H, 2.63, N, 14.48. ^1H NMR (D-$CDCl_3$): 5.28 (s, 5H), 6.02 (s, 5H).

Preparation of Sulfonamide derivative, II-25.

N,N-Dichlorobenzenesulfonamide (0.39 g, 1.7 mmol) was added to a slurry of **II-26** (0.65 g, 1.7 mmol) in 75 mL of CH_3CN. The green solution immediately turned red-brown. After 2 h at room temperature the mixture was filtered, and the filtrate evaporated to dryness in *vacuo* to leave a mixture Cp_2TiCl_2 (red) and a yellow crystalline material. This mixture was extracted with 50 mL of warm toluene and the extract evaporated to leave a solid which was dissolved in 50 mL of warm CH_3CN. The solution was then cooled to 0°C overnight. Subsequent filtration afforded yellow needles of the benzenesulfonamide **II-25** (0.30 g, 0.80 mmol, 49%), mp 184-86°C. Transparent yellow blocks suitable for X-ray work were grown by sublimation at 130-80° C/10^{-2} Torr. IR (1600-400 cm^{-1}): 1582 (w), 1403 (w), 1324 (w), 1313 (w), 1296 (w), 1250 (w), 1195 (w), 1175 (s), 1171 (s), 1129 (m), 818 (m) 813 (m), 781 (s), 757 (s), 726 (s), 689 (s), 637 (m), 599 (s), 569 (s), 549 (s), 494 (w), 472 (m), 424 (w) cm^{-1}. MS (EI, m/e): 355 (M^+, 16%), 291 ($[M - SO_2]^+$, 8%), 214 ($[M - SO_2Ph]^+$, 100%), 141 (SO_2Ph^+, 64%), 77 ($C_6H_5^+$, 100%). Anal. calcd for $C_{10}H_5N_5O_2S_4$: C, 33.79; H, 1.42; N, 19.70. Found: C, 33.87; H, 1.44; N, 19.81.

Preparation of 1,3,2-TDTA radical, II-28

Solid $S_3N_3Cl_3$ (1.50 g, 6.1 mmol) was added to a slurry of the dithiol **II-24** (1.20 g, 5.9 mmol) in 50 mL of CH_3CN, and the mixture was heated at a gentle reflux for 4 h. The resulting mixture, a red solution and a dark brown solid, was filtered, and the solid dried in *vacuo*. IR analysis of this mixture revealed the presence of neutral TDTA and the salt S_4N_3Cl (by comparison of its IR spectrum with that of a known sample[45]). The latter was removed by reducing the whole with excess Ph_3Sb (1.06 g, 3.0 mmol) in refluxing CH_3CN for 30 min (this effected the conversion of S_4N_3Cl to the more soluble S_4N_4). Hot filtration then afforded black microcrystals of TDTA **II-28** which were purified by fractional sublimation over the range 110-60°C/ 10^{-2} Torr as lustrous black needles (0.56 g, 2.6 mmol, 44%), dec. >186°C. IR (1600-400 cm^{-1}), 1429 (w), 1379 (w), 1316 (br, m), 1246 (w), 1136 (w), 906 (w), 880 (m), 867 (m), 805 (s), 713, 694 (m), 665 (m), 641 (w), 534 (s), 503 (s), 426 (m) cm^{-1}. MS (EI, m/e): 214 (M^+, 85%), 168 ([M - SN]$^+$, 7%), 78 (S_2N^+, 15%), 46 (SN^+, 100 %). Anal. calcd for $C_4N_5S_3$: C, 22.42; N, 32.69. Found: C, 22.91; N, 33.01.

Preparation of 2,3-dihydroxy-6,7-dichloro-pyrazino[2,3-b]-pyrazine, II-31 [38]

In 100 mL side armed flask, 2,3-diamino-5,6-dichloropyrazine **II-22** (1.5 g, 8.4 mmol) and diethyl oxalate (1.35 g, 9.3 mmol) in 50 mL of freshly made absolute ethanol were heated to boiling. Sodium (0.42 g, 18.7 mmol) ethoxide solution (10 mL) was added slowly through dropping funnel. The slurry was then allowed to reflux for two hours. The content of the flask was poured to 10% aqueous HCl to precipate the product (1.1 g, 5.2 mmol, 56%). mp. >250°C. IR (4000 - 400 cm^{-1}): 3259(w), 1726(s), 1706(s), 1580(m), 1494(s), 1401(m), 1338(m), 1291(m), 1232(s), 1218(s), 1022(s), 912(w), 828(w), 699(s),

657(m), 557(m), 504(m), 487(m), 446(m) cm^{-1}. MS (EI, m/e): 232 (M^+, 100% with correct DCl isotope pattern), 204 ($[M-CO]^+$, 68%), 176 ($[M-2CO]^+$, 28%), 150 (15%).

Preparation of 2,3,6,7-tetrachloropyrazino[3,4-b]pyrazine, II-32

Phosphorus pentachloride (8.23 g, 39.5 mmol) and dihydroxy derivative **II-31** (2.27 g, 10.2 mmol) were stirred with 60 mL of $POCl_3$ under nitrogen. The red slurry was refluxed for 3 hours to produce a red clear solution. The $POCl_3$ was removed *in vacuo* and crushed ice carefully added to destroy excessive PCl_5. After filtration and washing with water, the crude product (2.30 g) was recrystallized from toluene (100 mL); yield 1.9 g, 28 mmol, 72%. mp. 165°C (sublime), IR (1600-400 cm^{-1}): 1571(w), 1545(w), 1403(s), 1268(s), 1144(s), 1006(s), 803(m), 722(w), 626(s), 533(s), 520(s) cm^{-1}. MS (EI, m/e): 270 ($[M+2]^+$, 100%), 268 (M^+, 86%), 233 ($[M-Cl]^+$, 25%), 172(53%).

Preparation of 5,6-diamino-1,2,5-thiadiazolo-[3,4]-pyrazine, II-34 [27, 42]

Potassium phthalimide (7.5 g, 40 mmol) was added to a 250 mL RBF containing 5,6-dichloro-1,2,5-thiadiazolo[3,4-b]pyrazine **II-23** (4.2 g, 20 mmol) dissolved in 100 mL of DMF, and the resultant red brown slurry stirred at room temperature for 18 hours. The slurry was poured into 200 mL of water. The yellow precipitate so formed was filtered and washed with water. Hydrazine hydrate (98%, 20 mL) was added to a slurry of this yellow powder in 100 mL of water held at 0°C. The mixture was kept at 0°C and then warmed to room temperature for an hour. The brown solid (3.5 g) was filtered, dried and used directly for the next step. Later it was found that this compound can be prepared by bubbling NH_3

gas to **II-23** in boiling toluene. Purification was achieved by recrystallization from ethanol. mp, > 250°C. IR (4000-400 cm^{-1}): 3425 (w), 3384 (w), 3340 (w), 1686 (s), 1647 (s), 1528 (s), 1111 (m), 861 (s), 795 (s), 663 (s), 543 (br, s), 440 (m) cm^{-1}. MS (EI, m/e):168 (M^+, 100%), 141 ($[M-HCN]^+$, 48%), 99 (18%), 84 ($[C_2N_2S]^+$, 15%), 68 (90%).

Preparation of 2,3-dihydroxy-1,2,5-thiadiazolo[3,4-b]pyrazino[3,4-b]pyrazine, II-35

This compound was prepared in a manner similar to that described in the literature.[41] Sodium (0.83 g, 36 mmol) was added to 20 mL of anhydrous ethanol (distilled from Mg) in a dropping funnel. The resultant solution was slowly added to a slurry of diamino **II-34** (2.64 g, 15.7 mmol) and diethyl oxalate (2.64 g, 18 mmol) in 50 mL of freshly distilled anhydrous ethanol. After the addition was completed, the brown slurry was allowed to reflux for 4 hours. The content of the reactor was poured into 100 mL of 10% aqueous HCl. The bright brown solid was filtered and dried at 70°C overnight. Yield: (2.92 g, 13 mmol, 84%). mp. 179°C, IR (4000-400 cm^{-1}): 3434(bm), 1736(s), 1715(s), 1418(m), 1310(m), 969(w), 903(m), 820(m), 770(m), 721(w), 691(w), 631(m), 550(m), 520(m), 480(w), 454(m) cm^{-1}. MS (EI, m/e): 222 (M^+, 90%), 194 ($[M-CO]^+$, 60%), 166 ($[M-2CO]^+$, 26%), 99 (52%), 72 (52%), 67 (45%), 53 (97%), 46 (100%).

Preparation of 2,3-dichloro-1,2,5-thiadiazolo[3,4-b]pyrazino[3,4-b]pyrazine, II-33

Dihydroxy derivative **II-35** (2.8 g, 12.6 mmol) and PCl_5 (11.0 g, 52.8 mmol) were refluxed 4 hours in $POCl_3$ (40 mL). The solvent was then removed *in vacuo* and crushed ice slowly added to the residue in order to destroy residual PCl_5. The precipitate was filtered and

washed with water. The crude product was recrystallized from chlorobenzene. Yield (1.88 g, 31 mmol, 58%). mp. 247°C (dec), IR (4000-400 cm^{-1}): 1715 (w), 1511 (w), 1352 (s), 1263 (s), 1238 (m), 1213 (m), 1173 (s), 1158 (s), 1010 (s), 954 (s), 924 (s), 785 (w), 723 (w), 560 (m), 540 (m), 496 (s), 435 (w) cm^{-1}. Anal. calcd for $C_6N_6Cl_2S$: C, 27.80; N, 32.43. Found: C, 27.88; N, 32.43. MS (EI, m/e): 262 ($[M+4]^+$, 16%), 260 ($[M+2]^+$, 74%), 258 (M^+, 100%), 223 ($[M-Cl]^+$,33%), 171 ($[M-ClC_2N_2]^+$, 31%), 87 (48%).

Attempt of preparation of PPDTA, II-37

Dichloro derivative **II-33** (1.73 g, 6.8 mmol) and excessive thiourea (3.05 g, 39 mmol) were stirred in refluxing anhydrous ethanol for 2 hours. The red slurry was hot filtered to remove most of thiourea and the mixture then hydrolyzed with NaOH. Acidification with acetic acid afforded the product **II-36** (0.87 g, 51%). Dithiol derivative **II-36** and two equivalent $S_3N_3Cl_3$ was refluxed in CH_3CN overnight and the dark red precipitate was filtered and pumped dry. The sublimed product (230°C/ 10^{-4} torr) was analyzed by MS (DEI, m/e): 267 ($[M+H]^+$, 68%), 250 (100%), 239 ($[M-N_2]^+$ 14%), 233 (25%), 194 (13%). (CI, m/e): 268 ($[M+2H]^+$, 100%), 251 (44%), 240 (9%), 222 (8%), HRMS : for $[M+H]^+$, found, 266.947900, calcd 266.94555600. MS (CI, m/e), 267 (M^+, 9%), 250 (49%), 223 (12%), 43 (100%). IR (1600-400 cm^{-1}): 1570 (w), 1531(w), 1419 (w), 1303 (w), 1270 (w), 1069 (w), 908 (w), 841 (w), 782 (w), 737 (s), 681 (w), 634 (w), 543 (w), 534 (w), 517 (m), 448 (w) cm^{-1}.

2.8 References

1. (a) Lee, F. L.; Preston, K. F.; Williams, A. J.; Sutcliffe, L. H.; Banister, A. J.; Wait, S. T. *Magn. Reson. Chem.* **1989**, 27, 1161. (b) Markovski, L. N.; Polumbrik, O. M.; Talanov, V. S.; Shermolovich, Y. G. *Tetrahedron, Lett.* **1982**, *23*, 761. (c) Fairhurst, S. A.; Sutcliffe, L. H.; Preston, K. F., Banister, A. J.; Partington, A. S.; Rawson, J. M.; Passmore, J.; Schriver, M. J. *Magn. Reson, Chem.* **1993**, *31*, 1027.
2. SOMO pictures of 1,3,2- and 1,2,3-DTA are drawn based on the theoretical calculated data.
3. Parsons, S.; Passmore, J.; Schriver, M. J.; Sun, X. *Inorg. Chem.* **1991**, *30*, 3342.
4. Wolmershäuser, G.; Schnauber, M.; Wilhelm, T. *J. Chem. Soc., Chem. Commun.* **1984**, 573.
5. Barclay, T. M.; Cordes, A. W.; George, N. A.; Haddon, R. C.; Oakley, R. T.; Palstra, T. T. M.; Patenaude, G. W.; Reed, R. W.; Richardson, J. F.; Zhang, H. *J. Chem. Soc., Chem. Commun.* **1997**, 873.
6. Gray, M. A.; Rees, C. W. *J. Chem. Soc,. Perkin Trans. 1* **1993**, 3077.
7. Wolmershäuser, G.; Kaim, W.; Heckmann, G.; Lichtblau, A. *Z. Naturforsch* **1992**, *47 B*, 675.
8. Wolmershäuser, G.; Kraft, G. *Chem. Ber.* **1990**, *123*, 881.
9. Chandrasekhar, V.; Chivers, T.; Parvez, M.; Vargas-Beca, I.; Ziegler, T. *Inorg. Chem.* **1997**, *36*, 1669.
10. Fairhurst, S. A.; Pilkington, R. S.; Sutcliffe, L. H. *J. Chem. Soc., Faraday Trans. 1* **1983**, *79*, 925.
11. Chung, Y. L.; Fairhurst, S. A.; Gillies, D. G.; Kraft, G.; Krebber, A. M. L.; Preston, K. F.; Sutcliffe, L. H.; Wolmershäuser, G. *Magn. Reson. Chem.* **1992**, *30*, 774.
12. Hechman, G.; Johann, R.; Kraft, G.; Wolmershäuser, G. *Synth. Met.* **1991**, *41-43*, 3287.
13. Awere, E. G.; Burford, N.; Haddon, R. C.; Parsons, S.; Passmore, J.; Waszczak, J.

14. Wolmershäuser, G.; Johann, R. *Angrew. Chem. Int. Ed. Engl.* **1989**, *28*, 920.

15. Fujita, W.; Awaga, K. *Science* **1999**, *286*, 261.

16. Barclay, T. M.; Cordes, A. W.; De laat, R. H.; Goddard, J. D.; Haddon, R. C.; Jeter, D. Y.; MacKinnon, C. D.; Oakley, R. T.; Palstra, T. T. M.; Patenaude, G. W.; Reed, R. W.; Westwood, N. P. C. *J. Am. Chem. Soc.* **1997**, *119*, 2633.

17. (a) Figuly, G. D.; Loop, C. K.; Martin, J. C. *J. Am. Chem. Soc.* **1989**, *111*, 654. (b) Block, E.; Eswarakrishnan, V.; Gernon, M.; Ofori-Okai, G.; Saha, C.; Tang, K.; Zunieta, J. *J. Am. Chem. Soc.* **1989**, *111*, 658. (c) Smith, K.; Lindsay, C. M.; Pritchard, G. J. *J. Am. Chem. Soc.* **1989**, *111*, 665.

18. Gavezzotti, A.; Desiraju, G. R. *Acta Crystallogr.* **1988**, *44 B*, 427.

19. Dunitz, J. D.; Brock, C. P. *Acta Crystallogr.* **1982**, *38 B*, 2218.

20. Brock, C. P.; Dunitz, J. D. *Acta Crystallogr.* **1990**, *46 B*, 795.

21. This is a collaborative work, all magnetic susceptibility measurements on 1,3,2- and 1,2,3 radicals were performed by Drs. Haddon and Itkis at University of Kentucky.

22. Morrison, D. C. *J. Org. Chem.* **1956**, *21*, 470.

23. Heintzelman, R.W.; Swern, D. *Synthesis* **1976**, *11*, 731.

24. Allison, C. G.; Chambers, R. D.; MacBride, J. A. H.; Musgrave, W. K. R. *J. Chem. Soc., C* **1970**, 1023.

25. Palamidessi, G.; Luini, F. *Farmaco, Ed. Sci.* **1966**, *21*, 811 *(Via CA*, **1967**, *66*, 37886).

26. Tong, Y. L. *US.* Patent 3,987,044.

27. Tong, Y. C. *J. Heterocycl. Chem.* **1975**, *12*, 451.

28. (a)Chung, Y. L.; Sandall, J. P. B.; Sutcliffe, L. H.; Joly, H.; Preston, K. F.; Johann, R.; Wolmershaüser, G. *Magn. Reson. Chem.* **1991**, *31*, 625. (b) Preston, K. F.; Sutcliffe, L. H. *Magn. Reson. Chem.* **1990**, *28*, 189. (c) Chung, Y. L.; Fairhurst, S. A.; Gillies, D. G.; Preston, K. F.; Sutcliffe, L. H. *Magn. Reson. Chem.* **1992**, *30*, 666.

29. Hobza, P.; Selzle, H. L.; Schlag, E. W. *J. Am. Chem. Soc.* **1994**, *116*, 3500.

30. Bondi, A. *J. Phys. Chem.*, **1964**, *68*, 441.

31. (a) Cordes, A. W.; Haddon, R. C.; Oakley, R. T.; Schneemeyer, L. F.; Waszczak, J. V.; Young, K. M.; Zimmerman, N. M. *J. Am. Chem. Soc.* **1991**, *113*, 582. (b) Andrews, M. P.; Cordes, A. W.; Douglass, D. C.; Fleming, R. M.; Glarum, S. H.; Haddon, R. C.; Marsh, P.; Oakley, R. T.; Palstra, T. T. M.; Schneemeyer, L. F.; Trucks, G. W.; Tycko, R.; Waszczak, J. V.; Young, K. M.; Zimmerman, N. M. *J. Am. Chem. Soc.* **1991**, *113*, 3559. (c) Cordes, A. W.; Haddon, R. C.; Hicks, R. G.; Oakley, R. T.; Palstra, T. T. M.; Schneemeyer, L. F.; Waszczak, J. V. *J. Am. Chem. Soc.* **1992**, *114*, 5000. (d) Cordes, A. W.; Haddon, R. C.; Hicks, R. G.; Kennepohl, D. K.; Oakley, R. T.; Schneemeyer, L. F.; Waszczak, J. V. *Inorg. Chem.* **1993**, *32*, 1554. (e) Bryan, C. D.; Cordes, A. W.; Goddard, J. D.; Haddon, R. C.; Hicks, R. G.; Mackinnon, C. D.; Mawhinney, R. C.; Oakley, R. T.; Palstra, T. T. M.; Perel, A. S. *J. Am. Chem. Soc.* **1996**, *118*, 330. (f) Bryan, C. D.; Cordes, A. W.; Haddon, R. C.; Glarum, S. H.; Hicks, S. H.; Kennepohl, D. K.; MacKinnon, C. D.; Oakley, R. T.; Palstra, T. T. M.; Perel, A. S.; Schneemeyer, L. F.; Scott, S. R.; Waszczak, J. V. *J. Am. Chem. Soc.* **1994**, *116*, 1205. (g) Bryan, C. D.; Cordes, A. W.; Fleming, R. M.; George, N. A.; Glarum, S. H.; Haddon, R. C.; MacKinnon, C. D.; Oakley, R. T.; Palstra, T. T. M.; Perel, A. S. *J. Am. Chem. Soc.* **1995**, *117*, 6880. (h) Bryan, C. D.; Cordes, A. W.; George, N. A.; Haddon, R. C.; MacKinnon, C. D.; Oakley, R. T.; Palstra, T. T. M.; Perel, A. S. *Chem. Mater.* **1996**, *8*, 762.

32. Dunitz, J. D.; Bernstein, J. *Acc. Chem. Res.* **1995**, *28*, 193.

33. (a) Smallman, R. E. "*Modern Physical Metallurgy*" 3rd Ed., **1970**, Butterworth, London. (b) Etter, M. C.; Siedle, A. R. *J. Am. Chem. Soc.* **1983**, *105*, 641.

34. Ding, J.; Herbst, R.; Praefcke, K.; Kohne, B.; Saenger, W. *Acta Crystallogr.* **1991**, *47B*, 739.

35. (a) De´coret, C. *Molecules Phys. Chem. Bio.* **1988**, *1*, 159. (b) Megaw, H. D. *"Crystal Structures, a Working Approach"*, **1973**, W. B. Saunders Co. London.

36. (a) Reid, W.; Tsiotis, G. *Liebigs. Ann. Chem.* **1988**, 1197. Via *CA*, **1989**, *110*, 38955t. (b) Cort, L. A.; Francis, N. R. *J. Chem. Soc.* **1964**, 2799.

37. Mackinnon, C. D., *Ph. D. Thesis*, University of Guelph, **1997**.

38. Societa Farmaceutici Italia, ***Brit.*** *1,145,730. Via CA*, **1969**, *71*, 30505.

39. Ellingson, R. C.; Henry, R. L. *J. Am. Chem. Soc.* **1948**, *70*, 1257.

40. Cheeseman, G. W. H.; Cookson, R. F., "*Condensed Pyrazines*" John Wiley & Sons, **1979**, 576.

41. (a) Taylor E. C.; Sherman, W. R. *J. Am. Chem. Soc.* **1959**, *81*, 2464. (b) Adembri G.; de Sio, F.; Nesi, R. *Ric. Sci.* **1967**, 37, 440. Via *CA*, **1968**, *68*, 21903. (c) Niegel, H.; Goldner, H.; Meyer, H.; Lorenz, D. *Ger (East) DD 280,007*, **1990**. Via *CA*, **1991**, *114*, 102044.

42. Suzuki, T.; Fujii, H.; Yamashita, Y.; Kabuto, C.; Tanaka, S.; Harasawa, M.; Mukai, T.; Miyashi, T. *J. Am. Chem. Soc.* **1992**, *114*, 3034.

43. Barclay, T. M.; Cordes, A. W.; George, N. A.; Haddon, R. C.; Itkis, M. E.; Mashuta, M. S.; Oakley, R. T.; Patenaude, G. W.; Reed, R. W.; Richardson, J. F.; Zhang, H. *J. Am. Chem. Soc.* **1998**, *120*, 352.

44. Ferraro, J. R.; Williams, J. M., "*Introduction to Synthetic Electronic Conductors*", Academic Press Inc., **1987**, 129.

45. Jolly, W. L.; Maguire, K. D. *Inorg. Synth.* **1967**, *9*, 102.

Chapter 3 Electrochemistry and theoretical studies on 1,3,2-DTAs

This chapter serves as both a break and connection between the two halves of the thesis. In Chapter 1 we reviewed the history of synthetic organic conductors, and traced the development of neutral radical based materials. In chapter 2, we described several 1,3,2-DTA radicals, their preparation, crystal structure and other properties. In order to build upon these results, and generate new radicals with potentially better solid state properties, we decided to return to the basic design principles behind the Haddon model for neutral radical conductors. Towards this end, a knowledge of the trends in molecular ionization potentials (IP) and electron affinities (EA) is of paramount importance.

This chapter presents the results of various electrochemical studies on 1,3,2-DTAs. Also provided are the results of DFT theoretical calculations on both 1,3,2- and 1,2,3-DTAs. The calculated gas phase disproportionation energies (ΔH_{disp} = IP-EA) are then compared with the electrochemical data and used as a guide for the design of new radicals with improved charge transfer characteristics. It will be shown that 1,2,3-DTAs are more sensitive to substituents and therefore open the way to modification. Based on these conclusions several new 1,2,3-DTA derivatives have been pursued. These latter results are presented in Chapters 4 and 5.

3.1 Electrochemistry

3.1.1 Introduction

Effective conductivity in molecular conductors requires reducing electron-electron Coulombic repulsion (U) to minimize the ionic fluctuation during current flow through the

solid. A chemical expression of weak Coulombic repulsion is a low disproportionation energy (ΔH_{disp}), *i.e.*, for the reaction:

$$R + R = R^{+} + R^{-} \qquad U \approx \Delta H_{disp} = IP - EA \qquad (15)$$

An estimate of the extent of this process in the solid state can be obtained from solution electrochemistry. The electrochemical cell potential, E_{cell} for reaction (Eqn. 15) has been obtained for classical charge-transfer donors and acceptors. For example, for TTF the cell potential E_{cell} (for $2\ TTF^{+} = TTF^{0} + TTF^{2+}$) = 0.3 V,[1] and for TCNQ, E_{cell} (for $2\ TCNQ^{-} = TCNQ^{0} + TCNQ^{2-}$) = 0.42 V.[2] This E_{cell} value is numerically identical to the electrochemical estimate of bandgap, which has been used extensively to characterize small-bandgap conjugated polymers.[3] In such polymers, estimation of the actual bandgap of the polymer (E_g) from the solution oxidation (E_{ox}) and reduction (E_{red}) potentials has been facilitated with the help of the empirical equation (Eqn.16):

$$E_g \approx (E_{ox} - E_{red})(S^{+} - S^{-})\left(1 - \frac{1 - \frac{1}{\varepsilon_2}}{1 - \frac{1}{\varepsilon_1}}\right) \qquad (16)$$

where S is the solvation energy of the ionized molecule minus the solvation energy of the neutral molecule, and e_1 and e_2 are the dielectric constants of the solution and the solid, respectively.

3.1.2 Cyclic Voltammetry on 1,3,2-DTAs

Generally speaking, the change of the redox window (E_{cell}) in a series of structurally similar molecules reflects the energy difference between HOMO and LUMO of the molecules. For example, polycyclic aromatic compounds can be chemically or electrochemically reduced, often forming stable radical anions. Benzene itself has a very large redox stability window from approximately –3 to +3 volts. As the number of conjugated rings is increased, an ever-smaller separation between the reduction and oxidation potentials is observed. E_{cell} of naphthalene (**III-2**) is 4.04 V in acetonitrile and for anthracene (**III-3**) only 2.87 V.[4] In the phenalenyl radical derivative, 2,5,8-tri-tert-phenalenyl, the redox window decreases to only 1.57 V.[5] Recently Haddon has reported the spiro-biphenalenyl (**I-26**) with $E_{cell} = 0.37$ V,[6] which is comparable to the redox window of TTF^{+}. Clearly larger delocalized aromatic systems possess narrower redox windows.

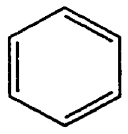

III-1

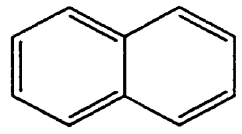

III-2

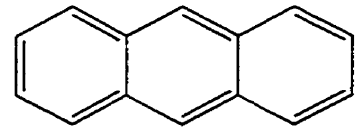

III-3

Phenalenyl based radicals are thus excellent candidates for NRCs. However dimerization has always been a problem. One approach to circumventing this issue, while at the same time stabilizing the radicals, is to introduce heteroatoms, such as N, P, S, Se. Since these elements have higher electronegativities, the redox windows widen, correspondingly the energy gaps become larger, and electrons are more localized. For example, six-membered thiatriazine derivatives, with three nitrogen and one sulfur atoms, have an E_{cell} around 1.43 V. For 1,2,3,5-dithiadiazolyls, E_{cell} is also around 1.43 V [7] with

many different substituents because the SOMO is nodal at the substituted carbon, and the unpaired electron cannot be delocalized.[8]

In contrast, for both 1,3,2- and 1,2,3-dithiazoyl rings, spin density can be delocalized to the substituents or to fused rings, and this leads to dramatic variations in redox potentials. Of the two groups, the 1,3,2-series has been studied more extensively. In Chapter 2 we noted that BDTA, NDTA reacts very rapidly with atmospheric oxygen, but QDTA does not. Indeed QDTA can be generated from its imide by treatment with oxygen and it is very stable in air. TDTA is also quite resistant to oxidation, and chloride salts of the cationic state readily disproportionate on mild heating back to the neutral form (with loss of chlorine). To quantify these observations we have performed cyclic voltammetric (CV) measurements over the triad of oxidation states, *i.e.*, anion, radical, and cation, available to these systems. The CV waves are illustrated in Figure 3.1, and the half-wave potentials for reduction and oxidation are summarized in Table 3.1, along with the values of E_{cell} ($E_{cell} = E_{1/2}(ox) - E_{1/2}(red)$). For all 1,3,2-DTA radicals oxidation is essentially reversible. Electrochemical reduction of NDTA and QDTA is, however, strongly irreversible, as is the case for BDTA, PDTA and BBDTA.[9] Only for TDTA, both the oxidation and reduction steps are reversible. Also presented in Table 3.1 are computed (B3LYP/6-31G**) values for adiabatic ionization potentials (IPs) and electron affinities (EAs) as well as the difference IP-EA, the enthalpy change ΔH_{disp} for the gas-phase disproportionation reaction (Eqn. 15).

Table 3.1 Redox and E_{cell} potentials[a] (V *vs* SCE), and computed (B3LYP/6-31G**) adiabatic IP, and EA and ΔH_{disp} values (eV) for 1,3,2-dithiazolyls

compd	DTA	BDTA	PDTA	NDTA	QDTA	TDTA	PPDTA
$E_{1/2}$(ox)	0.02[10]	0.15	0.53	0.27	0.62	1.00	---
$E_{1/2}$(red)	---	-1.24 [b]	-0.88 [b]	-1.08 [b]	-0.73 [b]	-0.06	---
E_{cell}	---	1.39 [c]	1.41 [c]	1.29 [c]	1.30 [c]	1.06	---
IP	6.77	6.58	7.15	6.47	6.95	7.60	7.36
EA	-0.41	0.16	0.85	0.68	1.33	2.14	1.83
ΔH_{disp}	7.18	6.42	6.30	5.79	5.63	5.46	5.53

[a] All potentals are from solutions in CH_3CN, reference SCE.

[b] Irreversible. [c] This value is taken as the difference between the cathodic peak potentials.

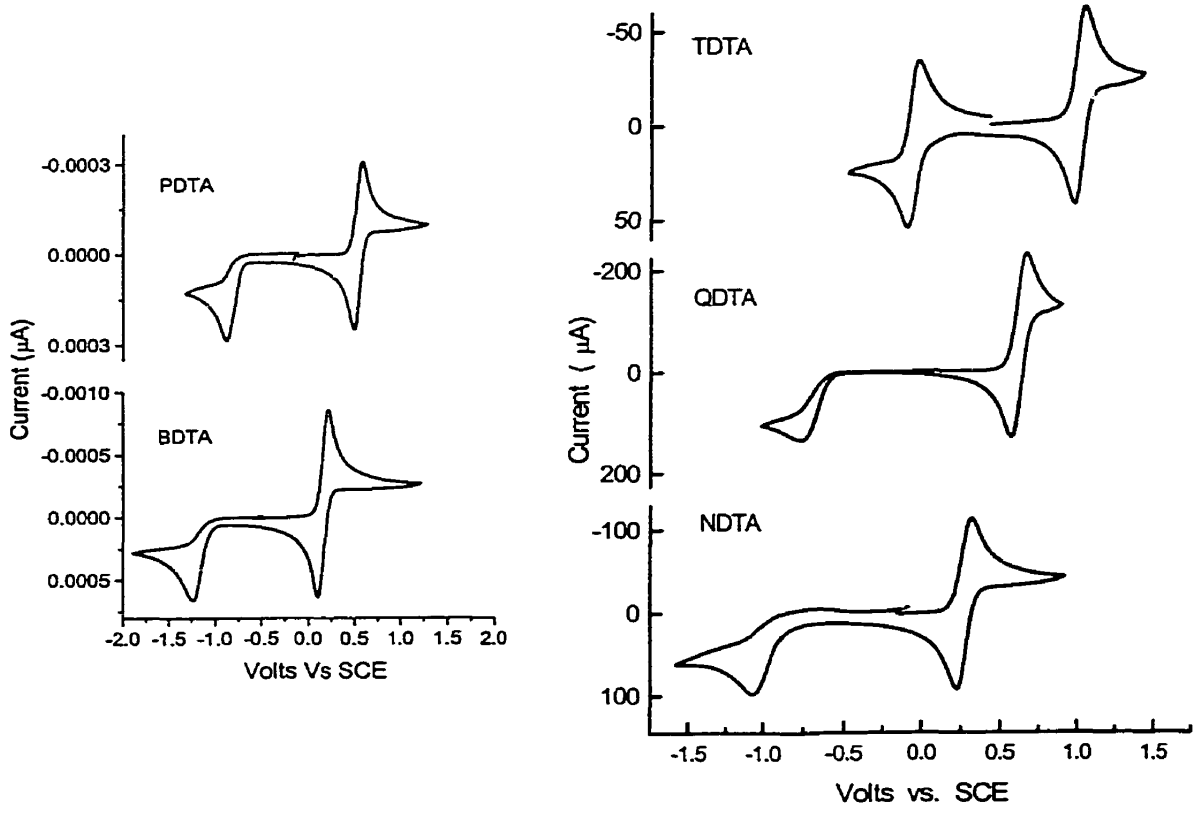

Figure 3.1 Cyclic voltammetry waves on BDTA, PDTA, NDTA, QDTA, and TDTA radicals (in CH_3CN, n-Bu_4NPF_6, supporting electrolyte, ref. SCE).

It is immediately apparent that the electrochemical properties of BDTA, PDTA, NDTA, QDTA, and TDTA parallel their chemical redox behavior. Thus, while BDTA, NDTA are the remarkably powerful donors, rivaling, for example, TTF ($E_{1/2}$ (ox) = 0.30 V *vs.* SCE),[1] TDTA is a strong acceptor, akin to closed shell heterocyclic systems containing the thiadiazole unit, *e.g.*, ($E_{1/2}$ (red) = 0.10 V vs SCE).[11] This variation in redox potentials is in striking contrast to the behavior of DTDA radicals, where ligand effects (at the 4-position) have relatively little influence on redox potentials,[12] ionization energies, and spin distributions. [13]

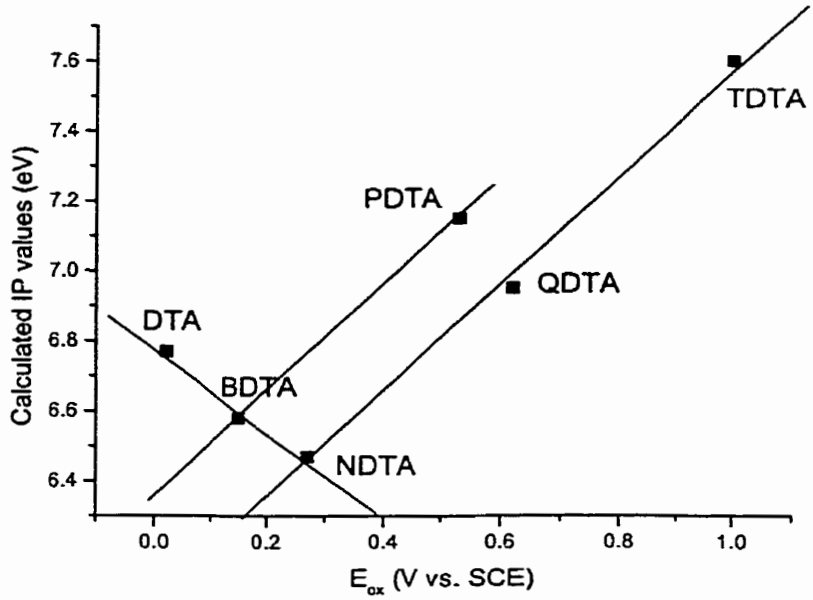

Figure 3.2 The relationship between theoretical IP and measured E_{ox} in CV experiments.

Perhaps more notable than the shift in potentials is the change in the value of E_{cell}, which drops markedly as the electron accepting ability of the heterocyclic residue attached to the DTA ring is increased. The drop in E_{cell} is most pronounced for TDTA. These

experimental (solution) results are supported by the calculated gas phase disproportionation energies (discussed in detail below), the increase in IP along the series of NDTA, QDTA and TDTA is more than offset by the larger increase in EA in TDTA, and the value of ΔH_{disp} drops by 0.17 eV (compare to NDTA).

If we compare E_{ox} in CV experiments with calculated IP values for 1,3,2-DTA radicals, it is found that two nearly linear relations are observed (Figure 3.2). From monocyclic DTA, to bicyclic BDTA and tricyclic NDTA, while one or two phenyl rings are fused to DTA ring, E_{ox} shifts anodically and IP values decrease. We will discuss these later in more detail.

3.2 Computational modeling studies of 1,3,2-DTA systems

In order to generate a reliable and consistent set of computed IP and EA for DTA radicals we have performed Density Functional Theory (DFT) calculations over a range of basis sets. The DFT method itself is well proved as being both economical and reliable for problems where electron correlation is important. Several basis sets, ranging from STO/3G, 3-21G to 6-31G** were employed, and molecular geometries were fully optimized save for a constraint on planarity; the MNDO method was generally used to provide a starting point. The total energies of the triad of oxidation states, *i.e.*, cation, radical and anion states, as obtained from the B3LYP/ 6-31G** calculations, were then used to derive the IP, EA and IP-EA values. The data based on the B3LYP/6-31G** calculations are listed in Table 3.2 while their IP, EA and the enthalpy changes (ΔH_{disp} = IP-EA) are plotted in Figure 3.3.

The similarity on the trends of IP and EA values is apparent. Generally when nitrogen replaces carbon, the IP value goes up since the electronegativity of nitrogen is larger than that

of carbon and the electron is held more tightly; on the other hand, if the larger aromatic ring attached onto the DTA system, the resultant cation will be stabilized by the more delocalized system and the IP value decreases slightly. These trends are clearly shown in Figure 3.2. For example, on moving from NDTA to QDTA, two CH groups are replaced by nitrogen, the electron withdrawing capacity of the substituent is increased, and the unpaired electron becomes more delocalized. The IP value of TDTA is even higher since the 1,2,5-thiadiazolopyrazine residue is an even more powerful electron withdrawing group than quinoxaline. From DTA, BDTA to NDTA, the increase of the number of aromatic rings reduces the IP values of the corresponding radicals.

Table 3.2 The calculated IP, EA, IP-EA values (eV) of various 1,3,2-DTA radicals

Radical	DTA	BDTA	PDTA	TTTA	NDTA	QDTA	PPTA	TDTA
IP	6.77	6.58	7.15	7.53	6.47	6.95	7.36	7. 60
EA	-0.41	0.16	0.85	1.18	0.68	1.33	1.83	2.14
IP-EA	7.18	6.42	6.30	6.35	5.79	5.65	5.53	5.46
q_N [a]	0.59	0.61	0.61	0.61	0.61	0.61	0.59	0.57

[a] *Spin density on the DTA nitrogen*

The trend of EA value generally follows the IP change since the larger, more delocalized systems also stabilize the extra electron. However, and more interestingly, the increase of EA value outpaces the increase of IP with the result that the difference IP-EA, *i.e.*, ΔH_{disp}, steadily decreases. These results mirror the trend in E_{cell}, and provide an indication of the Coulombic barrier to electron transfer in a neutral radical conductor.

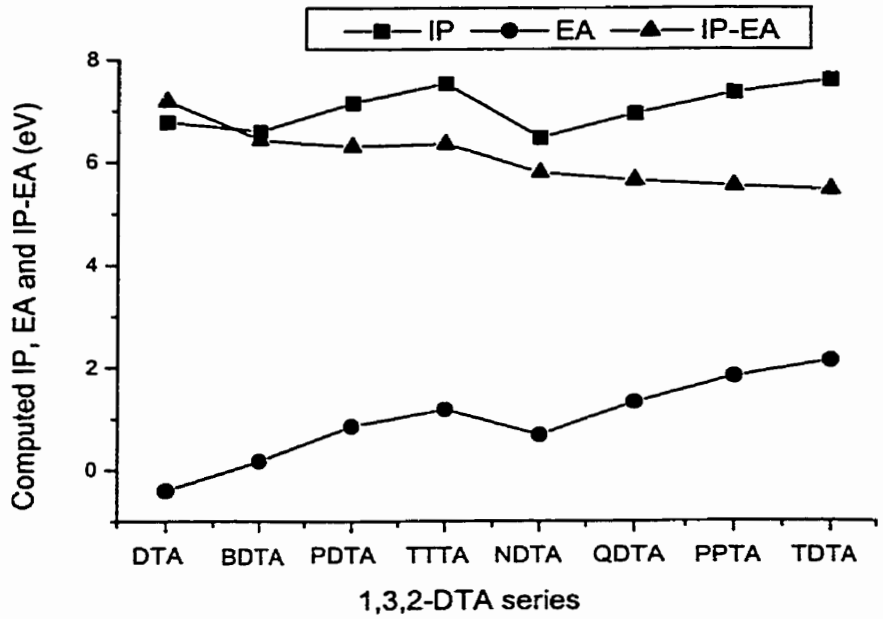

Figure 3.3 The calculated IP, EA and IP-EA values of various 1,3,2-DTA radicals.

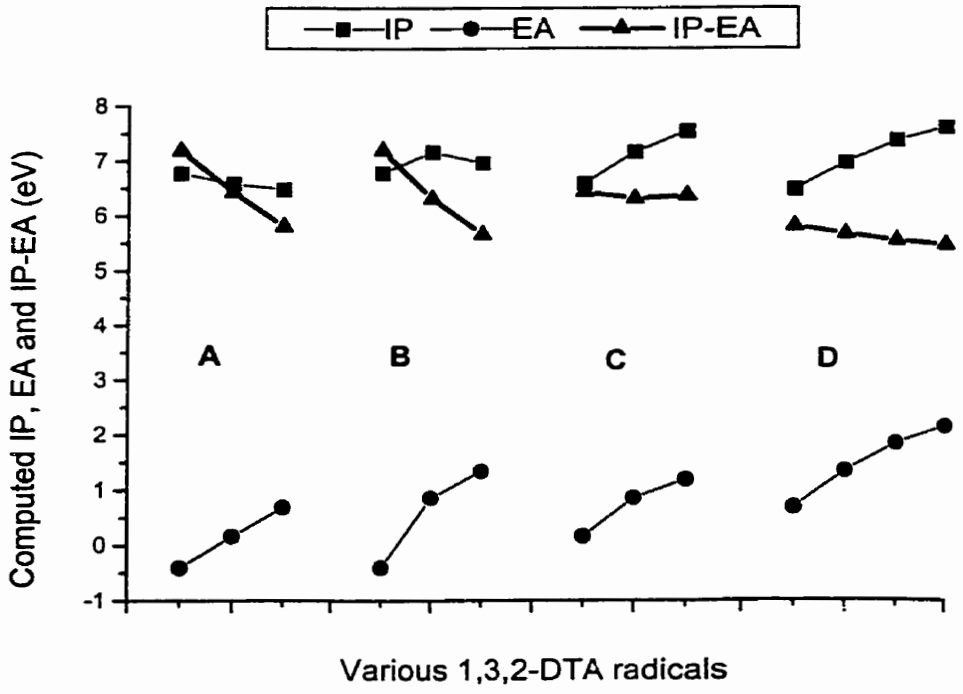

Figure 3.4 The calculated IP, EA, and IP-EA values of the grouped 1,2,3-DTA radicals. **A** (DTA, BDTA, NDTA), **B** (DTA, PDTA, QDTA), **C** (BDTA, PDTA, TTTA) and **D** (NDTA, QDTA, PPTA, TDTA).

To clearly show the various factors which effect IP, EA and IP-EA values of the radicals, the before-mentioned 1,3,2-DTA radicals were considered as four series [**A** (DTA, BDTA, NDTA); **B** (DTA, PDTA, QDTA); **C** (BDTA, PDTA, TTTA); **D** (NDTA, QDTA, PPTA, TDTA)]. The IP, EA and IP-EA values are plotted against these series in Figure 3.4.

Both **A** and **B** stand for the moving from monocyclic to bicyclic to tricyclic radicals. In the **A** series, the fully carbon based aromatic substituents result in large increase in EA and small decrease in IP. The total IP-EA values are thus greatly reduced (1.39 eV). Insertion of pyrazine ring in the **B** series also generates a large decrease in IP-EA (1.53 eV) at the cost of the increase of the IP value. The **C** and **D** series represent bicyclic and tricyclic systems, respectively, with the sequential replacement of CH by N (or S). Both series experience large increases in IP and EA, but the difference (IP-EA) remains relatively constant (0.12 eV in **C**) and (0.33 eV in **D**).

Here the structural and electronic factors, which determine the properties of the neutral radical conductors, have to be considered together. The systems with undimerized structures and low ΔH_{disp} values are highly desired. In the 1,3,2-DTA radical system, an increase in the size of the molecules greatly reduces the Coulombic barriers, such as in group **A** and **B**. However the structure maker CH groups in carbon based aromatics result in the herringbone arrangement (NDTA).[14] Increasing the number of heteroatoms in the radical skeleton leads to a preference for π-stacks , at the time that maintains or even slightly reduces the IP-EA value (QDTA and TDTA). In TDTA all the possible CH groups are removed and TDTA holds the lowest ΔH_{disp} not only in group **D**, but in all known 1,3,2-DTA radicals. The 1,3,2-DTA radical series displays great regularity between IP-EA values and molecular size and number of heteroatoms.

3.3 Computational modelling studies of 1,2,3-DTA systems

As a continuation of our modeling studies on 1,3,2-DTA radicals, we also explored a variety of 1,2,3-DTAs (shown in Scheme 3.2) at the B3LYP/6-31G** level. The computed IP, EA and IP-EA values of these compounds are listed in Table 3.3 and plotted in Figure 3.5 (Every 1,2,3-DTA was assigned a number and the corresponding molecular structure was shown in Scheme 3.1). The trend in IP-EA for the 1,2,3-DTA series is quite similar to that found for the 1,3,2-compounds. Thus, for example, replacement of hydrogen atoms in the 4,5-position in the parent 1,2,3-DTA radical by chlorine atoms does not change the IP-EA at all. However, with an increase of the molecular size and the introduction of the heteroatoms, both the IP and EA are increased, the latter more markedly, so that the IP-EA values are decreased remarkably. From the parent 1,2,3-DTA to (the best target) PBDTA (2,5), the difference of IP-EA is decreased by 1.72 eV.

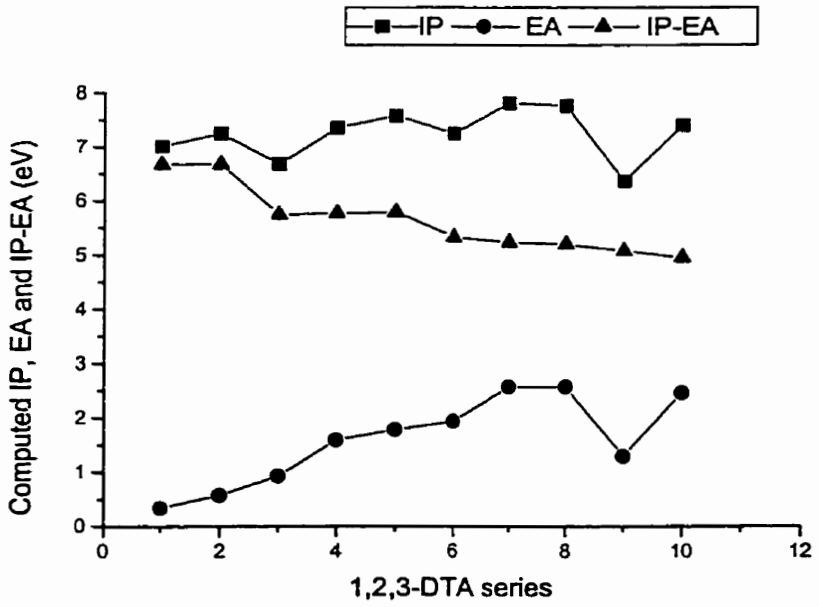

Figure 3.5 Computed IP, EA and IP-EA values for 1,2,3-DTA radicals (various 1,2,3-DTA radicals are labeled as integers, see Scheme 3.1 for structures).

Table 3.3 The calculated IP, EA, IP-EA values (eV) of various 1,2,3-DTA radicals

Radicals	IP	EA	IP-EA	Radicals	IP	EA	IP-EA
DTA	7.01	0.34	6.67	QDTA	7.24	1.93	5.32
DC-DTA	7.25	0.58	6.68	TDTA	7.81	2.57	5.23
BDTA	6.68	0.93	5.74	PTDTA	7.76	2.57	5.19
PDTA	7.35	1.59	5.76	PBDTA (3, 4)	6.36	1.29	5.07
PyDTA	7.57	1.78	5.78	PBDTA (2,5)	7.4	2.46	4.95

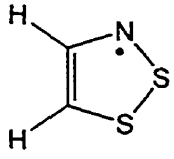

DTA **1**

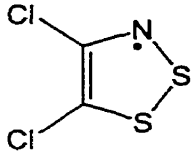

DC-DTA **2**

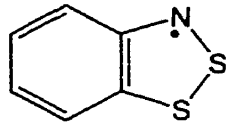

BDTA **3**

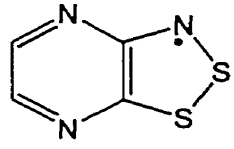

PDTA **4**

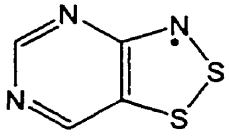

PyDTA **5**

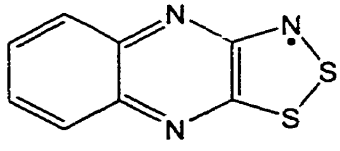

QDTA **6**

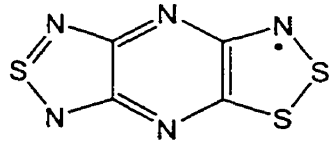

TDTA **7**

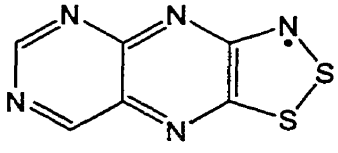

PTDTA **8**

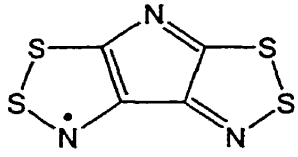

3,4-PBDTA **9**

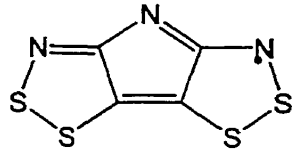

2,5-PBDTA **10**

Scheme 3.1

As in the case of 1,3,2-DTAs, we also can replot the IP-EA distribution for 1,2,3-DTAs based on the number of the rings and number of heteroatoms (Figure 3.6). The increase of the molecular size is a far more important factor than replacement by the

heteroatoms to reduce the IP-EA values. For example, in group **A** (DTA, PDTA, QDTA), the IP-EA value in tricyclic QDTA is much less than in monocyclic DTA ($\Delta = 1.34$ eV). In group **B** (BDTA, PDTA, PyDTA), addition of the heteroatoms or exchange of their positions in bicyclic radicals has little effect on the IP-EA value; In the tricyclic group **C** (QDTA, TDTA, PTDTA, 3,4-PBDTA and 2,5-PBDTA), with the fine tuning of the molecular structures, the IP-EA values slowly diminish from 5.32 eV in QDTA to 4.95 eV ($\Delta = 0.37$ eV).

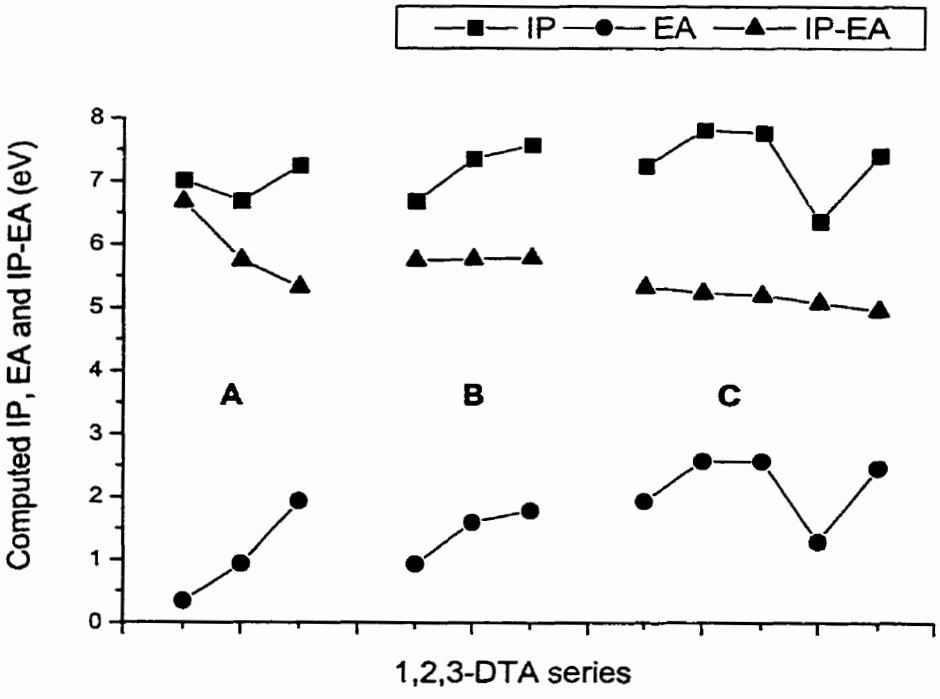

Figure 3.6 The calculated IP, EA and IP-EA values of the grouped 1,2,3-DTA derivatives. **A** (DTA, PDTA, QDTA), **B** (BDTA, PDTA, PyDTA), **C** (QDTA, TDTA, PTDTA, 3,4-PBDTA and 2,5-PBDTA),

Finally, a comparison of IP, EA and IP-EA values between 1,2,3 and 1,3,2-DTAs is plotted in Figure 3.7. In 1,2,3-DTA radicals, the DTA nitrogen is beside the fused aromatic

ring, and spin density is easier to delocalize. The EA values are therefore much higher than those of 1,3,2-DTAs. Based on these results we viewed 1,2,3-DTAs as being potentially better targets as molecular radical conductors. In the final three chapters, the results of our attempts to prepare and characterize 1,2,3-DTA radicals are described.

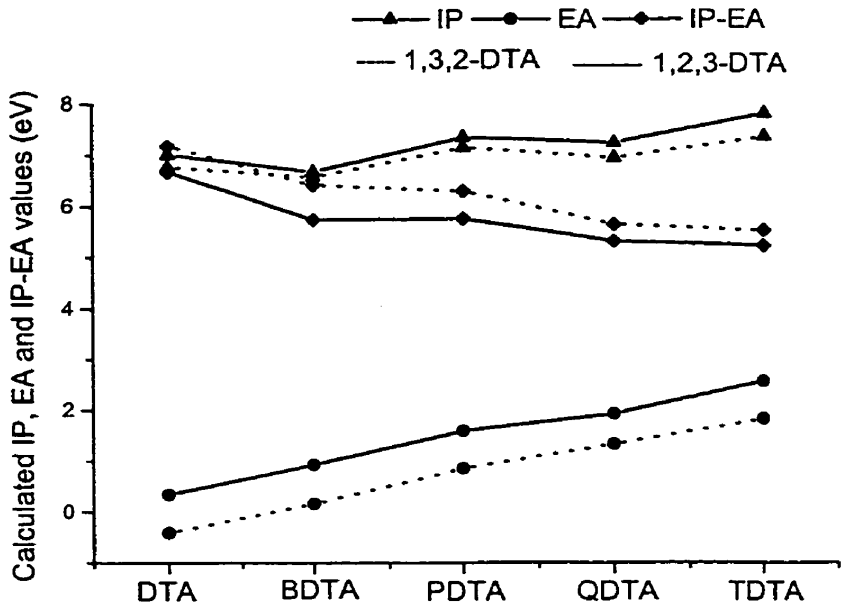

Figure 3.7 The comparison of IP, EA, and IP-EA values between the common 1,2,3 and 1,3,2- DTA.

3.4 References

1. (a) Sandman, D.J.; Zoski, G.D.; Burke, W.A.; Hamill, G.P.; Caesar, G.P.; Baker, A.D. *J. Chem. Soc., Chem. Commun.* **1981**, 829. (b) Lichtenberger, D. L.; Johnston, R. L.; Hinkelmann, K.; Suzuki, T.; Wudl, F. *J. Am. Chem. Soc.* **1990**, *112*, 3302.

2. Kaplan, M.L.; Haddon, R.C.; Bramwell, F.B.; Wudl, F.; Marshall, J. H.; Cowan, D.O.; Gronowitz, S. *J. Phys. Chem.* **1980**, *84*, 427.

3. Roncali, J. *Chem. Rev.* **1997**, *97*, 173.

4. (a) Zweig, A.; Hoffman K. *J. Org. Chem.* **1965**, *30*, 3997. (b) Weast, R.C., *CRC Handbook of Chemistry and Physics*, CRC Press, Inc., Boca Raton, Fl, **1989**, p. D-159.

5. Goto, K.; Kubo, T.; Yamamoto, K.; Nakasuji, K.; Sato, K.; Shiomi, D.; Takui, T.; Kubota, M.; Kobayashi, T.; Yakusi, K.; Ouyang, J. *J. Am. Chem. Soc.* **1999**, *121*, 1619.

6. Chi, X.; Itkis, M. E.; Patrick, B. O.; Barclay, T. M.; Reed, R. W.; Oakley, R. T.; Cordes, A. W.; Haddon, R. C. *J. Am. Chem. Soc.* **1999**, *121*, 10395.

7. (a) Boeré, R.T.; Moock, K.H. *J. Am. Chem. Soc.* **1995**, *117*, 4755. (b) Boeré, R.T.; Moock, K.H.; Parvez, M. *Z. Anorg. Allg. Chem.* **1994**, *620*, 1589.

8. (a) Lee, F. L.; Preston, K. F., Williams, A. J.; Sutcliffe, L. H.; Banister, A. J.; Wait, S. T. *Magn. Reson, Chem.* **1989**, *27*, 1161. (b) Markovski, L. N.; Polumbrik, O. M.; Talanov, V. S.; Shermolovich, Y. g. *Tetrahedron, Lett.* **1982**, *23*, 761. (c) Fairhurst, S. A.; Sutcliffe, L. H.; Preston, K. F., Banister, A. J.; Partington, A. S.; Rawson, J. M.; Passmore, J.; Schriver, M. J. *Magn. Reson, Chem.* **1993**, *31*, 1027.

9. Barclay, T. M.; Cordes, A. W.; De laat, R. H.; Goddard, J. D.; Haddon, R. C.; Jeter, D. Y.; MacKinnon, C. D.; Oakley, R. T.; Palstra, T. T. M.; Patenaude, G. W.; Reed, R. W.;Westwood, N. P. C. *J. Am. Chem. Soc.* **1997**, *119*, 2633.

10. MacLean, G.K.; Passmore, J.; Rao, M. N. S.; Schriver, M. J.; White, P.S.; Bethell, D.; Pilkington, R.S.; Sutcliffe, L. H. *J. Chem. Soc., Dalton Trans.* **1985**, 1405.

11. Yamashita, Y.; Saito, K.; Suzuki, T.; Kabuto, C.; Mukai, T.; Miyashi, T. *Angew. Chem., Int. Ed. Engl.* **1988**, *27*, 434.

12. Boeré, R. T.; Moock, K. H. *J. Am. Chem. Soc.* **1995**, *117*, 4755.

13. (a) Boeré, R. T.; Oakley, R. T.; Reed, R. W.; Westwood, N. P. C. *J. Am. Chem. Soc.* **1989**, *111*, 1180. (b) Cordes, A. W.; Goddard, J. D.; Oakley, R. T.; Westwood, N. P. C. *J. Am. Chem. Soc.* **1995**, *111*, 6147.

14. Barclay, T. M.; Cordes, A. W.; George, N. A.; Haddon, R. C.; Oakley, R. T.; Palstra, T. T. M.; Patenaude, G. W.; Reed, R. W.; Richardson, J. F.; Zhang, H. *J. Chem. Soc., Chem. Commun.* **1997**, 873.

Chapter 4 A special 1,2,3-dithiazolyl radical, TDTA

4.1 Introduction

The preparation and characterization of several polycyclic 1,3,2-dithiazolyl radicals were presented in Chapter 2. As predicted from theoretical calculations and later confirmed by experiment, the gas phase disproportionation energies ΔH_{disp} and cell potentials E_{cell} of these tricyclic systems are smaller than those found in simple 1,2,3,5-DTDA and 1,3,2-DTA radicals. The unpaired electron is delocalized onto the fused aromatic ring, as a result of which the tendency of the radical to dimerize is suppressed.[1] However, while the structures of both 1,3,2-QDTA and 1,3,2-TDTA consist of undimerized π stacks, the pressed pellet conductivities are still less than 10^{-6} S cm^{-1}. Charge correlation effects trap the unpaired electron on the radicals, and the bulk materials are Mott insulators.

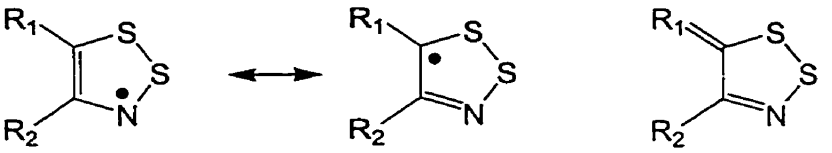

IV-1 **IV-2** **IV-3**

The asymmetric 1,2,3-DTA radical can be drawn with two resonance structures, one nitrogen-centered (**IV-1**) and one carbon centered (**IV-2**). The spin density at the 5-position of a 1,2,3-DTA radical is greater than in the 4,5-positions of a 1,3,2-DTA radical, and this feature should facilitate more extensive electron delocalization and, as a result, reduce the charge transfer barrier U ($\approx \Delta H_{disp}$). However, exocyclic double bonds can also be formed at this position, leading to closed shell neutral molecules (**IV-3**). The results described in this chapter relate to 1,2,3-DTA derivatives. While many closed shell molecules have been made, the focus will be on the radical states.

4.1.1 Closed shell 1,2,3-dithiazoles

Much of the chemistry of the dithiazole ring system has been developed from 4,5-dichloro-1,2,3-dithiazolium chloride ("Appel's salt" **IV-4**), the synthesis of which was established in 1985 (Scheme 4.1).[2] The reactions of this salt with nucleophiles to produce derivatives such as **IV-5** has received particular attention.[3]

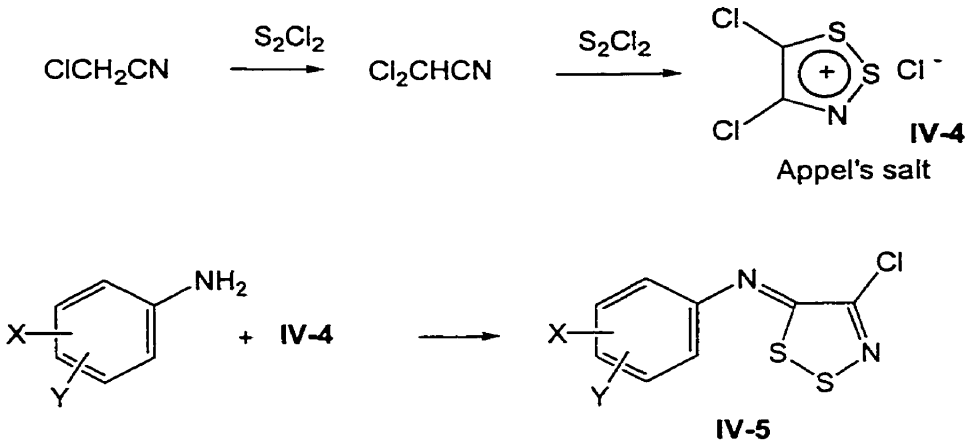

Scheme 4.1

Condensed ring DTA compounds are conveniently accessed by the Herz reaction,[4] *i.e.*, the cyclization of arylamines with S_2Cl_2. Diamino aromatic compounds can also undergo a Herz reaction, thus the bis(1,2,3-dithiazole). **IV-6** can be prepared in one step from 2,6-diaminonaphthalene.[5]

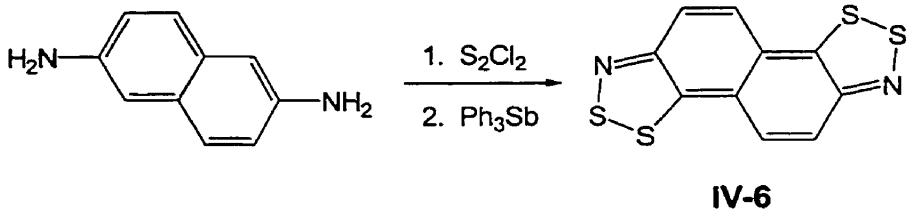

Oximes also undergo Herz-type chemistry. For example, both cyclopentaneoxime and cyclopenteneoxime react with S_2Cl_2 to form the stable 10 π-electron cyclopenta-1,2,3-

dithiazole **IV-7**.[6] These reactions (Scheme 4.2) can be facilitated by using an inert base, especially ethyldiisopropylamine (Hünig's base, HB)(**IV-8**). The introduction of chlorine atoms into the five carbocycle demonstrates the chlorination capacity of S_2Cl_2.

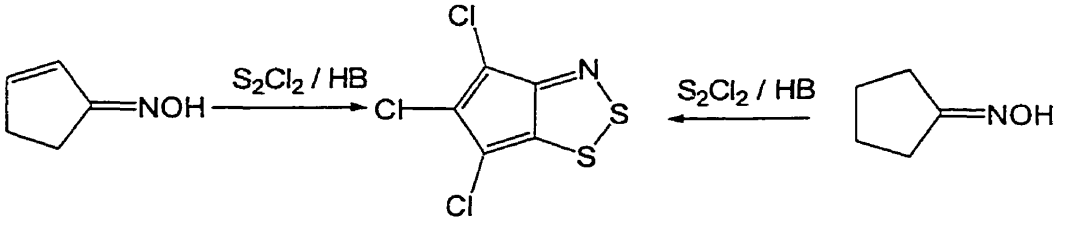

IV-7

Scheme 4.2

Rees[7] and coworkers have also shown that ethyldiisopropylamine, reacts with S_2Cl_2 at higher temperature. Complete sulfuration of all the C-H bonds of the isopropyl groups occurred when the slurry was refluxed in DBO for two hours; bis[1,2]dithiolo[3,4-b:4',3'-e]-[1,4]thiazine **IV-9** was the final product. The corresponding pyrrole derivative **IV-10** was obtained in this simple one-pot reaction if chlorobenzene was used as solvent (Scheme 4.3).

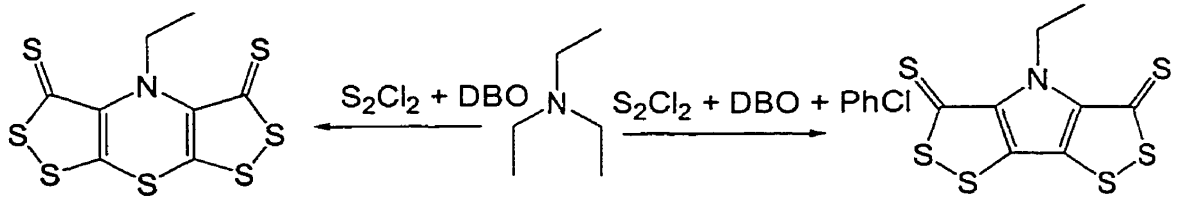

IV-9 **IV-8** **IV-10**

Scheme 4.3

Although the Herz reaction has been used to prepare many 1,2,3-dithiazoles, the mechanism of the reaction is far from well understood. In many cases, yields are low and it is difficult if not impossible to purify the products. On the other hand, aryl and heteroarylamines do not undergo the desired Hertz reaction with S_2Cl_2 if the ring is π-electron deficient,[2] *e.g.*, nitro-substituted. Cyclization only occurs with electron-rich systems

(*e.g.*, benzene, naphthalene); in the case of pyrazine or other nitrogen incorporated ring system, the method fails.

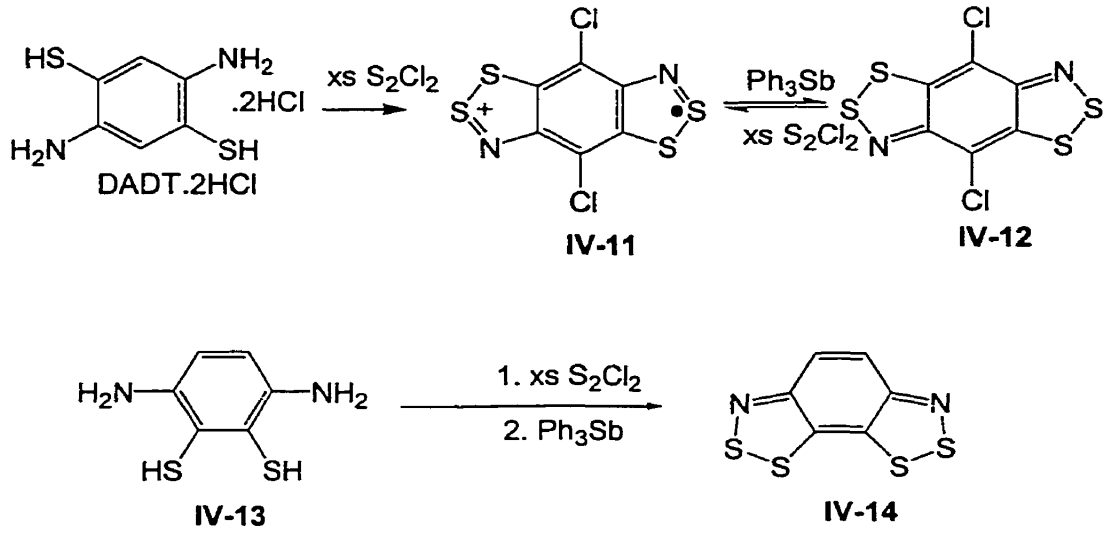

Scheme 4.4

Alternatively, the reactions of aminothiols with S_2Cl_2 can be used to make DTA rings. Thus, for example, while *p*-phenylenediamine does not react with S_2Cl_2 effectively,[8] the condensation of diaminobenzenedithiol dihydrochloride (DADT.2HCl) with sulfur monochloride generates the radical cation **IV-11** in good yield. Subsequent reduction affords the closed shell neutral compound **IV-12**. Similarly, the isomeric 1,4-diaminobenzene-2,3-dithiol (as its hydrochloride salt) **IV-13** reacts easily with excess S_2Cl_2 in refluxing chlorobenzene to yield, after reduction, the neutral cis-bis(1,2,3-dithiazole) compound, **IV-14**. The two reactions are shown in Scheme 4.4.

An unusual way to make 1,2,3-dithiazole compounds is shown in Scheme 4.5. The trithiadiazepine **IV-15**, prepared from condensation of (trimethylsilyl) sulfurdiimide and the sulfenyl chloride derivative of ethanedithiol,[9] was converted into the bromo derivative **IV-16**, which reacted with diphenyldiazomethance to afford the pyrazolotrithiadiazepine **IV-**

17. Thermolysis of the latter then yielded the condensed 1,2,3-dithiazole compound **IV-18**.[10]

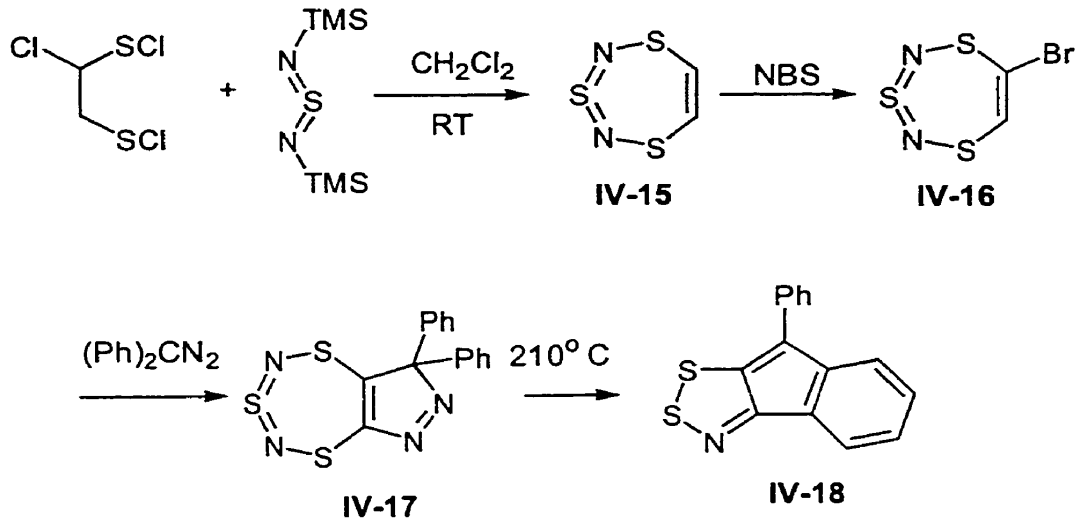

Scheme 4.5

4.1.2 1,2,3-dithiazolyl radicals

By means of the general Herz reaction, Mayer[11] was able to develop routes to a wide range of 1,2,3-DTA radicals (**IV-1**) with substituents in the 4,5-positions. These were characterized by ESR spectroscopy, which provided a valuable source of information on the effect of the substituents on the degree of delocalization of the unpaired electron; g-value and hyperfine coupling constant data have been reviewed and rationalized.[12] For example, in benzo-based 1,2,3-DTAs, the coupling constant a_N values vary from 0.65 to 0.87 mT and g-factors from 2.0075 to 2.0084. The a_N values correlate with the σ_p constants of the substituents; electron withdrawing groups (CF_3, Cl) in benzo-1,2,3-DTA reduce a_N value while electron donating groups (CH_3, CH_3O) increase it. On moving from benzene to naphthalene, a_N is also diminished, indicative of the fact that there is an increased electron delocalization effect in the latter.[12]

1,2,3-DTA radicals are usually obtained by reduction of the corresponding cation

generated from Herz reactions. Metals, sodium dithionite, triphenyl antimony and halogen anions (iodide) are common reducing reagents. However in some cases, the radical state can be reached directly (Schem 4.6). Thus, it has been reported that bis(o-aminoaryl) disulfide **IV-19** can be oxidized by SCl_2 to the radical in good yield. This radical was also obtained by irradiation or thermolysis of bis(azidoaryl) disulfides. Treatment of aminothiophenol **IV-20** with sulfur dichloride also gives stable radicals directly (Scheme 4.6). Although 1,2,3-DTA radicals have been known for many years, the first structural characterization of a monocyclic derivative was not reported quite recently. By careful selection of sterically bulky substituents at the 5-position, the radical **IV-22** was isolated from the cation form **IV-21**, and characterized structurally as its dimer. The two rings are linked by a single interannular S---S contact of 3.2987 (13)Å.[13]

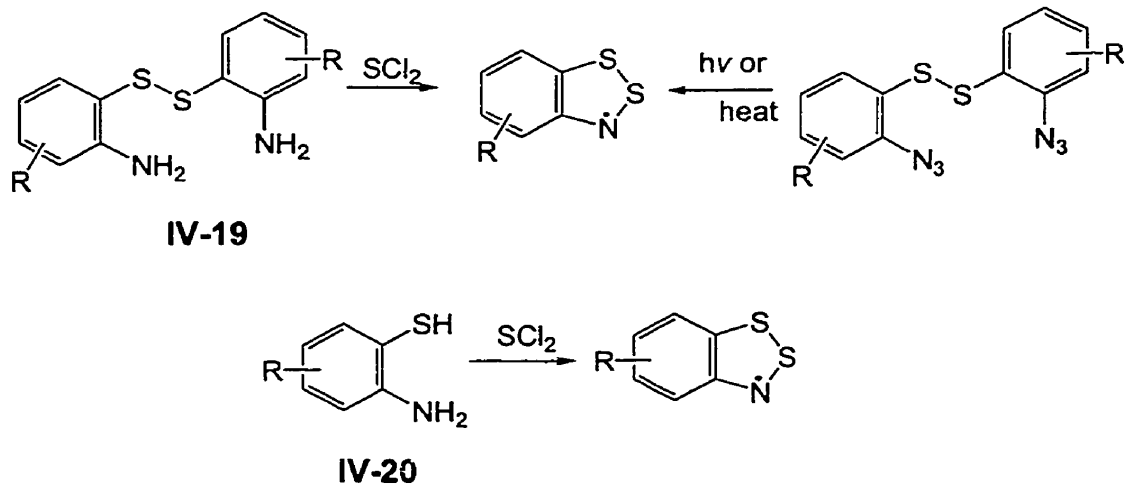

IV-19

IV-20

Scheme 4.6

In the absence of steric protection at the 5-position, association at this site is possible. Thus, reduction of Appel's salt under conditions similar to those described above lead, presumably, to a radical which undergoes a rapid irreversible association at carbon. While

the radical itself has not been observed, the final product is the fulvalene derivative **IV-25** (R = Cl).[14] No evidence was observed for the biradicals **IV-23** or **IV-24**.[15]

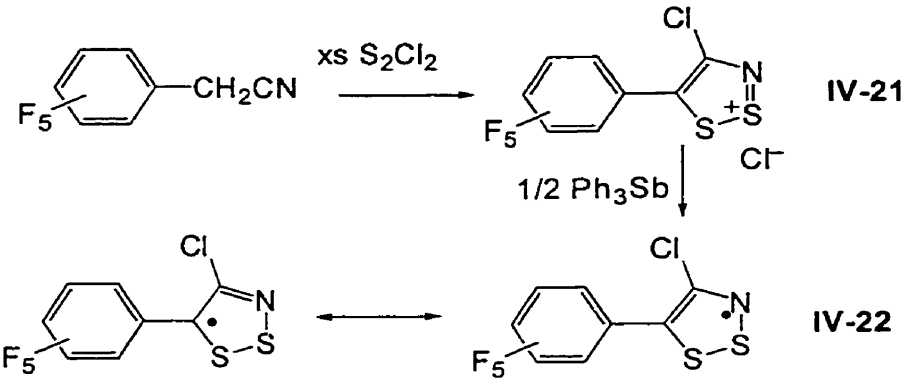

Scheme 4.7

Like tetrathiafulvalene, **IV-25** (R = Cl) can be electro-oxidized with small to medium sized counter anions such as FSO_3^-, ClO_4^- and BF_4^-, to form 1:1 CT salts. [16] Pressed pellet conductivities are in the range of 10^{-1} to 10^{-3} S cm^{-1}.

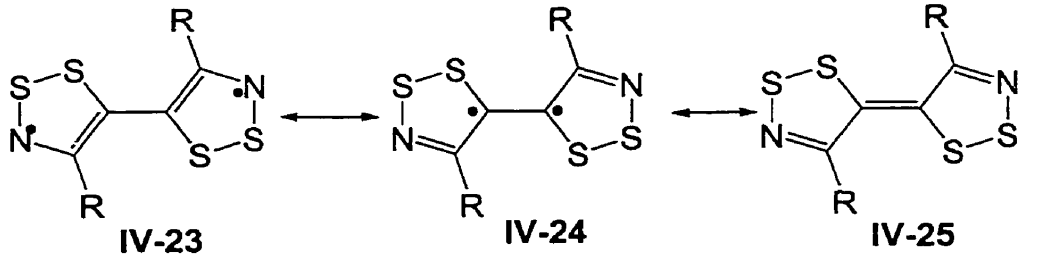

Low ΔH_{disp} should reduce the charge transfer barrier and we are moving towards the right direction. In an attempt to design heterocyclic radicals with still lower E_{cell} and ΔH_{disp} values, we set about the synthesis of 1,2,5-thiadiazolo[3,4-*b*]-1,2,3-dithiazolo[3,4-*b*]pyrazin-2-yl, or 1,2,3-TDTA (**IV-28**). As the isomer of 1,3,2-TDTA (covered in Chapter 2), 1,2,3-TDTA has extensively delocalized spin distribution. The preliminary estimates of the ΔH_{disp} value for 1,2,3-TDTA with B3LYP/6-31G** (Chapter 3) suggested a significant decrease

in the charge correlation effect (ΔH_{disp} = 5.23 eV compared with 5.46 eV in 1,3,2-TDTA). In the following section, the synthesis, redox properties, crystal structure and physical properties are presented.

4.2 Synthesis of 1,2,3-TDTA (IV-26)

Our synthesis of the 1,2,3-TDTA skeleton was based on the use of 5,6-dichloro-1,2,5-thiadiazolo[3,4-*b*]pyrazine, **IV-28** [17] the preparation of which had already been perfected during the 1,3,2-TDTA project (Chapter 2). Starting from **IV-28** preparation of the desired aminothiol **IV-27** required careful choice of reagents.

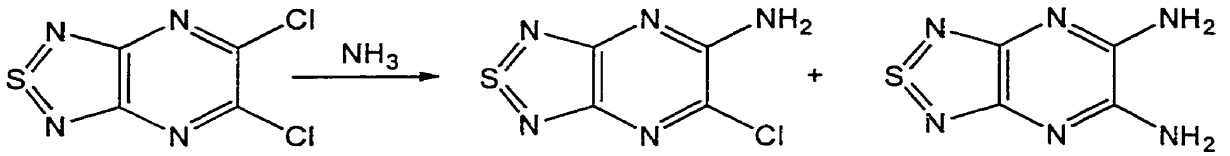

IV-28 **IV-29** **IV-30**

The activity of chlorine atoms towards substitution by ammonia varies. For example, the mono substituted product, 2-amino-3,5,6-trichloropyrazine can be prepared from tetrachloropyrazine at 90°C in a sealed tube with concentrated ammonia hydroxide, while the disubstituted products, diaminodichloropyrazine are generated at 140°C. Because of the unusual electron-withdrawing power of the 1,2,5-thiadiazole group, the chlorine atoms were greatly activated and both chlorines of **IV-28** were replaced easily by potassium phthalamide to give 5,6-diamino-1,2,5-thiadiazolo[3,4-*b*]pyrazine **IV-30** at room temperature.[18] To our surprise, the mono substituted product was not obtained, even when a deficit of potassium phthalimide was used. It appeared that, after the reaction with potassium phthalimide, the intermediate was hydrolyzed by hydrazine. The latter reagent not only broke up the

phthalimide, as predicted, but also replaced the second chlorine atom (which was reserved for thiol replacement). The reaction with ammonium hydroxide did not work well either.

Eventually we moved to the use of gaseous ammonia, and had more success. When NH_3 gas was bubbled into a toluene solution of **IV-28** at room temperature, a brown slurry was formed quickly and became very thick when it was cooled in a ice bath. This mixture contained starting material, as well as mono- and diamino derivatives (**IV-30**). However, the unreacted starting material could be filtered away and the diamino was removed during the recrystallization process. The overall yield was thus relatively low (about 50%), but a high purity of **IV-29** was achieved after double recrystallization from boiling toluene.

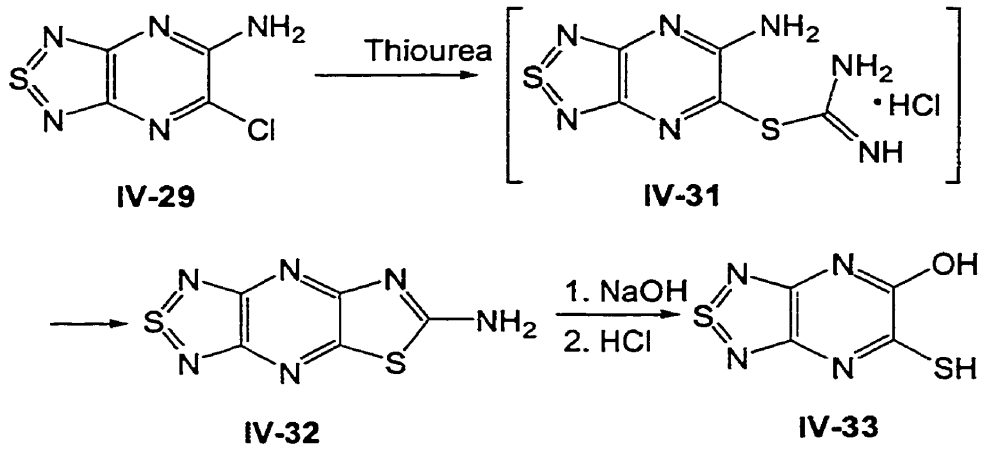

Scheme 4.8

For the conversion of the amino-chloro derivative **IV-29** to amino-thiol **IV-27**, we began by using thiourea to generate a thiouronium salt **IV-31**. However, while this step worked well, we eventually discovered that subsequent hydrolysis of the intermediate thiazole **IV-33** also converted the amine residue to an alcohol. When hydrolyzed, the thiazole ring was broken up and hydroxy group took the position of amino group (Scheme 4.8). The hydroxy-thiol compound, **IV-33** dominated the product.

We were therefore required to avoid strongly basic conditions in order to protect the amino group. This was achieved by using sodium sulfide which reacted cleanly with **IV-29** in refluxing anhydrous ethanol to afford the aminothiol **IV-27** with good yield. Crystallization of **IV-27** from boiling benzonitrile yielded brown red crystals.

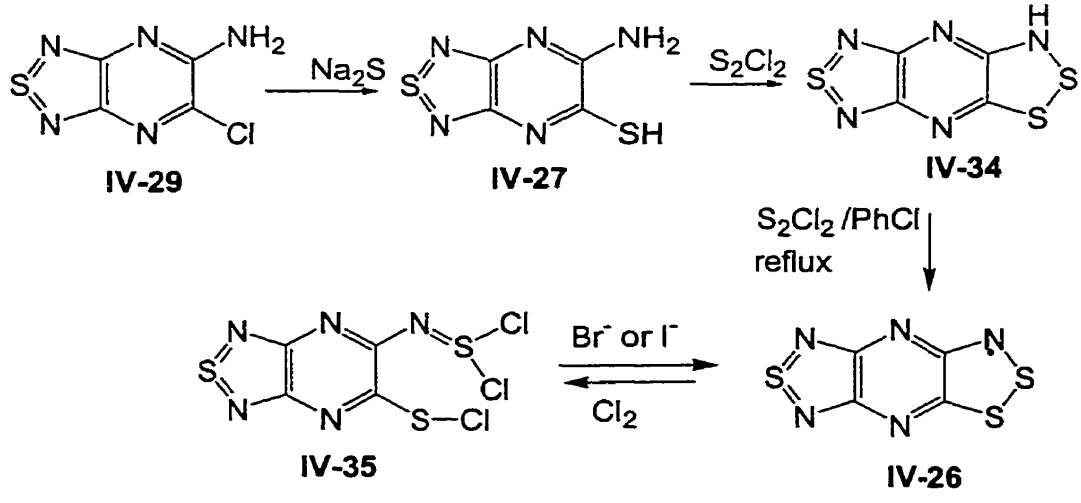

Scheme 4.9

Final cyclization of the **IV-27** with excess S_2Cl_2 took us a long time to perfect; initial attempts generated only the imide 1,2,3-TDTAH, **IV-34**. Conversion of the imide to the radical proved a challenging task. On one hand we were unable to oxidize **IV-34** to radical **IV-26** with either bromine or sulfuryl chloride, while on the other we found that chlorine was too harsh an oxidant, causing secondary cleavage of the S-S bond and formation of the trichloro-derivative 1,2,3-TDTACl_3 (**IV-35**). It was found later on that this could be achieved by direct reaction of aminothio **IV-27** with SCl_2. While reduction of the latter with bromide ion could be used to backtrack to the neutral radical (in low yield), we eventually discovered the simplest and most effective method for the conversion of imide to radical involved the use of sulfur monochloride in refluxing chlorobenzene. In this way, starting from either aminothiol or amide, the radical **IV-26** could be generated in good yield. The radical,

isolated as a lustrous black crystalline solid, was purified by fractional sublimation in vacuum. The total synthesis is shown in Scheme 4.9.

4.3 Redox chemistry of 1,2,3-TDTA

The thiadiazolopyrazine (TDP) ligand serves as a powerful electronwithdrawing ligand when attached to a 1,3,2-DTA radical (1,3,2-TDTA). Thus the redox potentials of 1,3,2- TDTA experience dramatic anodic shifts (Table 4.1) in comparison to the simple benzo derivative 1,3,2-BDTA. Computed estimates of IPs and EAs follow suit. In the context of molecular conductor design, the favorable shifts in EA and $E_{1/2}$(red) outpace the more adverse changes in IP and $E_{1/2}$(ox). The net effect is thus a diminution in both ΔH_{disp} and E_{cell} and an evolution toward a system with a lower barrier to charge transfer in the solid state.[19] As indicated in Table 4.1, the computed ΔH_{disp} values of both 1,2,3-BDTA and 1,2,3-TDTA are smaller than those seen in the 1,3,2-series, largely as a result of the higher electron affinity for the 1,2,3- DTA ring.

These computational predictions were confirmed by cyclic voltammetric analysis of 1,2,3-TDTA. The results of CV measurements on 1,2,3-BDTA[20] and 1,2,3-TDTA support these theoretical predictions. The reversible oxidation and reduction waves for the two 1,2,3- and 1,3,2-TDTA isomers are illustrated in Figure 4.1. In accord with its chemical behavior, notably the difficulty experienced in accessing the neutral radical from its imide **IV-34**, the electrochemical reduction of 1,2,3-TDTA occurs at 0.15 V vs SCE, a potential similar to that found for strong closed-shell acceptors, *e.g.*, TCNQ (0.127 V).[21] Oxidation also requires more forcing conditions, and most importantly, the overall cell potential E_{cell} is reduced from 1.06 V in the 1,3,2-isomer to 0.99 V in the 1,2,3-compound, the lowest value we have ever

observed for a heterocyclic thiazyl radical.

Table 4.1. Half-wave redox and E_{cell} potentials [a] (V *vs* SCE) and computed (B3LYP/6-31G**) IP, EA, and ΔH_{disp} values (eV) for 1,3,2- and 1,2,3-dithiazolyls

	compound			
param	1,3,2-BDTA	1,3,2-TDTA	1,2,3-BDTA	1,2,3-TDTA
$E_{1/2}$ (ox)	0.15	1.00	0.18	1.14
$E_{1/2}$ (red)	-1.24 [b]	-0.06	-1.0 [b]	0.15
E_{cell} [c]	1.33 [d]	1.06	1.15 [d]	0.99
IP	7.81	8.55	7.86	8.92
EA	1.45	3.02	2.44	4.03
ΔH_{disp}	6.36	5.53	5.41	4.88

[a] All potentials are from solutions in CH_3CN, reference SCE..

[b] *Irreversible.*

[c] E_{cell} defined as the difference in the half-wave potentials for oxidation and reduction, *i.e.*, $E_{cell} = E_{1/2}(ox) - E_{1/2}(red)$.

[d] This value taken as the difference in the cathodic peak potentials, since the reduction wave is irreversible

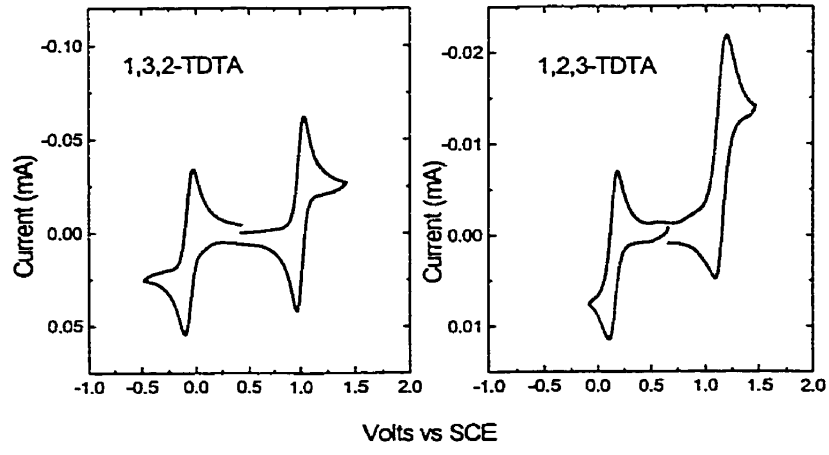

Figure 4.1 Cyclic voltammetry waves on 1,2,3-TDTA and 1,3,2-TDTA radicals (in CH_3CN, *n*-Bu_4NPF_6 supporting electrolyte, reference SCE).

4.4 ESR spectrum of 1,2,3-TDTA

The X-band ESR spectra (in CH_2Cl_2, 293 K) of the two TDTA isomers are shown in Figure 4.2. The signal ($g = 2.009$) of the 1,2,3-derivative is considerably more complex, but spectral simulation reveals the effects of hyperfine coupling to all five nitrogen nuclei. The assignments of the derived a_N values are also provided in Figure 4.2, along with the calculated ((B3LYP/6-31G**) spin densities q for both systems. The results reveal that while the thiadiazolopyrazine (TDP) residue simply refines the spin distribution of a 1,3,2-DTA radical, it causes a major reorganization of the electronic structure of a 1,2,3-DTA radical. In simple monofunctional 1,2,3-DTA radicals, spin density is heavily localized at the 5-position of the heterocycle; *i.e.*, they are carbon-centered radicals.[17] By contrast, in 1,2,3-TDTA, spin density is stripped away from the 5-position and is redistributed not only to the nitrogen attached to the 4-position of the DTA ring but also to the other three nitrogens of the TDP ligand. As a result of this reorganization of spin density, the 1,2,3-TDTA radical resists association via C-C bond formation.

An important point that can be drawn from the resonance structures of 1,2,3-TDTA (Scheme 4.10) is that the unpaired electron can be located on any of the nitrogen atoms, but not on carbon. As a result the potential for this species to associate by C-C bond formation is very low.

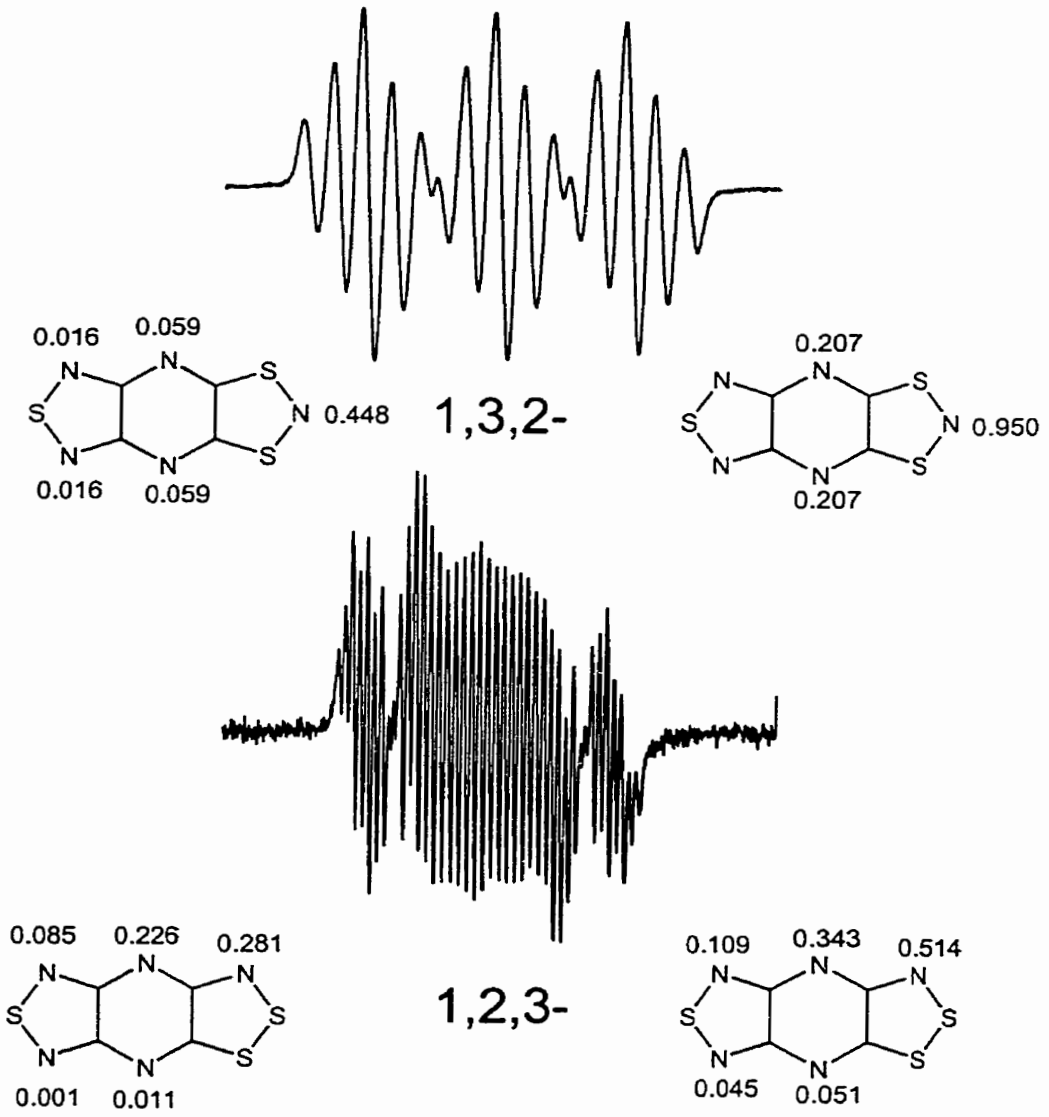

Figure 4.2 X-Band ESR spectra of 1,2,3-TDTA and 1,3,2-TDTA (in CH_2Cl_2, 293 K, sweep width 4 mT). Derived ^{14}N hyperfine coupling constants a_N are shown on the right, and calculated spin densities q_N are shown on the left.

4.5 Crystal structure of 1,2,3-TDTA

We determined two crystal structures in the course of work on 1,2,3-TDTA. That of the oxidized derivative 1,2,3-TDTACl_3 (**IV-35**) was performed in order to confirm its structural identity and also to provide a basis for comparison with the radical 1,2,3-TDTA itself. An ORTEP drawing of 1,2,3-TDTA, showing the atom numbering, is shown in Figure 4.4 (left). Table 4.2 summarizes the intramolecular distances in 1,2,3- TDTA and 1,2,3-TDTACl_3. Crystals of 1,2,3-TDTA belong to the monoclinic space group $P2_1/n$; there are four radical molecules per unit cell. The radicals, which are planar to within 0.07 Å, are loosely associated into centrosymmetric or head-to-tail dimers (Figure 4.3 right), the closest intradimer S-S contact $d1$ (S_2---S_3) being 3.2331(15) Å. This distance is shorter than the interannular contacts observed in the low-temperature phase of 1,3,2-TDTA, but longer than those seen in the dimer of 1,3,2-BDTA.[22a]

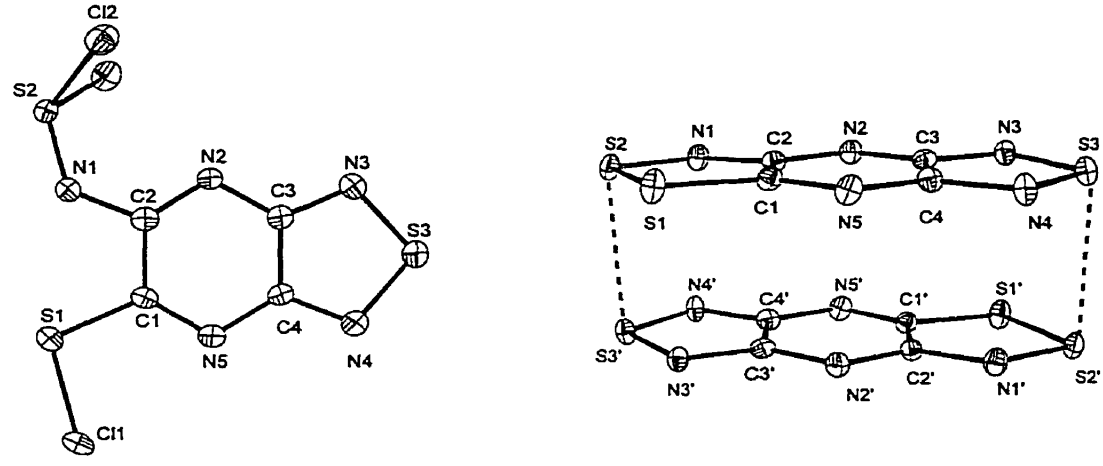

Figure 4.3 ORTEP drawings of the compound 1,2,3-TDTACl_3 (**IV-35**) (left) and a single dimer unit in 1,2,3-TDTA **IV-26**.

As the magnetic measurements (*vide infra*) indicate, interannular orbital interactions at this range are weak but sufficient to quench paramagnetism, *i.e.*, to generate a weak "chemical bond" between the two radicals. Within the individual halves of the dimer the bond lengths show changes from those seen in compound **IV-35** that reflect the long-range nature of the electron delocalization in the radical. The shortening of the N_1-C_2 bond relative to 1,2,3- $TDTACl_3$ heralds considerable double bond character. This change, coupled with the shortening of N_2-C_3 and N_5-C_4, and the lengthening of N_2-C_2, suggest the collective involvement of the series of valence bond resonance structures **IV-26 (A-C)** in Scheme 4.10.

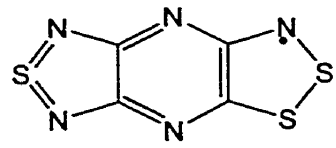

IV-26A

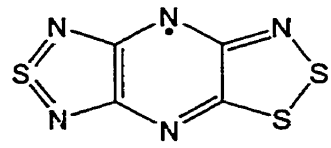

IV-26B

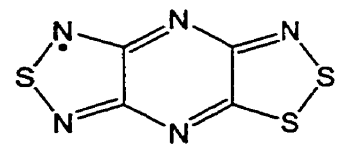

IV-26C

Scheme 4.10

Table 4.2 Intramolecular distances (Å) in **IV-26** and **IV-36**.

	IV-26	**IV-35**		**IV-26**	**IV-35**
S1-S2	2.0482 (13)	—	N2-C3	1.347(4)	1.369(5)
S1-C1	1.721(3)	1.754(4)	N3-C3	1.347(4)	1.335(5)
S2-N1	1.609(3)	1.516(3)	N4-C4	1.347(4)	1.333(5)
S3-N3	1.622(3)	1.618(4)	N5-C1	1.314(4)	1.301(5)
S3-N4	1.644(3)	1.619(4)	N5-C4	1.351(4)	1.364(5)
N1-C2	1.342(4)	1.403(5)	C1-C2	1.463(5)	1.451(5)
N2-C2	1.338(4)	1.293(5)	C3-C4	1.450(5)	1.417(6)

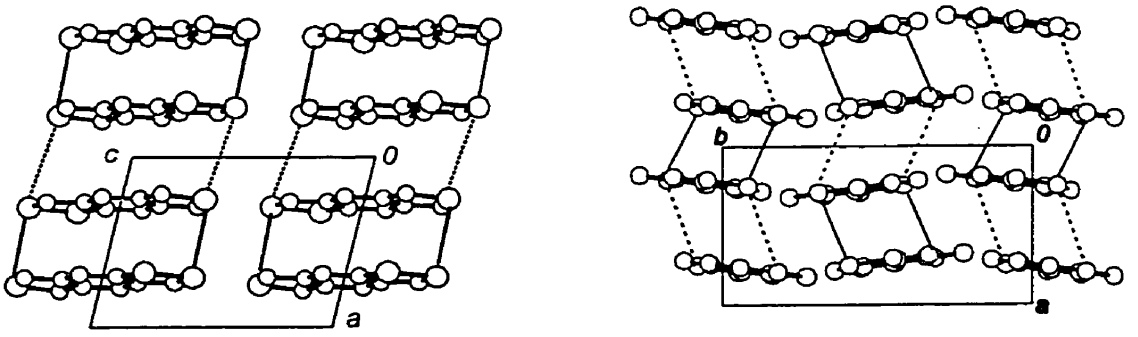

Figure 4.4 Two side views of the stacking structure of 1,2,3-TDTA

Several views of the packing of the dimers are shown in Figure 4.4 and Figure 4.5. The dimers adopt a slipped π-stack motif within which the closest interdimer S---S separation d_2 (S_2 ---S_3') is 3.8601(15) Å. In addition to these intrastack contacts there are two interstack S---S contacts d_3 (=3.5819(15) Å) and d_4 (=3.3610(13) Å) that are within the van der Waals approach (3.6 Å) for two sulfurs. [23]

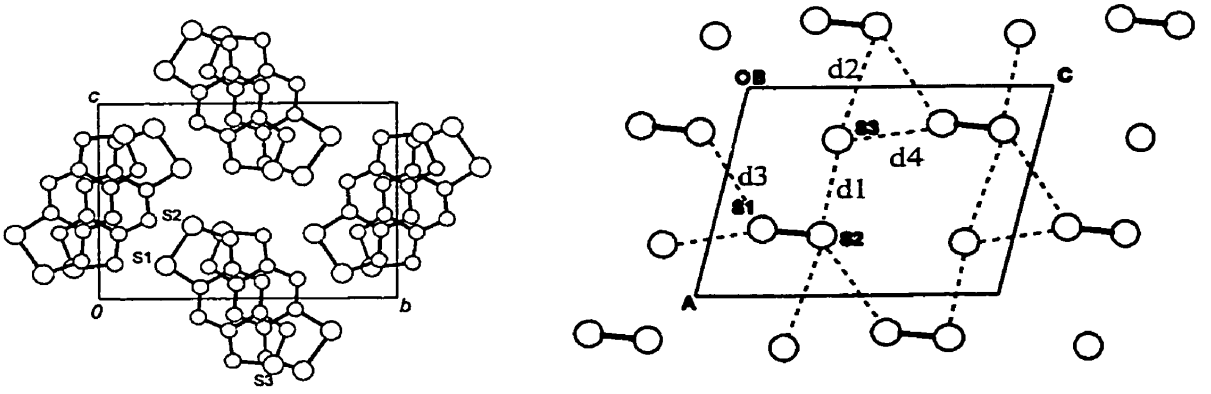

Figure 4.5 Packing of 1,2,3-TDTA, shown from above(left). Dashed lines show the intermolecular distances (right): d_1 =3.2331(15), d_2 =3.8601(15), d_3 =3.5819(15), and d_4 =3.3610(13) Å.

4.6 Magnetic susceptibility

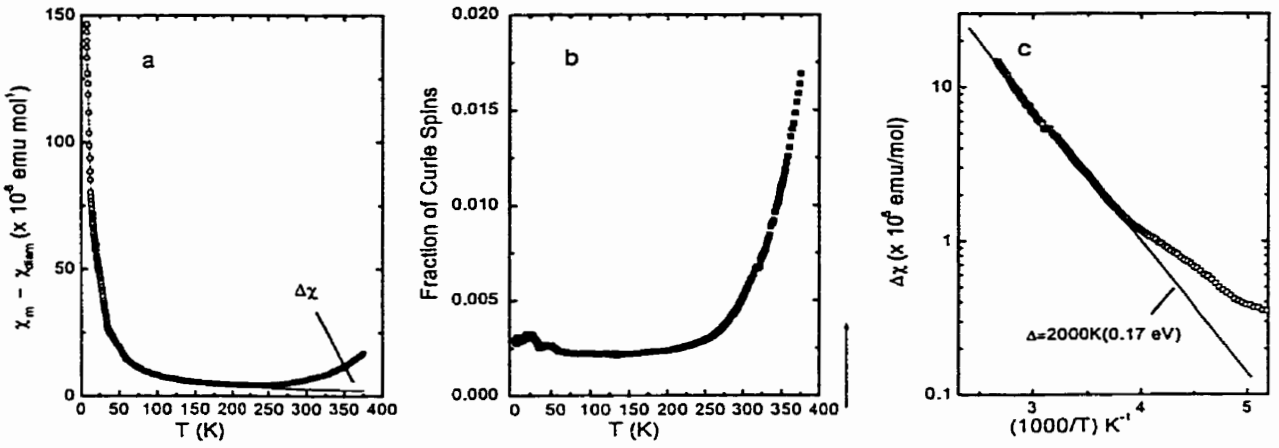

Figure 4.6 Magnetic susceptibility χ_M - χ_0 of solid-state 1,2,3- TDTA as a function of temperature (a), fraction of Curie spins as a function of T (b), and $\Delta\chi$ as a function of $1/T$ (c).

The magnetic susceptibility of 1,2,3-TDTA was measured over the temperature range 5-380 K; the results are plotted in Figure 4.6. The compound is essentially diamagnetic. In the low temperature regime the susceptibility exhibits a Curie-Weiss dependence (solid line in Figure 4.6a), with a derived diamagnetic contribution $\chi_0 = -133 \times 10^{-6}$ emu mol $^{-1}$, a Θ value of 6.4 K, and a residual spin concentration of 0.2% (Figure 4.6b). Above 200 K a deviation $\Delta\chi$ from Curie-Weiss behavior is observed (Figure 4.6a) in the form of an enhanced paramagnetism which reaches a value that corresponds to 2% of the molecules carrying free Curie spins at 380 K (Figure 4.6b). This enhancement $\Delta\chi$ shows an activated temperature dependence (see the plot of $\Delta\chi$ *vs* $1/T$ in Figure 4.6c) with activation energy Δ = 2000 K (0.17 eV). Similar paramagnetic enhancements of larger magnitude have been observed in the structures of dithiadiazolyl π-dimer stacks,[24, 25] and this behavior has been attributed to a lack of coupling of the weak intradimer bonds and the formation of spin

defects in the lattice. Such spin uncoupling can clearly also take place at elevated temperatures in 1,2,3-TDTA, but it is interesting, in view of the weakness of the interannular interactions (as evidenced by the molecular separation), that the degree of uncoupling is so small.

4.7 Conductivity Measurements

The single crystal conductivity (σ) of 1,2,3-TDTA was measured in a four probe configuration; the in-line contacts were made with silver paint. The crystal dimensions were $1 \times 0.3 \times 0.3$ mm^3 . The temperature dependence of the conductivity was measured in the range 345 - 75 K. At 75 K the sample resistance was over 10^{13} Ω, the limit of the experimental setup. The high-temperature limit was set by the sample degradation that appeared above 345 K as an irreversible increase in the sample resistance. The results are shown in Figure 4.7 a. The conductivity decreases by 8 orders of magnitude with decreasing temperature from 345 to 75 K. An Arrhenius plot of the same data (Figure 4.7b) shows activated behavior for σ with variable activation energy, the characteristic feature of hopping conductivity.[26] Near room temperature the activation energy Δ is about 2600 K (0.22 eV), which is close to the activation energy of the free Curie spins (Figure 4.6 c) and is consistent with a gap value $2\Delta = 0.4$ eV calculated in the next section. This correlation suggests that the thermally released free spins are the same carriers which contribute to the conductivity. Figure 4.7 c shows that the temperature dependence of the logarithm of conductivity is proportional to $T^{-1/2}$, as predicted for one-dimensional variable range hopping.[27, 28] The three- and two-dimensional variable-range hopping theories [29] ($T^{-1/4}$ and $T^{-1/3}$ dependencies, respectively) do not fit to our data. The observed behavior of the conductivity suggests that

defect states exist within the gap near the Fermi level and at least at low temperature the transport is dominated by variable-range hopping involving these states. The transport is preferentially one-dimensional in the x-direction along the molecular stacks. At high temperatures the hopping would involve states near the gap edge, $\Delta = 2600$ K, where the carrier mobility is higher.

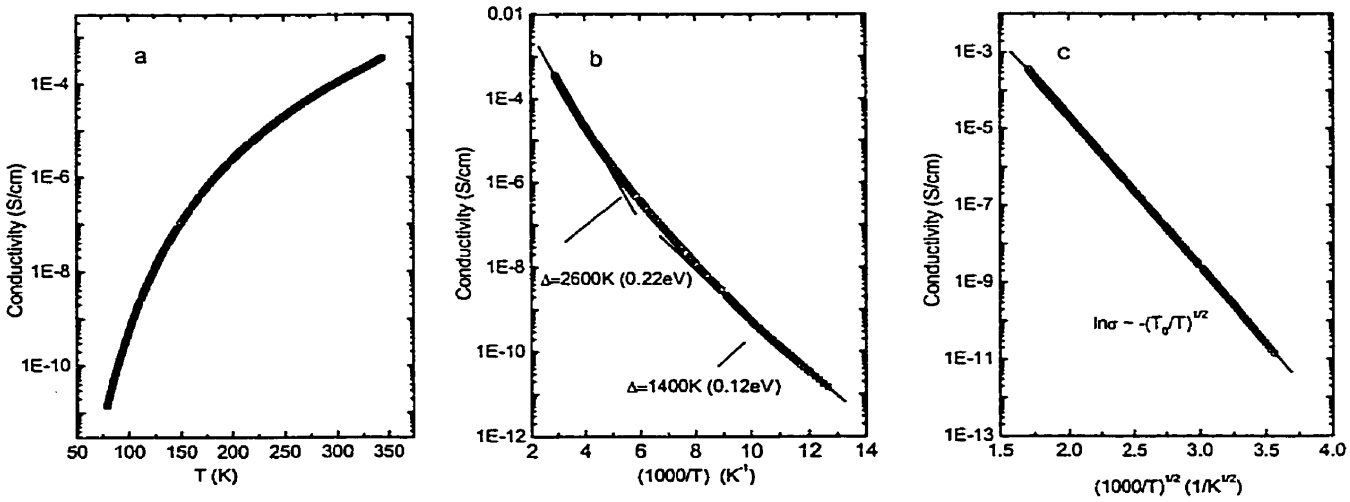

Figure 4.7 Conductivity of solid-state 1,2,3-TDTA, plotted as a function of (a) absolute temperature T, (b) $1/T$, and (c) $(1/T)^{1/2}$.

4.8 Band Structure Calculations

To probe the extent of intermolecular orbital interactions in 1,2,3-TDTA, we performed extended Hückel band structure calculations on the full solid state structure. Figure 4.8 (left) illustrates the dispersion curves of the highest lying occupied and lowest lying unoccupied molecular orbitals, plotted along the three principal directions of reciprocal space. As expected from the magnetic measurements, dimerization of the radicals leads to the opening of a band gap at the Fermi level, leading to a closed-shell semiconducting state.

The calculations suggest the band gap is ca. 0.4 eV, a value considerably smaller than that found in other radical dimer structures we have studied, and consistent with the magnetic and conductivity data reported above. The small size of the band gap cannot be ascribed to crystal orbital dispersion along the stacking direction.[29] Rather, the small valence/ conduction band splitting arises from the weakness of the *intra* dimer interactions, which we attribute to the unique head-to-tail mode of association. Uncoupling of the dimers will produce defects and midgap states which are important for conductivity (see below), but these cannot be adequately described by the ideal crystal model used for the band calculations.

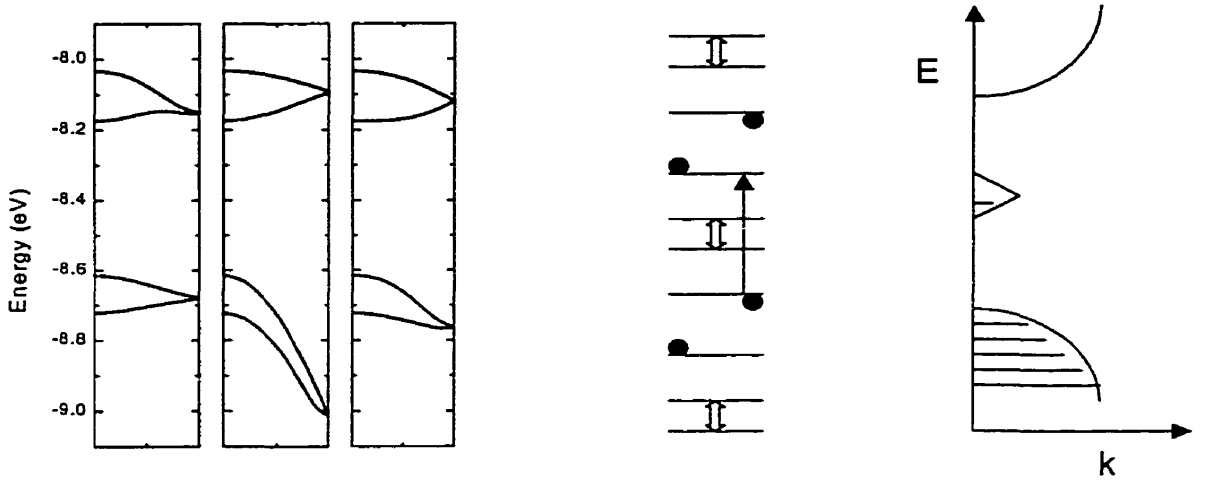

Figure 4.8 Dispersion of the valence and conduction bands of 1,2,3- TDTA (left). One-dimensional variable range hopping model for solid-state 1,2,3-TDTA. The mid gap states arise from topological defects in the lattice and thermal dissociation of dimers (right).

4.9 Conduction Model

The one-dimensional hopping model,[29] as it applies to 1,2,3-TDTA , is summarized in the right side of Figure 4.8. At low temperatures topological defects and some lattice disorder are responsible for the finite density of states within the gap that leads to hopping

conductivity. With increasing temperature the free spins that are created by dissociation of the dimers appear as midgap states at the Fermi level. Presumably the same situation arises with the dithiadiazolyl compounds, where a fairly large density of midgap states is generated. [27, 28] However these midgap states in the dithiadiazolyls do not contribute to the conductivity and the states are localized, apparently by the large onsite Coulomb correlation energy. Thus we consider the dithiadiazolyls as Mott insulators. The new feature for 1,2,3-TDTA is the identification of enhanced conductivity with these midgap states. Thus these states are not fully localized in 1,2,3- TDTA and they contribute to the conductivity by variable-range hopping. It may be appropriate to view these midgap states as separate donor and acceptor bands, [29] because these states will be split by the relatively large Coulomb correlations still remaining in this organic molecule. In this way the conduction in 1,2,3-TDTA would be viewed as arising from one-dimensional variable range hopping involving semi-metallic midgap states. In this model the low-temperature conductivity originates from hopping between midgap states (Figure 4.7 b, $\Delta = 0.12$ eV), whereas at high temperatures the conductivity is mainly associated with hopping that also involves midgap states and the band edges of either the valence or conduction bands ($\Delta = 0.22$ eV, in good agreement with the energy gap of 2Δ, discussed above).

At room temperature σ approaches 1×10^{-4} S cm^{-1}, rising to a value of 4×10^{-4} at 345 K. These values are significantly higher than those observed for 1,3,2-TDTA and, indeed, any heterocyclic thiazyl radical or radical dimer system we have yet encountered. We can estimate the mobility μ in 1,2,3-TDTA. Using the observed value of the fraction of free spins (0.5% at room temperature, Figure 4.6b) and the volume of the molecular unit cell ($1.6 \times 10\,2$ Å^3 mol^{-1}), we obtain a carrier (spin) density $n = 3 \times 10^{19}$ cm^{-3}. Hence $\mu = \sigma$

/(en) $= 2 \times 10^{-5}$ cm ^{2} V $^{-1}$ s $^{-1}$ at room temperature, a reasonably high value for this class of materials.[30]

4.10 Summary and conclusions

In our pursuit of neutral π-radical conductor materials we have faced two fundamental design challenges. First, we have endeavored to suppress the structural (Peierls) instability associated with a half-filled one-dimensional energy band, i.e., the tendency of π-stacked radicals to dimerize. Overcoming the self-association of radicals has required that the radical spins be highly delocalized at the molecular level and that in the solid state two- and three-dimensional intermolecular interactions be enhanced. We have addressed both of these issues by using ring systems in which carbon, along with its exocyclic ligand (even if only a C-H group), is replaced by a heteroatom. However, while aiding in the resolution of the structural issue the use of heteroatoms creates a second, energetic problem. The extreme electronegativity that results from incorporation of nitrogen and sulfur atoms into the skeletal framework leads to a higher ionization potential, a trend which is counterproductive to the design of radicals with a low disproportionation enthalpy ΔH_{disp}. Under these circumstances the radical spins become trapped on the molecular building blocks and in the solid state the materials are Mott insulators. The 1,3,2-TDTA radical provides a good example of such a system, i.e., an undimerized π-stacked structure in which the bandwidth is insufficient to overcome the Coulombic barrier U to charge transport. In the isomeric 1,2,3-TDTA radical reported here, U is lowered by virtue of a dramatic increase in electron affinity, one which more than offsets the small increase in ionization potential. However, in the solid state the 1,2,3-TDTA radical does not adopt a simple slipped π-stacked structure but rather a slipped

π-dimer stack in which the dimers are coupled in a hitherto unobserved head-to- tail arrangement. As a result of this association the radical spins are paired and a *small* energy gap is opened at the Fermi level. Nonetheless, the resulting material exhibits a remarkably high conductivity. Indeed it is, to our knowledge, the highest conductivity ever observed for a single-component [31] sulfur-based molecular material. More important, however, is the fact that the free spins generated by uncoupling of 1,3,2-TDTA dimers at elevated temperatures contribute to an enhancement in conductivity.

1,2,3-TDTA also confirmed that MNDO and, more particularly, DFT calculations are excellent tools for predicting the molecular electronic properties and guiding the design and engineering of new neutral radical conductors.

4.11 Experimental section

Preparation of 5-amino-6-chloro-1,2,5-thiadiazolo[3,4-*b*]pyrazine, IV-29

Ammonia gas was passed over a solution of 5,6-dichloro-1,2,5-thiadiazolo[3,4-*b*]pyrazine (**IV-28**) (5.00 g, 24.2 mmol) in 100 mL toluene for 30 min. The gas flow was halted and the mixture left to stir for 1 h at room temperature. The yellow solid was filtered off, washed with 50 mL ether, and sucked dry. The crude product was extracted by boiling with 300 mL of hot toluene (in which the presumed "diamino **IV-30**" derivative and ammonium chloride are insoluble). Hot filtration of the extract and cooling of the filtrate afforded canary yellow needles of **IV-29** (1.88 g, 10.0 mmol, 42%), mp 216-218°C. Evaporation of the toluene extracts afforded 0.4 g, 1.8 mmol of unreacted **IV-30**. IR (4000-400 cm^{-1}): 3419 (m), 3296 (w), 3127 (m, br), 1656 (vs), 1482 (m), 1343 (m), 1107 (s), 925 (w), 872 (m), 817 (m), 783 (w), 642 (m), 536 (vs), 474 (w), 434 (m) cm^{-1}. MS (EI, *m/e*): 187

(M^+, 100%), 152 (65%), 87 (14%), 74 (18%), 68 (50%), 53 (45%). Anal. calcd for $C_4H_2N_5SCl$: C, 25.61; H, 1.07; N, 37.33. Found: C, 25.74; H, 0.97; N, 37.50.

Preparation of 1,2,5-thiadiazolo[3,4-*b*]pyrazino [3,4-b]-1,3-thiazole, IV-32

The aminochloro derivative **IV-29** (2.37 g, 12.7 mmol) and thiourea (2.89 g, 38.0 mmol) were added to 100 ml of anhydrous ethanol. The yellow slurry was refluxed for about 3 hours and the orange precipitate filtered off and dried in the air. Yield, 2.6 g, 83%. IR (4000-400 cm^{-1}): 3357(w), 3275(w), 1684(s), 1623(w), 1600(w), 1568(m), 1317(s), 1212(m), 1124(s), 965(m), 873(w), 852(s), 806(s), 741(m), 714(m), 655(m), 643(w), 617(s), 604(m), 564(m), 521(s). MS (EI, m/e): 210 (M^+, 100%), 185 ($[M-HCN]^+$, 12%), 168 (13%),116 (12%), 70 (12%).

Preparation of 5-amino-6-hydroxy-1,2,5-thiadiazolo[3,4-*b*]pyrazine, IV-33

The thiazole derivative **IV-32** (1.0 g, 4.76 mmol) as intermediate was hydrolyzed with excess NaOH in about 40 ml of water for 30 minutes with gentle heating. All the solid went into the solution quickly and the clean red solution was acidified with acetic acid and generated a brown solid. Yield (0.56 g, 63%). MS (EI, m/e): 169 (M^+, 100%), 141 ($[M-CO]^+$, 41%), 99 (17%), 74 (36%), 68 (54%). IR (4000-400 cm^{-1}): 3434 (w), 3157 (w), 1686 (s), 1560 (w), 1545 (w), 1332 (s), 1114 (s), 925, 839 (s), 797 (s), 786 (s), 694 (s), 664 (s), 629 (s), 601 (m), 513 (w). No further characterization was performed on this material.

Preparation of 5-amino-6-mercapto-1,2,5-thiadiazolo[3,4-*b*]pyrazine, IV-27

Anhydrous sodium sulfide (1.84 g, 23.6 mmol) was added to a slurry of **IV-29** (4.00

g, 21.3 mmol) in 80 mL of anhydrous ethanol, and the resulting orange red slurry stirred under nitrogen for 16 h at 78 °C. Aqueous HCl (100 mL, 10%) was then added to the mixture, and the resulting orange precipitate filtered off, washed with water and ethanol, and sucked dry. The crude product was recrystallized from boiling benzonitrile (350 mL) as red brown microcrystals (3.07 g, 16.6 mmol, 78%), subl. >280 °C. IR (4000-400 cm^{-1}): 3402 (m), 3260-3070 (br, m), 1633 (s), 1601 (s), 1576 (s), 1312 (m), 1292 (m), 1126 (s) 852 (m), 806 (s), 778 (m), 693 (s), 516 (w), 467 (m) cm^{-1}. MS (*m/e*): 185 (M^+, 55%), 112 (21%), 68 (20%), 58 (100%). Anal. calcd for $C_4H_3N_5S_2$: C, 25.94; H, 1.63; N, 37.81 %. Found: C, 26.16; H, 1.56; N, 37.73 %.

Preparation of 1,2,5-thiadiazolo[3,4-*b*]pyrazino [3,4-b]-1,2,3-dithiazoline, IV-34

Excess sulfur monochloride (4 mL) was added to a slurry of aminothiol **IV-27** (0.50 g, 2.70 mmol) in 35 mL of distilled acetonitrile or dichloroethane, and the mixture stirred and heated at gentle reflux for 6 h. The mixture was cooled and the red microcrystalline solid filtered off, washed with 2 x 20 mL of dichloroethane, and dried *in vacuo* (yield 0.56 g, 2.62 mmol, 97%). The crude imide was purified, for analytical purposes, by fractional sublimation at 140-80 °C/10^{-2} Torr as orange microcrystals, dec >230 °C. IR (4000-400 cm^{-1}): 3188 (w), 1586 (s), 1564 (w), 1318 (s), 1277 (w), 1247 (m), 1079 (w), 838 (w), 828 (w), 785 (s), 717 (m), 693 (w), 508 (m) cm^{-1}. MS (EI, *m/e*): 215 (M^+, 100%), 84 (11%), 70 (11%), 64 (35%), 46 (26%). HRMS: Found, 214.9394, calcd 214.939408. Anal. calcd for $C_4HN_5S_3$: C, 22.32; H, 0.47; N, 32.53 %. Found: C, 22.54; H, 0.29; N, 32.70 %.

Preparation of 1,2,5-thiadiazolo[3,4- *b*]-1,2,3-dithiazolo[3,4-*b*]pyrazin-2-yl, IV-26.

An excess of sulfur monochloride (6 mL) was added to a slurry of **IV-27** (1.50 g, 8.10 mmol) in 50 mL of chlorobenzene, and the mixture stirred and heated at reflux for 3 hours. The black solid was filtered off, washed with 2 x 20 mL acetonitrile, and dried in *vacuo* (0.135 g, 6.31 mmol, 78%). The crude product was purified by slow, fractional sublimation (to remove traces of **IV-34**) at 155 -120 °C/10^{-2} Torr in a gradient tube furnace to afford jet black needles, dec >270 °C. Further purification was effected by a second sublimation at 140-80 °C/10^{-2} Torr in a sealed tube. IR (4000-400 cm^{-1}): 1417 (w), 1331 (s), 1293 (m), 1090 (w), 949 (m), 879 (s), 857 (m), 800 (m), 686 (m), 633 (m), 531 (m), 495 (w), 495 (m), 448 (m), 405 (s) cm^{-1}. Anal. calcd for $C_4N_5S_3$: C, 22.42; N, 32.69 %. Found: C, 22.53; N, 32.65 %.

Preparation of 1,2,3-TDTACl_3 (IV-35).

Chlorine gas was passed over a slurry of **IV-34** (0.250 g, 1.16 mmol) in 20 mL of CH_3CN. The mixture was gently warmed until all the solid dissolved to afford an orange solution (30 min). Canary yellow needles of 1,2,3-TDTACl_3 (**IV-35**) grew upon cooling the solution to -20 °C. These were filtered off under nitrogen, washed with 2 x 5 mL of cold CH_3CN, and pumped dry (yield 0.300 g, 0.94 mmol, 81%), dec >135 °C. IR (4000-400 cm^{-1}): 1521 (m), 1458 (s), 1384 (s), 1293 (s, br), 1246 (m), 1136 (s), 1021 (m) 917 (m), 869 (m), 814 (m), 759 (m), 681 (w), 636 (m), 549 (s), 467 (s), 431 (s) cm^{-1} . Anal. calcd for $C_4N_5S_3Cl_3$: C, 14.98; N, 21.84 %. Found: C, 15.10; N, 21.98 %. Crystals suitable for X-ray diffraction were grown by recrystallization from CH_3CN.

Reduction of 1,2,3-TDTACl_3 to 1,2,3-TDTA.

Tetra-*n*-butylammonium bromide (1.21 g, 3.75 mmol) was added to a slurry of 1,2,3-TDTACl_3 (**IV-35**) (0.400 g, 1.25 mmol) in 20 mL of CH_3CN. After 5 min a black precipitate of 1,2,3-TDTA (215 mg, 1.00 mmol, 80%) was filtered off and dried in *vacuo*. Its identity was confirmed by comparison of its IR spectrum with that of a known sample.

4.12 References

1. (a) Barclay, T. M.; Cordes, A. W.; Haddon, George, N. A.; R. C.; Itkis, M. E.; Mashuta, M. S.; Oakley, R. T.; Patenaude, G. W.; Reed, R. Richardson, J. F.; W.; Zhang, H. *J. Am. Chem. Soc.* **1999**, *121*, 969. (b) Barclay, T. M.; Cordes, A. W.; Haddon, R. C.; Itkis, M. E.; Oakley, R. T.; Reed, R. W.; Zhang, H. *J. Am. Chem. Soc.* **1999**, *121*, 969.
2. Appel, R.; Janssen, H.; Siray, M.; Knoch, F. *Chem. Ber.* **1985**, *118*, 1632.
3. (a) Rees, C. W. *J. Heterocyclic Chem.* **1992**, 639. (b) Khmelinitski, L.; Rakitin, O. A. "*Advance in Heterocyclic Chemistry*", **1996**, Chapter 4.11, P. 409. (c) Kim, K. *Sulfur Rep.* **1998**, *21*, 147. (d) Kim, K. *Phosphorus, Sulfur and Silicon*, **1997**, *120&121*, 229.
4. (a) Mayer, R.; Domschke, G.; Bleisch, S.; Bartl, A. *Z. Chem.* **1981**, *21*, 324. (b) Warburton, W. K. *Chem. Rev.* **1957**, 1011. (c) Inagaki, Y.; Okazaki, R. *Sulfur, Rep.* **1982**, *2*, 137.
5. Barclay, T. M.; Burgess, I. J.; Cordes, A. W.; Oakley, R. T.; Palstra, T. T. M.; Patenaude, G. W.; Reed, R. W. *Chem. Commun.* **1998**, 1935.
6. (a) Hafner, K.; Stowasser, B.; Sturm, V. *Tetrahedron Lett.* **1985**, *26*, 189. (b) Plater, M. J.; Rees, C. W.; Roe, D. G.; Torroba, T. *J. Chem. Soc., Chem. Commun.* **1993**, 293. (c) Plater, M. J.; Rees, C. W.; Roe, D. G.; Torroba, T.; *J. Chem. Soc., Perkin Trans.*1 **1993**, 769.

7. (a) Marcos, C. F.; Polo, C.; Rakitin, O. A.; Rees, C. W.; Torroba, T. *Angew. Chem. Int. Ed. Engl.* **1997**, *36*, 281. (b) Rees, C. W.; White, A. J. P.; Williams, D. J., Rakitin, O. A.; Marcos, C. F.; Polo, C.; Torroba, T. *J. Org. Chem.* **1998**, *63*, 2189. (c) Marcos, C. F.; Polo, C.; Rakitin, O. A.; Rees, C. W.; Torroba, T. *J. Chem. Soc., Chem. Commun.* **1997**, 879. (d) Marcos, C. F.; Rakitin, O. A.; Rees, C. W.; Torroba, T.; White, A. J. P.; Williams, D. J. *Chem. Commun.* **1999**, 29.

8. Barclay, T. M.; Cordes, A. W.; Goddard, J. D.; Mawhinney, R. C.; Oakley, R. T.; Preuss, K. E.; Reed, R. W. *J. Am. Chem. Soc.* **1997**, *119*, 12136.

9. (a) Morris. J. L.; Rees, C. W. *J. Chem. Soc., Perkin Trans. 1* **1987**, 211. (b) Morris. J. L.; Rees, C. W. *J. Chem. Soc., Perkin Trans. 1* **1987**, 217.

10. Plater, M. J.; Rees, C. W. *J. Chem. Soc., Perkin trans. 1* **1991**, 311.

11. Mayer, R. *Phosphorus Sulfur,* **1985**, *23*, 277.

12. Mayer, R.; Domschke, G.; Bleisch, S.; Fabian, J.; Bartl, A.; Staško, A. *Collection Czechoslovak Chem. Commun.* **1984**, *49*, 684.

13. Barclay, T. M.; Beer, L.; Cordes, A. W.; Oakley, R. T.; Preuss, K. E.; Taylor, N. J.; Reed, R. W. *J. Chem. Soc., Chem. Commun.* **1999**, 531.

14. Barclay, T. M.; Beer, L.; Cordes, A. W.; Haddon, R. C.; Itkis, M. E.; Oakley, R. T.; Preuss, K. E.; Reed, R. W. *J. Am. Chem. Soc.* **1999**, *121*, 6657.

15. Genin, H., Hoffmann, R. *Macromolecules*, **1998**, *31*, 444.

16. Barclay, T. M.; Cordes, A. W.; Oakley, R. T.; Preuss, K. E.; Reed, R. W. *J. Chem. Soc., Chem. Commun.* **1998**, 1039.

17. Tong, Y. C. *J. Heterocycl. Chem.* **1975**, *12*, 451.

18. (a) Yamashita, Y.; Saito,K.; Suzuki, T.; Kabuto, C.; Mukai, T.; Miyashi, T. *Angrew. Chem. Int. Ed. Engl.* **1988**, *27*, 434. (b) Suzuki, T.; Fujii, H.; Yamashita, Y.; Kabuto, C.; Tanaka, S.; Harasawa, M.; Mukai, T.; Miyashi, T. *J. Am. Chem. Soc.* **1992**, *114*, 3034.

19. (a) Haddon, R. C. *Nature* (London) **1975**, *256*, 394. (b) Haddon, R. C. *Aust. J. Chem.* **1975**, *28*, 2343.

20. Cyclic voltammetry on the 1,2,3-BDTA system has been reported by Tsveniashvili, V. Sh.; Malashkiya, M. V. *Electrokhimiya* **1984**, *3*, 357. The data provided in this table refer to measurements made in our laboratories.

21. Bard, A. J.; Faulkner, L. R. "*In Electrochemical Methods, Fundamental and Application*", J. Wiley and Sons, New York, **1980**, Appendix C.

22. (a) Awere, E. G.; Burford, N.; Haddon, R. C.; Parsons, S.; Passmore, J.; Waszczak, J. V.; White, P. S. *Inorg. Chem.* **1990**, *29*, 4821. (b) Wolmershaser, G.; Schnauber, M.; Wilhelm, T. *J. Chem. Soc., Chem. Commun.* **1984**, 573.

23. Bondi, A. *J. Phys. Chem.* **1964**, *68*, 41.

24. (a) Cordes, A. W.; Haddon, R. C.; Hicks, R. G.; Oakley, R. T.; Palstra, T. T. M.; Schnemeyer, L. F.; Waszczak, J. V. *J. Am. Chem. Soc.* **1992**, *114*, 1729. (b) Cordes, A. W.; Haddon, R. C.; Hicks, R. G.; Kennepohl, D. K.; Oakley, R. T.; Palstra, T. T. M.; Schneemeyer, L. F.; Scott, S. R.; Waszczak, J. V. *Chem. Mater.* **1993**, *5*, 820. (c) Bryan, C. D.; Cordes, A. W.; Goddard, J. D.; Haddon, R. C.; Hicks, R. G.; MacKinnon, C. D.; Mawhinney, R. C.; Oakley, R. T.; Palstra, T. T. M.; Perel, A. S. *J. Am. Chem. Soc.* **1996**, *118*, 330.

25. Beekman, R. A.; Boere R. T.; Moock, K. H.; Parvez, M. *Can. J. Chem.* **1998**, *76*, 85.

26. Mott, N. F.; Davis, E. A., "*Electronic Processes in Non-Crystalline Materials*"; **1979,** Oxford University Press, New York.

27. Shante, V. K. S.; Varma, C. M.; Bloch, A. N. *Phys. Rev.* **1973**, *B 8*, 4885.

28. Brenig, W.; Dohler, G. H.; Heyszenau, H. *Philos. Mag.* **1973**, *27*, 1093.

29. Given that the unit cell angles are equal to or close to 90°, and that there is a close correspondence between real and reciprocal space vectors, orbital dispersion along a^*, b^*, and c* can be equated with orbital interactions parallel to x, y, and z.

30. Haddon, R. C.; Siegrist, T.; Fleming, R. M.; Bridenbaugh, P. M.; Laudise, R. A. *J. Mater. Res.* **1995**, 1719.

31. We differentiate our neutral radical materials, which are single component, from highly polarized donor-acceptor compounds. For examples of the latter, see: Yamashita, Y.; Tomura, M. *J. Mater. Chem.* **1998**, 8, 1933.

Chapter 5 Quinoxaline-1,2,3-dithiazolyl Radicals (1,2,3-QDTA)

We have prepared and characterized 1,3,2- and 1,2,3-TDTA **V-1** and **V-2** as described in Chapter 2 and 4, respectively. The thiadiazolopyrazine substituents on these radicals is extremely electron withdrawing, and causes an increase in both the molecular IP and EA relative to those of simple (monocyclic) DTAs.[1, 2] More importantly the substitution causes a dramatic decrease in the disproportionation enthalpy ΔH_{disp} (= IP - EA) of the radical. Structural analysis on **V-1** revealed that the radical does not dimerize (at room temperature), but the molecular spins remain isolated, as a result of which the material is a Mott insulator. By contrast molecules of **V-2** dimerize in the solid state, but magnetic and conductivity measurements indicate that the free spins present as defects serve as carriers of charge. As a continuation of this work, *i.e.*, the development of structure/property relationships in heterocyclic radicals, we wished to compare the two quinoxaline based systems **V-3** and **V-4**. The results of the theoretical studies on 1,2,3-QDTA (**V-4**) presented in chapter 3 showed that a phenyl ring is as effective as other heterocyclic rings to stabilize the radicals and suggested **V-4** to be a better target radical molecule. Here we report the synthesis and characterization of a whole family of derivatives based on this "QDTA" skeleton.

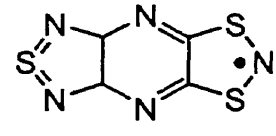

V-1

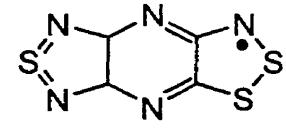

V-2

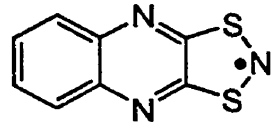

V-3

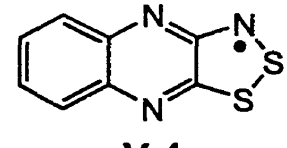

V-4

5.1 Synthesis

Quinoxalineaminothiol **V-8**, (QAT), the preferred starting material for the synthesis of QDTA **V-4**, is potentially accessible by a number of routes (Scheme 5.1). One involves the conversion of dichloroquinoxaline **V-5** (QCl_2) to the corresponding aminochloro derivative **V-6** (QACl),[3] followed by thiation of the latter with sodium sulfide. However, while the first step is straightforward, the second provides only a low yield (10%) of QAT. The alternative pathway, involving the amination of the intermediate dithiol **V-7** (QT_2),[4,5] which is easily accessible from QCl_2, affords QAT in much higher overall yields.

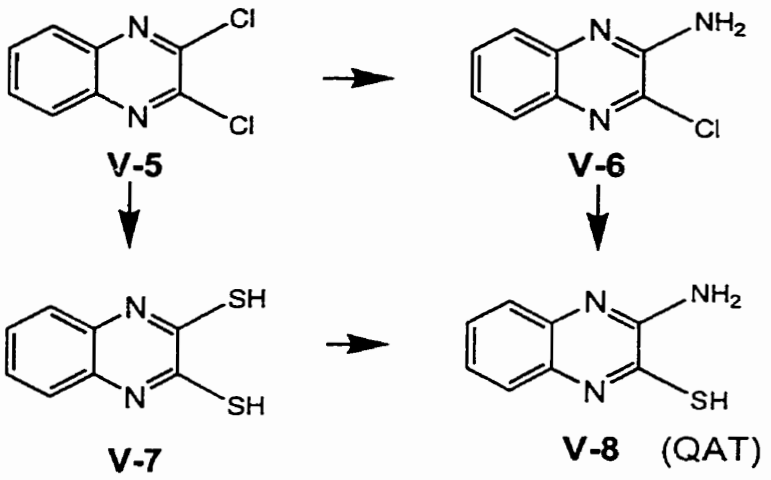

Scheme 5.1

Cyclization of **V-8** (QAT) by treatment with sulfur chlorides proved to be a far more complex process than we had anticipated. Elaboration of the overall sequence of events is facilitated by reference to the manifold of oxidation states illustrated in Scheme 5.2. Broadly speaking the nature of the product is a function of the oxidizing power of the sulfur chloride. Based on our experience with **V-2**, we were aware that sulfur monochloride would only produce an imide QDTAH. It was therefore not surprising to find that reaction of QAT with S_2Cl_2, in stoichiometric amounts or in excess, afforded an insoluble orange powder

exhibiting υ(NH) stretching bands in its infrared spectrum. Sulfur dichloride proved to be a stronger but less selective oxidant. Thus, when heated at reflux in acetonitrile with excess SCl_2, QAT was oxidized directly to the open chain "trichloro" derivative Cl-QDTA-Cl_3. Attempts to prevent oxidation of the quinoxaline residue were, for a long time, unsuccessful. Eventually, and somewhat to our surprise, we discovered that treatment of QAT with

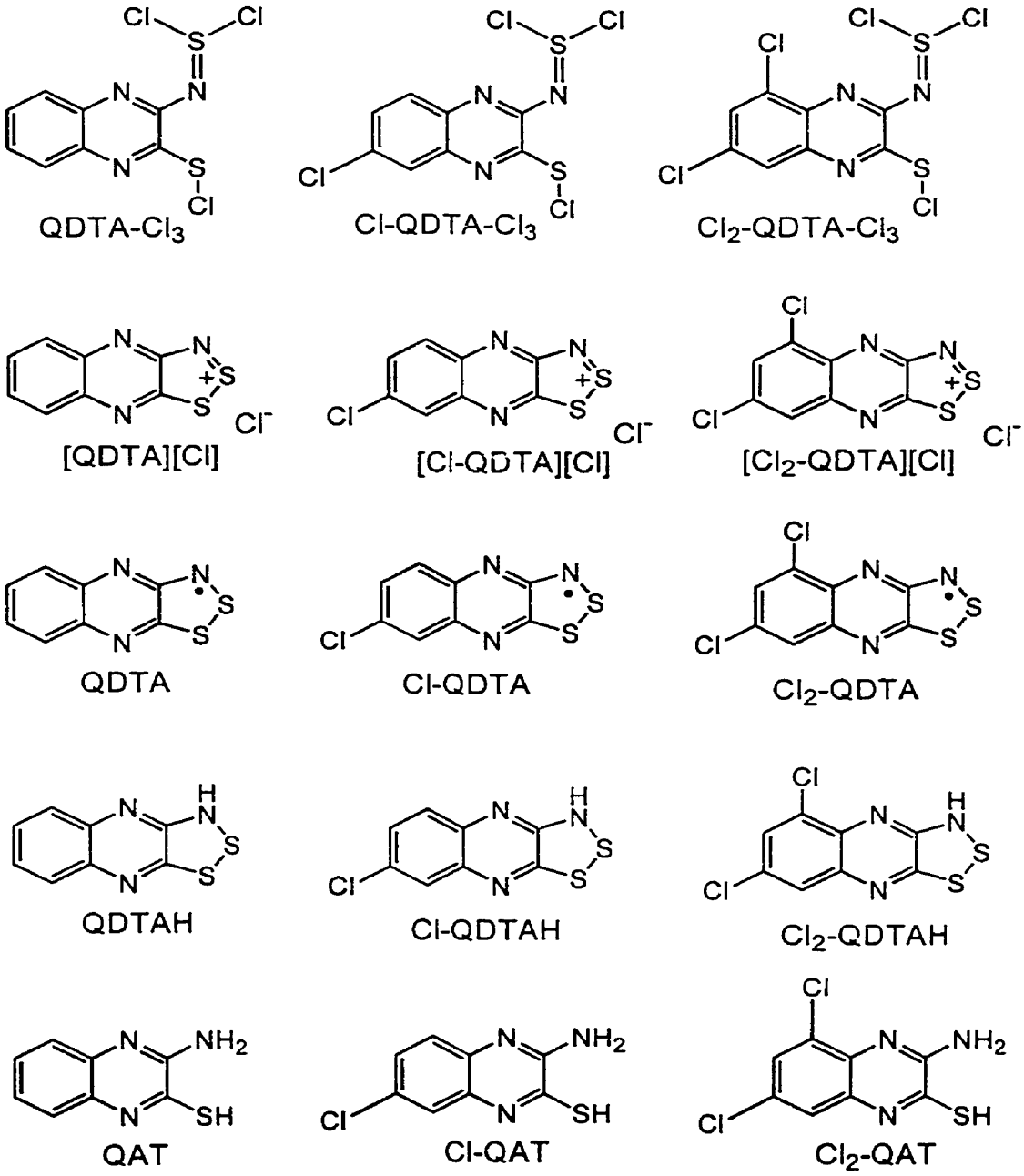

Scheme 5.2

chlorine gas for 2-3 min, followed by the addition of excess sulfur monochloride (at room temperature), gave rise to the precipitation of yellow crystals of QDTA-Cl_3. Attempts to recrystallize this material for analytical purposes were always thwarted by its partial conversion, upon dissolution, into Cl-QDTA-Cl_3. That the quinoxaline ring was unsubstituted was confirmed by hydrolysis of the compoundQDTA-Cl_3 and recovery of QAT.

Cl-QDTA-Cl_3 is resistant to further oxidation, indeed it is conveniently recrystallized from acetonitrile saturated with chlorine gas. However, when Cl-QDTA-Cl_3 is heated at reflux in acetonitrile with excess sulfur monochloride, a dark orange crystalline precipitate of the salt [Cl_2-QDTA][Cl] (as a CH_3CN solvate) is produced. In essence the open chain "trichloro" unit is closed to a dithiazolylium cation, while the quinoxaline ring is further chlorinated. [Cl_2-QDTA][Cl] was easily oxidized with chlorine to the corresponding "trichloro" derivative Cl_2-QDTA-Cl_3. Given the three "trichloro" compounds, we explored their reactions with reducing agents. While Cl_2-QDTA-Cl_3 was easily reduced with a stoichiometric amount of iodide ion or excess S_2Cl_2 to Cl_2-QDTA-Cl, reduction of Cl-QDTA-Cl_3 required a more careful choice of reducing agent. Eventually we found that hexamethyldisilane reacts with Cl-QDTA-Cl_3 to afford what we believe to be to [Cl-QDTA][Cl]. However, attempts to recrystallize this material led to its conversion to an insoluble solid exhibiting υ(NH) stretching bands and which, upon hydrolysis, afforded the dichlorinated aminothiol Cl_2-QAT. An analogous sequence of events was encountered upon reduction of QDTA-Cl_3. We interpret these observations in terms of the susceptibility of the dithiazolylium salts [QDTA][Cl] and [Cl-QDTA][Cl] to rearrange, with chlorination of the quinoxaline ring, to an imide (Scheme 5.3).

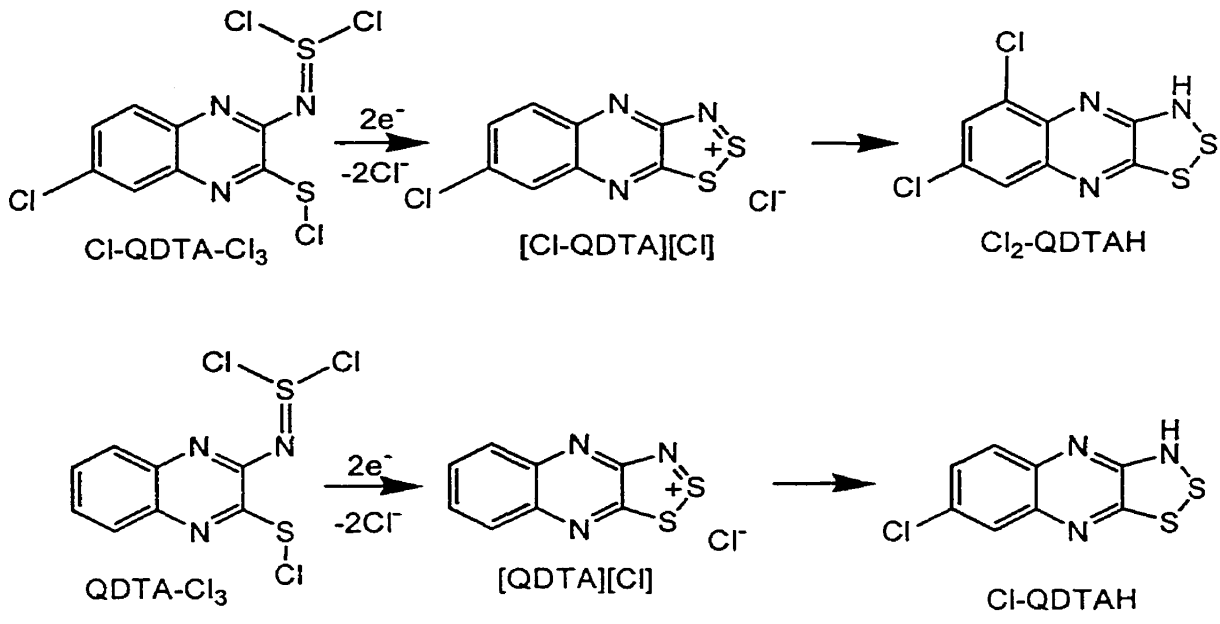

Scheme 5.3

Generation of the radical oxidation states QDTA, Cl-QDTA and Cl_2-QDTA required that we explore a variety of reducing agents (KI, Bu_4NI, Ph_3Sb, Zn), solvents (CH_3CN, SO_2) and starting oxidation states (Cl_n-QDTA-Cl_3 or [Cl_n-QDTA][Cl]). Each radical required a different combination for the best results (see Experimental section). All three radicals could be isolated in crude form, as black crystalline solids, but purification for analytical purposes was extremely inefficient. Vacuum sublimation of the products from the crude matrix, the preferred purification method for heterocyclic radicals, inevitably led to decomposition and low recovery of sublimed product (<5%). Curiously, once isolated, the sublimed material could be resublimed with little or no loss.

Along with the analogous derivative formed by chlorination of compound **V-2**, the "trichloro" compounds Cl_n-QDTA-Cl_3 (n = 0, 1, 2) are the first compounds of this type. In addition to being sources of QDTA radicals, these compounds are potentially interesting reagents for the construction of new heterocycles. As a first step in exploring these

possibilities, we examined the reaction of Cl_n-QDTA-Cl_3 (n = 1, 2) with nonamethyltrisilazane. In both cases condensation occured, to form the corresponding antiaromatic quinoxalinedithiadiazine Cl_n-QDTDA in good yield (Scheme 5.4). While other reported routes need stringent conditions,[6,7] this one was very easy and effective.

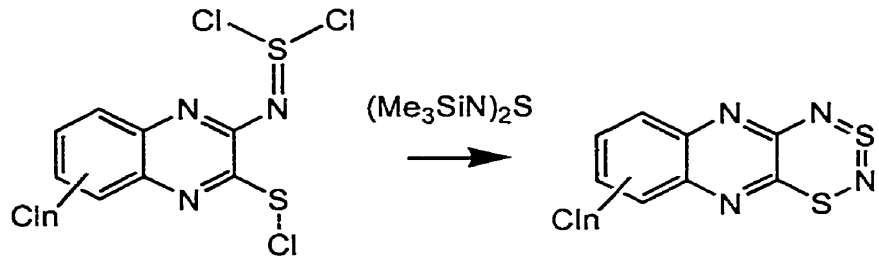

Cl_n-QDTA-Cl_3 (n = 1, 2) Cl_n-QDTDA (n = 1, 2)

Scheme 5.4

5.2 Crystal structure

During the exploration of the manifold of the reactions occuring when QAT was treated with SCl_2, or S_2Cl_2 and Cl_2, we identified the series of derivatives based on mono and di substitution of the quinoxaline framework. As yet we have been unable to grow crystals of any QDTA radical suitable for X-ray work. Thus, in order to establish unequivocally the positions of substitution of the quinooxaline frame in the Cl-Q and Cl_2-Q series, we pursued the structural determination of the two compounds: Cl-QDTA-Cl_3 and Cl_2-QDTA-Cl_3.

Crystals of these two compounds suitable for X-ray diffraction were grown from the solution of CH_3CN saturated with chlorine gas and the structures of both compounds are shown in Figure 5.1. As expected, on the basis of the resonance structures shown in Scheme 5.5, chlorination of the quinoxaline framework is expected to occur at the 5 and 7 positions. As observed in the two structures, the chlorination follows the free radical route rather than electrophilic substitution.

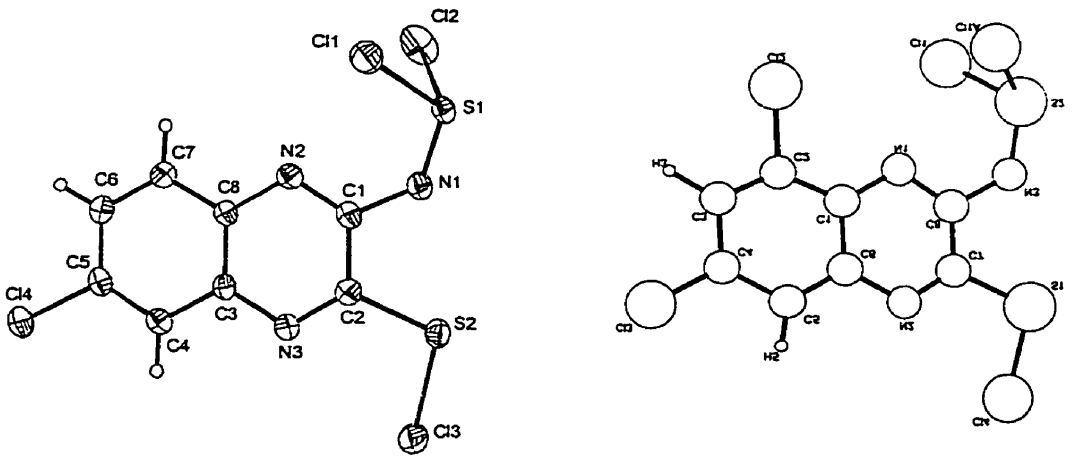

Figure 5.1 The crystal structure of Cl-Q-Cl_3 (left) and Cl_2-Q-Cl_3 (right)

This showed that the unpaired electron can be delocalized to the 5 and 7 positions making them more active than the other positions. Hence, when S_xCl_2 was employed, not only is aminothiol oxidized to form trichloro part, but also the 5 or 7 positions of the quinoxaline framework is chlorinated easily to form Cl and Cl_2-QDTA-Cl_3.

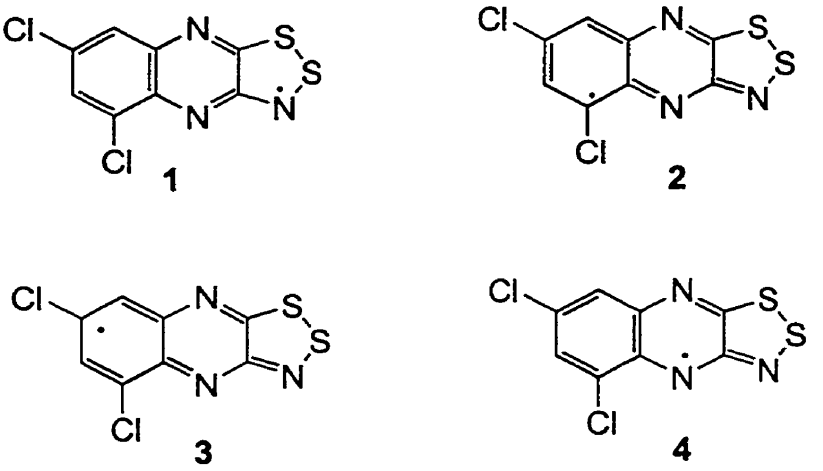

Scheme 5.5

5.3 ESR spectra

The X-band ESR spectra (in CH_2Cl_2, 293 K) of the 1,2,3-QDTA, Cl-QDTA and Cl_2-QDTA were recorded and are shown in Figure 5.2. The g values and the coupling constants a_N are listed in Table 5.1. The spectra are complex and if we compare the 1,2,3 and 1,3,2 isomers, the coupling constants on ^{14}N are very different. By simulation,[8] it was found that the effects of hyperfine coupling extend to all three nitrogen atoms. There are also relatively large hyperfine coupling constants to the hydrogen atoms. The unpaired electron is thus delocalized over the whole molecule in all three radicals.

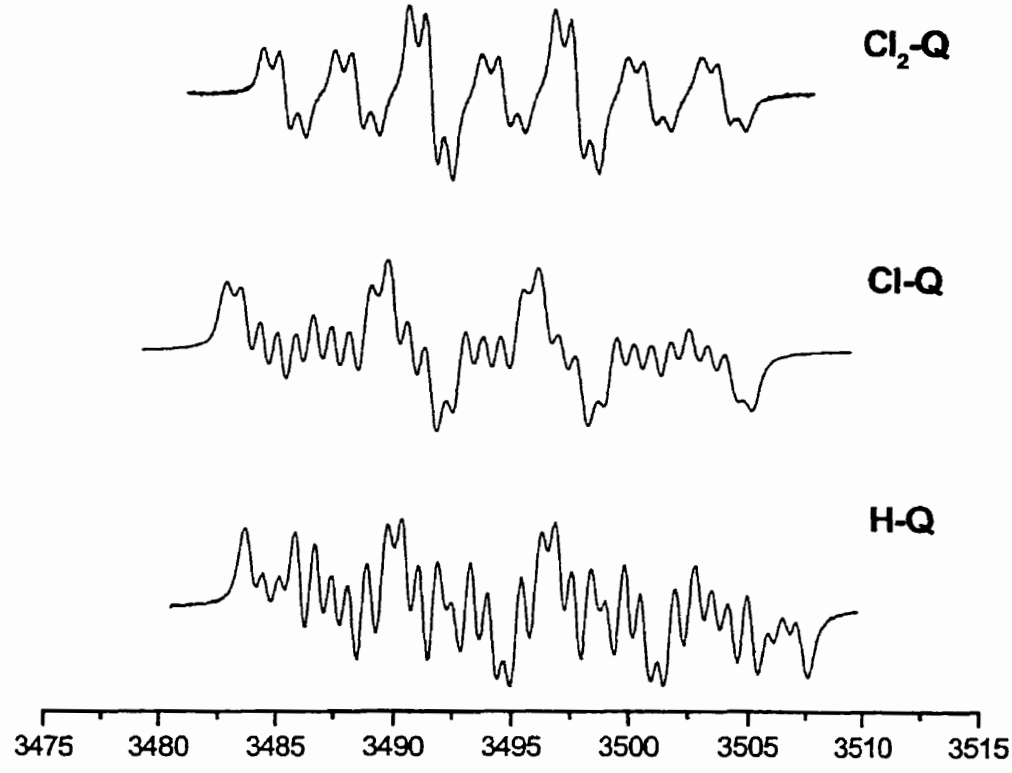

Figure 5.2 ESR spectra of 1,2,3-QDTA (below), Cl-QDTA (middle) and Cl_2-QDTA (above)

Table 5.1 ESR parameters of 1,3,2-QDTA and its 1,2,3 counterparts

parameters	1,3,2-QDTA	1,2,3-QDTA	1,2,3-Cl-QDTA	1,2,3-Cl_2-QDTA
g	2.0065	2.0079	2.0085	2.0068
a_N *(3)*	10.89 (a_N*(2)*)	6.53	6.45	6.2
a_N *(4)*	1.288	3.01	3.1	3.1
a_N *(9)*	1.288	0.06	0.4	0.4
a_H *(5, 7)*	0.645	2.18	1.5	0.75
a_H *(8)*	0.227	1.37	0.75	0.25
a_H (6)	0.227	0.7	0.2	---
a_H (5)	0.645	0.04	---	---

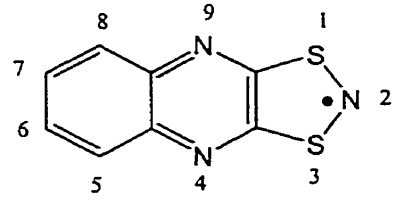

1,3,2-QDTA

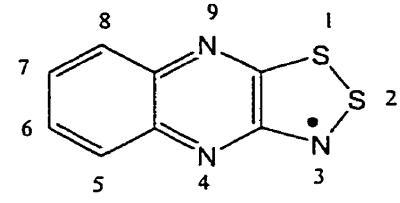

1,2,3-QDTA

5.4 Experimental section

Preparation of 2-amino-3-chloroquinoxaline (QACl) [3]

This compound was made by modificated procedure in ref 3. 2,3-dichloroquinoxaline (15 g, 76 mmol) was put into a steel bomb reactor with 200 mL of ethanol and NH_3 gas was bubbled through for 10 minutes. The sealed bomb was heated to 80°C for 16 hours. The bomb was then cooled to room temperature, and the solvent allowed to evaporate. The residue was extracted with 500 mL of methylene chloride to give a yellow solid. Yield: 11.4 g, 64 mmol, 84%. The solid was recrystallized from methylene chloride to give white

needles. mp. 137-9°C (lit. 141-3°C). IR (4000-400 cm^{-1}): 3478 (m), 3457 (w), 3293 (w), 1638 (s), 1606 (s), 1551 (s), 1353 (w), 1308 (m), 1245 (w), 1128 (s), 1053 (s), 950 (w), 821 (m), 757 (s), 597 (m), 470 (w).

Preparation of 2-amino-3-thio-quinoxaline (QAT)

This compound was prepared by modification of literature method.[3] 2,3-dithioquinoxaline (5.22 g, 27 mmol) was mixed with 30 mL of ethanol in a glass tube, through which anhydrous NH_3 gas was bubbled for 5 minutes. After that, the tube was sealed and heated to 110°C for 16 hours. The yellow crystalline product and solution was transferred onto 100 mL 1M KOH aqueous solution forming an almost clear red solution. The mixture was filtered and the filtrate acidified with acetic acid to give a yellow precipitate. Yellow crystalline solid was obtained by recrystallization from PhCN. Yield: 3.63 g, 20 mmol, 76%. mp, > 250°C. Anal. Calc'd . for $C_8H_7N_3S$, C: 54.22, H: 3.98, N: 23.71; found, C: 54.16, H: 4.13, N: 23.62. MS: 177 (M^+, 100%). IR (4000 - 400 cm^{-1}): 3394(m), 3274(w), 1636(s), 1611(m), 1593(m), 1553(m), 1507(m), 1313(w), 1271(w), 1253(w), 1136(s) ,1087(s), 940(m), 854(m), 749(s), 603(s), 443(m).

Preparation of QDTA-Cl_3

A gentle stream of chlorine gas was passed for 10 minutes over a slurry of **QAT** (1.0 g, 5.64 mmol) in 10 mL of acetonitrile at 0°C (ice bath). Within 60 s of initiating the chlorine flow, a solution of excess S_2Cl_2 (*ca.* 1.0 g) in 5 mL of CH_3CN was added dropwise to the mixture. After 5 min the chlorine flow was halted, and the flocculent yellow solid filtered off under nitrogen, washed with 2 × 5 mL acetonitrile saturated with chlorine, and dried in

vacuo. The crude (moisture sensitive) product, **QDTA-Cl_3** (0.845 g, 2.70 mmol, 48%), was used directly in all subsequent reactions. Attempts to recrystallize the compound led to its partial conversion to **Cl-QDTA-Cl_3**. IR (1600-400 cm^{-1}) 1329 (s), 1292 (w), 1228 (m), 1161 (m),1113 (m), 1017 (w), 903 (w), 805 (w), 754 (vs), 714 (w), 698 (w), 625 (vw), 593 (vw), 553 (vw), 539 (s),458 (s) cm^{-1}.

Preparation of Cl-QDTA-Cl_3

Excess (4 mL) of SCl_2 was added to a slurry of **QAT** (1.00 g, 5.64 mmol) in 30 mL of CH_3CN at room temperature. The mixture was stirred for an hour during which time it changed color from red to yellow. The canary yellow precipitate was filtered off, washed with 2 x 10 mL portions of CH_3CN, and dried in *vacuo*; (1.3 g, 3.75 mmol, 66%). The product Cl-QDTA-Cl_3 (0.500 g 1.44 mmol) was recrystallized from acetonitrile containing 2 mL of SCl_2 (to enhance the solubility of the compound). On cooling lustrous yellow needles were formed: mp, 85°C; IR (1600-400cm^{-1}) 1599(m), 1556(w), 1525(w), 1481(m), 1426(w), 1320(s), 1280(w), 1211(m), 1145(m), 1119(s), 1067(m), 1015(m), 964(w), 926(m), 878(m), 830(s), 710(m), 651(w), 622(m), 588(m), 557(m), 521(w), 494(w), 457(m), 425(m). Anal. Calcd for $C_8H_3Cl_4N_3S_2$: C: 27.68; H: 0.87; N: 12.11. Found: C: 27.92; H: trace; N: 12.07. MS: 241 ($[M-3Cl]^+$, 100%).

Preparation of Cl_2-QDTA-Cl_3

Excess S_2Cl_2 (4 mL) was added to a slurry of **QAT** (2.00 g, 11.3 mmol) in 60 mL of acetonitrile. The mixture was warmed gently to produce a red precipitate. Chlorine gas was then passed over the solid until a bright yellow precipitate was produced. Following the

addition of more S_2Cl_2 (4 mL) the mixture was heated at reflux for half an hour. As the mixture began to boil, the solid dissolved to give a dark red/brown solution. The mixture was then cooled to room temperature and reacted with a flow of chlorine to form the final product. The yellow precipitate was filtered off under nitrogen, washed with chlorine saturated acetonitrile and dried in *vacuo*. The product **Cl_2-QDTA-Cl_3** (2.83 g, 7.42 mmol, 66%) was recrystallized from chlorine saturated acetonitrile as yellow needles. IR (1600 - 400 cm^{-1}) 1590(m), 1529(w), 1334(w), 1304(s), 1281(w), 1216(m), 1191(m), 1137(s), 1082(m), 1029(m), 864(s), 807(s), 785(m), 676(m), 634(m), 586(m), 577(m), 534(m), 468(s), 433(m). Anal. Calcd for $C_8H_2Cl_5N_3S_2$: C: 25.19; H: 0.53; N: 11.01. Found: C: 25.30; H: trace; N: 10.93.

Preparation of [Cl_2-QDTA][Cl]·CH_3CN

Excess S_2Cl_2 (4 mL) was added to a slurry of Cl-Q-Cl_3 (1.50 g, 4.32 mmol) in 50 mL of CH_3CN. As the mixture was heated to reflux the solid dissolved to give a dark red/brown solution. After half an hour at reflux the solution was allowed to cool to room temperature. The orange brown crystalline solid which precipitated on cooling was filtered off, washed with 2 × 10 mL portions of CH_3CN, and dried in *vacuo*. The product [Cl_2-QDTA][Cl]·CH_3CN (1.25 g, 3.55 mmol, 82%) was recrystallized from acetonitrile containing a few drops of SCl_2. Infrared and elemental analysis confirmed that the compound was solvated with one mole of acetonitrile. mp (dec.) 85°C. IR (1600 - 400 cm^{-1}) 2247(w), 1661(w), 1589(m), 1537(w), 1299(w), 1276(m), 1191(m), 1091(m), 1004(m), 878(m), 858(m), 808(w), 791(w), 715(m), 612(m), 584(w), 544(w), 451(m) cm^{-1}. MS: 274 (M^+, 100%). Anal. Calcd for $C_{10}H_5N_4S_2Cl_3$: C: 34.15; H: 1.43; N: 15.93. Found: C: 33.89; H: 1.20;

N: 15.98.

Preparation of QDTA

QDTA-Cl_3 (0.845 g, 2.70 mmol, 48%) was treated with KI (1.48 g, 8.9 mmol) (dried in the oven and ground) in distilled CH_3CN at room temperature. The black precipitate was collected and dried *in vacuo*. It was further purified in very low yield (< 5%) by fractional sublimation and identified by its ESR spectrum. However no satisfactory element analysis could be obtained.

Preparation of Cl-QDTA

The freshly made **Cl-QDTA-Cl_3** (0.5 g, 1.4 mmol) in 10 mL of distilled CH_3CN in the Schlenk tube was added with predried KI and the immediately darkened slurry was stirred at room temperature for 20 min. The black crude material was filtered off and sublimed at 40-70-110°C/ 10^{-2} Torr. Yield: 50 mg, 0.22 mmol, 16%. mp. 163°C (dec.). IR (4000 - 400 cm^{-1}): 1560 (w), 1535 (w), 1344 (w), 1304 (w), 1279 (m), 1139 (w), 1200 (w), 1139 (w), 1076 (s), 942 (w), 898 (w), 815 (s), 793 (w), 665 (w), 597 (m), 578 (m), 512 (w), 435 (m). Anal. Calcd . for $C_8H_3N_3S_2Cl$: C: 39.92%, H: 1.26%, N: 17.46%. Found, C: 40.12%, H: 1.38%, N: 17.27%.

Preparation of Cl_2-QDTA

[Cl_2-QDTA-Cl][CH_3CN] (1.0 g, 3.6 mmol) was mixed with a stoichiometric amount of ground KI in 20 mL of CH_3CN. The slurry darkened quickly and after 30 minutes the black solid was filtered off and washed once with CH_3CN. The obtained solid was pumped

dry and was put in the furnace for fractional sublimation. Microcrystals were obtained in 50-70-110°C/10^{-2} Torr. Yield: 0.1 g, 12%. mp. 158°C. Anal. Calcd. for $C_8H_2N_3S_2Cl_2$, C: 34.92%, H: 0.73%, N: 15.27%. Found, C: 35.12%, H: 0.90%, N: 15.09%. MS (EI, m/e): 274 (M^+, 100%), 228 ([M-NS]$^+$, 34%), 210 (10%), 158 (31%). IR (4000-400 cm^{-1}): 1588 (w), 1527 (w), 1303 (m), 1277 (m), 1195(m), 1087 (m), 966 (m), 922 (m), 860 (m), 782 (w), 656 (w), 607 (w), 575 (w), 486 (w).

Preparation of Cl-QDTDA

Nonamethyltrisilazane (0.38 g, 1.6 mmol) was added to a slurry of Cl-QDTA-Cl_3 (0.50 g, 1.45 mmol) in 5 mL acetonitrile and the mixture stirred for 2 hours. The dark red solid was filtered off, washed with CH_3CN and dried in *vacuo*. This crude product Cl-QDTDA (0.30 g, 1.2 mmol, 81%) was filtered and recrystallized from dichloroethane. A sample for elemental analysis was prepared by gradient sublimation in vacuo at 100-60°C/10^{-2} Torr, mp. 169-170°C. MS (EI, m/e): 254 (M^+, 31%), 208 ([M-SN]$^+$, 37%), 156 (17%), 124 (8%), 78 (25%), 46 (SN^+, 100%). IR (4000 - 400 cm^{-1}):1591 (w), 1556 (w), 1423 (w), 1309 (m), 1198 (m), 1130 (s), 1102 (s), 1040 (m), 914 (w), 886 (s), 825 (s), 690 (s), 649 (m), 642 (m), 605 (w), 585 (s), 494 (s), 442 (s). Anal. Calcd for $C_8H_3N_4S_2Cl$: C: 37.72, H: 1.19, N: 22.00. Found, C: 37.90, H: 0.98, N: 21.98.

Preparation of Cl_2-QDTDA

Nonamethyltrisilazane (0.640 g, 2.74 mmol) was added to a slurry of Cl_2-Q-Cl_3 (1.00 g, 2.62 mmol) in 10 mL of acetonitrile and the mixture stirred for 2 hours. The dark red solid was filtered off, washed with CH_3CN and dried in *vacuo*. This crude product Cl_2-QDTDA

(0.67 g, 2.32 mmol, 88%) was purified by sublimation at 110-60°C /10^{-2} Torr in a gradient tube furnace to afford small black needles. IR (1600 - 400cm^{-1}) 1581(m), 1549(m), 1428(m), 1306(s), 1271(w), 1213(m), 1190(m), 1111(m), 1090(m), 1046(s), 987(m), 879(w), 857(s), 783(s), 715(w), 647(s), 618(m), 577(s), 498(m), 439(s), 426(m) cm^{1}. Anal. Calcd for $C_8H_2Cl_2N_4S_2$: C, 33.23; H, 0.70; N, 19.38. Found: C, 33.43; H, 0.49; N, 19.18.

5.5 References

1. Barclay, T. M.; Cordes, A. W.; George, N. A.; Haddon, R. C.; Itkis, M. E.; Mashuta, M. S.; Oakley, R. T.; Patenaude, G. W.; Reed, R. W.; Richardson, J. F.; Zhang, H. *J. Am. Chem. Soc.* **1998**, *120*, 352.
2. Barclay, T. M.; Cordes, A. W.; Haddon, R. C.; Itkis, M. E.; Oakley, R. T.; Reed, R. W.; Zhang, H. *J. Am. Chem. Soc.* **1999**, *121*, 969.
3. Saikachi, H.; Tagami, S. *Chem. & Pharm. Bull.* **1961**, *9*, 941.
4. Morrison, D. C.; Furst, A. *J. Org. Chem.* **1956**, *21*, 470.
5. Patel, N. R.; Castle, R. N. *J. Heterocyclic. Chem.* **1966**, *3*, 512.
6. (a) Koenig, H.; Oakley, R. T. *J. Chem. Soc., Chem. Commun.* **1983**, 73. (b) Cordes, A. W.; Hojo, M.; Koenig, H.; Noble, M. C.; Oakley, R. T.; Pennington, W. T. *Inorg. Chem.* **1986**, *25*, 1137.
7. (a) Bagryanskaya, I. Y.; Bock, H.; Gatilov, Y. V.; Haas, A.; Shakirov, M. M.; Solouki, B.; Zibarev, A. V. *Chem. Ber.* **1997**, *130*, 247. (b) Petrachenko, N. E.; Gatilov, Y. V., Zibarev, A. V. *J. Electron Spectrosc. Relat. Phenom.* **1994**, *67*, 489.
8. Bruker Simfonia software.

Chapter 6 Ongoing 1,2,3-dithiazolyl systems

In earlier chapters we have described the preparation and structures of several 1,3,2- and 1,2,3-DTA radicals. Based on the computational results provided in Chapter 3, the 1,2,3-DTAs were identified as more appealing building blocks for neutral radical conductors; in Chapter 4 and 5, we presented full case studies - synthesis, structure and transport properties - on the 1,2,3-TDTA and 1,2,3-QDTA related radicals. In this final chapter we provide the results of several ongoing projects, all designed to explore synthetic avenues to the three 1,2,3-DTA derivatives shown below.

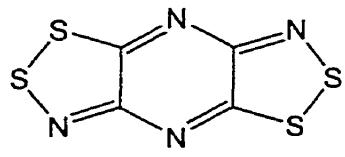

VI-9

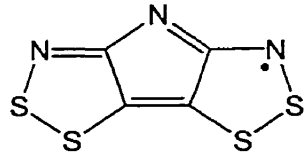

VI-11

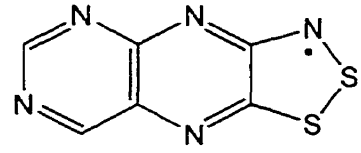

VI-41

6.1 Attempted Synthesis of *trans*-PT, VI-9

In the course of the 1,3,2-TDTA project, we encountered the problem of preparing and separating the isomeric diaminodichloropyrazines **II-21, II-22.** Interestingly, from the reaction of tetrachloropyrazine with ammonium hydroxide,[1] only these two isomers of diaminodichloropyrazine were ever isolated. The third possible isomer, the 2,5-diamino-3,6-dichloropyrazine (**VI-5**) was never observed. The characterization of this potentially valuable intermediate was therefore of fundamental interest to us.

Other 2,5-disubstituted pyrazines have been known for some time. For example, 2,5-diaminopyrazine **VI-1** was made in 1951 by a multi-step reaction from pyrazine-2,5-dicarboxylic acid.[2] Similarly, the 2,5-dichloropyrazine **VI-2** was prepared from 3-amino-6-

chloromethylpyrazinoate after hydrolysis, decarboxylation, diazotization and chlorination steps.[3] 2,5-dichloro-3,6-bis(alkoxycarbonylamino)-1,4-benzoquinone **VI-3** has also been reported.[4] It seems that, by selecting different reaction pathways, it is possible to control the position that amino groups access. It was also known that tetrachloropyrazine reacts with pyridine to give a 2,5-substituted salt.[5] This may be due to the fact that the pyridine molecule is larger, and when it is used as reagent, the bulky groups try to separate far enough in order to reduce the steric congestion.

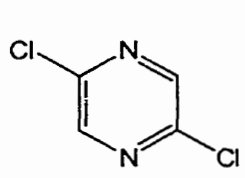

VI-1

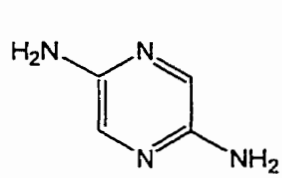

VI-2

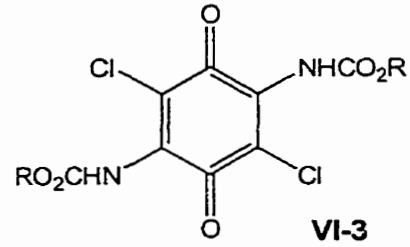

VI-3

Considering these factors, we selected potassium phthalimide as a potential nucleophile for reacting regiospecifically tetrachloropyrazine at the 2,5-positions (Scheme 6.1). To our satisfaction the reaction proceeded as anticipated, and the phthalimide adduct **VI-4** was hydrolyzed with hydrazine to afford yellow crystals of **VI-5**. The 2,5-regiochemistry was confirmed by X-ray crystallography (Figure 6.1). The structure can be compared to those of 2-amino-3-chloropyrazine[6] and *para*-phenylene-diamine.[7] As in the former the structure consists of pleated sheets linked via N-H---N (pyrazine) bonds.

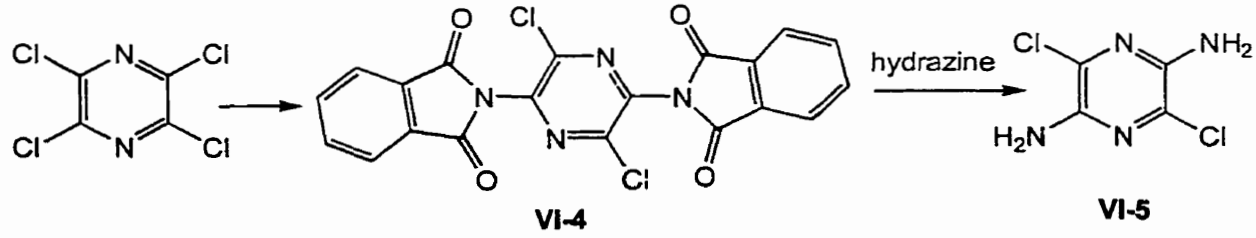

VI-4 **VI-5**

Scheme 6.1

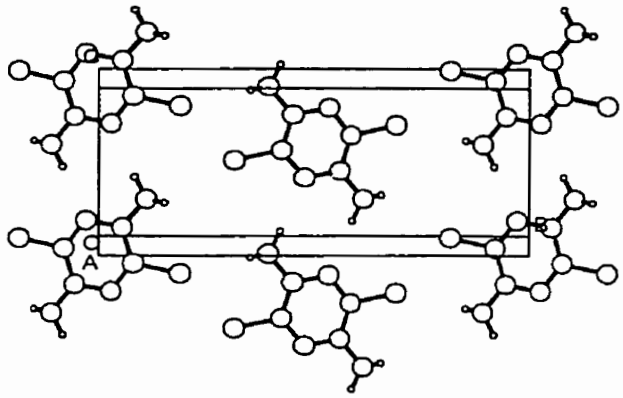

Figure 6.2 The crystal structure of 2,5-diamino-3,6-dichloropyrazine (**VI-5**).

Our main reason for seeking **VI-5** was to be able to use it as a starting point for the putative diaminodithiol **VI-8**. This idea was by analogy with other work in the Oakley laboratories (Scheme 6.2), which had led to the isolation of the *trans*-benzobis(1,2,3-dithiazole) **VI-7** starting from the benzenediaminodithiol **VI-6**. However, while substitution of **VI-5** with sodium sulfide could be driven to **VI-10**, we have to date been unable to replace both chloro groups with the thiol functionality.

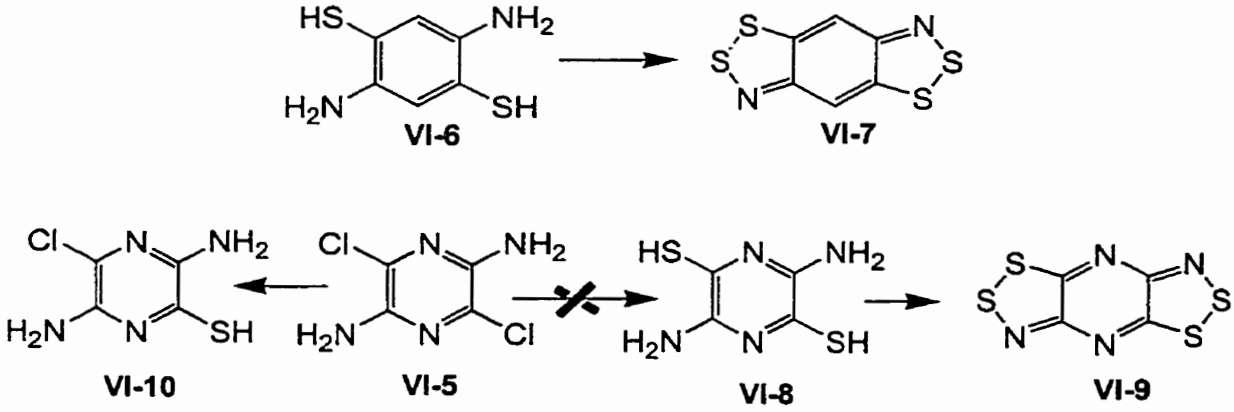

Scheme 6.2

6.2 Attempted Synthesis of PBDTA, a pyrrole based bis(DTA), VI-11

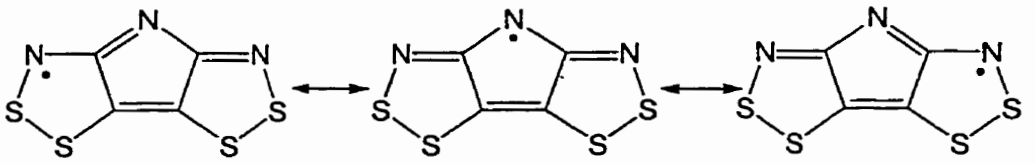

VI-11a VI-11b VI-11c

After completion of the 1,2,3-TDTA project (Chapter 4), we decided to pursue a more ambitious synthetic target. Based on the theoretical calculations presented in Chapter 3, we selected 1,2,3-PBDTA (**VI-11**) as a suitable candidate, as it has even lower IP-EA value than that of 1,2,3-TDTA. This neutral radical has three low energy resonant structures (**VI-11**, a-c), all of them are nitrogen centered. As in the case of trans-PT, **VI-5** , the key intermediate for the preparation of this compound was a pyrrole derivative, **VI-12** (Scheme 6.3). Here too, however, we encountered problems.

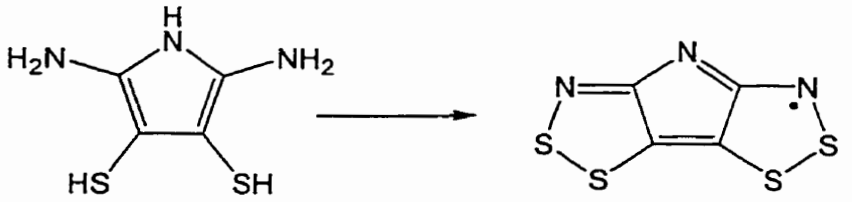

VI-12 VI-11

Scheme 6.3

6.2.1 Approach 1 - from Bähr's salt (VI-13)

Compared to other heterocyclic rings, the pyrrole ring framework is not very stable. The nitrogen position is especially active and easily attacked; as a result the ring is opened or alkylated.[8] Given these concerns the Bähr salt **VI-13** [9] looked a perfect starting point for the design of the functionalized pyrrole **VI-12.** It provided both the necessary sulfur functionality and served as the precursor of diamine groups. In the latter context it is well

known that dicyano derivatives afford imidines when treated with ammonia or hydrazine.[10] For example, in Scheme 6.4, 2,3-dicyanopyrazine **VI-14** with ammonia gas generates **VI-15**. Likewise dicarboxylic acids or their anhydrides in the presence of $(NH_4)_2MoO_4$ as catalyst with urea gives the imidine derivative,[11, 12] and tetracyanoethane reacts with hydrazine hydrate to form 3,4-dicyano-1,2,5-triaminopyrrole.[13] We therefore expected that the Bähr salt **VI-13** would lead to similar chemistry.

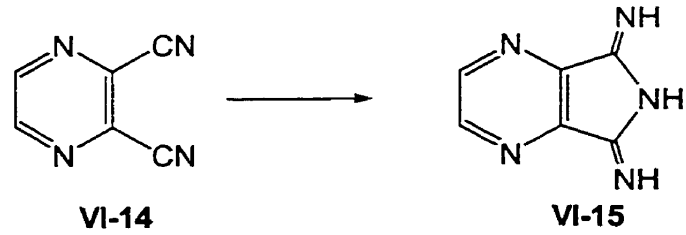

VI-14 **VI-15**

Scheme 6.4

The generation of **VI-13**, from CS_2 and NaCN, followed the literature procedure (Scheme 6.5). After the addition of various alcohols (not only isopropanol[9]), a high yield of the intermediate salt **VI-16** was always obtained. The dried product was put into a sublimation pot and heated to 130°C under vacuum to facilitate the dimerization. Recrystallization in ethanol gave a yellow solid of disodium dimercaptomalenitrile **VI-13**.

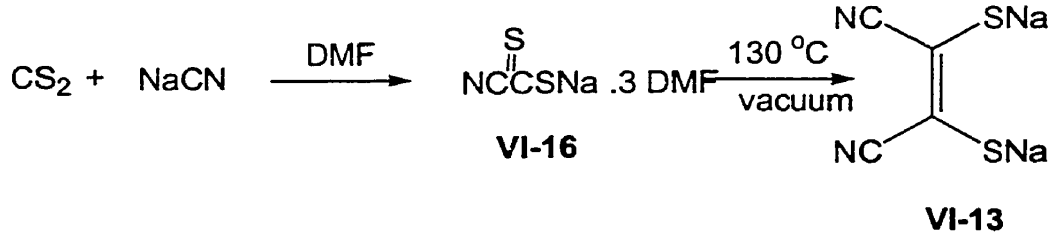

VI-16 **VI-13**

Scheme 6.5

At this point we decided to protect the two sulfur positions in **VI-13** by alkylation. The shortcoming of this idea is that we still needed these sulfur functionalities later on, and

we were concerned that dealkylation of the S-alkyl groups would require forcing conditions.[14] We nonetheless were able to make the 1,4-dithiin **VI-17**, and when ammonia gas was passed though a solution of **VI-17** in ethylene glycol at 70°C, the yellow diimine derivative **VI-18** was generated.[15] However we had no way to break the C-S bond we had previously attached (Scheme 6.6).

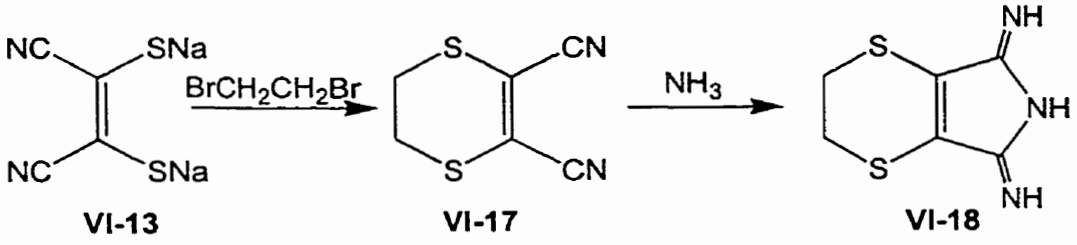

VI-13 **VI-17** **VI-18**

Scheme 6.6

Another attempt involved benzoylation of the thiols (Scheme 6.7), since this group can be easily replaced by base; the benzoyl derivative **VI-19** was thus easily prepared. However, attempts to close the pyrrole ring, by condensation of **VI-19** with hydrazine, led to reaction at the benzoyl groups rather than the nitriles, affording **VI-21**. We also tried methylation of **VI-13** , but the product appeared not to react with ammonia at all.

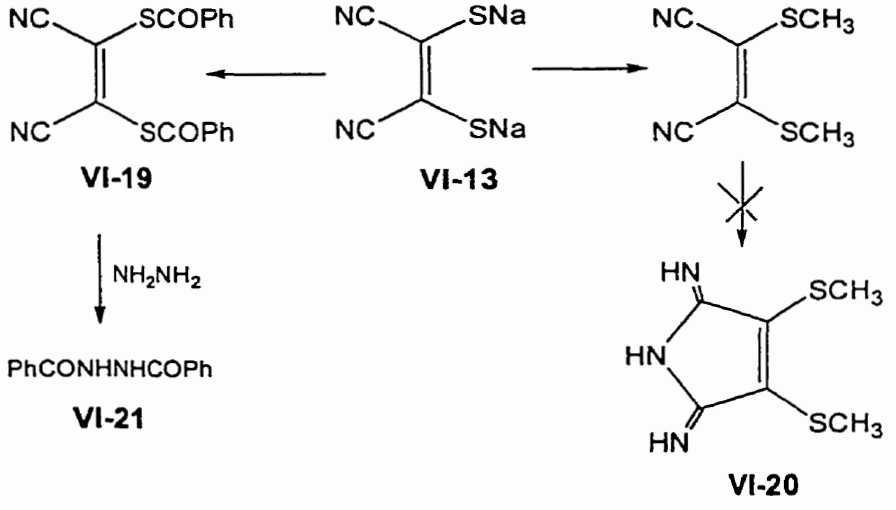

VI-19 **VI-13** **VI-21** **VI-20**

Scheme 6.7

6.2.2 Approach 2 - from an oxime derivative (VI-22)

An alternative systhesis of **VI-11** involved, as a first step, the construction of a pyrrole ring bearing the diimine functionality. Along these lines, it has been reported that succinonitrile forms an amidine with NH_3.[16] We were unable, however, to duplicate these results. Nonetheless we did make a dioxime derivative. Interestingly two products, **VI-22** and **VI-23**, can be obtained from the reaction of succinonitrile with hydroxylamine (Scheme 6.8). The relative yields of the two can be controlled by altering the amount of base used. With **VI-22** in hand we hoped that, as with other hydroxyamine derivatives,[17] it would undergo a double Herz reaction with S_2Cl_2 to afford **VI-11**. However, attempts to effect this cyclization gave no identifiable products.

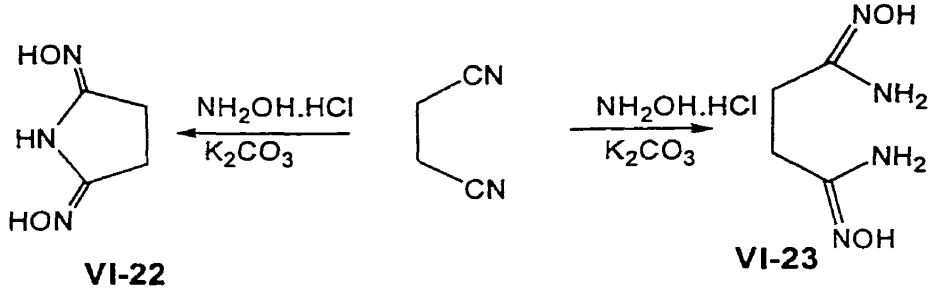

VI-22 **VI-23**

Scheme 6.8

6.2.3 Approach 3 - from pentachloropyrrole (VI-27)

A variety of halogenated pyrroles are known. Then can be reached by oxidation of pyrrole with a variety of strong halogenation reagents, such as Cl_2, Br_2, or SCl_2, SO_2Cl_2, usually one or more sites are halogenated with many side-reactions.[18] In a more unusual reaction, phosphorus pentachloride chlorinates succinonitrile to afford 2,3,4-trichloro-5-imino-N-tetrachlorophosphopyrrolenine **VI-24**. [19]

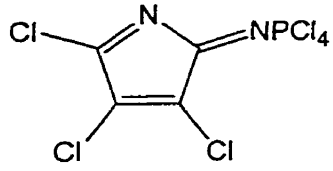

VI-24

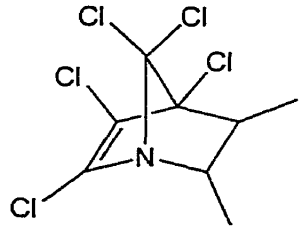

VI-25

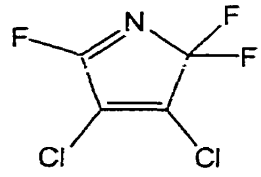

VI-26

The fully chlorinated material pentachloropyrrole (pentachloroazacycloopentadiene) **VI-27** is a very reactive molecule.[18] It can be employed as a Dies-Alder diene addend [20] to make some unusual [4+2] and [2+2] cycloadducts like **VI-25**.[21] It also reacts with silver fluoride to afford the 3,4-dichloro-2,2,5-trifuloropyrrolenine[22] **VI-26**, and with Me_3SiNMe_2 to give azacyclo-pentadienylium chlorides .[23] In both reactions, the chlorines in 2- and 5-positions are replaced.

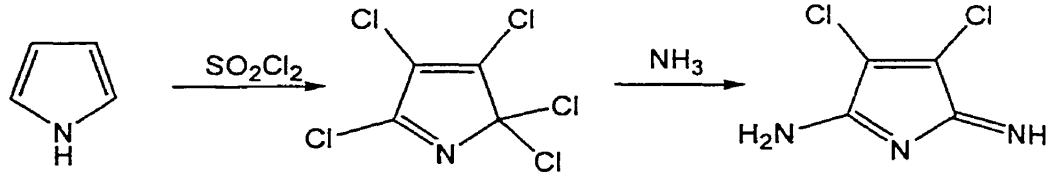

VI-27 VI-28

Scheme 5.9

When pentachloropyrrole (**VI-27**) was treated by NH_3 gas at room temperature, an off-white precipitate was quickly formed. The recrystallized product gave good mass spectral evidence for a diaminopyrrole. Based on the regiochemistry noted earlier, we are confident to assign the 2,5-diaminopyrrole structure **VI-28**. At the time of writing this thesis, no further work was done on this compound. Its reactivity with sulfide and hydrosulfide ions deserves careful study.

6.3 Pteridine based DTA (1,2,3-PTDTA)

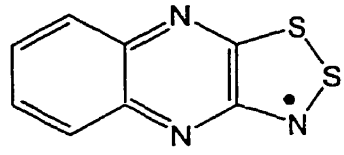

VI-29

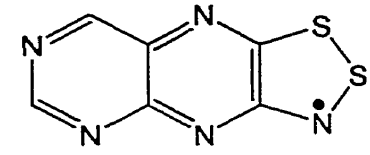

VI-30

As presented in Chapter 5, three quinoxaline-1,2,3-dithiazolyl (QDTA) radicals were obtained and characterized by ESR, MS and IR spectroscopy. Growing crystals of these systems was unexpectedly difficult, and while attempts are continuing, we have been unable to characterize structurally any one of these systems. In the belief that one of the problems associated with the 1,2,3-QDTA skeleton (**VI-29**) is its vulnerability to attack by chlorine, we decided to build a new radical in which the ring chlorination at these sites could not occur. The selective replacement of carbon by nitrogen on the phenyl ring would, we believed, stabilize the corresponding radical and prevent chlorination.

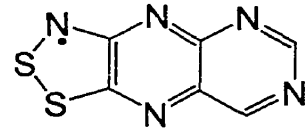

1

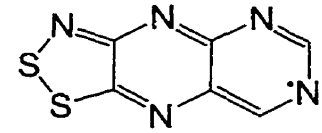

2

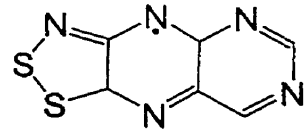

3

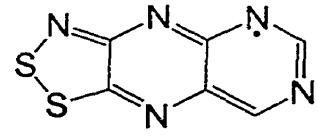

4

VI-30

Based on the chlorine substitution pattern in Cl_2-QDTA the new radical system was one in which the benzene ring of the quinoxaline framework was replaced by a pyrimidine ring. In addition to blocking substitution, we believed the two nitrogen atoms in the

pyrimidine ring would draw electron density away more effectively than the benzene ring of quinoxaline, and therefore stabilize the radical state. For example, if we consider the resonance structures of the radical (**VI-30, 1-4**), all possible positions for the unpaired electron are on the nitrogen atoms. In **VI-30**, the carbon-centered resonance structures found in 1,2,3-QDTA can be effectively avoided.

6.3.1 Buildup of the pteridine frame

Pteridine systems without substitution on 2,4-positions are relatively rare. In the words of Brown:[24] "*4,5-diaminopyrimidine is an essential intermediate for the direct synthesis of those pterdines and purines that are unsubstituted in the pyrimidine. Because this diamine has been so troublesome to prepare, there has been a strong tendency to avoid research into purines and pteridines of this kind*". Considering this situation and the cost of materials, 6-hydroxy-4,5-diamino-2-mercaptopyrimidine (**VI-31**) was selected as the starting point.

The route involved a multi-step synthesis (Scheme 6.10) and, at the early stage, the reactions were scaled up as much as possible. 4,5-Diamino-2,6-dimercapto-pyrimidine (**VI-32**) was made from **VI-31** and phosphorus pentasulfide under reflux in pyridine (Scheme 5.17).[25] 4,5-Diaminopyrimidine (**VI-33**) was originally made from 4-hydroxy-2-mercaptopyrimidine **VI-34** by Brown[24] after 6 steps. However we took advantage of a new route involving Raney nickel.[26] Usually this step was a large scale reaction which consumed up to 150 g of 4,5-diamino-2,6-dimercaptopyrimidine. The crude product was extracted and recrystallized from acetonitrile. 6,7-Dihydroxypteridine (**VI-35**)[27] and the following 6,7-dichloropterdine [28] (**VI-36**) were also prepared by modification of the literature methods.

Chlorination with $PCl_5/POCl_3$ only generated tetrachloropteridine.[29]

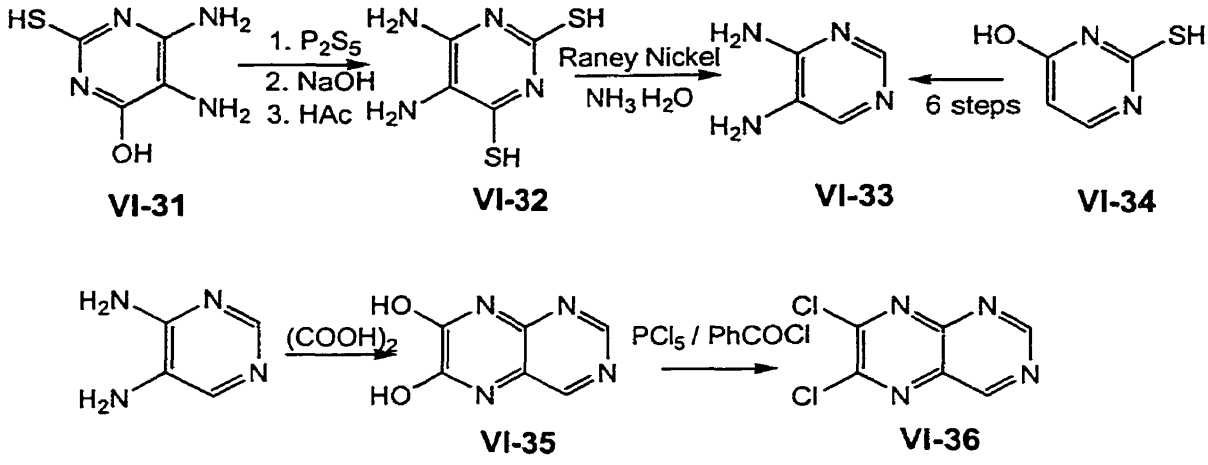

VI-31 VI-32 VI-33 VI-34

VI-35 VI-36

Scheme 6.10

6.3.2 Preparation of a trichloro compound, VI-39

Compared to other heterocycles, the 4-position of the pteridine ring is more reactive. For example, in aqueous solution, 6- and 7-chloropteridine and 6,7-dichloropteridine undergo the rapid reversible addition of water at the 3,4-double bond as well as normal nucleophilic replacement of a reactive chlorine atom.[28] This dual reactivity determined its sensitivity to pH, temperature, concentration and the nature of acids and bases. Although no kinetic work has been done on the relative reactivity of a chloro substituent at the 2-, 4-, 6-, 7- position of pteridine,[29] it is known that the replacement of chlorine atoms is stepwise, and that the aminolysis of 2,4,6,7-tetrachloropteridine with ammonia proceeds in three stages (6,7-dichloropteridine undergoes two steps). Therefore, and to avoid the unwanted side reaction, 7-amino-6-chloropteridine (**VI-37**) was made with careful control temperature of reaction (< 5°C). Once isolated, **VI-37** was immediately converted to the corresponding aminothiol.

In the course of this thesis several methods were developed to make aminothiol derivatives. For example, 2-amino-3-thiopyrazine was prepared from 2-amino-3-

chloropyrazine and anhydrous Na_2S in DMF at 100°C for 5 hours [30]; while the aminothiol for 1,2,3-TDTA was from the corresponding aminochloro and anhydrous Na_2S in ethanol.[31] In the case of 2-amino-3-thioquinoxaline, the best product was obtained using 2,3-dithioquinoxaline with NH_3 in a bomb reactor at 110°C overnight.

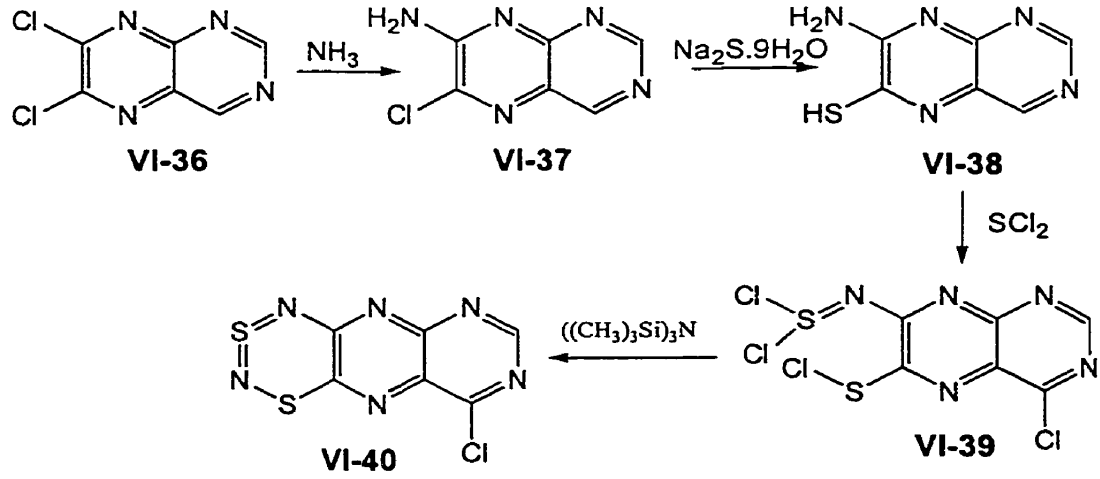

Scheme 6.11

The route employed in the quinoxaline case (the dithiol reaction with NH_3 gas) did succeed for pteridine; the reaction of 6,7-dithiopteridine with NH_3 gas only gave partial conversion. However the reaction of 7-amino-6-chloropteridine (**VI-37**) in aqueous solution with Na_2S was effective. The product was recrystallized from PhCN even though the yield was not good. The replacement of CH by nitrogen was expected to prevent the chlorination. Surprisingly, however, the reaction of **VI-38** and SCl_2 at room temperature generated the trichloro compound (**VI-39**) with chlorination at the 4-position of the pyrimidine ring.

Since crystals of **VI-39** suitable for X-ray crystallography were not available and also in order to determine the chlorination position in the pyrimidine ring, the trichloro compound was treated with tris(trimethylsilyl)amine to generate the dithiadiazine (**VI-40**). The position of nitrogen was confirmed by a crystal structure determination of **VI-40** (shown in Figure

6.2). The molecule is planar within 0.085(5) and the crystal structure consists of antiparallel ribbons of dithiadiazines running parallel to the y direction. The interlocking structure is similar to that of NDTA radical. This time we certainly can not attribute the structure to the structure-making CH--ring interaction which favors the herringbone arrangement, since the benzo based dithiadiazine (**VI-43**) possesses 4 CH, and yet exhibits a π-stacked structure. The intermolecular H---Cl interaction may be the determining effect.

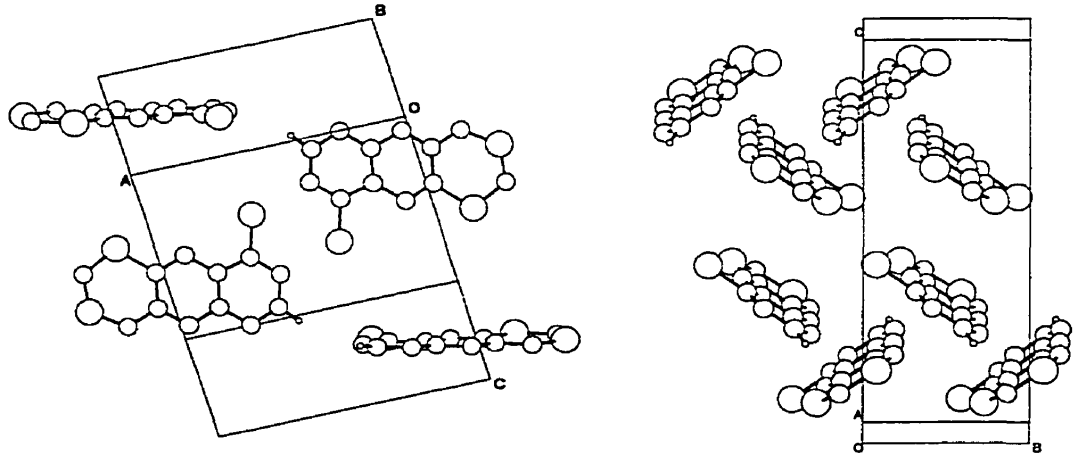

Figure 6.2 The crystal structure of **VI-40**. Top view (left) and side view (right).

6.3.3 Attempts to generate the radical

The final problem remaining was to bring trichloro **VI-39** down to the radical state. In contrast to our work on QDTA radicals, reagents such as, triphenylantimony, zinc, bromide and iodide salts, afforded ESR silent products. In one experiment with KI we successfully sublimed orange microcrystals whose IR spectrum had no sign of a υ(N-H) band, yet the mass spectrum gave a (M+1) peak in both low and high resolution modes. Elemental analysis could not distinguish the 1 unit difference, either. Another experiment, using thiophene as reducing agent, afforded a red fine precipitate which, upon sublimation,

generated orange microcrystals with the same IR spectrum as that of the KI reaction.

Thi

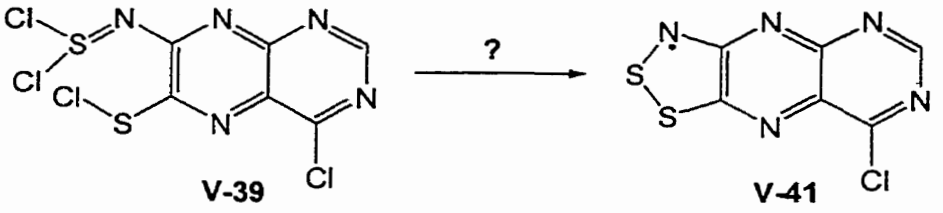

V-39 V-41

6.4 Experimental section

Preparation of 2,5-diamino-3,6-dichloropyrazine (VI-5)

Tetrachloropyrazine (6.0 g, 27.5 mmol) and potassium phthalimide (10.2 g, 27.5 mmol) in 80 mL of DMF was stirred at 50°C for 16 hours. The reaction was quenched with water and the precipitate was filtered and dried. This intermediate in 150 mL of water was treated with 10 mL of hydrazine hydrate and, after 2 hour stirring at room temperature, the yellow slurry was filtered, washed with water and dried. Yield: 3.1 g, 17.3%, 63%. Purification was achieved by recrystallization from ethanol with 84% of recovery and the crystal suitable for X-ray work was grown by fractional sublimation. mp, 269-271°C: Anal. calcd for $C_4H_4N_4Cl_2$: C: 26.84, H: 2.25, N: 31.30. Found: C: 27.01, H: 1.98, N: 31.57. Low Resolution MS: 178 (M^+ 100%), 180($[M+2]^+$, 66%), 153 ($[M-Cl]^+$, 12%). ^1H NMR (D-DMSO): 5.84 ppm (s). IR(4000- 400 cm^{-1}): 3446 (m), 3301(s), 3176 (m), 1610 (s), 1348 (m), 1262 (w), 1220 (m), 1206 (m), 1145 (s), 1055 (m), 848 (w), 725 (w), and 464 (w).

Preparation of disodium dimercaptomaleonitrile (VI-13)

This compound was prepared and purified as described in literature.[9] CS_2 (16.2 g, 0.21 mol) was added slowly to the slurry of NaCN (9.9 g, 0.2 mol) in 60 mL of DMF and

stirred for an hour at room temperature. The solution became dark red quickly. Ethanol (500 mL) was added and the solution was heated to gentle reflux for another hour. This dark red solution was hot filtered to remove any unreacted NaCN and cooled in the freezer (sometimes, a small seed crystal was needed to induce crystallization). The red crystals so formed were filtered and dried overnight. At this stage, sodium cyanodithioformate exists in the form of the complex with DMF. The dried DMF complex was put into a sublimation pot and heated to 130°C (oil bath) for about 12 hours until a yellow solid was obtained. Anhydrous ethanol was used to recrystallize the product. Yield: 12.6 g, 71 mmol, 68%. IR (4000-400 cm^{-1}) : 2196 (w), 1650 (w), 1157 (w), 1119 (m), 1019 (w), 861 (m), 679 (w), 542 (w), 467 (w).

Preparation of diimino derivative in ethylene glycol ($C_6H_7N_3S_2$), VI-18 [15]

This compound was made based on ref. 15. Ammonia gas was bubbled through a slurry of 2,3-Dicyano-5,6-dihydro-1,4-dithiin (0.5 g, 2.7 mmol) in 5 mL of ethylene glycol while the temperature was raised up to 70°C and maintained for half an hour. Then the heating bath was removed and the reaction was allowed to cool down to room temperature. The ammonia flow was kept up for another 10 minutes before the tube was sealed up and cooled in the freezer. The yellow precipitate was filtered off and washed with small amount of hexane/ether and pumped dry. Yield: 0.4 g, 45%. mp, 110°C start to decompose, (lit. 138-9°C). Anal. calcd for $C_6H_7N_3S_2$: C: 38.90, H: 3.81, N: 22.68; Found, C: 38.88, H: 3.90, N: 22.49. IR (4000-400 cm^{-1}): 3272 (w), 1699 (m), 1641 (s), 1571 (s), 1527 (s), 1318 (w), 1143 (s), 1125 (s), 1080 (s), 1049 (s), 1029 (s), 883 (m), 857 (m), 745 (w), 671 (w), 650 (w), 511 (m).

Preparation of 2,5-diamino-3,4-dichloropyrrole (VI-28)

When ammonia gas was passed through a solution of pentachloropyrrole [18] in methylene chloride at room temperature, the solution was converted into a pale yellow slurry. The gas flow was stopped 20 minutes later and the slurry was left to stir for an hour. The precipitate was was filtered off and recrystallized from dichloroethane. IR (4000-400 cm^{-1}): 3303 (w), 3261 (w), 1708 (s), 1633 (s), 1613 (s), 1566 (s), 1435 (s), 1300 (s), 1134 (s), 1118 (s), 1058 (m), 1015 (s), 903 (m), 862 (s), 813 (w), 743 (w), 662 (w), 448 (w). MS (EI, m/e): 163 (M^+, 100%).

Preparation of 6,7-dichloropteridine (VI-36) [28]

Finely ground 6,7-dihydroxypteridine (4.9 g, 30 mmol) and phosphorus pentachloride (15.2 g, 73 mmol) in about 80 mL of benzoyl chloride were heated to 145°C for 5 hours. The majority of the solvent was then removed under vacuum to leave a semi-solid which was extracted with boiling petroleum ether (150 mL x 4). The combined yellow extracts were concentrated to 50 mL and cooled in the freezer. The yellow product was collected by filtration, and washed with petroleum ether. Recrystallization was achieved from hexane. Yield, (2.3 - 2.8 g, 38 - 47%). mp, 135°C (lit. 140-1°C). MS (EI, m/e): 200 (M^+, 100%), 173 ($[M-HCN]^+$, 18%), 165 ($[M-Cl]^+$, 19%), 146 ($[M-H_2C_2N_2]^+$, 18%). IR (4000-400 cm^{-1}): 1582 (s), 1539 (s), 1340 (m), 1224 (w), 1152 (m), 1132 (m), 1092 (w), 1031 (s), 1003 (s), 855 (w), 811 (s), 665 (w), 599 (s), 568 (m), 549 (m), 492 (s), 431 (m).

Preparation of 7-amino-6-thiopteridine (VI-37)

A solution of 7-amino-6-chloropteridine made from 7-amino-6-chloropteridine

(4.9 g, 24.5 mmol) and Na_2S .$9H_2O$ (6.2 g, 26 mmol) in water was warmed to 70°C for 2 hours. The almost clear red solution was filtered and acidified with acetic acid. The precipitate was filtered off, washed with a small amount of acetonitrile and dried in vacuum. The crude product was recrystalled from benzonitrile even though the recovered rate was relatively low (average 2.0 g, 46 %). Anal. calcd for $C_6H_5N_5S$, C: 40.21%, H: 2.81%, N: 39.08%; found, C: 40.33%, H: 2.84%, N: 36.41%. The sample for IR was made by sublimation at 150°C. MS (EI, m/e): 179 (M^+, 42%), 163 ($[M-NH_2]^+$, 14%), 152 ($[M-HCN]^+$, 29%), 135 ($[M-CS]^+$, 12%), 93 (18%), 43 (100%). IR (4000-400 cm^{-1}): 3124 (w), 3281(w), 1630 (m), 1606 (w), 1564 (w), 1544 (w), 1405 (w), 1247 (w), 1123 (w), 1102 (s), 926 (w), 842 (w), 794 (m), 609 (w), 586 (w), 468 (w).

Preparation of trichloro derivative (VI-39)

A solution of 7-amino-6-thio-pteridine, **VI-38** (0.5 g, 2.8 mmol) in acetonitrile (5 mL) was treated with excess S_2Cl_2, and then chlorine gas bubbled through the slurry for 5 min. The initially red slurry turned yellow. The mixture was sealed and stirred for additional 2 hours, then placed in the freezer for half an hour. The yellow crystalline solid so formed was filtered off and dried *in vacuo*. Yield (0.55 g, 1.4 mmol, 51%). mp. 178°C. Anal. calcd for $C_6H_1N_5S_2Cl_4$, C: 20.65%, H: 0.29%, N: 20.06%; found, C: 20.79%, H: 0.40%, N: 19.96%. MS (EI, m/e): 347 ($[M]^+$, 25%), 312 ($[M-Cl]^+$, 70%), 266 (70%), 242 ($[M-3Cl]^+$, 100%), 210 ($[M-SCl_3]^+$, 78%), 170 (78%), 102 (100%). IR (4000-400 cm^{-1}): 1564 (s), 1520 (s), 1418 (s), 1299 (s), 1233 (s), 1168 (s), 1122 (s), 1041 (s), 962 (s), 860 (s), 814 (s), 739 (m), 669 (s), 644 (s), 607 (s), 559 (s), 539 (s), 492 (m), 464 (s), 430 (s), 418 (w).

Preparation of dithiadiazine derivative (VI-40)

To a solution of the freshly prepared trichloro derivative (0.3 g, 0.86 mmol) in acetonitrile (5 mL) was added tris(trimetylsilyl)amine (0.29 g, 1.2 mmol). The initial slurry turned to dark red then black after stirring for an hour at room temperature. This precipitate was filtered and recrystallized from acetonitrile. Crystals suitable for X-ray crystallographic work was recrystallized from dichloroethane. mp, 240°C, Anal. calcd for $C_6H_1N_6S_2Cl$, C: 28.07%, H:, 0.39%, N: 32.74%; found, C: 27.98%, H: 0.18%, N: 33.00%. MS (EI, m/e): 256 (M^+, 100%), 221 ([M-Cl]$^+$, 22%), 210 ([M-NS]$^+$, 30%), 196 ([M-N_2S]$^+$, 42%), 147 (25%), 131 (31%). IR (4000-400 cm^{-1}): 1556 (s), 1530 (s), 1433 (m), 1342 (m), 1281(s), 1224 (m), 1164, (s) 1112 (s), 1045 (s), 1010 (m), 931 (s), 858 (m), 811 (s), 703 (s), 652 (s), 642 (w), 552 (s), 449 (m), 437 (s).

Attempted reduction of trichloropteridine (VI-41).

Trichloropteridine was treated with a variety of reagents, such as thiophene, KI, $(Bu_4N)I$ and $(Bu_4N)Br$. In a typical experiment, After for about 10 - 30 min at room temperature, the precipitate was filtered and pumped dry. The solid was sublimed at 50 - 80 -140°C/ 10^{-3} Torr. All of these reactions gave the same product with low yield, and mp.> 250°C. Anal. calcd for $C_6H_1N_5S_2Cl$, C: 29.69, H: 0.42, N: 28.86, found, C: 29.62, H: 0.62, N: 29.26. MS (EI, m/e): 243 ([M]$^+$, 100%), 215 ([M-N_2]$^+$, 15%), 197 ([M-NS]$^+$, 62%), 185 [M-N_2S]$^+$,28%). HRMS (ESI) for (M+1), calcl. 243.9518, found, 243.9748. IR (4000-400 cm^{-1}): 1605 (s), 1575 (m), 1538 (m), 1422 (w), 1404 (w), 1351 (w), 1286 (m), 1249 (m), 1218 (w), 1165 (w), 1075 (w), 1012 (s), 886 (m), 818 (w), 690 (s), 635 (s), 603 (s), 549 (s), 524 (s), 425 (m).

6.6 References

1. Palamidessi, G.; Luini, F. *Farmaco, Ed. Sci.* **1966**, *21*, 811.
2. Sharefkin, D. M.; Spoerri, P. E. *J. Am. Chem. Soc.* **1951**, *73*, 1637.
3. Palamidisessi, G.; Bernardi, L. *J. Am. Chem. Soc.* **1964**, 2491.
4. Dzielendziak, A.; Butler, J. *Synthesis*, **1989**, 643.
5. Chambers, R. D.; Kenneth, W.; Musgrave, R.; Urben, P. G. *Chem. & Indust.* **1975**, 89.
6. Morrow, J. C.; Huddle, B. P. *Acta Cryst.* **1972**, *B 28*, 1748.
7. Povet'eva, Z. P.; Zvonkova, Z. V. *Kristallografija,* **1975**, *20*, 69.
8. Various reagents can react with pyrrole nitrogen to open the ring, see Gilow, H. M.; Burton, D. E. *J. Org. Chem.*, **1981**, *46*, 2221.
9. (a) Bähr, G.; Schleitzer, G. *Ber.* **1955**, 1771. (b) Bähr, G. *Angew. Chem.* **1956**, *68*, 525.
10. (a) Armand, P. J.; Deswarte, S.; Pinson, J.; Zamarlik, H. *Bull. Soc. Chem. France*, **1971**, 671. (b) Leglanc, R.; Corre, E.; Soenen-Svilarich, M.; Chasle, M. F.; Foucaud, A. *Tetrahedron*, **1972**, *28*, 4431.
11. (a) Bakibaev, A. A.; Yagovkin, A. Y. *Russian Chemical Review*, **1998**, *67*, 294. (b) Waltherwolf, V.; Defener, E.; Petersen S. *Angrew. Chem.* **1960**, *72*, 963.
12. Brach, P. J.; Grammatica, S. J.; Ossanna, O. A.; Weinberger, L., **1970**, 1403.
13. Dickinson, C. L.; Middleton, W. J.; Engelhardt, V. A. *J. Org. Chem.* **1962**, *27*, 2470.
14. (a) Velázquez, C. S.; Broderick, W. E.; Sabat, M.; Barrett, A. G.; Hoffman, B. M. *J. Am. Chem. Soc.* **1990**, *112*, 7409. (b) Schramm, C. J.; Hoffman, B. M. *Inorg. Chem.* **1980**, *19*, 383.
15. (a) Degener, E.; Petersen, S. *US 2,991,292*, Via *CA*, **1961**, 26456 i. (b) Wolf, W.; Roesch, G.; Klappert, H.; Degener *E. Ger. 1,101,422*, Via *CA*, **1961**, 7331c.
16. Coon, C. L. *US* 3,642,824. **1972.**

17. (a) Plater, M. J.; Rees, C. W.; Roe, D. G.; Torroba, T. *J. Chem. Soc., Chem. Commun.* **1996**, 427. (b) Plater, M. J.; Rees, C. W.; Roe, D. G.; Torroba, T. *J. Chem. Soc., Perkin Trans. 1* **1993**, 769.

18. Gilow, H. M.; Burton, D. E. *J. Org. Chem.* **1981**, *46*, 2221.

19. (a) Shevchenko, V. I.; Kukhar, V. P. *Zh. Obshch. Khim.* **1966**, *36*, 735 (Via *CA*, **1966**, *65*, 8858). (b) Kukhar, V. P.; Koval, A. A.; Kirsanov, A. V. *Zh, Obshch. Khim.* **1968**, *38*, 1270 (Via *CA*, **1968**, *69*, 106391).

20. (a) Daniels, P. H.; Wong, J. L.; Atwood, J. L.; Vanada, L. G.; Rogers, R. D. *J. Org. Chem.* **1980**, *45*, 435. (b) Rammash, B. K.; Atwood, J. L.; Weeks, J. A.; Wong, J. L. *J. Org. Chem.* **1987**, *52*, 1712.

21. Eibler, E.; Hoecht, P.; Prantl, B., Rossmaier, H.; Schuhbauer, H.; Wiest, H.; Sauer, J. *Liebigs Ann. Recl.* **1997**, *12*, 2471 (via *CA 128*, 88460).

22. Ulrich, H.; Kober, E.; Schroeder, H.; Ratz, R.; Grundmann, C. *J. Org. Chem.* **1962**, *27*, 2585.

23. Gompper, R.; Junius, M. *Tetrahedron Letter.* **1980**, *21*, 2883.

24. Brown, D. J. *J. Appl. Chem.* **1952**, 239.

25. (a) Dille, K. L.; Christensen, B. E. *J. Am. Chem. Soc.* **1954**, *76*, 5087. (b) Levin, G.; Kalmus, A.; Bergmann, F. *J. Org. Chem.* **1960**, *25*, 1753.

26. Beaman, A. G.; Gerster, J. F.; Robins, R. K. *J. Org. Chem.* **1962**, *27*, 986.

27. Albert, A.; Brown, D. J.; Cheeseman, G. W. S. *J. Chem. Soc.* **1952**, 1620.

28. Albert, A.; Clark, J. *J. Chem. Soc.* **1964**, 1666.

29. Taylor, E. C.; Sherman, W. R. *J. Am. Chem. Soc.* **1958**, *81*, 2464.

30. Safonova, T. S., Myshkina, l. A. *Chem. Heterocycl. Compd.*, **1970**, *6*, 1019.

31. Barclay, T. M.; Cordes, A. W.; Haddon, R. C.; Itkis, M. E.; Oakley, R. T.; Reed, R. W.; Zhang, H. *J. Am. Chem. Soc.* **1999**, *121*, 969.

Appendix 1: Starting materials

A1.1 Chemicals obtained commercially and used without purification

acetic anhydride	Fisher
acetic acid	BDH
acetonitrile (anhydrous)	Caledon
4-aminopyrimidine	Aldrich
2-aminopyrazine	Aldrich
1-aminopyrene	Aldrich
ammonia gas	Matheson
ammonium hydroxide	BDH
argon	Canox
benzosulfonamide	Aldrich
benzonitrile	Aldrich
benzoyl chloride	Aldrich
bromine	Fisher
butyllithium	Aldrich
carbon disulfide	Aldrich
chlorine	Matheson
chloroform	Fisher
2-chloropyrazine	Aldrich
4,5-diaminopyrimidine	Aldrich
4,5-diamino-2,6-dimecaptopyrimidine	Aldrich
4,5-diamino-6-mecapto-2-hydroxypyrimidine	Aldrich

1,2-dibromoethane	Aldrich
1,2-dichloroethane	Fisher
dichloroquinoxaline	Aldrich
3,4-dichlorothiadiazole	Aldrich
N,N-dimethylformamide	Fisher
dimethylsulfoxide	Fisher
ethanol anhydrous	Fisher
ethanol 95%	Fisher
ether (anhydrous)	Aldrich
hexane	Fisher
hydrazine anhydrous	Aldrich
hydrazine hydrate	Aldrich
hydrochloric acid	BDH
hydroxy amine hydrochloride	Fisher
iodine	Fisher
Linde 4Å molecular sieves	Anachemia
lithium aluminum hydride	Aldrich
magnesium sulfate	Fisher
magnesium turnings	Fisher
mercury	Fisher
methanol	Fisher, BDH
1-methylpyrrole	Aldrich
naphthalene-2-thiol	Aldrich
nitric acid	BDH

nitrogen (high purity)	Canox
oxalic acid hydrate	BDH
p-xylene	Fisher
phosphorus pentoxide	Fisher
phosphorus pentachloride	Aldrich
phosphorus oxychloride	Aldrich
potassium carbonate (anhydrous)	BDH
potassium hydroxide	BDH
potassium bromide	Fisher
potassium iodide	Fisher
pyrazine	Aldrich
pyridine	BDH
pyrrole	Aldrich
Raney nickel	Aldrich
selenium	Aldrich
sodium borohydride	BDH
sodium sulfate	Fisher
sodium cyanide	Fisher
sodium hydroxide	BDH
sodium carbonate	BDH
sodium	BDH
sodium sulfide (anhydrous)	Aldrich
sodium sulfide nonahydrate	Aldrich
sodium acetate (hydrated)	Fisher

sulfur monochloride	Aldrich
sulfenyl chloride	Aldrich
tetrabutylammonium iodide	Aldrich
thiophene	Aldrich
thionyl chloride	Aldrich
thiourea	BDH
thiosemicarbazide	Aldrich
titanocene	Aldrich
triethylamine	Aldrich
trimethylsilylamine	Aldrich
trimethylsilylazide	Aldrich
triphenylantimony	Aldrich
zinc	Fisher

A1.2 Chemicals obtained and purified before use

acetonitrile (Fisher and BDH) ---distilled from P_2O_5

chlorobenzene (Fisher) --- distilled from P_2O_5

dichloromethane (Fisher and BDH) --- distilled from P_2O_5

dichloroethane (Fisher and BDH) --- distilled from P_2O_5

diethyl ether (Fisher) --- distilled from lithium aluminum hydride

toluene (Fisher) ---distilled from sodium

anhydrous ethanol --- distilled from magnesium

A1.3 Commonly used chemicals made in the laboratory

Dichloroiodobenzene

Cl_2 gas was passed over an ice-cooled solution of iodobenzene (10 g, 49 mmol) in 50 mL of methylene chloride for 20 minutes, to form a canary yellow precipitate. The slurry was allowed to warm up slowly to release excess Cl_2 in the solution. The yellow crystalline product was filtered off and pumped dry and stored for further use. Yield (12.6 g, 45 mmol, 93%).

Selenium tetrachloride

Selenium powder (10 g, 125 mmol) was slurried in 100 mL of acetonitrile and the mixture stirred and cooled in an ice bath. Chlorine gas was passed over the solution (*c.a.* 20 min) which resulted in a gradual color change from black to white. The solution was filtered *in vacuo* and the white precipitate rinsed three times with acetonitrile and dried *in vacuo*. The $SeCl_4$ was stored in the dry box. The yield was 24 g , 106 mmol, 85%.

Sulfur dichloride

A few milligrams of ferric chloride as the catalyst was added to 100 mL of sulfur monochloride and the orange solution cooled in an ice bath. Chloride gas was bubbled through the solution until the color changed to deep red (*c.a.* 30 min). Atmospheric distillation of the solution yielded approximately 50 mL of sulfur dichloride, which was stored in the refrigerator. The yellow residue was also stored for next use.

Appendix 2 General procedures and instrumentation

A2.1 General procedures

Air-sensitive reactions were performed using standand Schlenk techniques under an inert atmosphere (nitrogen) provided by a double manifold vacuum line (vacuum/nitrogen). Air-sensitive compounds were handled in a Braun MB-150 M dry box under argon or nitrogen. Gradient sublimations were performed on ATS 3210 series three-zone tube furnace with an ATS 1400 series programmable temperature controller. The bomb reactions was carried on Parr bomb reactor with automatic temperature controller.

A2.2 Instrumentation

Melting points are uncorrected and were obtained on an Electrothermal Melting Point Apparatus. Infrared spectra were recorded on a Nicolet 20SX/C and Avatar 320 Infrared Spectrometer with KBr optics. Solid samples were ground with Nujol to form mulls and liquids were put on the KBr plate neat. ^{1}H NMR were recorded either on a Varian Gemini 200 MHz spectrometer in $CDCl_3$ except where specified. Mass spectra were recorded by EI or CI techniques on a Kratos MS890 spectrometer at the University of Guelph, on a Finnigan 4500 quadrupole mass spectrometer (70 eV, DEI and DCI) at the McMaster Regional Centre for Mass Spectrometry or a VG 7070E at University of Waterloo. Cyclic voltammetry experiments were run on a PINE spectrochemical working system (EG&G Instruments). n-Bu_4NPF_6 (0.01 M) in CH3CN was used as supporting electrolyte. X-band ESR spectra were recorded on a Varian E-109 spectrometer and Bruker EMX 200 with DPPH as field marker. Elemental analysis were performed by MHW Laboratories, Phoenix, AZ.

A2.3 Collaborative work

X-ray crystal structures were solved by the Prof. A. W. Cordes group at the University of Arkansas and Prof. J. F. Richardson at the University of Louisville. Data were collected on Nonius CAD-4 diffractometers with monochromated Mo Kα radiation (λ = 0.07107Å). Magnetic susceptibility and conductivity measurements were performed by Prof. R. C. Haddon at AT&T Bell Laboratories and later at University of Kentucky. Further details can be found in the literature cited in this thesis.

Appendix 3 Crystal Structure Data

The selected crystallographic information of the crystal structures appearing in this thesis are presented in the following table. Only 1,3,2-dithiazolyl or 1,2,3-dithiazolyl ring related bond lengths and bond angles are of concern. Further details may be found in the literature. Table abbreviations are defined as follows:

Z - number of formula units in the unit cell

f.wt. - formula weight

R, R_w - R-factor and weighted R-factor

V- unit cell volume

d_{calcd} - calculated density

compound	NDTA	QDTA	TDTA-SO_2Ph	TDTA
formula	$C_8H_6NS_2$	$C_8H_4N_3S_2$	$C_{10}H_5N_5O_2S_4$	$C_4N_5S_3$
f.wt.	204.28	206.26	355.42	214.26
space group	$P\ \bar{1}$	$P2_1$	$P\ \bar{1}$	$P\ \bar{1}$
Z	4	2	4	2
V, Å^3	892.5(3)	406.10 (15)	1324.7 (2)	342.2(1)
d(calcd), g cm	1.52	1.69	1.78	2.08
temp. K	293	293	293	293
R	0.037	0.041	0.050	0.032
R_w	0.058	0.056	0.052	0.055
a, Å	9.4516(18)	3.7105 (8)	10.2388 (8)	4.4456 (8)
b, Å	9.5167(19)	19.009 (5)	11.8299(9)	8.407 (2)
c, Å	10.5397(13)	5.7864 (9)	13.1024(12)	9.671(3)
α, deg	76.911(13)	90	115.066(7)	71.34(2)
β, deg	86.139(12)	95.724 (14)	94.083(8)	89.28(2)
γ, deg	75.144(15)	90	108.405(6)	87.80(2)
d(S-N), Å	1.644(4)	1.649	1.73(3)	1.636(3)
d(S-C), Å	1.749(3)	1.736	1.755(16)	1.728(2)
d(C-C), Å	1.364(5)	1.435	1.467(6)	1.448(2)
∠(SNS)	114.83	115.0	110.55(12)	115.83(9)

compound	TDTA	1,2,3-TDTA	$TDTACl_3$	2,5-diamino
formula	$C_8N_{10}S_6$	$C_4N_5S_3$	$C_4N_5S_3Cl_3$	$C_4H_4N_4$
f.wt.	428.52	214.26	320.61	108.10
space group	$P\bar{1}$	$P2_1/n$	$P2_1/m$	$P2_1/n$
Z	2	4	2	4
V, Å^3	667.5 (9)	655.7(2)	520.67(16)	335.05(6)
d(calcd), g cm^{-1}	2.13	2.17	2.04	1.774
temp. K	150	293	293	293
R	0.111	0.037	0.030	0.033
R_W	0.137	0.050	0.036	0.062
a, Å	7.489(7)	6.6749(16)	8.6990(11)	3.7582(4)
b, Å	9.593(4)	11.7178(14)	6.8203(17)	14.5505(15)
c, Å	10.759(6)	8.6148(14)	9.4167(10)	6.2451(6)
α, deg	65.77(4)	90	90	90
β, deg	74.10(6)	103.297(16)	111.261(16)	101.162(8)
γ, deg	74.64(6)	90	90	90
d(S-S), Å	---	2.0482(13)	---	---
d(S-N), Å	1.627(14)	1.609(3)	1.516(3)	---
d(N-C), Å	---	1.342(4)	---	1.362(3)
d(S-C), Å	1.73(3)	1.721(3)	1.754(4)	---
d(C-C), Å	1.45(2)	1.463(5)	1.451(5)	1.388(3)
∠(SNS)	116.5(6)	---	---	---
∠(SSN)	---	99.75(16)	---	---

compound	Cl-Q-Cl_3	VI-40
formula	$C_8H_3N_3S_2Cl_4$	$C_6HN_6S_2Cl$
f.wt.	347.06	256.7
space group	C2/c	$P2_1/c$
Z	8	4
V, Å^3	2521.4(9)	906.2(4)
d(calcd), g cm $^{-3}$	1.83	1.88
temp. K	293	293
R	0.043	0.048
R_w	0.049	0.063
a, Å	30.561(5)	10.248(2)
b, Å	4.9764(9)	5.772(2)
c, Å	22.247(4)	15.391(4)
α, deg	---	---
β, deg	131.822(14)	95.93(2)
γ, deg	---	---
planarity (Å)	0.08(5)	0.058(6)
d(S-N), Å	1.498(4)	1.540/1.664
d(N-C), Å	1.400(5)	1.392(6)
d(S-C), Å	1.766(4)	1.774(5)
d(C-C), Å	1.438(6)	1.450(7)